Examination committee:
Prof. dr. ir. Koen Dewettinck (Chain, Ghent University)
Prof. dr. ir. Stijn Van Hulle (Ghent University)
Prof. dr. ir. Geraldine Heynderickx (Ghent University)
Dr. Jim Wicks (The Fluid Group)
Prof. dr. Olivier Potier (University de Lorraine)

Promotors:
Prof. dr. ir. Ingmar Nopens*
dr. ir. Youri Amerlink*

*Department of Mathematical Modelling, Statistics and Bioinformatics
BIOMATH research group: Model-based analysis and optimisation of bioprocesses
Faculty of Bioscience Engineering
Ghent University

Dean:
Prof. dr. ir. Marc Van Meirvenne

Rector:
Prof. dr. Anne De Paepe

Usman ur Rehman

Next generation bioreactor models for wastewater treatment systems by means of detailed combined modelling of mixing and biokinetics

The thesis is submitted for the fulfilment of the requirement for the degree of Doctor (PhD) in Applied Biological Sciences

Please refer to this work as follows:
Usman Rehman (2016). Next generation bioreactor models for wastewater treatment systems by means of detailed combined modelling of mixing and biokinetics, PhD thesis, Ghent University, Belgium

ISBN 978-90-5989-932-2

Acknowledgements

I can so much relate the journey of completing my PhD with this Earl Nightingale's quote,

"We are at our very best, and we are happiest, when we are fully engaged in work we enjoy on the journey toward the goal we've established for ourselves. It gives meaning to our time off and comfort to our sleep. It makes everything else in life so wonderful, so worthwhile."

The journey which I started in 2012 has finally come to an end. It was a journey of discovery. There were moments when I celebrated small milestones as if I have vanquished the Mount Everest. Then there were moments of setbacks when the destination looked awry. But I've to say, there were people who inspired me and encouraged me to keep working hard. I am writing these lines, hoping that I may express my gratefulness for all those people who have been a support to me during my PhD.

First of all, I would like to express my gratitude to my promotor Prof. Ingmar Nopens. I feel honoured to have worked with him and be part of his research group BIOMATH. Ingmar, I have really enjoyed working with you and find myself very fortunate to complete my PhD under your supervision. You have always inspired me and I've learnt to work hard and be innovative at the same time. I'm thankful for all the opportunities you gave me to disseminate my research and represent BIOMATH at numerous conferences. I also feel immensely grateful for your consideration regarding my personal circumstances and for giving the freedom to tackle all the problems.

I'd like to thank Youri Amerlinck for his utmost support and guidance throughout my PhD. Youri has played a vital role in the completion of this PhD by providing much needed critical review of my work. He has been there whenever I needed his advice and assistance. It is always good to have somebody like Youri who is not only my co-promoter but also a good friend.

I thank members of the examination committee who evaluated this thesis and provided invaluable feedback. Their feedback certainly improved the quality of the thesis. Thankyou Geraldine, Stijn, Olivier and Jim for reading this thesis and for attending the defence.

For the first three years of my PhD, I was part of a European project SANITAS. It was a life changing experience as it helped enormously in my career development through training events and secondments. I thank all those people who were involved in this project as it was a great professional and personal experience working with them. Special thanks to Alexandra Popartan for managing and arranging all the events during this project.

During my PhD I worked at ACCIONA's pilot plant at Almunecar, Spain for three months. I would like to thank Teresa de la Torre for giving me this opportunity. It was a special experience as it included living at a mountain top next to a Costa Tropical beach. I would like to mention specially Marina for her continuous help on and off the plant. Thank you for your exceptional company firstly in Almunecar and then in Ghent as well. I hope the friendship continues hereafter.

I also spent three months at LEQUIA, a research unit of Girona university, Spain. I would like to thank Prof. Joaquim Comas to give this opportunity. Moreover, I'd like to thank Montse, Antonia and Julian for making it an exciting stay. Special thanks to Ignasi Aymerich for his fantastic company and support.

Working at BIOMATH was a fantastic experience and I have to say it is a group of extraordinary people. I'd like to thank Tinne for her delicious cakes and assistance in several matters. Thanks to Timpe, Ruth and Annie for their administrative support and Jan Roels for his technical support. I would like to thank my colleagues and friends at BIOMATH: Severine, Wim, Elena, Thomas, Mehul, Stijn (Van Hoey), Niels, Daan, Michael, Ivaylo, Ashish, Timothy, Giacomo, Chaim, Sophie, David, Roop and Andreia. All of them have contributed in creating a friendly working environment where everybody is willing to help each other. Special thanks to my friend Wouter for all the support, interesting conversations and for accompanying me in memorable trips to Lisbon (2014) and Australia (2015). I hope all the friendships and professional relationships I developed during these years will last long.

I would like to thank my friends Saqib, Raja Usman, Naeem, Mehmood, Waqar and Mehboob, they have been a moral support and always cheered me up when needed.

Last but not the least, thanks to my family: father, mother, Sidra, Mona, Zohaib & Mavra. It wasn't possible without their support and well wishes. I dedicate this thesis to my family because they always gave me immense love and trusted my decisions.

The few lines I wrote above are unable to do the justice with the amount of appreciation I have for all these nice people. I hope I'll keep seeing them in future and will never forget the time I spent with them.

Usman

Ghent, October 2016

Table of Contents

List of abbreviations

1D	1-dimensional
2D	2-dimensional
3D	3-dimensional
ADCP	Acoustic Doppler Current Profiler
AOB	Ammonia oxidising bacteria
ASM	Activated sludge models
ASM1	Activated sludge model number 1
ASM2	Activated sludge model number 2
ASM2d	Activated sludge model number 2d
ASM3	Activated sludge model number 3
ASMG1	Activated sludge model number 1 for greenhouse gases
BOD	Biological oxygen demands
CDP	Concentration distribution plot
CFD	Computational fluid dynamics
CM	Compartmental model
COD	Chemical oxygen demand
CSD	Cumulative species distribution
CSO	Combined sewer overflows
CSTR	Continuous stirred tank reactor
DNS	Direct numerical simulation
DO	Dissolved oxygen
HRT	Hydraulic retention time
IWA	International Water Association
$K_{O,A}$	Oxygen half saturation index in ammonia oxidizing bacteria
K-values	Half saturation indices
LES	Large eddy simulation
MBR	Membrane bioreactor
N_2	Dinitrogen
NO_2^-	Nitrite
NO_3^-	Nitrate
N_2O	Nitrous oxide
NOB	Nitrate oxidizing bacteria
PAOs	Phosphorous accumulating organisms

RANS	Reynolds averaged Navier-Stokes
SND	Simultaneous nitrification-denitrification
TIS	Tanks-in-series
TSS	Total suspended solids
UDF	User defined function
VOF	Volume of fluid model
WFD	Water Framework Directive
WWT	Wastewater treatment
WWTP	Wastewater treatment plants
NO	Nitric oxide

Chapter 1

Introduction

This chapter includes problem statement, objectives and layout of the thesis.

1.1. Problem statement

Wastewater treatment plants (WWTP) are needed to treat municipal and industrial wastewater to reduce the impact of pollutants on the natural environment. The discharge of treated wastewater and the disposal of sludge from treatment plants treating domestic or industrial wastewater are subject to regulations imposed by the authorities. In the European Union, the Water Framework Directive (WFD) enforces a good ecological and chemical status of all surface waters. River basin management plans are drawn up in Europe for the implementation of the WFD. Basic measures within these plans, include the control of pollution at their source through the setting of emission limits as well as through the setting of environmental quality standards. Many surface waters throughout Europe still do not meet the WFD requirements due to discharges of combined sewer overflows (CSO) and of WWTP effluent (Commission report, 2009).

During the wastewater treatment process greenhouse gas emissions are produced. These emissions from WWTPs are a matter of growing concern. The global warming potential of nitrous oxide (N_2O) is 298 times greater than carbon dioxide (IPCC, 2014). Therefore, research on N_2O emissions has become a point of attention in recent research (Ni and Yuan, 2015).

The increased importance of wastewater treatment has led to development of mathematical models for optimization and design of wastewater treatment plants (Belia et al., 2009; Gernaey et al., 2004; Glover et al., 2006). The use of these models has

increased with the increase in computational power of computers and consequently more and more complex models have surfaced. However, in the wastewater treatment field, more modelling efforts have been made towards comprehending the underlying biological processes rather than the hydrodynamic aspects of the reactor design. Currently, hydrodynamic modelling is based on an over-simplified approach of tanks-in-series (TIS) modelling developed by Levenspiel (1962). The TIS models are commonly used along with activated sludge models (ASM) for modelling WWTPs. The TIS approach models the mixing behaviour of the whole reactor as a number of completely mixed continuous stirred tank reactors considering the flow in only one direction. However, complete mixing is unlikely to exist in a full scale WWTP. In most current modelling efforts, the TIS approach is used and detailed spatial variations in substrate and electron acceptor concentrations in the bioreactors are typically not taken into account, even though it is plausible that they have a significant impact on the plant performance. Therefore, these models are unsuitable to evaluate the detailed impact of different operational conditions on the performance of the biological processes.

The activated sludge models (ASM) are based on the Monod equation (Monod, 1942), which uses half saturation indices (K-values) to describe the dependence of microbial growth to substrate availability. In Monod's equation, growth (and thus substrate consumption) largely depends on the local substrate (e.g. ammonium) and electron acceptor concentrations (e.g. oxygen and nitrate) (Henze et al., 1987). Changing the half saturation indices is typically applied in the regularly required calibration exercise, especially in those cases where low contaminant concentrations exist (Coen et al., 1998). The difficulties arise when considering different operational conditions and recalibration is usually needed when moving from dry to wet weather conditions. Therefore, there is a need for further investigation to understand the factors influencing the process variables and calibration efforts.

Computational fluid dynamics (CFD) is a method for detailed hydrodynamic modelling. The CFD discretises the domain into a three dimensional computational grid and Navier-Stokes equations are solved at each grid point to simulate the flow field (Batchelor, 1967). The method allows to visualise the impact of design parameters and operational strategies on the local hydrodynamic of the system. In addition, the inclusion of turbulence and multiphase modelling enables the detailed modelling of the aeration system of the WWTP. Currently, the CFD modelling framework is mainly used for basic hydraulic design and troubleshooting in WWTP modelling. However, CFD

has not extensively been used to evaluate the impact of local mixing conditions on the process rates and subsequent process concentrations in a WWTP.

One of the major bottlenecks in using CFD as a main modelling tool for process design, is its high computational requirement. Hence, it is unlikely to become mainstream in the first decades to come and there is a need for a methodology that combines the improved insight of CFD and the low computational cost of TIS. Previously, CFD results have been used to develop a so-called compartmental model (CM) (Alvarado et al., 2012; Delafosse et al., 2010; Le Moullec et al., 2010). A CM is a conceptual network of spatially localized compartments connected through convective and exchange fluxes based on the findings of detailed CFD modelling. Hitherto the compartmental models have been solely based on hydrodynamic results of CFD studies. A CFD hydrodynamic model can indicate the mixing limitation but is unable to quantify mixing inefficiencies in terms of concentration variations which might provide exact knowledge about the calibration needs. Hence, a compartmental model which does not only take into account hydrodynamics but also consequential concentration variations still needs to be developed.

1.2. Objective

In the wake of the problem statement, the main objective of the thesis is to improve current WWTP modelling practice and point out the limitations of the currently employed models. Hence, this thesis aims at providing detailed modelling including both hydrodynamics and biokinetics in the first step and quantifying the mixing limitations to develop a simplified model in the next step. It also aims at evaluating the impact of mixing conditions on model calibration efforts. The stepwise objectives are more specifically summarized as:

a) To determine the detailed hydrodynamics and local mixing heterogeneities in a WWTP

b) To evaluate and quantify the impact of local mixing heterogeneities on the process variables

c) To translate the impact of quantified process variations into simplified modelling

d) To better understand the impact of mixing inefficiencies on model calibration efforts

1.3. Outline

In order to achieve the abovementioned objectives, a systematic approach is used in the thesis. The approach is elaborated in Figure 1.1. It starts with detailed hydrodynamic modelling of the WWTP using CFD modelling. It is followed by scenario analysis which includes the CFD simulations with varying operational conditions. In the next step, biokinetic models are integrated with the CFD model. The biokinetic models include both the full ASM1 model to predict carbon and nitrogen removal (Henze et al., 2000) as well as the ASMG1 to predict nitrous oxide production (Guo and Vanrolleghem, 2014). These simulations are also performed at varying process conditions. In the next step, model reduction is performed using the process knowledge gained from CFD-biokinetic modelling and a compartmental model is derived. It is followed by developing a dynamic compartmental model which can be used under dynamic process conditions.

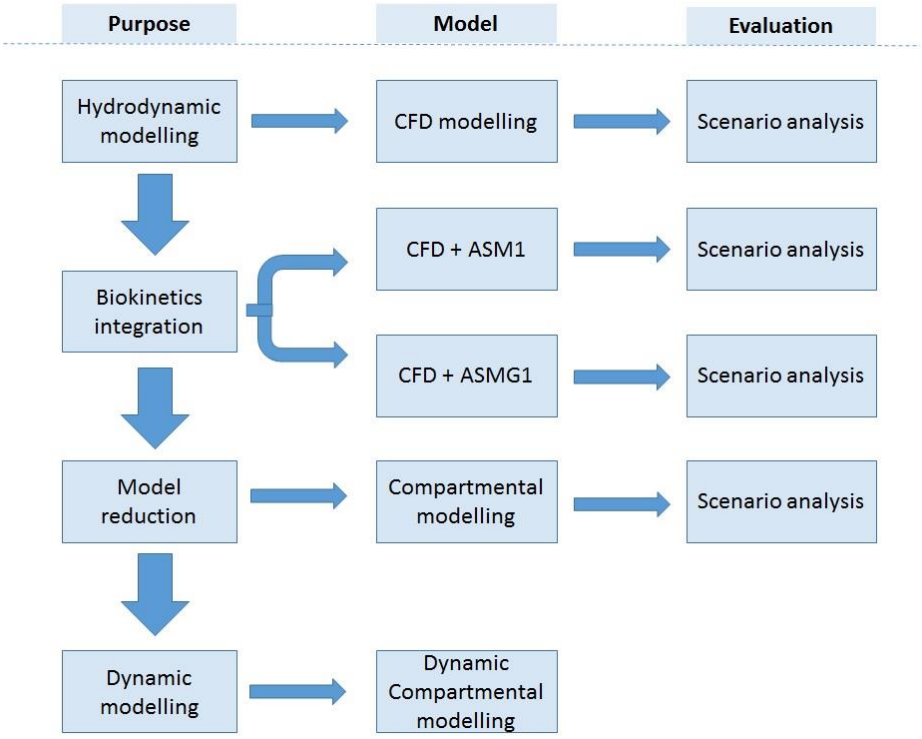

Figure 1.1 Description of modelling approach applied in the PhD

A structural layout of the thesis is provided in Figure 1.2. Primarily, all the modelling is performed for a bioreactor at the WWTP in Eindhoven (The Netherlands). In addition, the modelling methodologies are verified on other case studies. Therefore, the layout in Figure 1.2 shows different chapters divided into two columns. One column represents the Eindhoven WWTP modelling efforts whereas the other compiles the other case studies. Henceforth, the PhD thesis is structured into four distinct parts where each part addresses the different objectives mentioned in section 1.2.

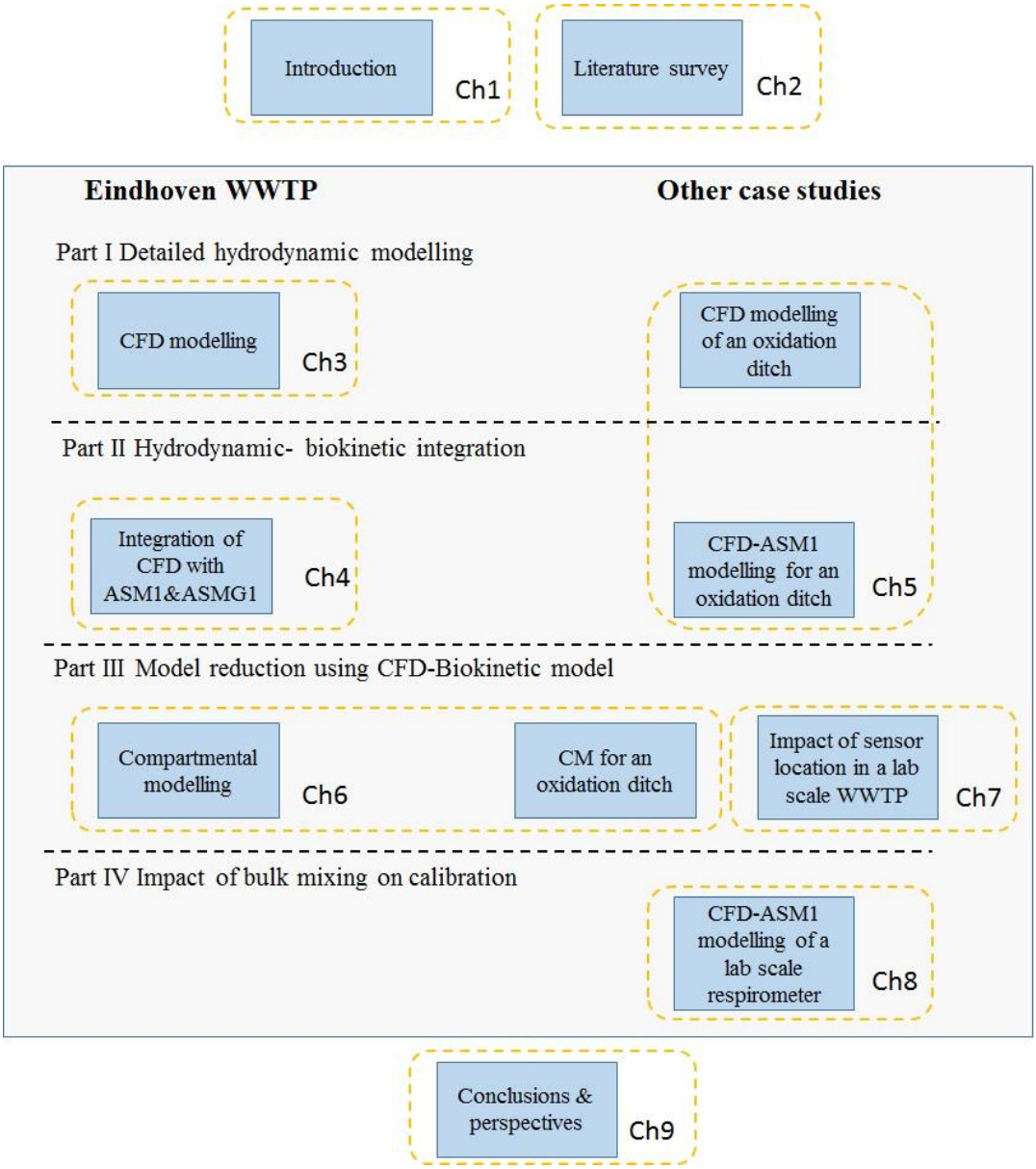

Figure 1.2 The structural layout of the thesis

The first chapter discusses the problem statement and clarifies the objectives of the thesis. The second chapter provides a literature survey and background of WWTP modelling. The last chapter addresses the conclusions & perspectives. The details about the remaining chapters in the main part of the PhD are provided here.

Part I: Detailed hydrodynamic modelling

Chapter 3: This chapter provides the detailed CFD hydrodynamic modelling for the full scale WWTP of Eindhoven (The Netherlands) and evaluates the mixing patterns due to changes in process conditions

Part II: Hydrodynamic-biokinetic integration

Chapter 4: This chapter provides the method to integrate the biokinetic model (ASM1) with the CFD hydrodynamic model. In the next step the nitrous oxide model is also included.

Chapter 5: This chapter provides the application of integrated CFD-ASM1 model for an oxidation ditch (La Bisbal d'Empordà, Spain).

Part III: Model reduction

Chapter 6: This chapter explains the derivation of the compartmental model from CFD-ASM model for both the case studies (Eindhoven and La Bisbal WWTPs).

Chapter 7: This chapter provides a proof of principle study to evaluate the impact of sensor location on the performance of a controller in a lab scale WWTP.

Part IV: Impact of bulk mixing on calibration

Chapter 8: This chapter describes the use of the integrated CFD-biokinetic model to study the impact of mixing conditions on the calibrated half saturation indices in detail using a lab scale respirometric vessel as a case study.

Chapter 2

Literature Review

This chapter includes a literature survey and background of WWTP modelling.

2.1. Wastewater treatment

Municipal wastewater treatment plants (WWTP) can have different configurations based on desired output and regional regulations. However, the general treatment process can be outlined in three steps: primary, secondary and tertiary treatment (Tchobanoglous et al., 2003) (Figure 2.1). Primary treatment includes mechanical separation of large particles from wastewater, whereas secondary treatment includes biological treatment and secondary settling. Tertiary treatment refers to effluent polishing e.g. sand filtering & disinfection. These steps are further divided into several sub-processes depending on the influent and desired effluent quality. The research presented in this thesis is mainly focused on the biological treatment step.

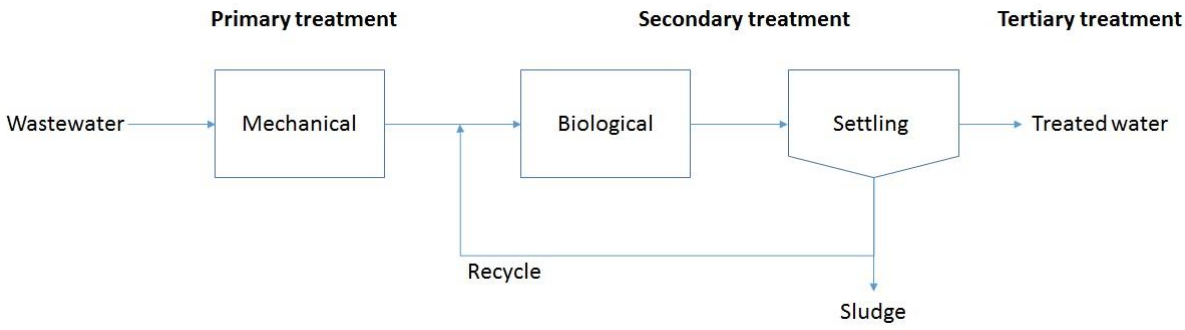

Figure 2.1 General outline of a wastewater treatment plant

During the biological treatment, the organic compounds and nutrients (phosphorous and nitrogen) in the wastewater are degraded by micro-organisms. This treatment is most

commonly based on the Activated Sludge (AS) system which was first used for a sequencing batch reactor by Ardern and Lockett (1914). The AS process is the most commonly employed method for biological treatment of wastewater (Eckenfelder and Grau, 1998; Kolarik and Priestley, 1995).

2.1.1. Activated sludge process

An activated sludge process plant conventionally involves aeration of wastewater in a bioreactor and is followed by solids-liquid separation in a settler/clarifier in order to retain the sludge in the system. In the bioreactor suspended biomass (activated sludge) is responsible for the removal of pollutants. It includes the removal of organic carbon by heterotrophic bacteria under aerobic conditions, i.e. in the presence of dissolved oxygen (DO). The presence of DO also triggers autotrophic nitrifying bacteria to convert ammonium into nitrate (nitrification). In WWTPs with N-removal, denitrifying bacteria remove organic matter, in absence of DO, with the use of nitrates as electron acceptor (i.e. under anoxic conditions) (denitrification). During the denitrification process, nitrate is converted into atmospheric nitrogen (Henze et al., 2000, 1987). Therefore, an activated sludge process needs both aerobic and anoxic conditions to remove organic compounds and nitrogen and hence the availability of DO plays a vital role in the AS process.

The aerobic and anoxic conditions are developed in an activated sludge bioreactor WWTP by creating aerated and non-aerated regions either in a single or separate bioreactors. However, in either situation (single or separate reactor), mixing is important as it impacts the availability of substrate and DO concentrations in all parts of the bioreactor (Arnaldos et al., 2015; Gresch et al., 2011b). The mixing in WWTP is achieved by propellers and adequate aeration. The propellers keep the biomass suspended and maintain a desired flow velocity in the bioreactors, while aeration is a source of oxygen and also induces mixing energy by creating turbulence in the system. Mixing becomes even more important where simultaneous nitrification and denitrification is desired in a single bioreactor because both aerobic and anoxic conditions are required (Samstag and Wicklein, 2014; Samstag et al., 2012).

In such systems strict DO control is needed to achieve the desired process conditions and as well as to minimize aeration costs. The major energy expenditure of a WWTP is its aeration (up to 65%) and pumping costs (Duchène et al., 2001; Maere et al., 2009; Rieger et al., 2006). Therefore, optimization of WWTP performance with reduced

aeration costs has been a major driving force for wastewater treatment modelling (Pittoors et al., 2014).

2.2. Wastewater treatment plant modelling

Process models have been used for decades to assess the performance of a wastewater treatment plant. The main goal of WWTP process modelling is usually to improve the performance with reduced operational costs. Inherently, modelling of a process which contains physical-chemical/bio reactors (such as a WWTP) has two modelling aspects. Firstly, the modelling of physical-chemical/biological reactions (biokinetics) and secondly, hydrodynamic modelling of a reactor. In a conceptual process design, the biokinetic modelling is usually performed to decide upon the processes and aims at predicting the biological conversions and corresponding conversion rates. However, in technical process design, hydrodynamic modelling is performed to look into the impact of reactor design on the process and aims at predicting the flow or mixing regime of a bioreactor. However, the hydrodynamics and kinetics have joint impact on the reaction yields.

Hydrodynamic models are needed to model the flow and diagnose the poor flow regions in a reactor. Two different types of modelling approaches have been used to determine the hydrodynamics of the reactors. A first modelling approach being the most common was developed by Levenspiel (Levenspiel, 1999) conventionally termed as “systemic modelling”. During the last decade a more advanced second modelling method known as computational fluid dynamics (CFD) has been used for modelling chemical reactors. However, the potential of CFD for bioreactors has not been fully utilized within wastewater treatment plant modelling (Karpinska and Bridgeman, 2016).

A structural summary of the above discussion can be seen in Figure 2.2. The description of activated sludge modelling, systemic modelling and computational fluid dynamics is provided in the subsequent sections 2.3, 2.4 & 2.5 respectively.

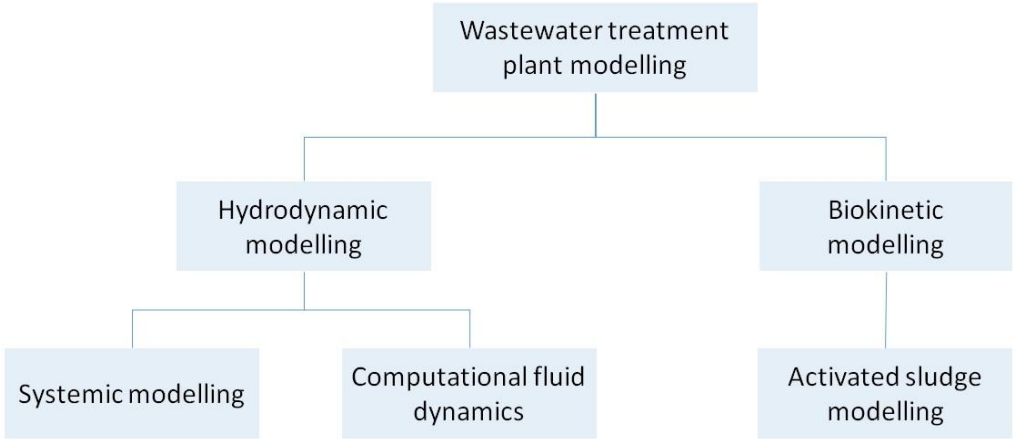

Figure 2.2 Overview of different modelling approaches used for WWTP modelling

2.3. Biokinetic modelling

Biokinetic modelling refers to the modelling of biological reactions involved in any bioreactor. In WWTP modelling, the activated sludge models (ASM) are widely employed as biokinetic models to predict different biological processes and their impact on the overall system performance.

2.3.1. Activated sludge modelling

The ASM concept has been developed by "The International Association on Water Pollution Research and Control" (IAWPRC), refurbished into "The International Association on Water Quality" (IAWQ) (Henze et al., 1987) and nowadays known as the “International Water Association” (IWA). The ASM concept has been extensively tested for describing biological processes. Numerous experiments for testing the ASM concepts’ applicability for activated sludge systems in process tanks with both alternating and recirculation operation have been performed. Gernaey et al. (2004) gives an extensive overview of the application of the ASM models to different wastewater treatment plant cases.

There are a lot of ASM models, however, ASM1, ASM2 and ASM3 form the basis for most of them. These models are based on deterministic descriptions of the biological turnover of organic matter and nutrients. These models are represented in a matrix form

(based on Petersen (1965)) commonly known as a Gujer matrix and constitutes stoichiometric and kinetic coefficients of state variables for different processes.

2.3.1.1. Activated sludge model No. 1

Among the ASM models, ASM1 is considered the reference model and has been used most widely (Roeleveld and van Loosdrecht, 2002). Due to its universal appeal and practical verification, it has been chosen as the biokinetic model in the COST Simulation Benchmark, a benchmark WWTP model developed to evaluate different activated sludge WWTP controlling strategies via simulations (Copp, 2000).

The ASM1 is developed primarily for municipal activated sludge WWTPs to describe the removal of organic carbon compounds and nitrogen, with simultaneous consumption of oxygen and nitrate as electron acceptors. It also aims at yielding a good description of the sludge production. In the model, the wide variety of organic carbon compounds and nitrogenous compounds are subdivided into a limited number of fractions (which form the state variables) based on biodegradability and solubility considerations. There are in total 13 state variables defined in ASM1 (Table 2.1). The model consists of eight processes which are fundamental to the activated sludge process. These are aerobic growth of heterotrophs, anoxic growth of heterotrophs, decay of heterotrophs, aerobic growth of autotrophs, decay of autotrophs, ammonification of soluble organic nitrogen and hydrolysis of entrapped particulate organic matter and organic nitrogen. The complete ASM1 matrix is provided in Appendix A 1. It can be observed that ASM1 consists of 5 stoichiometric parameters and 14 kinetic parameters (Table 2.2). The values of these parameters are the characteristics of wastewater and are needed to be measured or estimated to conduct a successful modelling. However, few of these parameters show little variation from wastewater to wastewater and thus can be considered constants (Henze et al., 1987). It is a common practice in WWTP modelling to calibrate these parameters to achieve the desired results.

Table 2.1 The ASM1 components (Henze et al., 1987)

Components	Description
S_I	Soluble inert organic matter
S_S	Readily biodegradable substrate
X_I	Particulate inert organic matter
X_S	Slowly biodegradable substrate
$X_{B,H}$	Active heterotrophic biomass
$X_{B,A}$	Active autotrophic biomass
X_P	Particulate products arising from biomass decay
S_O	Oxygen
S_{NO}	Nitrate and nitrite nitrogen
S_{NH}	NH^+_4+NH_3 nitrogen
S_{ND}	Soluble organic biodegradable nitrogen
X_{ND}	Particulate biodegradable organic nitrogen
S_{ALK}	Alkalinity

2.3.1.2. Activated sludge model No. 2 and No. 3

The other models (ASM2 & ASM3) are extensions of ASM1. The ASM2 forms a basis for modelling biological phosphorous (bio-P) removal by extending the ASM1. Chemical-P removal via precipitation is also included (Gujer et al., 1995). However, it is clearly mentioned that the model does not include all the observed phenomena for the description of the bio-P processes. In order to mediate the weaknesses, ASM2d extends ASM2 by including denitrifying activity of PAOs (phosphorous accumulating organisms) which allows a better description of phosphate and nitrates (Henze et al., 1999). ASM3 is similar to ASM1 with the objective of modelling organics and N-removal. However, it corrects a number of defects in ASM1 (Gujer et al., 1999). The major difference between the two is that ASM3 recognizes the importance of storage polymers in heterotrophic activated sludge conversions. The detailed description of these activated sludge models is provided in Henze et al. (2000) for the interested reader.

Table 2.2 Stoichiometric and kinetic parameters of ASM1 (Henze et al., 1987)

Symbol	Description
Stoichiometric parameters	
Y_A	Yield for autotrophic biomass
Y_H	Yield for heterotrophic biomass
f_P	Fraction of biomass leading to particulate products
i_{XB}	Mass of nitrogen per mass of COD in biomass
i_{XP}	Mass of nitrogen per mass of COD in products from biomass
Kinetic parameters	
b_A	Decay coefficient for autotropic biomass
$K_{O,H}$	Oxygen half-saturation coefficient for heterotrophic biomass
K_{NO}	Nitrate half-saturation coefficient for denitrifying heterotrophic biomass
$K_{O,A}$	Oxygen half-saturation coefficient for autotrophic biomass
Y_H	Yield for heterotrophic biomass
$\hat{\mu}_{\mathrm{A}}$	Maximum specific growth rate for autotrophic biomass
K_{NH}	Ammonia half-saturation coefficient for autotrophic biomass
b_H	Decay coefficient for heterotrophic biomass
η_g	Correction factor for $\mu_H$under anoxic conditions
η_h	Correction factor for hydrolysis under anoxic conditions
$\hat{\mu}_{\mathrm{H}}$	Maximum specific growth rate for heterotrophic biomass
K_S	Half-saturation coefficient for heterotrophic biomass
k_h	Maximum specific hydrolysis rate
K_X	Half-saturation coefficient for hydrolysis of slowly biodegradable substrate
k_a	Ammonification rate

2.3.1.3. Activated sludge models for nitrous oxide emissions

Greenhouse gas emissions from wastewater treatment plants (WWTP) are a matter of growing concern. The global warming potential of nitrous oxide (N_2O) is 298 times greater than carbon dioxide ((IPCC) Intergovernmental Panel on Climate Change, 2014). Therefore, research on N_2O emissions has become a point of attention in recent years.

N_2O in a wastewater treatment plant is produced during nitrogen removal processes and can be attributed to autotrophic AOB (ammonia oxidizing bacteria) (Chandran et al., 2011; Kampschreur et al., 2009; Tallec et al., 2006) and heterotrophic denitrifiers (Kampschreur et al., 2009; Lu and Chandran, 2010; Pan et al., 2013). N_2O might be potentially also produced through a chemical pathway (Harper et al., 2015; Schreiber et al., 2009) however, there are three microbial pathways (Wunderlin et al., 2013, 2012): heterotrophic denitrification (Lu and Chandran, 2010; Schulthess et al., 1994), AOB denitrification (Bock et al., 1995; Chandran et al., 2011; Kampschreur et al., 2007; Tallec et al., 2006) and from PAOs (phosphorous accumulating organisms) (Ahn et al., 2001).

Ni and Yuan (2015) presented a detailed review about current mathematical models available for N_2O emissions from wastewater treatment. The research on nitrous oxide production through different pathways has grown (Ni and Yuan, 2015) and subsequently activated sludge models have been updated by adding new processes and state variables along with respective kinetic parameters. Several modelling studies have been performed to quantify N_2O emissions taking different pathways into account (Flores-Alsina et al., 2011; Guo and Vanrolleghem, 2014; Hiatt and Grady, 2008; Mampaey et al., 2013). Common consensus is found on Hiatt and Grady's ASMN model (Hiatt and Grady, 2008) of four step heterotrophic denitrification which includes N_2O as an intermediate. Mampaey et al. (2013) on the other hand, also included N_2O and nitric oxide (NO) production due to AOB. The model combining heterotrophic denitrification and AOB denitrification is commonly known as ASMG1. Guo and Vanrolleghem (2014) modified the original ASMG1 by modifying the DO kinetic term. Research suggests that for N_2O production by AOB denitrification, a maximum rate occurs at relatively low DO conditions (Ni et al., 2013; Yu et al., 2010). This behaviour may be explained by the hypothesis that a low DO stimulates N_2O production, while high DO inhibits it, meaning that the influence of DO can be expressed by Haldane kinetics (Haldane, 1930). This kinetic approach is in accordance with and is a simplification of the model proposed by Ni et al.(2013). The overall effect of DO is described by the DO kinetic term (similar to a switching function) defined in equation 2.1.

$$DO_{Haldane} = \frac{S_O}{K_{SO,AOBden} + \left(1 - 2\sqrt{K_{O,AOBden}/K_{IO,AOBden}}\right)S_O + S_O^2/K_{IO,AOBden}} \qquad \textbf{2.1}$$

Here, $K_{SO,AOBden}$, $K_{O,AOBden}$ and $K_{IO,AOBden}$ are the kinetic parameters and S_O is the dissolved oxygen concentration.

The new model incorporating DO Haldane kinetics is now referred to as modified ASMG1 (Guo and Vanrolleghem, 2014). This model comprises of 18 state variables and 15 processes. In this model, autotrophic biomass is subdivided into AOB (ammonium oxidizing bacteria) and NOB (nitrate oxidizing bacteria). Nitrates are subdivided into nitrate (NO_3^-), nitrite (NO_2^-), nitric oxide (NO), nitrous oxide (N_2O) and dinitrogen (N_2). The additional processes and variables lead to a tremendous increase in stoichiometric and kinetic parameters totalling to 62. The detailed matrix for all the processes and default values for the kinetic parameters is provided by Guo and Vanrolleghem (2014). It must be noted that DO Haldane is used in the process rate terms of AOB denitrification of nitrite to nitric oxide and nitric oxide to nitrous oxide.

2.4. Systemic modelling

The systemic modelling approach has been extensively used for modelling the hydrodynamics of both chemical and biological reactors (Levenspiel, 1999; Nauman, 1987). It is a simplified approach in which the non-ideal flow behaviour of a reactor is approximated by the help of virtual structures/units. These units can be CSTRs (continous stirred tank reactors), plug flow reactors and/or dead volumes. The systemic modelling aimed at understanding the hydrodynamics only by knowing inlet and outlet of a reactor, thus mainly by tracing and RTD (residence time distribution) studies.

Systemic modelling can be further classified into axial dispersion and tanks-in-series (TIS) modelling. Axial dispersion models are limited to describe the longitudinal dispersion of a flow with small deviations from the plug flow. However, in systems with large recirculation flows (as is the case in industrial scale plants) the effectiveness of axial dispersion models is uncertain (Levenspiel, 1999). Therefore, the TIS models are commonly employed for modelling of WWTPs.

In the TIS approach, the flow behaviour of the whole reactor is modelled as a number of completely mixed continuous stirred tank reactors considering the flow in only one direction. This approach can account for some recirculation by maintaining the liquid

longer in the system by manipulating the recirculation rate (Figure 2.3). The number of tanks are usually determined with the help of tracer tests.

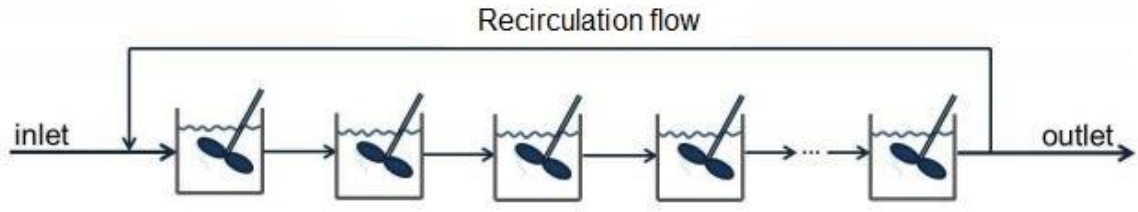

Figure 2.3 Tanks-in-series with back recirculation flow (Levenspiel, 1999)

However, in the TIS approach detailed spatial variations in substrate and electron acceptor concentrations in the bioreactors (stemming from design characteristics and operational conditions) are typically not taken into account, even though it is plausible that they have a significant impact on model predictions. Therefore, these models are unsuitable to evaluate the detailed impact of certain design parameters (such as tank geometry, number and type of propellers and aerator system design) on the performance of the biological process, as well as different operational strategies. Considering an optimal number of tanks to some extent can better predict the overall behaviour of a reactor by taking into account the longitudinal variation. However, all the tanks are considered completely mixed. In this way they average out local variations occurring in the other two dimensions and thus lead to inaccurate predictions.

2.4.1. Systemic modelling in WWTP modelling

The systemic approach along with ASM models has been used widely to model WWTPs. These modelling practices have not only been used to assess and optimize the performance of current WWTPs but also to design new treatment plants (Cheng and Ribarova, 1999; Hreiz et al., 2015; Maurer and Gujer, 1998; Zhou et al., 2015). Hreiz et al. (2015) provided a very detailed overview of previous activated sludge modelling efforts in various applications. However, a brief account of relevant WWTP modelling practices is provided below.

Pons et al. (1993) developed a tool for WWTP modelling based on activated sludge and tanks-in-series modelling. The underlying model was based on the assumption of complete mixing in the tanks and detailed hydrodynamics of the system were not taken into account. The article mentioned that the tool would need rigorous calibration of the parameters to get successful results. Garcia-Olivares and Becares (1995) performed

activated sludge modelling and calibrated the model for a two stage pilot scale WWTP. The authors provided a method to dynamically calibrate the model over time instead of using constant values. Xu and Hultman (1996) performed activated sludge modelling of a full scale WWTP and demonstrated the model calibration procedure using experimental data. Maurer and Gujer (1998) performed dynamic modelling for the description of enhanced biological phosphorus removal using ASM2. The model included two additional processes for the anoxic growth of phosphorus accumulating organisms (PAO) and anoxic storage of polyphosphate. The successful modelling included estimation of kinetic parameters using batch experimental data. Cheng and Ribarova (1999) used ASM1 to model a full scale WWTP for nitrogen removal. The authors found a very good correlation between model and measured data and the model was calibrated for the characterization of actual wastewater. Samuelsson (2007) used the COST simulation benchmark to decide upon the choice of optimal set-points and cost minimizing control strategies for the denitrification process in an activated sludge process. Ni and Yu (2008) extended the ASM3 by taking oxygen transfer, microbial maintenance, and biomass decay into account, in order to describe the heterotrophic storage and growth processes in activated sludge. The authors also performed model calibrations to match the measurements. Xie et al. (2011) modelled a full-scale carrousel oxidation ditch WWTP and optimized through integrating the ASM2d with advanced numerical algorithms. The ASM2d model after calibration and validation with the operating data was used to simulate the process. However, detailed hydrodynamics were not taken into account in this study. Li et al. (2013) performed modelling of a full scale oxidation ditch process for treating sewage with the ASM2d and optimized for minimal cost with acceptable performance in terms of ammonium and phosphorus removal.

The systemic approach has also been used to develop new control strategies for various purposes. Chachuat et al. (2005) and Fikar et al. (2005) developed an aeration control strategy to optimize effluent quality of a single basin wastewater treatment plant using TIS modelling approach. Ayesa et al. (2006) developed various control strategies to optimise the nitrogen removal in pre-denitrifying WWTPs using the TIS approach. Valverde-Peres et al. (2016) devised nitrogen to phosphorous ratio control for a novel enhanced biological phosphorus removal and recovery process.

In all these works it can be observed that detailed calibration of kinetic parameters was required to match the measurement data. The primary reason behind the need of calibration are the uncertainties in the determination of kinetic parameters. While the

biokinetic models have uncertainties regarding the kinetic parameters, the systemic modelling also has its limitation in terms of its inability to take spatial heterogeneities into account. All these aforementioned research lacked detailed hydrodynamic modelling (assumed completely mixed tanks using systemic approach) and performed calibrations based on the real wastewater treatment plant data where complete mixing is hard to realise and is subject to detailed hydrodynamic modelling. Therefore, by using the TIS approach, there is always a tendency of over calibration of kinetic parameters by correcting the errors which are induced by hydrodynamic limitations. Hence, there is a need for detailed hydrodynamic modelling to be included to correctly calibrate and partly avoid unnecessary and erroneous calibration efforts.

2.5. Computational fluid dynamics modelling

Computational fluid dynamics is a method which can model the flow in all three directions and can take into account the impact of geometrical structure on the hydrodynamics of the system. The CFD modelling discretises the domain into small volumes (grid/mesh) and Navier-Stokes equations along with continuity equations are solved at each grid point to simulate the flow field in 2D or 3D. The Navier-Stokes equations consist of momentum conservation equations in all directions, whereas, continuity equation is a mass conservation equation.

The general continuity equation for compressible and incompressible flow is given as

$$\frac{\partial \rho}{\partial t} + \nabla.(\rho \vec{v}) = S_m \qquad \textbf{2.2}$$

where ρ is the density, $\vec{v}$ is the velocity and S_m is the mass source. For incompressible flows the first term becomes zero and for a 3D incompressible steady state flow the continuity equation can be explicitly written as.

$$\rho\left(\frac{\partial u}{\partial x} + \frac{\partial v}{\partial y} + \frac{\partial w}{\partial z}\right) = S_m \qquad \textbf{2.3}$$

where *u, v* & *w* are the velocity components in *x, y* & *z* directions respectively.

A general momentum conservation equation can be written as.

$$\frac{\partial \rho \vec{v}}{\partial t} + \nabla.(\rho \vec{v}\vec{v}) = -\nabla P + \nabla.(\bar{\bar{\tau}}) + \rho \vec{g} + \vec{F} \quad \textbf{2.4}$$

where P is the static pressure, $\rho \vec{g}$ is the gravitational force, F represents the external forces and $\bar{\bar{\tau}}$ is the stress tensor.

For a steady state flow, the first term on the left side in equation 2.4 vanishes. Therefore, the momentum equations for a steady state 3D flow can be explicitly written as.

$$u\frac{\partial u}{\partial x} + v\frac{\partial u}{\partial y} + w\frac{\partial u}{\partial z} = -\frac{1}{\rho}\frac{\partial P}{\partial x} + \frac{\mu}{\rho}\frac{\partial^2 u}{\partial x \partial x} + g_x + F_x \quad \textbf{2.5}$$

$$u\frac{\partial v}{\partial x} + v\frac{\partial v}{\partial y} + w\frac{\partial v}{\partial z} = -\frac{1}{\rho}\frac{\partial P}{\partial y} + \frac{\mu}{\rho}\frac{\partial^2 v}{\partial y \partial y} + g_y + F_y \quad \textbf{2.6}$$

$$u\frac{\partial w}{\partial x} + v\frac{\partial w}{\partial y} + w\frac{\partial w}{\partial z} = -\frac{1}{\rho}\frac{\partial P}{\partial z} + \frac{\mu}{\rho}\frac{\partial^2 w}{\partial z \partial z} + g_z + F_z \quad \textbf{2.7}$$

Equations 2.2-2.7 are sufficient to model a simple laminar flow. However, the solution of extra equations is required if other phenomenon such as heat/mass transfer and/or species transfer needs to be modelled. Moreover, extra transport equations and models are needed for complex flows which include turbulent and multiphase flows. Plenty of literature is available for the underlying physics and the corresponding equations for these models (Andersson et al., 2011; Çengel and Cimbala, 2014; Versteeg and Malalasekera, 2007). The development of these models is considered standard (Ishii and Hibiki, 2011). In the remainder of this thesis, only if deemed necessary for better comprehension, models and selection criteria are described.

The CFD modelling process can be primarily divided into pre-processing, processing and post-processing steps and these are elaborated below

a. Pre-processing

i. Development of the 3D model (geometry) of the bioreactor
ii. Discretization of the geometry into a grid (meshing)
iii. Characterization of the boundary conditions

b. Processing

i. Selection of the suitable models
ii. Achieving the convergence (solution)

c. Post-processing

i. Comparison with the measurements (validation)
ii. Extraction of the eloquent results

The most important steps which include geometry development, meshing, boundary conditions and turbulence & multiphase modelling are described further in detail.

2.5.1. Geometry development

The pre-processing step basically concerns the setting up of the model for the CFD simulations. The first step during pre-processing is to determine the geometrical domain of the system under study. It comprises the determination of exact dimensions and structural layout of the system.

A CFD study can be either 2 or 3-dimensional (2D or 3D) based on the configuration of the system and the level of accuracy needed. In depth analysis of certain processes (such as turbulence, boundary layer separation, interphase interactions and/or interface determination) can be performed in 2D because a very fine mesh or a fine time step is sometimes needed to resolve all the length and time scales. Hence using a 3D geometry might lead to very high computational demands. For large scale studies, 2D can only be used when there is a geometrical symmetry in the system configuration and the fluid is not expected to flow in third dimension. It must be noted that majority of the fluid flow problems are 3D and 2D modelling will always be an approximation. 3D modelling is recommended for achieving more accurate and realistic modelling results (Andersson et al., 2011).

The geometry should be kept as simple as possible without neglecting the necessary details which can impact the hydrodynamics of the system. The necessary details can be the sizes, exact locations and shapes of the different structural components of the system such as inlets, outlets, and propellers etc.

2.5.2. Meshing

In the next step meshing is performed in which the geometry is discretized into small cell volumes (commonly called cells). The resulting discretized geometry is called a mesh or grid. In a mesh, each cell has a certain shape and size and can be characterized based on its shape into several types such as hexahedral, tetrahedral, pyramid and wedge (Figure 2.4). A mesh can contain different types of cells with different sizes and can be classified into structured, unstructured and hybrid/mixed mesh. A structured mesh contains similar types of cells whereas an unstructured mesh contains different types of cells throughout the domain. A hybrid or mixed mesh is a mesh which contains structured mesh in some parts and unstructured in other parts of the domain.

It is difficult to generalize the impact of different types of meshes on the stability and resulting numerical errors in the solution (Andersson et al., 2011). However, a structured mesh is recommended because it needs less memory storage compared to an unstructured mesh. If a complete structured mesh is not possible (which is the case for most 3D problems), a hybrid mesh with maximum possible structured mesh can be used.

Some advances have been made towards mesh free methods in the field of numerical analysis (Li and Ren, 2010). These methods use numerical algorithms to define interactions between each node instead of mesh elements. However, the method is highly computationally intensive and is mostly used for simpler problems.

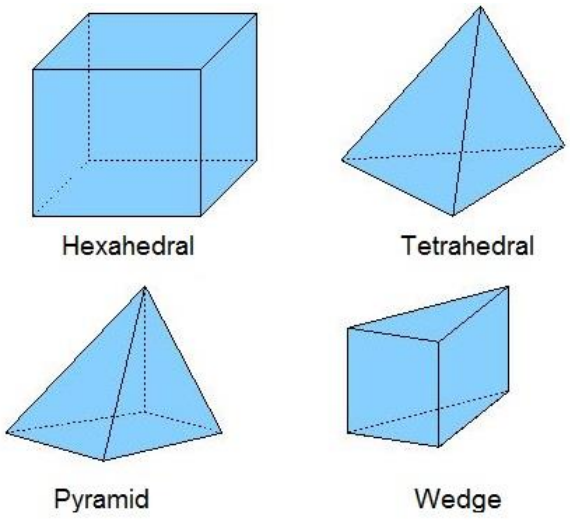

Figure 2.4 Different cell types for 3D mesh (Andersson et al., 2011)

The meshing plays a vital role in the quality of modelling results. Therefore, it is always good to have a mesh independent solution and the procedure to achieve this is commonly known as grid/mesh independence tests. Generally during a mesh independence test, a coarse mesh (with large sized cells) is created in the beginning and after a first set of simulations the mesh is further refined. The refinement is normally based on velocity and pressure gradients and as well as on gradients of any other parameter of interest. For example, in heat transfer studies, the temperature gradient can also be used for the mesh refinement. The mesh is refined until a solution is reached where the further refinement of the mesh does not significantly impact the solution.

2.5.3. Boundary conditions

Every CFD problem needs initial and boundary conditions to be defined. The most common boundary conditions are inlet, outlet, wall, constant pressure and symmetry boundary conditions. Inlet/outlet boundary conditions are specified when the inlet/outlet flow is known and it can be defined simply as a velocity magnitude or flow rate with the correct specification of direction (going into or out of the system). A wall boundary condition is used to specify the physical bounds of the system and it makes sure that no flux goes in or out of the boundary. The wall boundary condition sets the velocity zero at the wall. The constant pressure boundary condition is used when pressure is known but the exact flow conditions are unknown at the boundary. A symmetry boundary condition is used when symmetry is expected across a plane or along an axis. The symmetry boundary condition does not allow the flux across the boundary and acts as a mirror that reflects all the flow distributions on the other side. The symmetry boundary condition is also useful where flux across a boundary is not desired but velocity at the boundary is non-zero (for example the top open surface of a bubble column). In other words, the symmetry boundary condition acts just like a wall but with zero wall friction (ANSYS Inc., 2011). This approach is a safe approximation in such cases where the boundary interface is not of interest. Figure 2.5 illustrates different boundary conditions where $P_{in\ or\ out}$ & $V_{in\ or\ out}$ are pressure and velocity respectively at inlet and outlet.

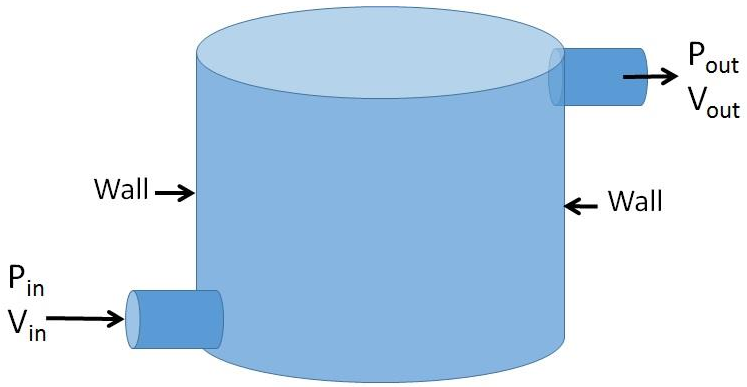

Figure 2.5 Summary of different possible boundary conditions used in CFD

2.5.4. Turbulence modelling

Turbulence is encountered in most flows in nature and in industrial applications. Natural turbulent flows can be found in oceans, in rivers and in the atmosphere, whereas industrial turbulent flows can be found in heat exchangers, chemical/biological reactors etc. Most flows encountered in industrial applications are turbulent, since turbulence significantly enhances heat and mass transfer rates (Borghi and Anselmet, 2013). In industry a variety of turbulent multiphase flows can be encountered. Turbulence plays an important role in this type of flows since it affects processes such as break-up and coalescence of bubbles and drops, thereby controlling the interfacial area between the phases. Thus, turbulence modelling becomes one of the key elements in CFD.

A truly turbulent flow involves a large number of different length scales, velocity scales and time scales. Accurate turbulence modelling would involve modelling of the smallest length and time scale. However, it is not always desired to model the smallest length scale and thus models are needed to make an approximation of turbulence. There are several turbulence models available and they can be categorized based on the accuracy and number of extra equations needed (Figure 2.6). A higher accuracy requires the solution of more equations as well as a higher resolution (i.e. a finer mesh) and thus leads to an increase in computational demand. Therefore, a trade-off is needed between computational costs and accuracy. For example, for direct numerical simulation (DNS) and for large eddy simulation (LES) the computational grid (mesh) and time step has to be very small to be able to take into account all the turbulent length and time scales. Therefore, it is practically impossible to use DNS for high turbulence problems which are encountered usually at industrial scale (Borghi and Anselmet, 2013). The DNS and

LES approaches are normally used to better understand the phenomenon at a small scale. However, Reynolds Averaged Navier-Stokes (RANS) based models are commonly used in industrial applications and provide a reasonable level of accuracy at a lower computational cost (Andersson et al., 2011). Among RANS models, the Reynolds stress model is the most intricate model which uses six extra equations to model the turbulence. However, it is still computationally expensive to be used for a full scale industrial problem which may also involve multiphase flow. The two equation RANS based models are the most commonly employed models for industrial applications. These models are validated for a wide range of applications and flow conditions. Among them, the k-ε model is the most widely used for highly turbulent conditions. However, it is unstable and gives erroneous predictions where adverse pressure and jet flow is expected (Mohammadi and Pironneau, 1993; Wilcox, 1998). Realizable k-ε and RNG k-ε model are modified k-ε models which can model such instances (jet flows & swirling flows) more realistically. Furthermore, the k-ω model is a very useful model where both high and low turbulent flow is expected. The one equation and zero equation models are oversimplified models and are normally no longer used for complex industrial flows.

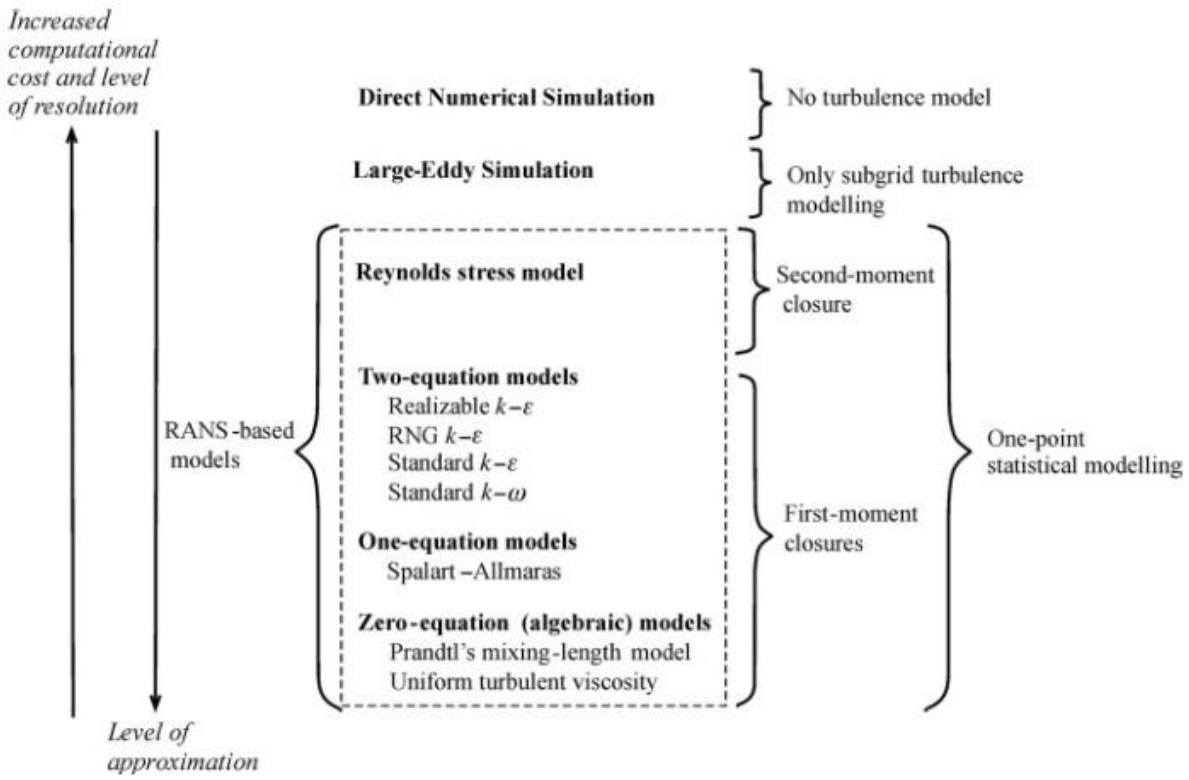

Figure 2.6 A schematic overview of turbulence models (Andersson et al., 2011)

2.5.4.1. Wall functions

The flow near the walls is affected by the walls and viscosity plays a vital role in such regions. The turbulence models are not valid in the viscosity affected near-wall regions. Therefore, wall-functions are employed to avoid wrong boundary values at the walls. The wall-functions are empirical rules based on the logarithmic law of the wall and apply boundary conditions some distance away from the wall such that the turbulence models are not solved close to the wall (Andersson et al., 2011). There are several wall-functions available in the Fluent solver, but the most common are the 'Standard wall-functions'. This wall-function is applicable for highly turbulent flows and for flows where boundary layer separations or high impinging flows are not expected (Figure 2.7). In the case where such flows are expected it is recommended to use advanced wall functions such as non-equilibrium wall functions. It is important to note that standard wall-functions reduce the computational requirements because they do not require a fine mesh near the wall. Moreover, these are considered to be more robust for highly turbulent flows.

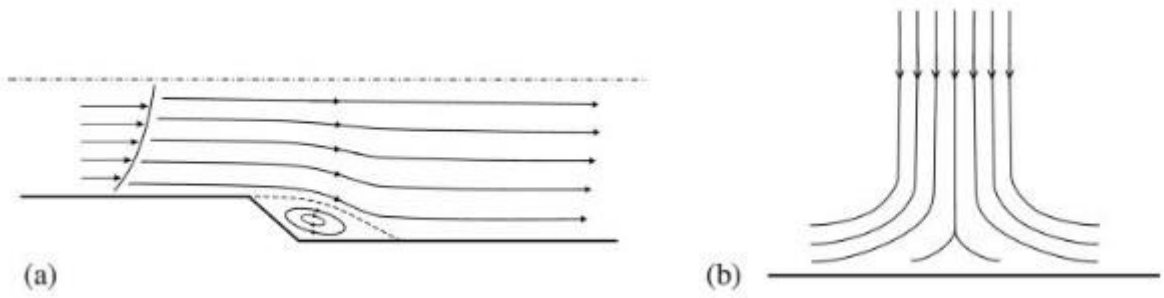

Figure 2.7 Flows with (a) boundary layer separations (b) and impinging flows

2.5.5. Multiphase modelling

The term 'phase' in multiphase refers to the solid, liquid or gas state of matter. Therefore, multiphase flows are flows which consist of more than one state of matter i.e. liquid-solid, liquid-gas, solid-gas or all three. Typical examples of multiphase flows are bubble columns, fluidized bed reactors, dryers and scrubbers.

There are several multiphase models available to choose from. The choice of the multiphase model depends on the types of the phases (liquid, solid & gas) involved and

the interaction between the different phases. The multiphase models can be primarily divided as follows (Andersson et al., 2011)

- Euler–Lagrange model
- Euler–Euler model
- Mixture or algebraic-slip model
- Volume-of-fluid (VOF) model
- Porous-bed models.

2.5.5.1. Euler–Lagrange modelling

In Euler–Lagrange modelling the fluid phase is modelled as a continuum by solving the Navier–Stokes equations, while for the dispersed phase (can be solid particles, vapours or bubbles) a large number of individual particles is modelled. The dispersed phase can exchange momentum, mass and energy with the fluid phase. Since the particle or droplet trajectories are computed for each particle or for a bundle of particles that are assumed to follow the same trajectory, the approach is limited to systems with a low volume fraction of dispersed phase as the computational load is significant.

2.5.5.2. Euler–Euler models

In Euler–Euler models the different phases are all treated as continuous phases, and momentum and continuity equations are solved for each phase. The Euler–Euler model can handle very complex flows, but does not always give the best results since empirical information is needed in order to close the momentum equations. Typical applications are risers and fluidized beds.

2.5.5.3. Mixture model

In the mixture model (algebraic-slip model) the flows of two or more phases are assumed to interact strongly and it is not necessary to solve the momentum balances for the different phases separately. In this model the viscosity is estimated for the mixture. The velocities of the different phases are thereafter calculated from buoyancy, drag and other forces, giving the relative velocities in comparison with the mean velocity of the mixture. Typical applications are bubble columns, fine particle suspensions and stirred-tank reactors.

2.5.5.4. Volume of fluid model

The volume-of-fluid (VOF) model is an Euler–Euler model whereby the interface between the different phases is tracked. The model is suitable for stratified flow, free surface flows and movement of large bubbles in liquids. Since the interface between the fluids must be resolved, it is not applicable for a system with many small drops or bubbles.

2.5.5.5. Porous bed model

In the porous-bed model, the pressure drop across a porous bed is modelled. In a bed containing many particles, it is not possible to resolve the geometry and solve the Navier–Stokes equations. Instead, the pressure drop is calculated from an equation similar to the Ergun equation for the pressure drop in fixed beds (Kolev, 2005).

2.5.6. Governing equations for mixture model

In the current study, the mixture model is used and thus the governing equations for this model are being provided here.

The mixture model solves the continuity equation for the mixture, the momentum equation for the mixture and the volume fraction equation for the secondary phases, as well as algebraic expressions for the relative velocities (as the phases are expected to move at different velocities). The governing equations are given below.

The continuity equation for the mixture '*m'* is

$$\frac{\partial}{\partial t}(\rho_m) + \nabla.\ (\rho_m\ \vec{v}_m) = 0 \qquad \textbf{2.8}$$

where ρ_m is the mixture density and $\vec{v}_m$ is mass averaged velocity for the mixture.

The mixture density ρ_m is calculated as,

$$\rho_m = \sum_{k=1}^{n} \alpha_k \rho_k \qquad \textbf{2.9}$$

where k is any phase, n is the total number of phases (in this case only 2), α_k is the volume fraction and ρ_k is the density of a phase k.

The mass averaged velocity $\vec{v}_m$ is calculated as,

$$\vec{v}_m = \sum_{k=1}^{n} \frac{\alpha_k \rho_k \vec{v}_k}{\rho_m} \qquad \textbf{2.10}$$

where $\vec{v}_k$ is the velocity of phase k.

The momentum equation for the mixture is given in equation 2.11 and is obtained by summing the individual momentum equations for each phase.

$$\begin{aligned} \frac{\partial}{\partial t}(\rho_m \vec{v}_m) + \nabla.(\rho_m \vec{v}_m \vec{v}_m) \\ = -\nabla P + \nabla.[\mu_m (\nabla \vec{v}_m + \nabla \vec{v}_m^T)] + \rho_m \vec{g} + \vec{F} \\ + \nabla.\left(\sum_{k=1}^{n} \alpha_k \rho_k \vec{v}_{dr,k} \vec{v}_{dr,k}\right) \end{aligned} \qquad \textbf{2.11}$$

where P is the static pressure, $\rho_m \vec{g}$ is the gravitational force, $\vec{F}$ is the external body force (such forces arise from interaction between the phases), μ_m is the mixture viscosity and $\vec{v}_{dr,k}$ is the drift velocity for the phase k.

The mixture viscosity μ_m is calculated as

$$\mu_m = \sum_{k=1}^{n} \alpha_k \mu_k \qquad \textbf{2.12}$$

where μ_k is the viscosity of the phase k.

The drift velocity $\vec{v}_{dr,k}$ of a phase k is defined as,

$$\vec{v}_{dr,k} = \vec{v}_k - \vec{v}_m \qquad \textbf{2.13}$$

The relative velocity also known as slip velocity ($\vec{v}_{qp}$) is defined as the velocity of a secondary phase (q) with respect to the primary phase (p).

$$\vec{v}_{qp} = \vec{v}_q - \vec{v}_p \quad \textbf{2.14}$$

The drift velocity and slip velocity can be correlated as shown in equation 2.15 (ANSYS Inc., 2011)

$$\vec{v}_{dr,k} = \vec{v}_{qp} - \sum_{k=1}^{n} \frac{\alpha_k \rho_k \vec{v}_{pk}}{\rho_m} \quad \textbf{2.15}$$

The slip velocity is then calculated based on the algebraic correlation given by equation 2.16 (Manninen et al., 1996)

$$\vec{v}_{qp} = \frac{d_q^2(\rho_q - \rho_m)\vec{a}}{18\mu_p f_{drag}} \quad \textbf{2.16}$$

where d_q is the diameter of secondary phase particles (i.e. bubble size in this case), $\vec{a}$ is the secondary phase particle acceleration and f_{drag} is the drag function. In this case, the simplest algebraic formulation of slip velocity (i.e. drift flux model) is used in which acceleration is due to gravity and/or a centrifugal force. The drag function is calculated based on the following correlation (Schiller and Naumann, 1935):

$$f_{drag} = \begin{cases} 1 + 0.15Re^{0.687} & Re \leq 1000 \\ 0.183Re & Re \geq 1000 \end{cases} \quad \textbf{2.17}$$

Finally, another equation is solved for the volume fraction of the secondary phase:

$$\frac{\partial}{\partial t}(\alpha_q \rho_q) + \nabla.(\alpha_q \rho_q \vec{v}_m) = -\nabla.(\alpha_q \rho_q \vec{v}_{dr,q}) + \sum_{p=1}^{n}(\dot{m}_{pq} - \dot{m}_{qp}) \quad \textbf{2.18}$$

where, $\dot{m}_{qp}$ & $\dot{m}_{pq}$ are the mass transfer between the phases.

2.5.7. Recent advances in CFD modelling of WWT

CFD models have been commonly used in various engineering fields such as automotive engineering, chemical engineering, mechanical engineering and aerospace engineering. Recently, the use of CFD modelling in wastewater treatment (WWT) has steadily grown. This growth is mainly due to increased importance of drivers (such as effluent quality, operational cost and greenhouse gas emissions) for optimization of municipal and industrial WWT unit processes. Previously CFD has been used for the modelling of primary and secondary settlers, stabilization ponds, membrane bioreactors and activated sludge bioreactors. The details of a few of the CFD studies regarding WWT are provided below.

Weiss et al. (2007) performed 3D CFD modelling of a secondary settler equipped with a suction-lift removal system. The model included the multiphase modelling of sludge rheology and successfully predicted the concentration profiles for two different plant loadings. Liu and Garcia (2011) performed 3D CFD modelling of a primary settler and successfully modelled the solids removal efficiencies based on the particle size distributions. The modelling resulted in establishing the design basis of a new primary settler with improved performance and reduced capital costs. Rostami et al. (2011) performed 2D CFD studies of a primary settler to evaluate the impact of inlet on the prevailing flow patterns. They concluded that the different inlet aperture configurations resulted in different flow patterns in the settling basin. Tarpagkou and Pantokratoras (2013) performed 3D CFD modelling of a primary sedimentation tank. The authors included the detailed modelling of the solid particles using a Lagrangian model (a discrete phase model) and evaluated the impact of continuous and discrete phases on one another and on the performance of the settler with varying particle sizes. Guyonvarch et al. (2015) used statistically designed CFD simulations as numerical experiments for the identification of a one-dimensional (1-D) advection-dispersion models in secondary settlers and resulted in prediction of solids distribution with high accuracy at a reasonable computational cost. Torfs (2015) performed 2D CFD modelling of a full scale secondary settler and integrated a flocculation model with the CFD model. The author showed that the qualitative analysis of the effect of aggregation and breakage on the distribution of the flocs can be made through coupling of a flocculation model with a CFD model.

Wood et al. (1995) performed 2D CFD studies of a stabilization pond. It was a very basic modelling effort which included laminar modelling of the flow in the pond. Later,

Wood et al. (1998) concluded that 2D modelling is not enough to predict the flows realistically in the pond. Alvarado et al. (2013) also performed CFD studies of a stabilization pond to evaluate different aerator configurations. The authors concluded that a configuration with 4 or 6 aerators can be enough to achieve a uniform mixing regime in the pond and thus it would minimize the sediment oxygen demand enhancing the oxygen level in the pond.

Wang et al. (2013) provided a detailed overview of the application of the CFD for modelling of membrane bioreactors (MBR). They also provided information about different available models which can be useful in modelling single or multiphase modelling of MBRs. Liu et al. (2015) performed the CFD modelling of an MBR incorporating an empirical rheology model and porous media model. The model was validated with velocity measurements. Shirazi et al. (2016) reviewed the application of CFD for membrane distillation processes. It concluded that CFD has mostly been used for studying the impact of different geometry configurations on the hydrodynamics.

Furthermore, CFD has been used for modelling mixing and aeration in activated sludge reactors. Fayolle et al. (2007) modelled oxygen mass transfer in aeration tanks using CFD. They presented a validated numerical model which successfully predicted mass transfer coefficient within +/- 5% of experimental results. However, the author did not include the biokinetic model and hence was unable to explain the impact of local oxygen concentrations on the process performance. Le Moullec (2010a) performed CFD modelling of a lab scale bioreactor and successfully modelled mixing limitations of the bioreactor. In another study (Le Moullec et al., 2011), it is shown that by considering mixing inefficiencies, CFD predictions were much better than the conventional TIS approach. However, both studies were limited to lab scale under controlled conditions. Gresch et al. (2011a, 2011b) performed tracer tests and CFD modelling of aeration system in a full scale wastewater treatment plant. It was observed that aeration has a major impact on mixing patterns and CFD is a useful tool to model the mixing variations. More recently (Karpinska and Bridgeman, 2016) presented a detailed review of CFD applications in activated sludge systems. This review discussed the rationale behind the use of CFD to model aeration, facilitating enhancement of treatment efficiency and reduction of energy input. However, the full potential of CFD has not been utilized in WWTP modelling but its capability to improve biokinetics model predictions has been preliminarily shown in some of these previous studies (Gresch et al., 2011b, 2009; Le Moullec et al., 2010a).

An International Water Association (IWA) working group has been formed to investigate a variety of issues and challenges related to CFD modelling in water and WWT (Nopens, 2013). Nopens et al., (2012) stressed upon the need for good modelling practices for CFD modelling in WWT for the practitioners and researchers. As a result Wicklein et al., (2016) summarized the recommendations for good modelling practices of the IWA working group on CFD. It provided a detailed principle overview of the modelling practices which should be adopted to conduct the CFD studies and hence improve the quality of research. A complete overview of a CFD modelling practice is provided in Figure 2.8. It provides a structural layout which should be followed to conduct a successful CFD study.

2.6. General conclusions

Most of the current modelling approaches in WWTP assume complete mixing and thus ignore spatial heterogeneities arising due to different operational conditions or the geometrical structure of the reactors. However, it is very unlikely to have a completely mixed full scale reactor (Gresch et al., 2011a, 2011b). Therefore, the resulting models might have inherent errors and thus always need calibration. The calibration is performed by changing half saturation indices (K-values) in ASM models to match the measurement data and might correct errors induced due to certain mixing conditions. As a consequence, with changes in process conditions, new mixing conditions might develop and recalibration is needed to correct for the new errors. Hence, these models do not possess a good predictive power. Therefore, instead of calibrating and recalibrating, detailed process models need to be developed which can better account for inherent mixing inefficiencies.

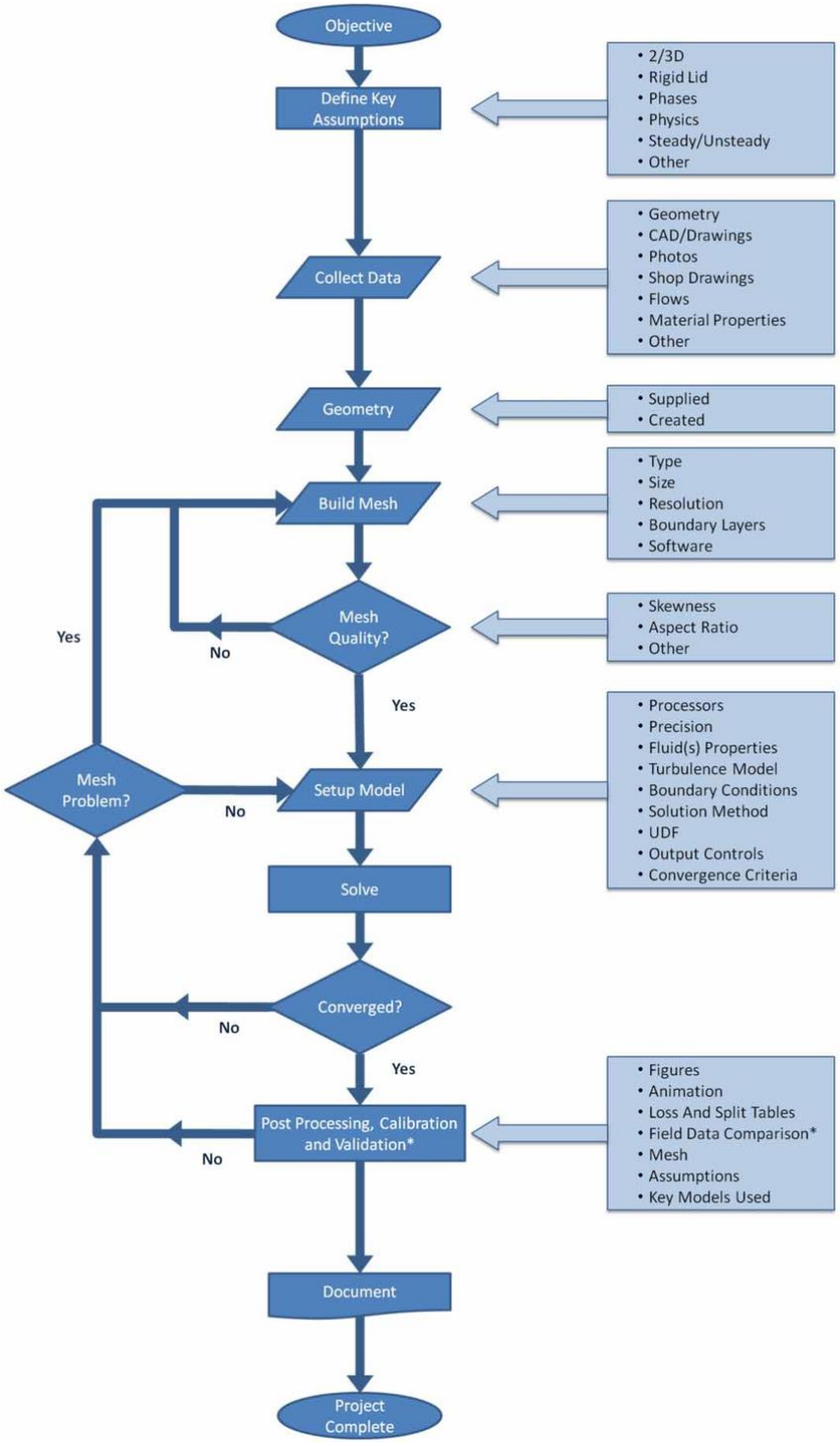

Figure 2.8 Complete flow of a CFD modelling practice (Wicklein et al., 2016)

PART I

Detailed hydrodynamic modelling

Chapter 3

CFD hydrodynamic modelling of a full-scale WWTP

This chapter includes the detailed CFD hydrodynamic modelling of a full-scale WWTP.

3.1. Introduction

The current process models for WWTPs use a tanks-in-series (TIS) modelling approach and, hence, are based on the assumption of complete mixing within each tank and thus ignore the spatial heterogeneities. These process models at best can model the flow in one direction and ignore the flows in other directions. However, complete mixing is hard to achieve in large bioreactors, thus current models are unable to model the mixing inefficiencies. The computational fluid dynamics modelling is a method which models the flow in all three dimensions and thus can model the mixing in a better way. Previously, CFD studies have been performed to show that the CFD is a useful tool to model the hydrodynamics accurately in WWT systems (Alvarado et al., 2013; Fayolle et al., 2007; Gresch et al., 2011a; Le Moullec et al., 2010a). Therefore, detailed CFD modelling is used to model the hydrodynamics of a full-scale WWTP in this chapter.

The main objective of this chapter is to demonstrate that a full-scale bioreactor is not homogeneous due to its complex configuration and multiphase system. The current TIS-based models exhibit quite some deviation from reality and hence a more detailed hydrodynamic modelling is needed. In order to achieve the objective put forward, detailed CFD modelling including turbulence and multiphase (gas and liquid) modelling of a full scale wastewater treatment plant is performed. The model includes ample detail of the aeration system full-scale and is validated with experimental measurements. The impact of reactor configuration and the multiphase interactions on the prevailing flow patterns and gas holdup distributions is presented. Finally, the

impact of different operational conditions such as liquid and air flow rate on the reactor's hydrodynamics is evaluated and analysed.

3.2. Materials & methods

3.2.1. Eindhoven WWTP configuration

The full-scale plant modelled in this study is the Eindhoven WWTP in The Netherlands. This plant treats the wastewater of 750,000 population equivalents (PE) with a design load of 136 g COD day^{-1} PE^{-1}. The incoming wastewater is treated in three parallel lines, each containing a primary settler, a biological tank and four secondary settlers. The plant is a modified UCT (University Cape Town) configuration (biological COD, N and P removal) (Figure 3.1). It is a carrousel type reactor in which the circular inner ring (an anaerobic tank) is intended to perform like a plug flow reactor, consisting of four compartments in series, with no aeration and minimal recycled nitrate (the purpose of recycle is to bring back activated sludge). The middle ring is anoxic from where the mixed liquor enters the outer ring, which is a facultative aerobic/anoxic carrousel ring. It contains membrane plate aerators installed at the bottom in certain locations. Two zones of aerators can be distinguished: the "summer package", which is always active and its airflow is controlled by a NH_4-DO cascade controller accounting for the load, and the "winter package", which can be switched on during winter time or rain events for additional nitrification capacity. Finally, three recycles are active: one to recycle sludge from the anoxic middle to the anaerobic inner ring, a second one to recycle nitrate from the outer ring to the anoxic middle ring, and a third one recycling settled secondary sludge to the anoxic tank (Amerlinck, 2015).

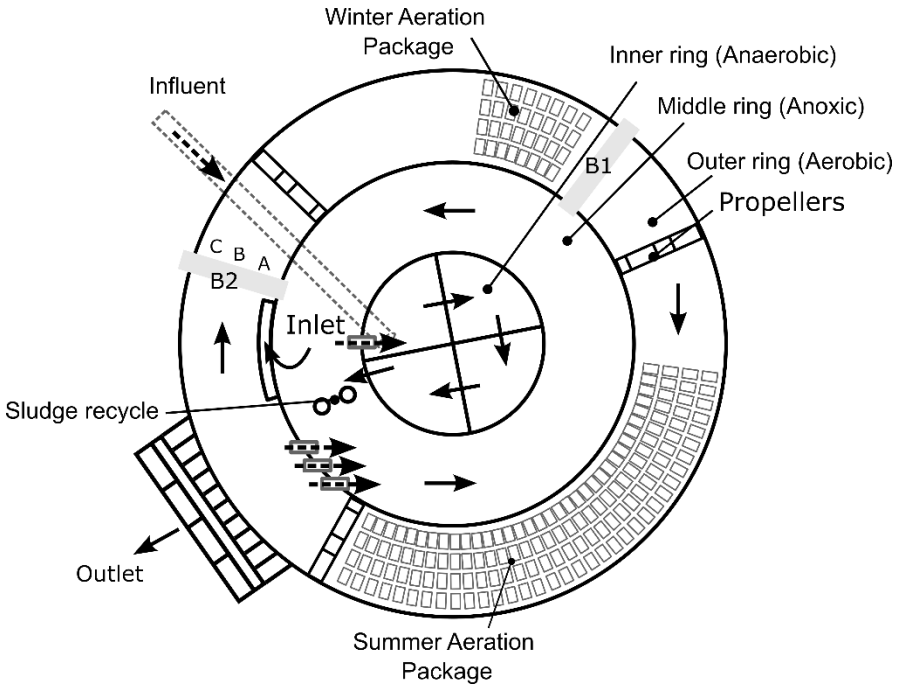

Figure 3.1 Configuration of the bioreactor at the Eindhoven WWTP

In this study, the outer ring of one of the three biological reactors (ATII) of the Eindhoven WWTP has been modelled. The outer ring of the bioreactor consists of one inlet (flow coming from the middle ring) and four outlets (1 outflow and 3 recycle pumps). There are three pairs of propellers installed along the length of the bioreactor to keep the flow in one direction and provide extra energy for better mixing. The two aeration packages (summer & winter package) installed at the bottom of the bioreactor comprise of total 196 plate diffusers (168 in summer and 28 in winter package). These plate diffusers are spread uniformly along the width and length of the reactor (Figure 3.1). An inside view of the reactor is shown in Figure 3.2.

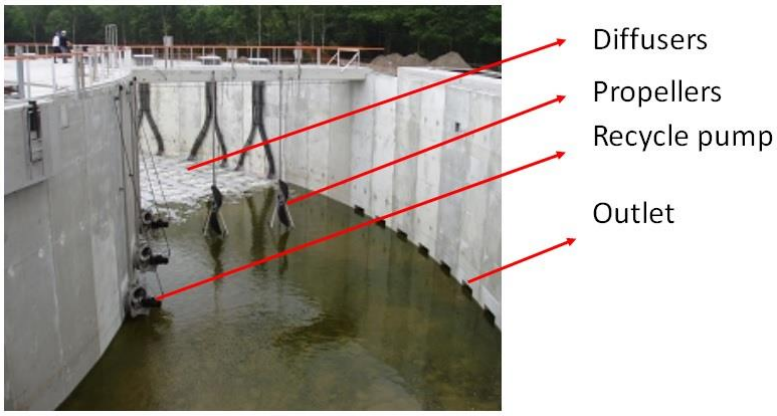

Figure 3.2 Inside view of the reactor at the Eindhoven WWTP

3.2.2. Experimental Setup

In order to validate hydrodynamics, velocity measurements with the help of a non-invasive Acoustic Doppler Current Profiler (ADCP) Workhorse Rio Grande (Teledyne RD instruments - Figure 3.3a) were performed.

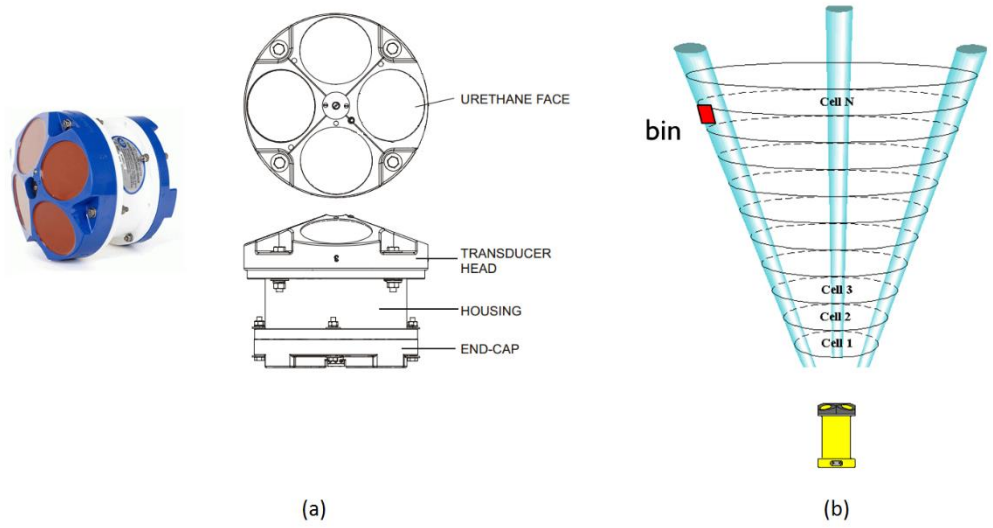

Figure 3.3 (a) The Acoustic Doppler Current Profiler (ADCP) and (b) its working principle (Torfs, 2015)

The working principle of the ADCP is based on the Doppler effect (Ballot, 1845). The device has four transducers which transmit sound signals at a constant frequency into the water. These sound waves travel through the water column and partially scatter back by particles suspended in the moving water. The ADCP records these echoes at precise time intervals corresponding to fixed depths in the water column which can be determined based on the traveling time of the signals. The water column is thus divided in successive vertical elements (called bins) along the axis of the beams (Figure 3.3b). The ADCP measures the change in wavelength between the emitted signal and the received signal coming from successive bins (Doppler frequency shift). This allows the determination of the particle velocity over a range of depths (Cobb, 1993; Kinnear and Deines, 2001; Mullison et al., 2011). The software package WinRiver II R (Teledyne RD Instruments) is used for data collection and processing. Measurements in this work were performed with the Rio Grande High Resolution Mode (Mode 12) which is

characterised by an acoustic frequency of 1200 kHz, a sampling interval of 1 s, a velocity resolution of 1 mm/s and which allows measurements down to 25 m depth.

The four transducers are positioned around a horizontal circle every 90 degrees and directed outwards at a certain angle to the vertical. This configuration allows to estimate the 3-dimensional velocity components: a tangential, radial and vertical component (Mullison et al., 2011). However, only three beams are required to determine these three velocity components. The fourth beam allows to calculate two separate vertical velocities and hence the difference can be considered as an estimate of the measurement error in order to check the homogeneity of the flow field (Kinnear and Deines, 2001; Mullison et al., 2011). The larger the beam angle with the vertical, the more sensitive the ADCP becomes to horizontal velocity measurements. However, simultaneously the capacity of the ADCP to measure particle velocities at larger depth decreases. This can be explained by the occurrence of side lobes when an acoustic signal is transmitted by the transducers. If these side lobes reach the bottom or any other internal structures (baffles or the scraper mechanism) before the main signal the transducers will first receive the reflected side lobe signals (typically stronger than the signals reflected from particles). This may blur the particle return signals and hamper the measurements (Cobb, 1993). Consequently, the ADCP is not able to measure velocities near the wall or other internal structures (for example close to the walls of the reactor) nor can it record velocity measurements at the bottom region of the tank due to acoustic reflection of the bottom wall. In addition, the ADCP cannot conduct measurements within 0.5 m of its head due to the time needed to convert the equipment head from transmitter to receiver (the blanking period).

The measurements in the current study were performed at two bridges (B1 & B2) (Figure 3.1). Measurements at the third bridge were too disturbed by aeration and thus could not be implemented. At each bridge, time-averaged radial, vertical and tangential velocity components at different depths were measured at three radial locations (A, B & C). These locations were chosen, based on the fact that the ADCP needs to be away from the possible hindrances such as walls and propellers. At each location for every measurement, 15 minutes of data was collected and each measurement was repeated three times to reduce the variations induced by the dynamic inflow.

3.2.3. Computational fluid dynamics modelling

The CFD modelling discretises the domain into small volumes (grid/mesh) and the Navier-Stokes equations are solved at each grid point to simulate the flow field. It is a stepwise method and is divided into pre-processing, processing and post-processing steps. The CFD methodology is explained in detail in section 2.4 in chapter 2. Therefore, following the methodology, the first step is to develop a 3D geometrical model of the reactor. Next step is the meshing followed by defining appropriate boundary conditions. Turbulence and multiphase models along with suitable numerical algorithms are then chosen before running the simulations. Suitable convergence criteria are needed to achieve the solution. Finally, the post-processing which includes evaluation of the modelling results is performed.

3.2.3.1. Geometry Development

Based on full-scale dimensions, the 3-dimensional (3D) model of the bioreactor is developed with the help of a commercial tool (AutoCAD Siemens NX 9.0 ("NX: Siemens PLM Software," 2016)) (Figure 3.4a). All the necessary details that may impact the hydrodynamics are included such as exact locations and sizes of propellers, inlets, outlets and recycle pumps. These are important details because potentially they can have a significant impact on the hydrodynamics of the reactor.

The minor details such as pores in the aerator plates are not modelled. However, one of the most significant improvements to the model was the detailed modelling of the aerators. Aerators are designed by calculating the total flow area of air on the basis of pore sizes (provided by the manufacturers). It was foreseen that a mixture model (CFD model for modelling dense bubbly flows) would be used, where individual bubbles are not modelled and tracked, but rather the fluid domain is simulated as a mixture of both phases. Therefore, instead of designing individual pores, an aerator equal to the area of pores is modelled, keeping the geometrical symmetry with the real diffusers (Figure 3.4b). This makes sure that the superficial velocity of the gas phase remains realistic.

The propellers are also simplified and individual propeller blades are not modelled as modelling of their motion was not intended (due to high computational requirements for modelling of moving parts). Instead, propellers are modelled as thin cylindrical vessels equal to the size of real propellers and are modelled as merely a momentum source. Furthermore, it is a good modelling practice to model the flow boundaries (inlets

& outlets) away from their actual locations to achieve a developed flow and avoid backflow due to boundary layer separations at these boundaries (Versteeg and Malalasekera, 2007). Therefore, inlet, outlet and recycle pumps are extended in this case.

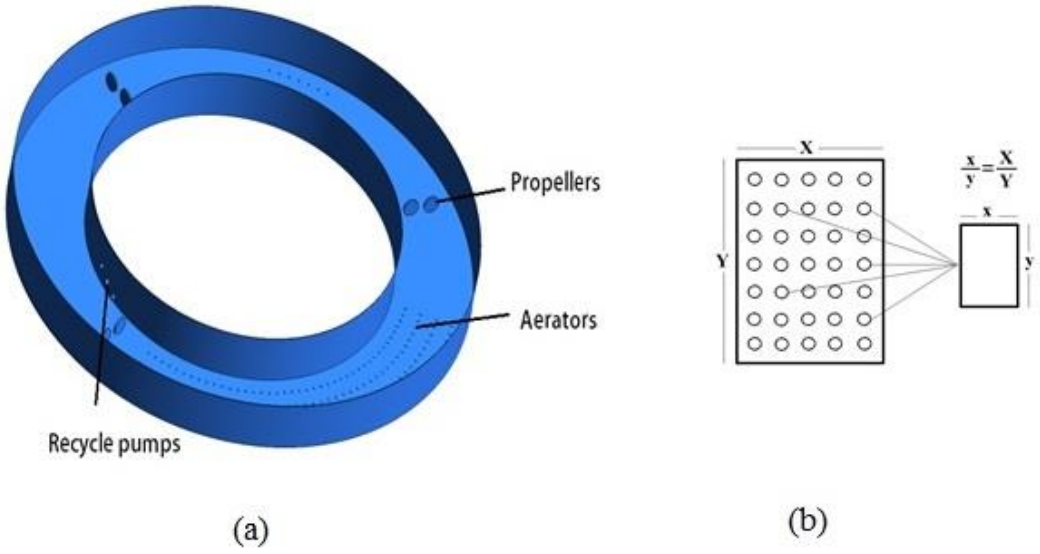

Figure 3.4 (a) The 3D model (geometry) of the bioreactor and (b) the plate diffuser simplification

3.2.3.2. Meshing

In the next step, meshing using a commercial mesh/grid generator tool (ICEM CFD, ANSYS) is performed. Different meshes (coarse, fine & very fine) are generated to check for grid independence. The coarse mesh comprises of 0.7 million cells, the fine mesh 1.5 million cells and the finest mesh 2.5 million cells. The fine and very fine mesh provide the best match with the experimental values (velocity measurements) but the fine mesh is used for all the simulations due to its lower computational needs. It must be noted that the very fine mesh did not change the results compared to the fine mesh. The mesh includes different sizes and shapes of cells but is kept structured as much as possible. 90% of the cells are hexahedral cells which will eventually lead to less numerical instabilities (Andersson et al., 2011) (Figure 3.5). The mesh is kept very fine in regions near the diffusers (i.e. smaller than the size of diffusers) and coarser in regions where small velocity gradients are expected (i.e. regions of bulk flow). These refinements are made during the grid independence check. The different views of the

resulting mesh (fine mesh with 1.5 million cells mesh) are shown in Figure 3.6 and Figure 3.7.

The bioreactor is divided into several zones to apply different conditions in different zones. Mainly, the reactor's top is separated from the main reactor to implement a degassing boundary condition and is termed as degassing zone. The reactor's height is 6.7m and an additional layer of 0.2m height is added on top of it (this layer is visible in Figure 3.6a). The height of 0.2 is chosen so that the mesh inside this region is neither too coarse nor too fine with an average size equal to the rest of the reactor's mesh. Moreover, the propellers are also modelled as separate zones to apply the momentum source to mimic the real propellers.

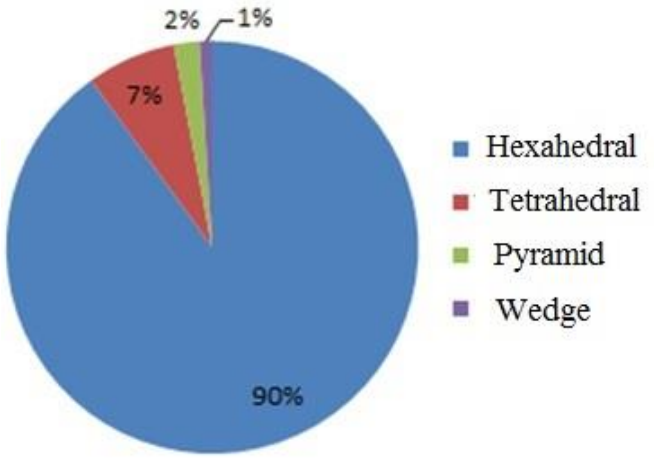

Figure 3.5 The distribution of the fine mesh cell types

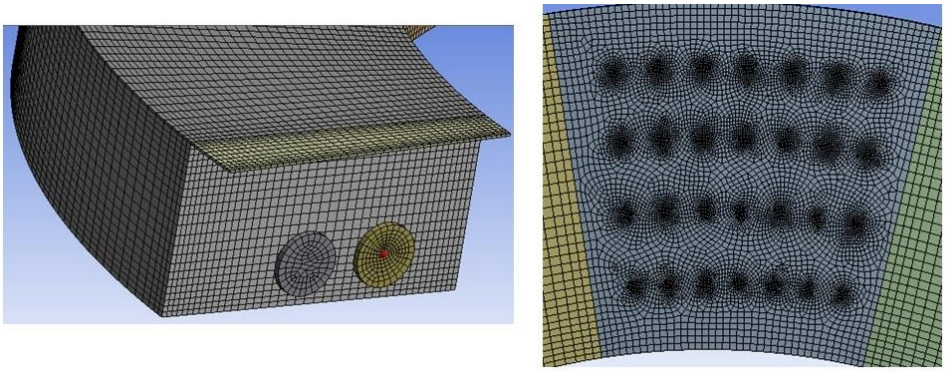

Figure 3.6 (a) An inside view and (b) bottom view of the fine mesh

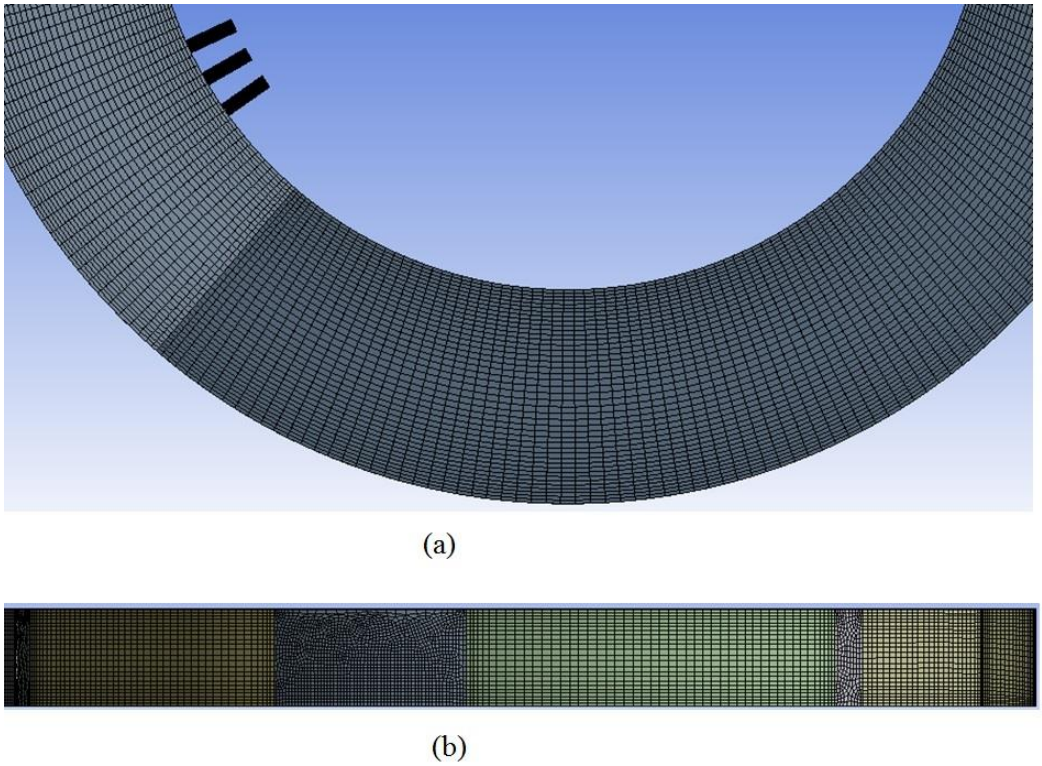

Figure 3.7 (a) A top and (b) side view of the fine mesh

3.2.3.3. Boundary conditions

In the next step, the boundaries of the system are characterized. It includes naming of the boundaries, choosing a suitable type for the boundaries and determination of the boundary condition values at these boundaries.

First, there are two types of inlet boundaries, one for the liquid inflow and another for the gas inflow (diffusers). The inlet for liquid is simply named as ***'Inlet'***, whereas, inlet for gas is further characterized as ***'Summer'*** **and** ***'Winter'*** to distinguish between the two aeration packages. All the diffusers in each package are grouped as one boundary condition (i.e. uniform flow through each diffuser is assumed). Next, there are four outlets of the reactor, one for the main liquid outflow and three for the recycle pumps. The liquid outflow is simply named as ***'Outlet'*** and the rest of the three are named as ***'P1, P2 & P3'*** for the recycle pumps. It must be noted that all the recycle pumps are separately characterized so that if needed different flowrates can be evaluated and the contents being recycled can be examined separately. The top of the reactor is a free surface (not covered) and is just named as ***'Top'***. The rest of the boundaries are physical

bounds of the reactor and are thus named as ***'Walls'***. Hence, there are 9 boundaries of the reactor in total which need to be either defined or calculated.

Boundary conditions are set based on the given knowledge of the system. As the flow coming into bioreactor, aeration rate and recycle ratios are known, these boundaries can be calculated. The 'velocity inlet' boundary condition is used for inlet, summer and winter boundaries. The recycle pumps P1, P2 & P3 are also set with 'velocity inlet' but with direction vector pointing out of the system (negative velocity inlet). It is done to mimic the recycle pumps because pumps have a certain capacity and flow through them which do not depend on the flow in reactor. The outlet is set with the boundary condition of 'outflow' and is calculated with the help of CFD mass and momentum conservation equations. It must be noted that outlet does not have a pump, therefore flow entirely depends upon the hydrostatic pressure and inertial forces in the reactor. The top boundary is slightly more delicate because it is a free surface that allows the gas to leave the top surface but liquid remains within the reactor. A straightforward approach would be to set separate boundary conditions for both the phases i.e. outlet boundary condition for the gas phase and wall for the liquid phase. However, it was foreseen to use a mixture model for multiphase modelling and it does not allow separate boundary conditions for each phase. The other way around which is commonly used and is also suggested by the commercial tool users is to set up a symmetry boundary condition for free surfaces (Witt et al., 2012). It is a similar to wall boundary condition but with zero wall friction. Therefore, the 'symmetry' boundary condition is used for the top. The 'wall' boundary condition is used for the walls with no slip condition. It means no flux goes in or out through walls and velocity is zero at the wall.

In the next step, boundary conditions are calculated based on the plant data. The flow coming into the bioreactor is dynamic. However, only steady state simulations are performed at varying flow conditions to capture the impact of dynamics of the system. The flow into the outer ring is calculated based on the average daily inflow and the respective recycle ratios. Similarly, the aeration rate is averaged as well. The average lower bound of the liquid flowrate into the outer ring is 1867 m^3/h (L) and average higher bound is approximately double, i.e. 3734 m^3/h (2L). Similarly, the average lower bound of aeration rate is 2000 Nm^3/h (G) and the higher bound is approximately triple, i.e. 6000 Nm^3/h (3G). The winter package is kept turned off because it is turned on only when summer package reaches its full capacity which is not the case under these conditions. The outlet flowrate will be calculated from the CFD solution. The

corresponding boundary conditions for the base case defined for CFD modelling are given in Table 3.1.

Table 3.1 The boundary conditions for the base case CFD modelling

No.	Boundary condition	Type	Value/Description
1	Inlet	Velocity inlet	1867 m^3/h
2	Summer package	Velocity inlet	2000 Nm^3/h
3	Winter package	Velocity inlet	0
4	P1, P2, P3	Negative velocity inlet	332 m^3/h
5	Outlet	Outflow	To be calculated from the CFD
6	Walls	Wall	No slip condition
7	Top	Symmetry	

In the degassing zone (top layer of the reactor) a user defined function (UDF) is implemented which acts as a sink term for the secondary phase (air). It acts such that the secondary phase disappears whenever it enters this zone. This is applied to mimic the air bubbles leaving the top surface of the water.

The propeller zones are provided with a momentum source to mimic the propeller behaviour. The momentum source is the thrust provided by the mechanical motion of the propeller in the direction of flow and can be correlated to the power of the propeller as in equation 3.1 (Huang and Li, 2013; Jiang et al., 2010; Yang et al., 2010).

$$P = 2\pi N_r \int F_\theta \, dV \qquad \textbf{3.1}$$

where P is the power of the impeller, N_r is the rotational speed, F_θ is the tangential momentum source and V is the volume is each cell in the propeller zone. Power of a propeller can be calculated from the power number correlation as in equation 3.2

$$P = N_p \rho N_r^3 D^5 \qquad \textbf{3.2}$$

where N_p is the power number, ρ is the fluid density and D is the diameter of the impeller. It must be noted that this is an approximated method and does not model the exact motion of the propellers. However, it provides an educated guess about the propellers thrust transmitted to the fluid.

3.2.3.4. Selection of suitable models

The flow inside the reactor under study is turbulent due to the high flow rates and aeration. Therefore, a suitable turbulence model is needed to capture all the important features of the fluid flow. Moreover, due to aeration, it is also important to model both phases (i.e. liquid & gas), thus a multiphase model is needed to accurately capture the gas dispersion in the system. All the CFD simulations are performed in Fluent (v14.5) (ANSYS). It is one of the most commonly used CFD solver and is chosen for its ease of use. In this solver, several validated turbulence and multiphase models are available to choose from (ANSYS Inc., 2011).

3.2.3.4.1 Turbulence modelling

For the initial simulations, the k-ε turbulence model was tested, however, the k-ε model is unstable and gives erroneous predictions where adverse pressure and jet flow is expected. The reactor under study has diffusers installed at the bottom and injection of air into the liquid can result into jet flow, therefore, the k-ε model is not an appropriate choice for turbulence modelling in this case. The realizable k-ε model, which is a modified k-ε model, is able to model such instances (jet flows & swirling flows) more realistically and is therefore applied in this study to model turbulence.

The flow near the walls is affected by the walls and viscosity plays a vital role in such regions. The turbulence models are not valid in the viscosity affected near-wall regions. Therefore, standard wall functions are employed for the bioreactor under study to model the near wall regions. These wall-functions are applicable for highly turbulent flows (not limited to) and for flows where boundary layer separations or high impinging flows are not expected. In the current bioreactor, there is no possibility of have impinging flows but boundary layer separation can be expected at the inlet or outlets of the liquid flow. However, these boundary layer separations are not expected to be huge or having an impact on the overall flow behaviour of the reactor, therefore, standard wall-functions can safely be employed. It is important to note that standard wall-functions reduce the computational requirements because they do not require a fine mesh near the

wall. The Fluent solver also adjusts the standard wall-functions according to the mesh, therefore, these are considered to be more robust.

3.2.3.4.2 Multiphase Modelling

There are several multiphase models available in the Fluent solver to choose from. The choice of the multiphase model depends on the types of the phases (liquid, solid & gas) involved and the interaction between the different phases. In the current study, primarily all three phases are present in the bioreactor i.e. wastewater being the liquid phase, biomass and particulates being the solid phase and air bubbles (due to aeration) being the gas phase. Although solids are important to model the rheology of the system the added computational demand for modelling all three phases is overwhelming. Therefore, only liquid and gas phases are modelled for the current study to be able to model the impact of aeration on the flow patterns. The solid particles will have even less impact on the rheology in the aerated regions. Later, after the integration with biokinetics model the impact of solids is taken into account by calculating the sludge density as a function of total suspended solids (TSS) concentration (see Chapter 4). The sludge density cannot be modelled as a function of TSS unless the biokinetic models are integrated.

Hence, the current case is a bubbly flow system, where liquid is considered as the primary (continuous) phase and air as the secondary (dispersed) phase. The mixture model is the most suitable and recommended model for such systems where individual dispersed phase particles (bubbles) tracking is not needed (Andersson et al., 2011). This model provides a good level of accuracy with lower computational requirements. It solves one momentum equation for the mixture and estimates the viscosity of the mixture. This model also calculates the relative velocities of the different phases using buoyancy, drag and other external forces. Therefore, in this study, the mixture model is employed and it will provide the gas dispersion in terms of volume fraction of the secondary phase (gas hold-up). The details of the model equations can be found in Chapter 2.

3.2.3.5. Additional model considerations and convergence

There are two flow solvers available in ANSYS Fluent, i.e. a density based solver and a pressure based solver. The density based solver is traditionally used for compressible high speed flows whereas the pressure based solver is employed for incompressible low

speed flows. In the current study the continuous phase is an incompressible liquid flow, therefore the pressure based solver is used.

The CFD solver stores values at the cell centres of the grid and, hence, an algorithm is required to interpolate these values to the cell faces to calculate the convective flux through each cell face. There are various numerical algorithms/schemes available in Fluent for such spatial discretization. These schemes are commonly called upwind schemes, as they interpolate the face values from the downstream cell centre. It is good modelling practice to use the higher order schemes to solve the momentum and turbulence equations (Andersson et al., 2011). Therefore, in this study, a second order upwind scheme is used which will eventually boost the convergence speed and reduce the numerical errors.

After deciding the models and numerical algorithms, next step is to set a criterion for convergence. As solving the partial differential equations requires an iterative method, the solution needs to be initialized with initial values (guessed from the boundary conditions). During each iteration each cell computes a new value for each variable (for example the x-coordinate of velocity i.e. v_x). After each iteration the difference between the old and the new value is computed and is commonly called a residual. Next, as a convergence criterion an acceptable residual value is set, such that when the calculated residual is less than the set residual value, the iteration stops. If the convergence criterion is not met, a new value is assumed and the iterative procedure is repeated until the residuals fall below the set values. The residual criterion for all variables is set separately according to their magnitudes. The residual values for the different variables in the current study are given in Table 3.2. Another way of checking the convergence and making sure that the solution is correct is to check the mass imbalance of the solution. It computes the difference between the flux coming in and leaving a cell. Ideally it should be zero.

Table 3.2 The residual values for the convergence criteria

Variable	Residuals
Continuity	10^{-5}
x-coordinate of velocity	10^{-5}
y-coordinate of velocity	10^{-5}
z-coordinate of velocity	10^{-5}
Volume fraction (secondary phase)	10^{-4}
Turbulent kinetic energy	10^{-5}
Turbulent dissipation energy	10^{-5}

3.3. Results & discussion

3.3.1. Comparison between measurements and CFD simulations

The absolute velocity magnitudes derived from the ADCP-measured tangential and axial fluid velocity components along with the corresponding CFD predictions at the B1 & B2 location are shown in Figure 3.8. At bridge B1, the CFD velocity profiles at locations B & C are close to the measured values. However, at location A the CFD values are over-predicted. At bridge B2, velocity profiles at locations B & C are over-predicted and at location A the CFD values are close to the measured values.

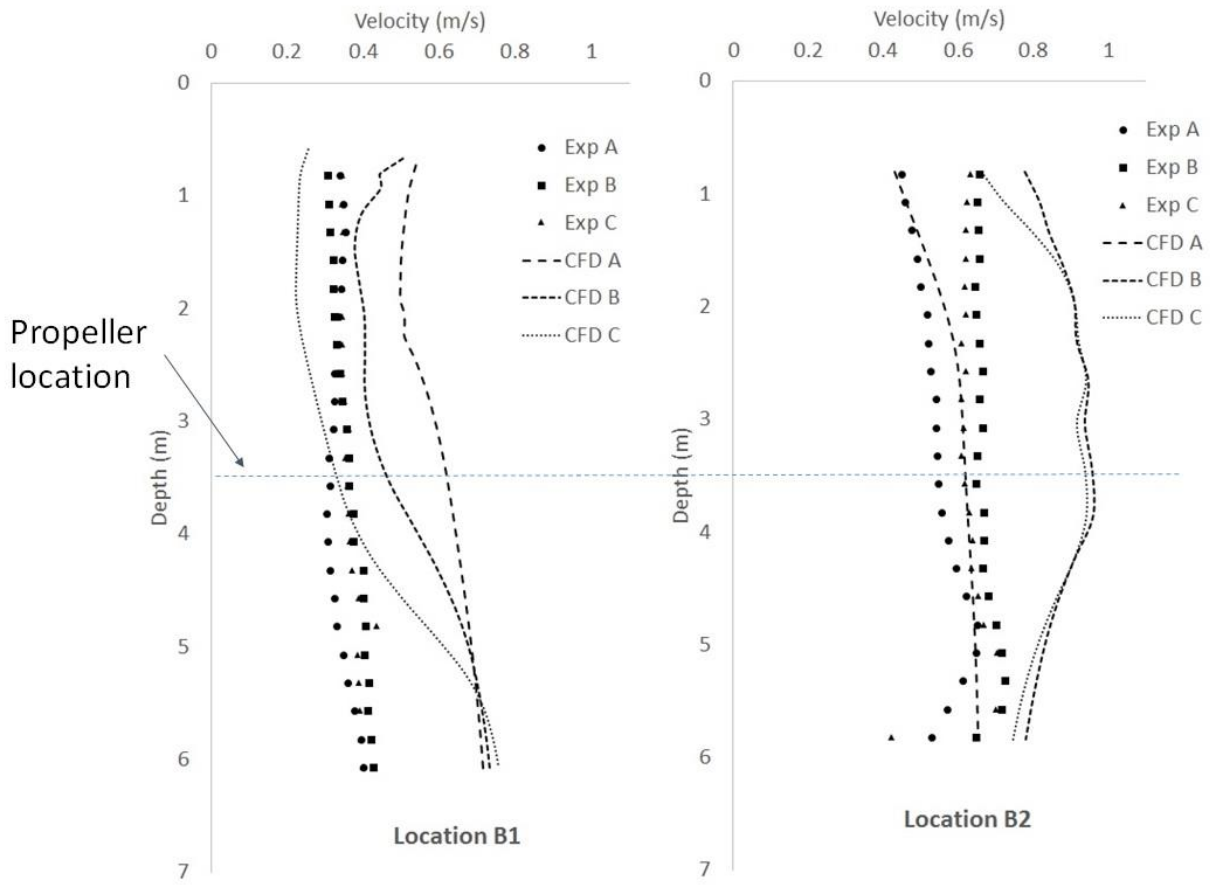

Figure 3.8 Comparison between the CFD and measured velocities at locations B1 & B2 (A: Near the inner wall, B: In the middle and C: Near the outer wall) (Average measurement error is ±0.0315 m/s)

The underlying causes for these over-predictions could be several. It is particularly important to note that the velocity data were collected under dynamic hydraulic conditions, whereas the model was run at steady-state conditions using the average inflow rate. Moreover, an approximation (momentum source method) was made for the propellers, whereas in reality these propellers cause swirling flows which is not taken into account. The standard water density was used for modelling liquid flow instead of sludge density. It can be expected that by using the sludge density the velocity profiles will come closer to the measured values (the sludge density is eventually used later in chapter 4). Whether these are the only causes for model-experiment divergence would require further investigation. Preliminary investigation showed that the over-prediction was reduced by 10-15% when using the bulk density function instead of the standard

water density indicating the importance of using the correct density (results of using a bulk density function are provided in Chapter 4).

3.3.2. Base case results

In Figure 3.9, liquid velocities and air volume fractions (gas hold up) are shown for horizontal cross sections of the reactor (3.45 m of depth), respectively. In these Figures, flow variations and non-ideal mixing in the reactor can be observed even in areas close to the propellers (indicated in Figure 3.9a) and the aeration system (summer aeration package). In Figure 3.9a the impact of propellers on the flow is evident and the regions of lower velocities near the outer wall in the aerated region can be observed. The impact of aeration on the flow patterns is also evident as the aeration causes more fluctuations and turbulence. Figure 3.9b shows the non-uniform distribution of gas holdup (volume fraction of the gas phase) in the aerated region as well as in the rest of the reactor. It can be seen that the gas holdup decreases, expectedly, moving downstream from the aerated region. In the aerated region, the gas holdup is higher near the inner wall and lower near the outer wall. This could be due to the fact that the aeration plume is pushed towards the inner wall due to the bulk flow. This can be further investigated by looking at the gas hold up distribution at different depths in the reactor (Figure 3.10). Here, it can be observed that the distribution changes moving from top to bottom. As the gas moves towards the top of the reactor it distributes more evenly compared to the bottom region. It can also be stated that the aeration plume expands towards the top. These results show that the air from each diffuser does not rise perpendicularly instead it is pushed towards the wall which hints at the possible recirculating flow pattern. These findings are important because these patterns will eventually impact the mass transfer between the phases and will be decisive from a mixing point of view.

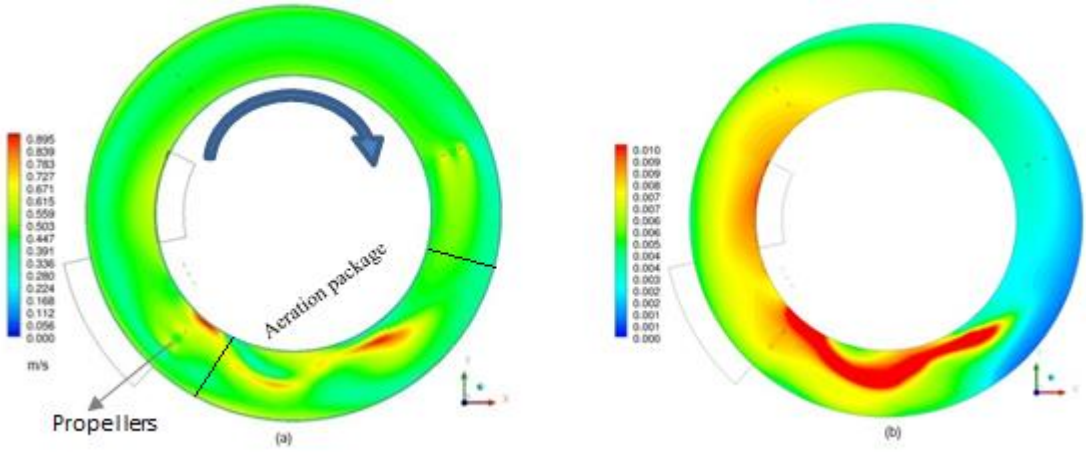

Figure 3.9 (a) Velocity contour plot (blue arrow shows the direction of flow) and (b) gas hold up (volume fraction of the gas phase) contour plot at 3.45m depth in the reactor

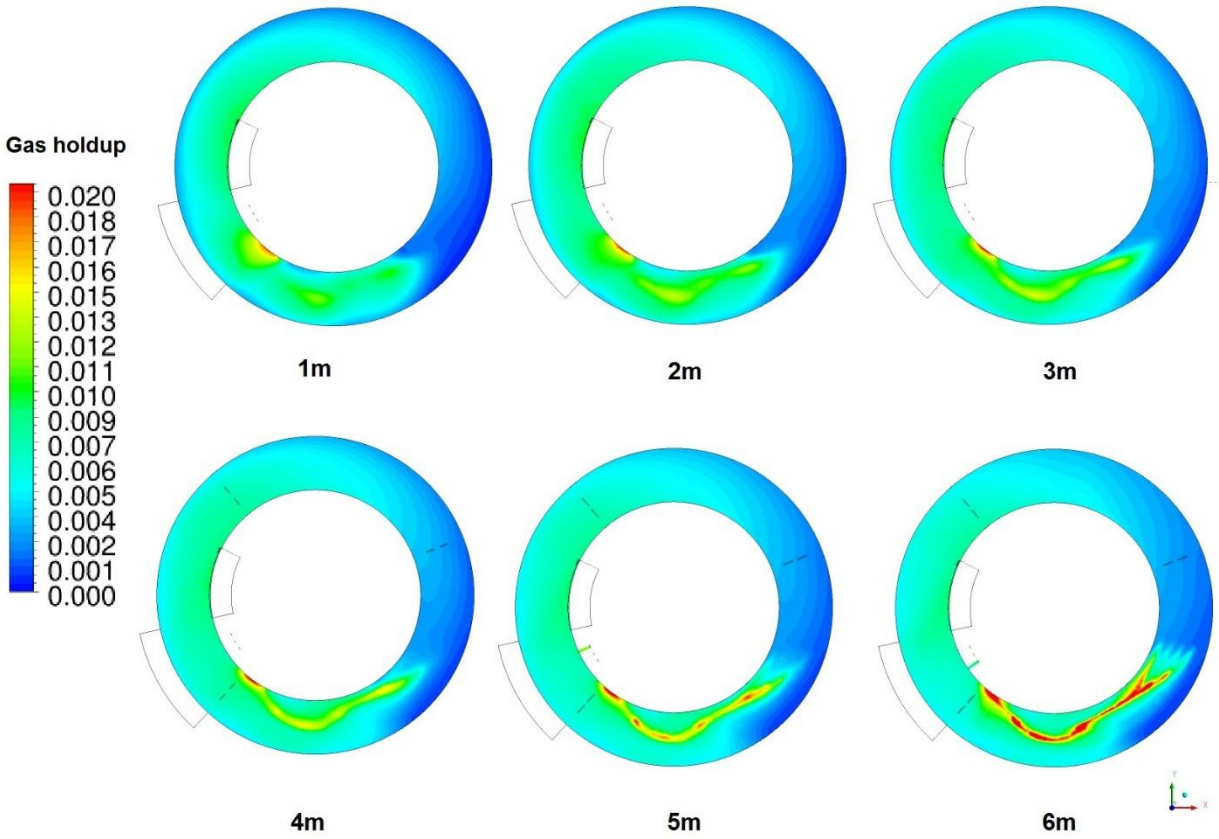

Figure 3.10 Contour plots of gas hold up at horizontal cross-sections at different depths in the reactor (1m is near the top and 6m is near the bottom)

In order to further investigate the flow patterns in the reactor, velocity streamlines are plotted in Figure 3.11. It shows that the flow is not streamlined, instead it is a swirling flow throughout the reactor. The swirling flow originates mainly due to the aeration and the reactor's circular design. It is similar to the flow through a pipe elbow where the flow becomes swirling due to the pipe's bend. It is useful information for understanding the mixing in the reactor.

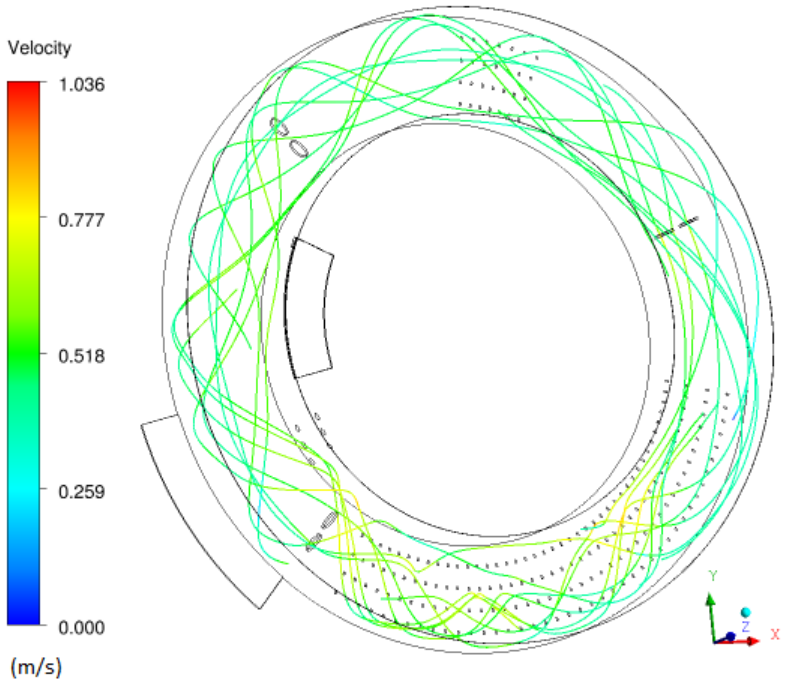

Figure 3.11 Illustration of the velocity streamlines in the reactor

In order to further investigate the flow patterns, the velocity vectors are plotted in a vertical cross-section of the reactor at different locations. The locations for these plots are shown in Figure 3.12 and Figure 3.13 shows the vector plots at these locations. It should be noted that in each vertical cross-section plot left side is the inner wall and right side is the outer wall denoted by 'i' & 'o' respectively. In the aerated region velocity vectors are plotted at three different locations i.e. at the beginning, middle and end. Furthermore, locations are plotted for each of the inlets, the outlet and the non-aerated regions. It can be observed that throughout the reactor a recirculating/swirling

flow prevails which is also visible in Figure 3.11 (swirling flow). In the beginning of the aerated region a major recirculating flow can be seen but the magnitude of arrows suggests that the intensity of the recirculation is small. However, in the middle of the aerated region the magnitude of recirculation increases and two recirculation zones with unequal sizes are developed. At the end of the aerated region these two recirculation zones become almost equal in size. At the outlet region (moving downstream from the aerated region), these recirculation zones merge into one big recirculation zone again. This recirculation zone then prevails in the inlet and non-aerated regions.

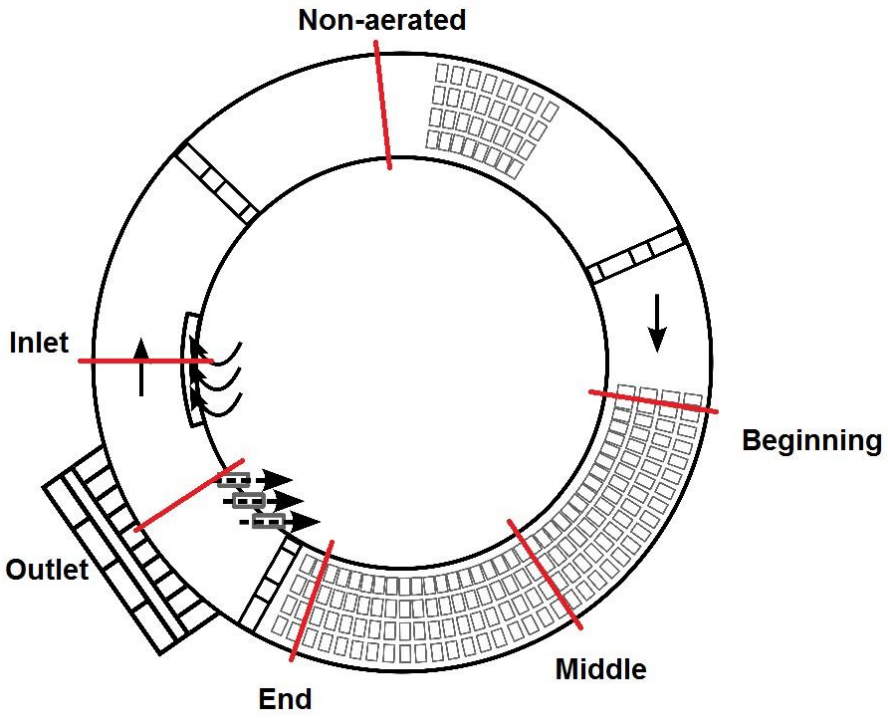

Figure 3.12 Plot locations for the vertical cross-sections in the reactor

The vertical plots in Figure 3.13 can be used to explain the gas holdup distributions along the depth in Figure 3.10, which shows that the gas holdup is squeezed (concentrated red region) at depths of 6m and 5m. This is because of the formation of the plume at the bottom which can be observed in the vertical plot of the middle section of the aerated region in Figure 3.13. However, this plume expands towards the top and this explains the wide distribution of the gas holdup in Figure 3.10 at 1m and 2m. The flow is recirculating (rising towards the top & falling back towards the bottom) but the gas phase leaves the top surface and does not completely recirculate back to the bottom.

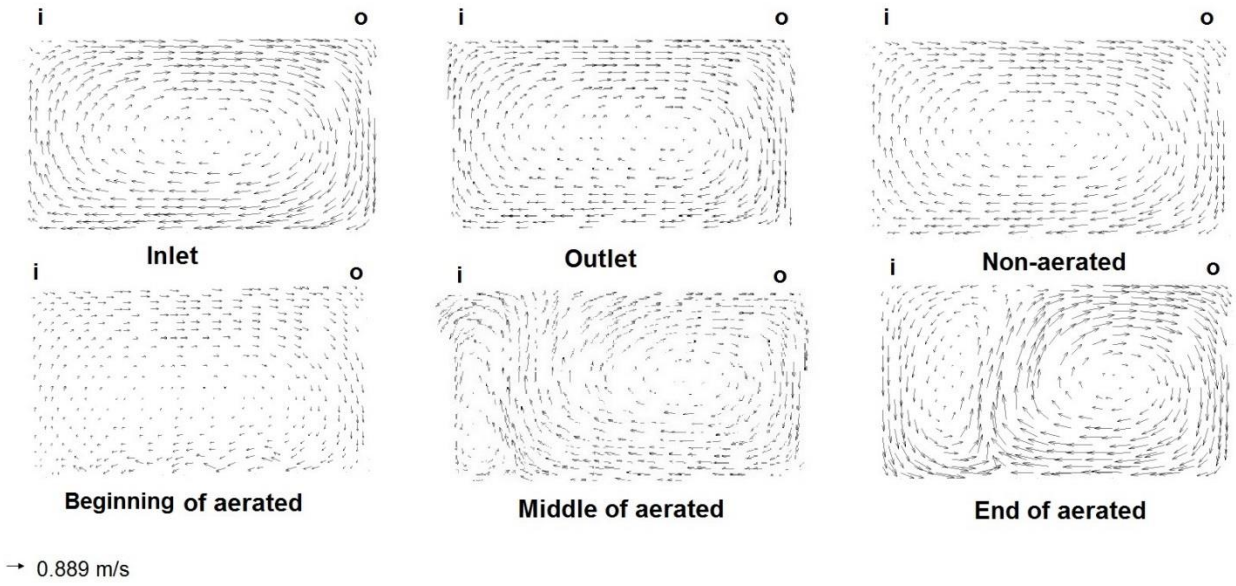

Figure 3.13 Velocity vector plots in the vertical cross-section at different locations in the reactor (plot locations shown in the Figure 3.12)

The impact of the recirculation zones on the vertical distribution of gas holdup is shown in Figure 3.14. The vertical plot for the beginning of the aeration zone shows that the gas plume does not completely reach the top. This is because the bulk flow is pushing the gas plume in the direction of the bulk flow. For better understanding, these graphs can be looked at in combination with Figure 3.10, where the plot at 6m depth shows gas hold up near the bottom. Here in the beginning of the aerated region, the gas holdup pattern suggests that it is pushed in the direction of the bulk flow. This explains the resulting gas holdup in the Figure 3.14 for the beginning of the aeration region. Therefore, it is always important to bear in mind that these graphs are a result of 3 dimensional (3D) modelling and should not be conceived only as a result of 1D gas dispersion when interpreting them. Similarly, the remainder of the gas holdup plots are also the result of 3D gas dispersion and show that bulk flow combined with aeration has a major impact on the prevailing mixing patterns.

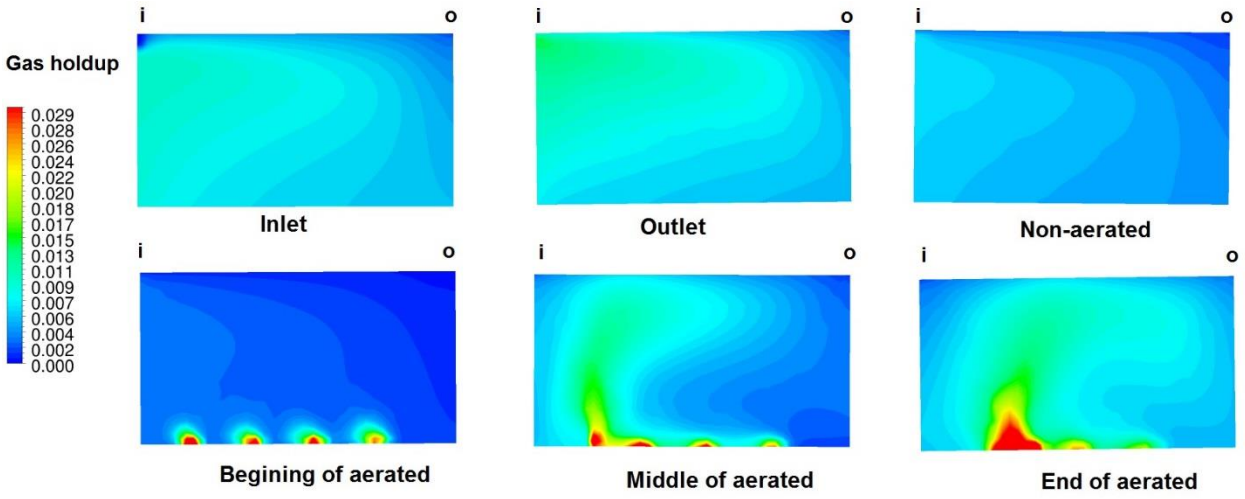

Figure 3.14 Gas holdup in the vertical cross-section at different locations in the reactor (plot locations shown in Figure 3.12)

3.3.2.1. Scenario analysis

Dynamic conditions are encountered in a WWTP and, therefore, it should be evaluated how different combinations of aeration and liquid flow rates impact the mixing patterns shown in the previous section. Therefore, 8 more different scenarios have been modelled combining different liquid and air flowrates (Figure 3.15). The flowrates for these scenarios are provided in Table 3.3.

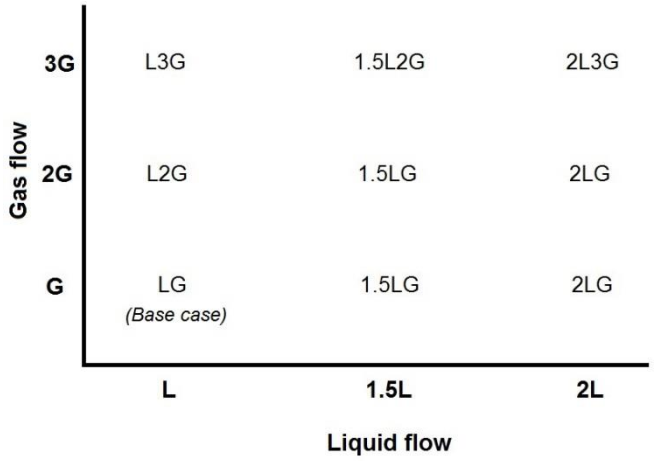

Figure 3.15 Scenario analysis layout

Table 3.3 Flow rates for different scenarios

Scenario	Liquid Flow (m^3/h)	Gas flow (Nm^3/h)
LG (*Base case*)	1867	2000
1.5LG	2800	2000
2LG	3734	2000
L2G	1867	4000
1.5L2G	2800	4000
2L2G	3734	4000
L3G	1867	6000
1.5L3G	2800	6000
2L3G	3734	6000

3.3.2.2. Impact of the different scenarios on the flow patterns

All scenarios are simulated and investigated and serve as the basis to choose relevant scenarios to be investigated in combination with the biokinetic model (see chapter 4). Figure 3.16 shows the velocity vector plots in the middle of aerated region for all the scenarios (see Figure 3.12 for the plot location). It can be seen that the change in either aeration or bulk flowrate leads to significant different flow patterns. For the base case (LG) two unequal sized recirculation zones were observed, i.e. one minor and one major recirculation zone. When the aeration rate is increased from G to 2G (keeping the liquid flow unchanged), the size of the minor recirculation zone reduces. Further increase in aeration rate leads to the vanishing of the minor zone (L3G). However, at a higher liquid flow rate, change in aeration rate does not bring about the same results. It can be seen that moving from 1.5LG to 1.5L2G reduces the recirculation zone but further increase in aeration to 1.5L3G makes the recirculation zone even more pronounced. Similarly, case 2LG exhibits two recirculation zones (one minor & one major). Increase in aeration to 2L2G enlarges the recirculation but further increase to 2L3G leads to the vanishing

of the recirculation zone. Similarly, these plots can be analysed by keeping the gas flow rate constant e.g. moving from LG to 1.5LG and then to 2LG. Firstly, it shows the enlargement of the minor recirculation zone (1.5LG) and then further increase in liquid flow rate causes the significant reduction of the minor zone. Therefore, it is hard to predict the outcome solely based on the flowrates, as different combinations of flowrates result in distinct mixing patterns with no clear logic.

Another way of looking at these graphs is to look only at LG, 1.5L2G and 2L3G cases. These cases show a simultaneous increase in both liquid and aeration rate which is normally expected at a WWTP i.e. a higher inflow triggers a control action increasing the aeration flow rate. It can be seen that moving from LG to 1.5L2G, the minor recirculation zone reduces in size. Further increase to 2L3G almost completely leads to the vanishing of the minor recirculation zone, leaving just one major recirculation zone. This shows an important trend in mixing patterns when both liquid and gas flowrates are increased simultaneously. Moreover, it brings our attention towards the fact that the mixing patterns change with the change in flow conditions and hence can impact the process performance.

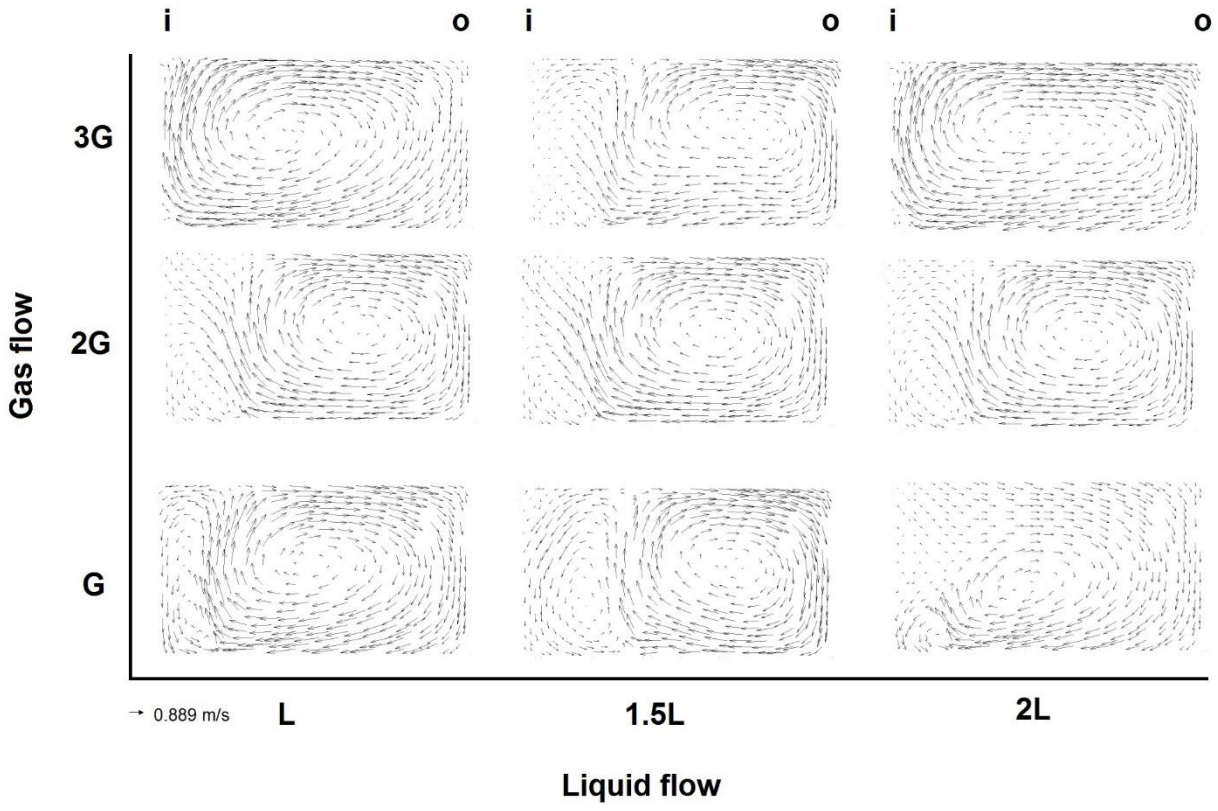

Figure 3.16 Vector plots in the vertical cross-section in the middle of the aerated region

3.3.2.3. Impact of different scenarios on gas holdup distribution

The impact of varying flowrates on the gas holdup is provided in Figure 3.17. It can be observed that variation in aeration and liquid flowrates results in different gas dispersion. Figure 3.16 & Figure 3.17 should be investigated simultaneously to understand the gas dispersion. It is observed that gas dispersion is not only dependent on the aeration rate but also on the bulk flow. It was observed earlier as well (in section 3.3.2) that the bulk flow has a significant impact on the gas dispersion. This impact is visible in both low and high gas flowrates. In the LG case, the gas plume is near the inner wall, however, a change in bulk flow to 1.5LG pushes the gas plume away from the inner wall. Further increase in bulk flow to 2LG does not let the gas plume reach the top. In the L3G case the plume is near the inner wall and with increase in liquid flowrate to 1.5L3G the plume is pushed away from the inner wall. However, further increase in bulk liquid flowrate to 2L3G pushes the plume back towards the inner wall. Moreover, the LG, 1.5L2G and 2L3G cases show the impact of simultaneous increase in liquid and aeration rates on the gas holdup distributions. It can be observed that with the simultaneous increase in liquid and aeration rate, the gas holdup distribution changes indicating that changes in operational condition results in significantly different mixing conditions.

It is important to note that there are regions with strongly reduced gas holdup (dark blue regions) in the LG, L3G & 2LG cases. This indicates the bad mixing zones originating from the mixing patterns observed earlier in Figure 3.16. The aerated regions are commonly considered to be well mixed whereas the findings here show that the areas commonly assumed to be well mixed also exhibit regions of insufficient mixing. These findings will impact the mass transfer between the phases and hence the dissolved oxygen concentrations as well as the related aerobic biochemical reactions.

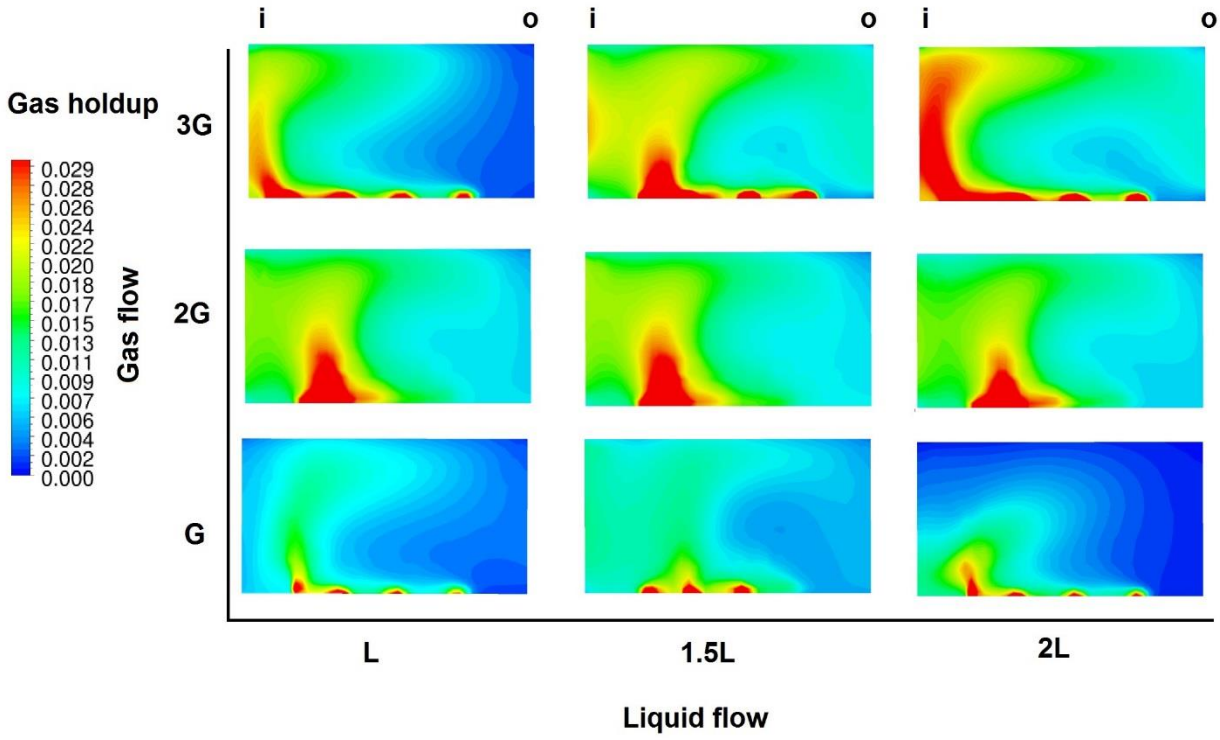

Figure 3.17 Gas holdup plots in the vertical cross-section in the middle of the aerated region

3.4. Conclusions

A hydrodynamic model with the detailed modelling of the aeration system of a full-scale wastewater treatment plant is presented in this chapter. The model takes into account all the important operational aspects of the reactor such as aeration packages, propellers and recycle pumps. The model demonstrates the ability of CFD modelling to model the complex local mixing phenomena.

The model includes the modelling of gas dispersion and prevailing mixing patterns due to aeration and turbulence. It is observed that not only aeration but also liquid flow rate impacts the gas dispersion. The results show that there are regions of insufficient mixing even in the aerated regions. These regions can have a significant impact on the mass transfer between the phases. Consequently, mass transfer between the phases will impact dissolved oxygen concentrations. As biological activity in the reactor is mainly driven by oxygen availability or unavailability, therefore, it can be stated that the

regions with insufficient mixing will impact the biological activity and thus the process performance.

Finally, a detailed scenario analysis is performed. It is observed that changes in flow rate conditions leads to significant changes in mixing patterns. Therefore, it is hard to predict a single mixing pattern for all the process conditions. The process performance will also be different with the change in mixing conditions as the gas dispersion varies with the flow conditions. In order to confirm the hypothesis, a biokinetic model is integrated with a CFD hydrodynamic model in the Chapter 4.

PART II

Hydrodynamic - biokinetic integration

Chapter 4

Hydrodynamic-biokinetic model integration applied to a full-scale WWTP

This chapter extends the model of chapter 3 by integrating a biokinetic model into the CFD model of the WWTP of Eindhoven (The Netherlands).

4.1. Introduction

Wastewater treatment plant (WWTP) modelling, and activated sludge modelling in particular, has been increasingly applied in the last couple of decades. Activated sludge models (ASM) have proven to be a useful tool for process evaluation, design and optimization (Fenu et al., 2010; Hauduc et al., 2013). However, most current modelling efforts use the traditionally introduced tanks-in-series (TIS) modelling approach that can only model the flow in one direction (i.e. the direction of bulk flow) and, hence, ignore the detailed spatial variations in substrate and electron acceptor concentrations in the other two directions. In contrast, CFD is a method which can model the flow in all three dimensions (as demonstrated in Chapter 3) and can take into account most of the spatial variations stemming from either geometrical configuration or operational dynamics. Currently, this modelling framework is mainly used for troubleshooting and basic hydraulic design. However, when integrated with biokinetic models, it becomes a powerful tool to gain insight into the impact of local mixing conditions in the reactor on the overall process performance and thus to be used for developing the next generation of flow sheet models (Laurent et al., 2014).

The potential of CFD to improve biokinetic model predictions has already been shown in a few earlier studies. The application potential of combined CFD and ASM models in both pilot and full scale systems was evaluated by Glover et al. (2006), concluding

that it can provide a more accurate description of system oxygenation capacity. Le Moullec et al. (2010a) performed detailed CFD modelling of a lab scale channel bioreactor showing better results than the conventional systemic approach (i.e. tanks in series - TIS). Detailed aeration modelling has been performed in terms of oxygen mass transfer at full scale to show the impact of different operational conditions on mixing by Fayolle et al. (2007). However, it is important to note that none of the previous efforts considered complete ASM-CFD integration at full scale along with detailed modelling of the aeration system, but were either limited to lab-scale or to only aeration modelling without complete ASM integration.

The ASM models are based on the Monod equation (Monod, 1942), which has been extensively used for modelling biological processes in wastewater treatment. In Monod's equation, microbial growth (and thus substrate consumption) largely depends on the local substrate and electron acceptor concentrations (dissolved oxygen, ammonium, etc.) and these dependencies are described by half saturation indices or K-values (Arnaldos et al., 2015; Henze et al., 1987). To compensate for the inaccuracies introduced by using TIS models (e.g. misrepresentation of dead or recirculation zones), often these K-values are calibrated, especially in those cases where low contaminant concentrations prevail given their sensitivity in those conditions (Arnaldos et al., 2015). However, one should be careful that this calibration does not result in a mere fitting exercise, which would be the case if mixing inhomogeneity would be at the basis of this need for calibration. In this case, difficulties will arise when considering different operational conditions and recalibration would usually be needed when for instance moving from dry to wet weather conditions. These difficulties could be overcome through the detailed analysis and better modelling of the impact of mixing conditions on the state variables.

There are several ASM models available for different objectives. These objectives include prediction of carbon and nitrogen removal (ASM1) and phosphorous removal (ASM2). These models are then extended to include various pathways to correctly model the important steps in biological conversions. In this chapter, first, the ASM1 model is used to predict carbon and nitrogen removal and subsequently a model (modified ASMG1) to predict nitrous oxide production is introduced.

The main objective of this chapter is therefore (1) to provide evidence that incomplete mixing leads to local heterogeneities in species concentrations and (2) to demonstrate the applicability of integrated CFD-ASM models for process analysis and evaluation

for full scale systems (i.e. knowledge buildup). In order to achieve these principal objectives, the CFD model is integrated with an ASM model to describe the impact of local mixing conditions on biological process performance. The complete model is then used to analyze the consequences at the process level of changing influent and aeration flowrates. In addition, the concept of concentration distribution plots (CDP) is introduced in order to quantify the heterogeneity of species concentrations. In addition, to demonstrate the added value of the CFD-ASM models over conventional methods, a simple TIS model is developed and the impact of K-values on concentrations and process rates is briefly discussed. Finally, the usefulness of employing this integrated CFD-ASM approach in terms of determining sensor location, control system design and process evaluation is briefly addressed.

The integration of biokinetic models into the CFD is divided into two parts. First, the integration of a model to predict carbon and nitrogen is provided with detailed description of methods and evaluation of the results. Second, a model to predict the nitrous oxide production is integrated and important findings are presented.

4.2. CFD-ASM1 integration

4.2.1. Materials & methods

The integration of the biokinetic models with the CFD hydrodynamic model is applied to the biological reactor of the WWTP facility of Eindhoven as presented in chapter 3 and the details of the reactor configuration are provided there (section 3.2) and not repeated here.

Given the objective to predict aerobic carbon and nitrogen removal, the hydrodynamic model is extended with a biokinetic model, i.e. the well-established Activated Sludge Model No. 1 (ASM1 (Henze et al., 2000, 1987). The Gujer matrix for the ASM1 is provided in the Appendix A 1. This integration is performed by adding 13 user defined scalars (UDS) representing each of the 13 components in the ASM1 model (Table 2.1). Fluent solves 13 transport additional equations for these UDS. Each transport equation for a scalar $\emptyset$ can generally be written as

$$\frac{\partial \alpha_l \rho_l \emptyset_l^k}{\partial t} + \nabla . \left(\alpha_l \rho_l \vec{u}_l \emptyset_l^k - \alpha_l \Gamma_l^k \nabla \emptyset_l^k\right) = S_l^k \quad k = 1, \dots, N \qquad \textbf{4.1}$$

where α_l, ρ_l and $\vec{u}_l$ are the volume fraction, density and relative velocity of the liquid phase, respectively. Γ and *S* are the diffusion coefficient and the source term for scalar $\emptyset$. k is the corresponding scalar and *N* is the total number of scalars (in this case 13). The first term in the equation is the unsteady term, which in this case is zero as only steady-state simulations are performed. The source terms are introduced by means of user defined functions (UDFs) based on the mass balance equations for each of the ASM1 components. The recommended standard values for all the stoichiometric and kinetic parameters are used (Henze et al., 1987). Note that this might not be correct as these values were determined by using TIS-based models. However, it is the best assumption at this point. The results and discussion in this chapter are limited to only dissolved oxygen and ammonium for improved clarity in conveying the message and reasoning.

In addition to all the standard processes of ASM1, an extra term for the oxygen mass balance is included describing the mass transfer from the gas to the liquid phase. The local oxygen mass transfer is modelled as

$$J = k_L a \, (C_S - C_O) \qquad \textbf{4.2}$$

where *J* is the local mass flux, k_L the mass transfer coefficient, *a* the interfacial area, C_S the saturation concentration of oxygen in water and C_O is the local concentration of oxygen in the water. k_L is calculated using the classical penetration theory (Higbie, 1935) based on the diffusion coefficient of oxygen in water:

$$k_L = 2\sqrt{\frac{D_L V_r}{\pi d_b}} \qquad \textbf{4.3}$$

where D_L is the diffusion coefficient of oxygen in water at 20 °C, d_b is the bubble diameter and V_r is the relative velocity between the phases.

The interfacial area a is based on bubble size and local volume fractions (equation 4.4) (Fayolle et al., 2007).

$$a = \frac{1}{d_b}\frac{\alpha_g}{1-\alpha_g} \qquad \textbf{4.4}$$

Here α_g is the local gas hold up (volume fraction of gas phase in each cell).

The coalescence and breakage phenomenon of the bubbles is not considered and thus a constant bubble size is assumed; an assumption that can and should probably be relaxed in the future. The membrane aerators are designed to provide a bubble size of about 3mm and this value is used to calculate the interfacial area and the mass transfer coefficient.

For species transport it is important to provide a good estimate of turbulent diffusivity. In the current study it is calculated based on a Schmidt number of 0.7 which is a safe assumption for such systems and have been used previously by Le Moullec et al., (2010).

Given the importance of density in reactive flows (Samstag and Wicklein, 2014; Samstag et al., 2012), bulk density is defined as a function of local suspended solids concentration (De Clercq, 2003) (equation 4.5).

$$\rho_b = \frac{\rho_l}{1-\Phi_s\left(1-\frac{\rho_l}{\rho_s}\right)} \qquad \textbf{4.5}$$

where Φ_s is the local mass fraction of suspended solids, ρ_b the bulk density and ρ_l & ρ_s the liquid and solids density, respectively. Solids density has been reported to range between 1250 and 1450 kg/m^3 (Lyn et al., 1992; Stamou et al., 2000). In this study, 1450 kg/m^3 was used to consider the maximum impact of solids. In this study, water viscosity is used because in highly turbulent flows (high Reynolds number) the impact of change in molecular viscosity is expected to be negligible (Wilcox, 1998). However, the impact of sludge viscosity is subject to more investigations, though debate on the correct measuring method and modelling is still ongoing (Ratkovich et al., 2013).

The simulations for biokinetic equations are performed on top of the "frozen" converged steady state hydrodynamic solution (at selected liquid and gas flowrates) to maintain a reasonable convergence time. Computational requirements to achieve convergence increased significantly from a 3-4 hours to 8-10 hours after including all the biokinetic equations for the steady-state solution using 8 parallel processors. It is important to mention that convergence time for the next simulation is significantly reduced to 4-6 hours when the solution is initialized from a previous converged steady state solution. It is recommended to initialize the solution with non-zero soluble substrate (S_S), oxygen (S_O) and ammonium (S_{NH}) concentrations. It will thus not lead to negative values in the beginning of the solution and hence smooth convergence can be achieved. The influent flowrate and composition is collected from the available plant historical data to use as inlet boundary condition and is provided in the form of ASM1 components in Table 4.1. Not all the data was available and the missing values which included X_I, S_I, X_{ND}, X_S and X_P. were borrowed from the Eindhoven WWTP model developed by Amerlinck (2015).

Table 4.1 Overview of the biokinetic boundary conditions

	ASM1 components	Values (mg/L)
1	S_I	42.70
2	S_S	41.00
3	X_I	1955.85
4	X_S	37.78
5	$X_{B,H}$	500.00
6	$X_{B,A}$	98.90
7	X_P	0
8	S_O	0.10
9	S_{NO}	15.20
10	S_{NH}	4.00
11	S_{ND}	0.44
12	X_{ND}	40.63
13	S_{ALK}	30.00

4.2.1.1. Simulation setup

Several simulations using the CFD-ASM model were carried out to investigate the impact of different realistic combinations of liquid and air flowrates on the local distribution of substrates and thus process performance. The combination of two

influent liquid flowrates and two air flowrates have been simulated to produce a total of 4 scenarios. The low inflow rate was selected to be Eindhoven's WWTP average dry weather flow (1,876 m^3/h referred to as scenario "L"), while the high inflow rate was double that (scenario "2L"). Similarly, the low gas flowrate was chosen to be the process base case (2,000 Nm^3/h referred to "G") and the high gas flowrate was three times that ("3G") representing the aeration rate at high peak load conditions. These scenarios were selected based on investigation of long term flow dynamics in the plant.

As traditional half-saturation indices in ASM models merge several processes (Arnaldos et al., 2015), and given the fact that the advection portion of this is explicitly modelled in CFD, it can be expected that K-values used in a combined ASM-CFD model would need to be lower. This is further investigated in the Chapter 8. To demonstrate this impact at this stage, the half saturation index of dissolved oxygen for autotrophic growth ($K_{O,A}$) is reduced by 15% to study its impact on local concentrations and process rates. The expression for the autotrophic growth rate (Henze et al., 1987) is given by:

$$Autotrophic\ growth\ rate = \mu_A \left(\frac{S_{NH}}{K_{NH} + S_{NH}}\right)\left(\frac{S_O}{K_{O,A} + S_O}\right) X_{BA} \qquad \textbf{4.6}$$

where μ_A is the maximum specific growth rate for autotrophic biomass, S_{NH} the concentration of ammonium, S_O the concentration of dissolved oxygen, X_{BA} the concentration of autotrophic biomass, K_{NH} the half saturation index of ammonium and $K_{O,A}$ the half saturation index of dissolved oxygen for autotrophic biomass.

4.2.1.2. Tanks-in-series modelling

A simple tanks-in-series (TIS) model (using ASM1 model) was developed in order to draw a comparison between TIS and CFD modelling. The reactor was divided into six tanks based on the reactor configuration and is shown in Figure 4.1a. Each of the tanks is named with reference to the reactor configuration. In Figure 4.1, T_{in} is the section receiving the inlet flow, T_{an1} is the anoxic section before the winter package, T_W is the winter aeration package section, T_{an2} is the anoxic section between summer and winter aeration packages, T_S is the summer aeration package and T_{out} is the section having the outlet & recycle pumps. Steady state simulations were then performed in the modelling and simulation platform WEST ("MIKE Powered by DHI," 2016) with the default K-

values and same influent composition and flowrates as the CFD simulations. The respective plant layout in WEST is shown in Figure 4.1b. Moreover, the volume of each tank is also provided in Table 4.2.

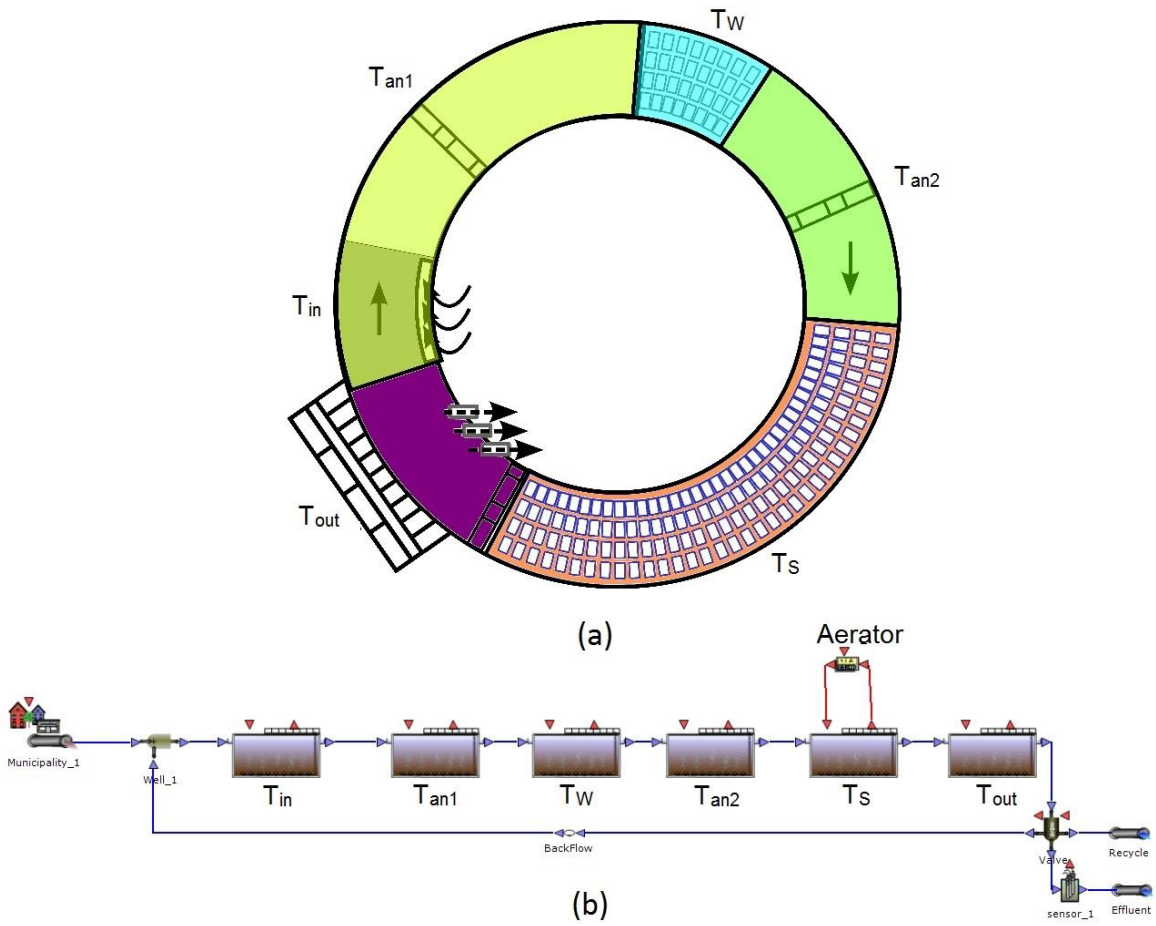

Figure 4.1 (a) The reactor division for the TIS modelling and (b) the plant layout in WEST

Table 4.2 The volumes of each tank shown in Figure 4.1

Tank	Volume (m^3)
T_{in}	1821
T_{an1}	3402.5
T_W	862.6
T_{an2}	3594.3
T_S	2060.7
T_{out}	17252.4

4.2.2. Results & discussion

4.2.2.1. Comparison between the CFD and velocity measurements

The use of the sludge density correlation (equation 4.5) resulted in different predictions of velocities as compared to the use of standard water density. The comparison between the CFD velocities and measured velocities is provided in Figure 4.2. It can be observed that the trend of velocities is similar to the water density based velocities (Figure 3.8), however, the difference between the CFD and measured velocities has been reduced by almost 10-15%. Therefore, the density correlation partially corrects the deviations from the measured data set. It can be observed for the location B1, the CFD velocities are similar to the measured velocities near the top and higher near the bottom. It can be due to the fact that the potential sedimentation impact is high near the bottom. More accurate predictions can be achieved by modelling the solids transport and taking into account possible sedimentation impacts. Bulk density should therefore always be included when simulating activated sludge systems.

The results from the integrated CFD-biokinetic model are provided and discussed below. The concentration distributions stem from the CFD hydrodynamic model; where necessary hydrodynamic results are provided as well for the sake of better understanding.

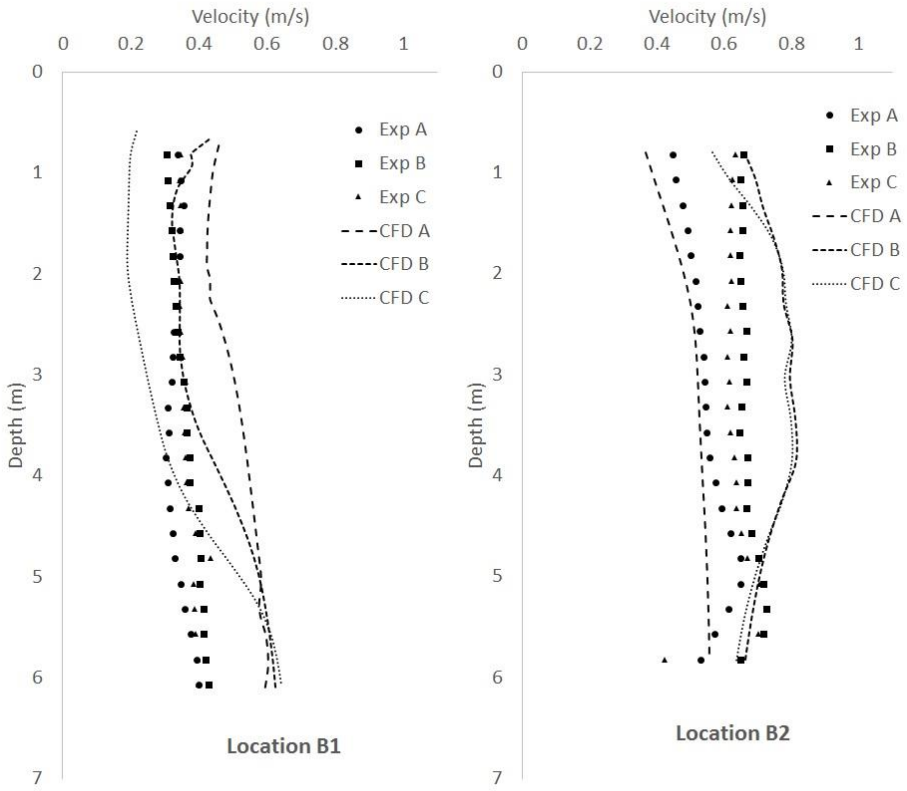

Figure 4.2 Comparison between the CFD (sludge density based) and measured velocities at the location B1 & B2 (A: Near the inner wall, B: In the middle and C: Near the outer wall) (Average measurement error is ±0.0315 m/s)

4.2.2.2. Local concentrations in the reactor

Results of the local concentrations of dissolved oxygen and ammonium from the ASM-CFD model are given for the base case (L-G) in Figure 4.3 for the horizontal cross section (at the middle of reactor's depth i.e. 3.45m deep). It must be noted that these concentration patterns are very similar to the gas holdup patterns observed in Figure 3.10. The dissolved oxygen and ammonium concentrations vary between 0.2-1.96 mg/L and 0.4-2.2 mg/L, respectively. These results clearly show the non–uniformity in both the dissolved oxygen and ammonium concentrations throughout the biological reactor. This non-uniformity also occurs in the part of the reactor corresponding to the aeration system, where uniform mixing and substrate concentrations are typically assumed. It must be noted that the concentration variations are not only in the direction of flow but also in the directions lateral to the bulk flow (i.e. along the width of the reactor). It eventually leads to differences between concentrations near the walls and in the bulk

flow. The outlet of the reactor is located near a wall and this heterogeneity would ultimately cause significant differences in ammonium and dissolved oxygen concentrations between the reactor outlet and the bulk flow. In terms of dissolved oxygen, a sensor used as input for the DO controller can lead to significantly different controller behaviour depending on its location (exactly at the outlet or in the bulk flow). Figure 4.3 shows the actual sensor location at the bioreactor near the wall next to outlet.

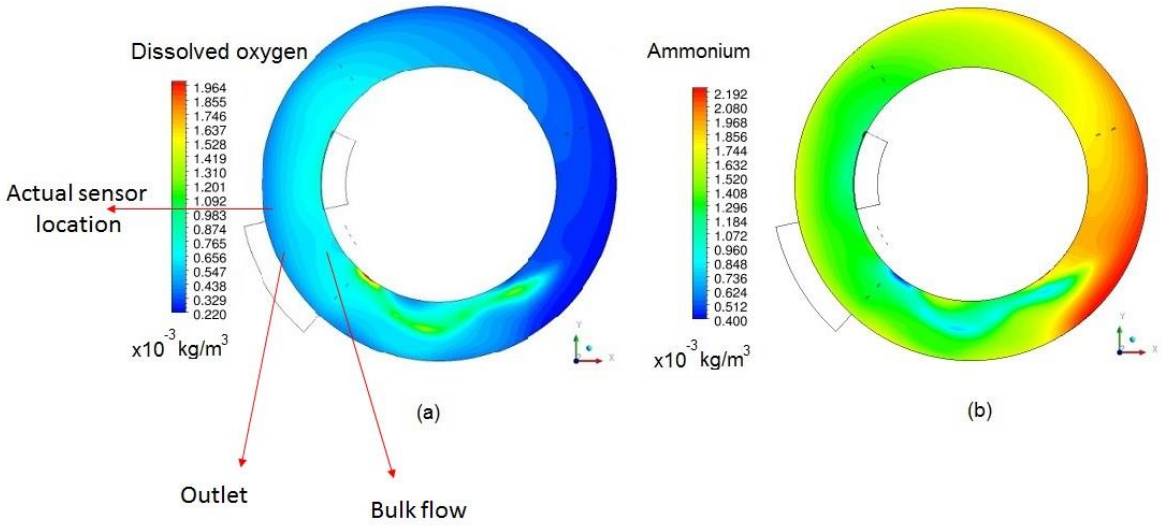

Figure 4.3 (a) Dissolved oxygen and (b) ammonium concentrations at 3.45m depth in the bioreactor for the L-G case

Figure 4.5 shows, for a vertical cross section of the reactor in the middle of the aeration zone (Figure 3.12), the impact of the flow patterns (Figure 4.4) on the local concentrations of dissolved oxygen and ammonium for the base case (L-G). These regions are traditionally considered to be well-mixed, whereas Figure 4.5 clearly shows the heterogeneity of dissolved oxygen and ammonium concentrations. The variations in dissolved oxygen concentration originate from the fact that aeration is causing a specific flow pattern, which creates significant recirculation. The latter creates a region within its core (dead zone) that becomes isolated from the bulk flow and thus leads to local mass transfer limitations (from the gas to liquid phase). This is causing a non-uniform distribution of the dissolved oxygen concentration and consequently it results in local variations in ammonium concentration since it is subject to an aerobic conversion process. Similarly, these variations impact other process variables, such as nitrate and organic carbon concentrations, as well.

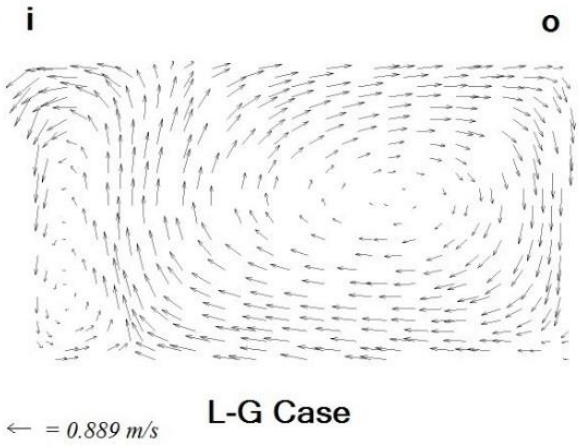

Figure 4.4 Velocity vector plot at a vertical cross section in the middle of the aerated region (plot location indicated in the Figure 3.12) for the L-G case

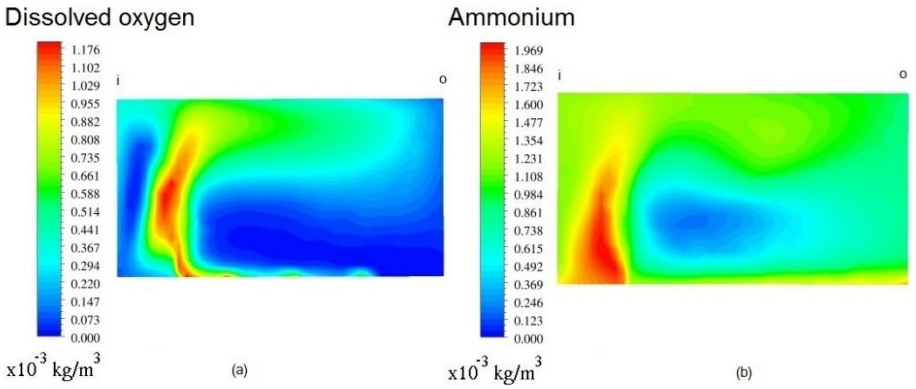

Figure 4.5 Dissolved oxygen (a) and ammonium (b) concentrations at a vertical cross-section in the middle of aerated region (plot location indicated in Figure 3.12 for the L-G case

Equation 4.6 shows the dependence of the autotrophic growth rate on dissolved oxygen and ammonia concentrations. In this equation the concentrations S_{NH} and S_O represent the concentration to which the microorganisms are exposed to, i.e. the local concentrations. As such, obviously, the varying local concentration impact the process rate locally. Figure 4.6 shows the impact of concentrations shown in Figure 4.5 on local autotrophic growth rate in the same vertical slice of the reactor in the aerated zone. As can be seen, there are major areas with significantly reduced dissolved oxygen concentrations (Figure 4.5a) leading to anoxic conditions and hence limiting aerobic growth of autotrophic biomass. Therefore, it is evident that local mixing is limiting the

process rate locally due to mass transfer limitations. However, as these details are typically ignored in the TIS model, reduced/enhanced process rates need to be achieved by altering either half saturation indices or maximum specific growth rates in order to match the experimental data.

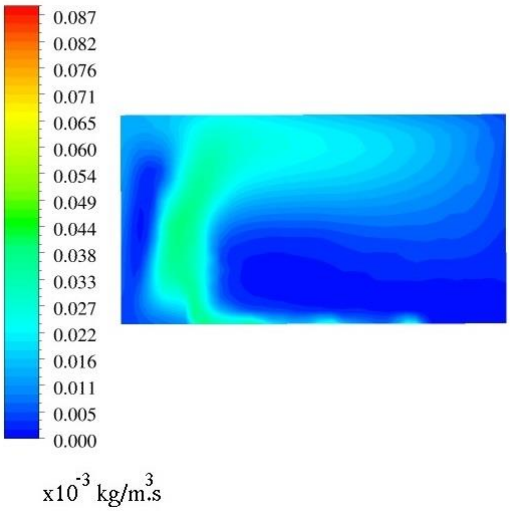

Figure 4.6 Autotrophic growth rate at a vertical cross-section in the aerated region (plot location indicated in Figure 3.12) for L-G case

4.2.2.3. Average concentrations in the reactor

Figure 4.7 shows the averaged substrate concentrations. These averages provide the information about the performance of different sections of the reactor. Here, ammonium and dissolved oxygen concentrations have been averaged for every section of the reactor and also the corresponding complete range bars (minimum and maximum values) are shown. Before evaluating these plots, the physical significance of these sections must be understood. Sections T1 & T2 are the first two sections sharing the inlet and T3 to T7 are the sections downstream from the inlet. Sections T8 to T11 are the aerated sections and T12 is the section having the outlet & recycle streams. As expected, the average dissolved oxygen concentration decreases from 0.65 mg/L in section T1 to 0.1 mg/L in section T8 (start of aerated region). Thereafter, thanks to aeration, the concentration increases to 0.76 mg/L in section T12. However, the trend in ammonium concentrations is quite different. The only source of ammonium is at the inlet (i.e. ammonium load coming into the system) and as a result there is an increase in its concentration from 1.3 mg/L in section T1 to 2.0 mg/L in section T2. Thereafter, the average ammonium concentration decreases almost linearly to 0.9 mg/L up to

section T12. The range bars in the plots provide an indication about the magnitude of the variation in a section. The larger range bars indicate higher variations and vice versa. Figure 4.7 shows that these range bars differ in size moving from one section to the next. For example, the range bar of dissolved oxygen concentration in section T10 is the largest (0.1 to 1.4 mg/L) and smallest for section T7 (0 to 0.5 mg/L). Hence, the heterogeneity in dissolved oxygen concentrations in section T7 is substantially lower than in section T10. It can be concluded that different sections of the reactor have different levels of heterogeneity which is currently not reflected in the modelling of such systems.

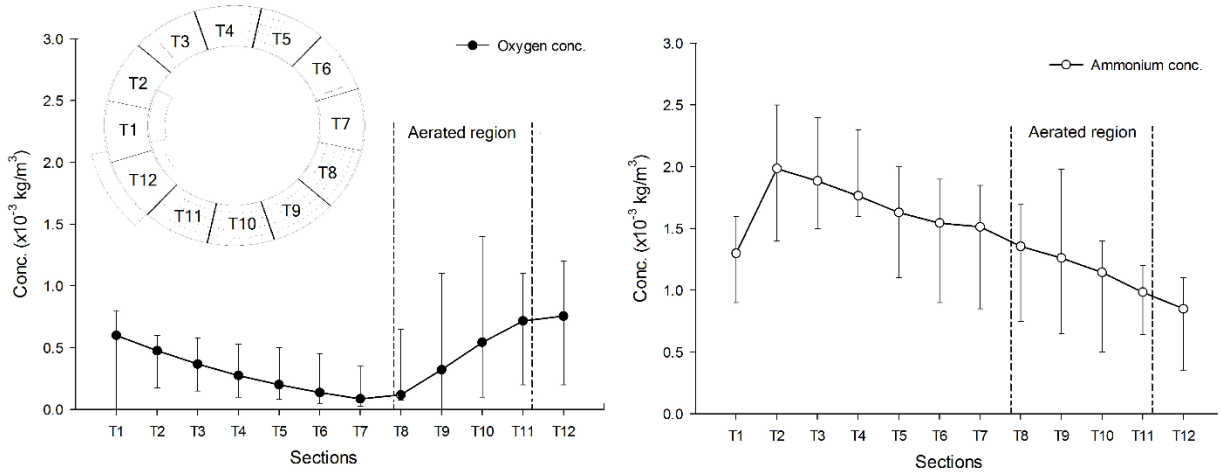

Figure 4.7 Averaged ammonium & dissolved oxygen concentrations in the different sections of the reactor

4.2.2.4. Results of the scenario analysis

Figure 4.8 and Figure 4.9 show the impact of different liquid and gas flowrates, respectively on the dissolved oxygen and ammonium concentrations, in a vertical cross section (same location as in Figure 4.5) of the aerated region. The impact of flow patterns observed in Figure 3.16 are also visible here. As can be seen, the doubling of liquid flowrate while keeping a constant air flowrate of 2,000 Nm^3/h does not cause improved mixing conditions. Nevertheless, significant changes are visible in terms of ammonium elimination originating from the limited availability of air at the doubled influent flowrate. Triplicating the gas flowrate brings about significant increases in the dissolved oxygen concentrations (with consequent decreases in ammonium concentrations). Additionally, at this high gas flowrate, the interaction in terms of mixing between the air and liquid flows becomes evident. At higher liquid flowrates,

an increased mixing non-uniformity prevails which would not be easy to predict without the application of CFD. These results are important to understand what will happen at the process level with dynamic influent flows, and the impact of varying gas flowrates in response to these dynamics. This information would be difficult to attain without the use of an integrated hydrodynamic-biokinetic model like the one developed in the present study. The dynamics of mixing with varying liquid and air flowrates is currently completely ignored in conventional tanks-in-series modelling.

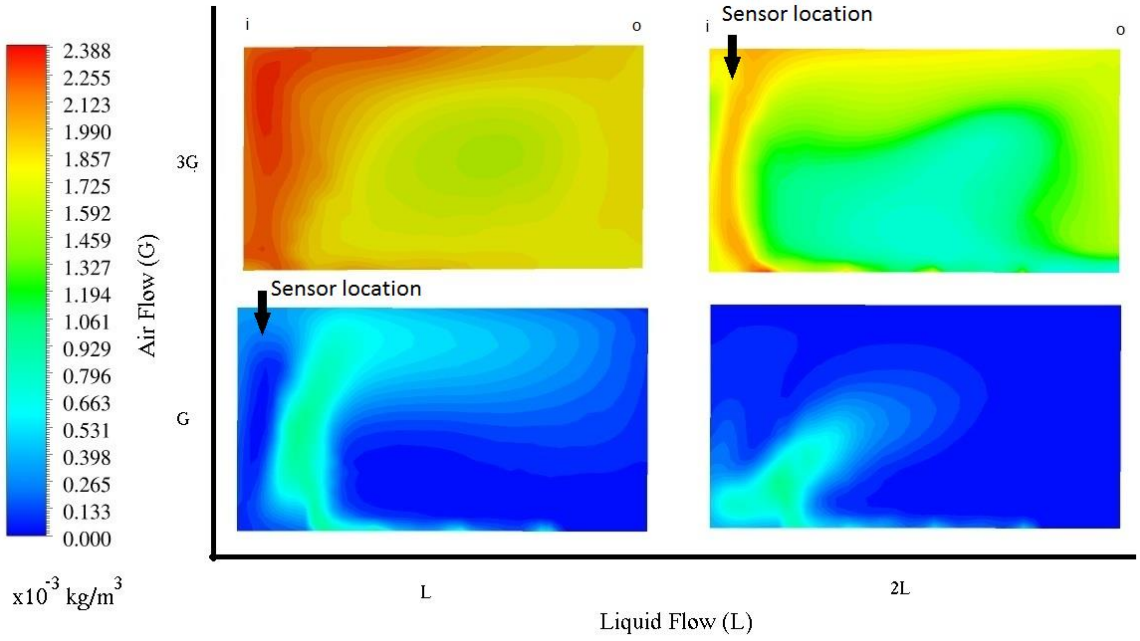

Figure 4.8 Dissolved oxygen concentrations in the middle cross section (plot location indicated in Figure 3.12 of the aerated region at different air and liquid flowrates (sensor locations shown here are virtual locations for discussion)

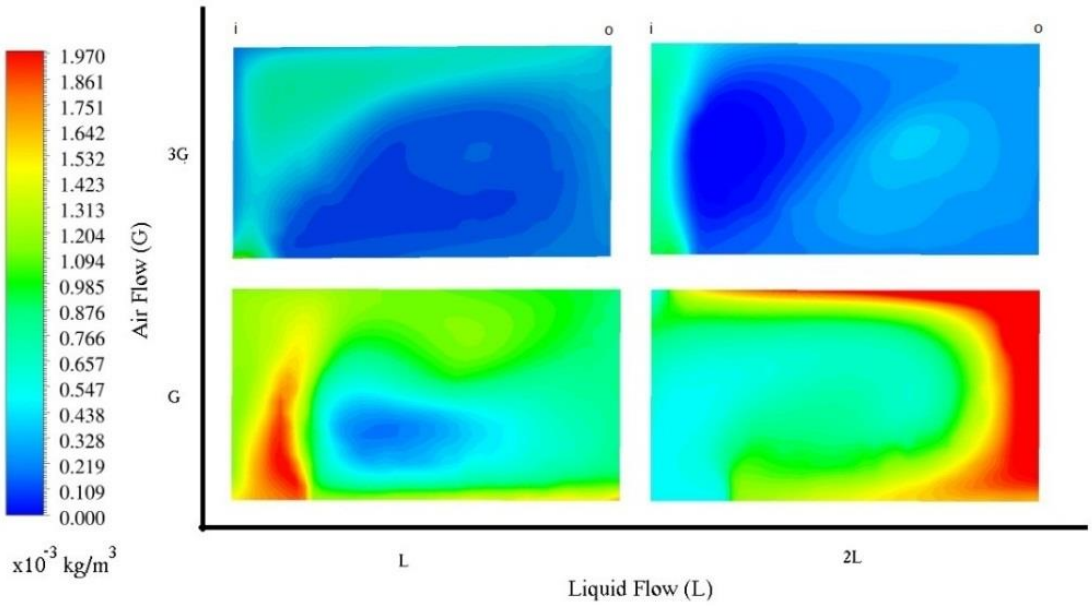

Figure 4.9 Ammonium concentrations in the middle cross section (plot location indicated in Figure 3.12) of the aerated region at different air and liquid flowrates

4.2.2.5. Concentration distribution plots

In order to quantify the heterogeneity of species, the concept of concentration distribution plots (CDP) is proposed. These are volume based cumulative frequency distributions for a species. Figure 4.10 illustrates how the CDP is calculated from the CFD model. The CFD-biokinetic model provides local concentrations for each cell of the grid (mesh). In a certain section of the reactor with volume 'V1', for each cell 'i', the local concentrations 'Ci' and the corresponding size 'Vi' of the cell is calculated (available from the CFD-biokinetic model). Therefore, the total volume of the cells having a concentration 'Ci' equals ∑Vi and the corresponding volumetric fraction $\Sigma Vi/_{V1}$. Similarly, such volumetric fractions can be calculated based on concentration ranges such as 'Ci to Ci+ΔC' and 'Ci+ΔC to Ci+2ΔC' instead of absolute concentrations. Finally, with the knowledge of minimum and maximum concentrations and by choosing a small step change (ΔC) (bin size), the CDP can be plotted for each species in any user-selected volume 'V1'. Hence, for each volumetric region selected by the user, a CDP can be constructed and this for every species computed by the integrated CFD-ASM model.

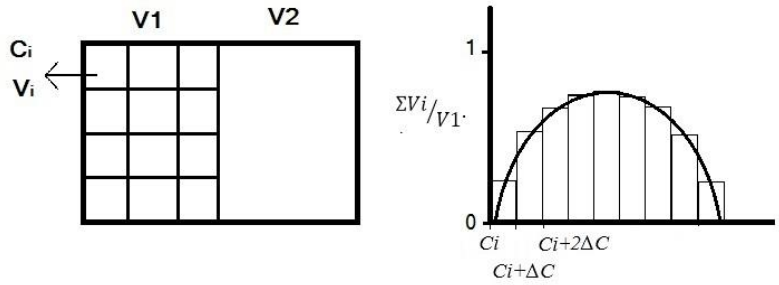

Figure 4.10 Illustration of volume based frequency distribution calculation

The CDPs for the DO concentrations in two different sections of the reactor and under different conditions are shown in Figure 4.11. A step change (bin size) of 0.1 mg/L is used for all these plots. Figure 4.11a shows the CDP for DO in the aerated and non-aerated sections of the reactor. It should be noted that the curves are merely extrapolated by joining the points which correspond to mid-points of each bin. For example, the first point in Figure 4.11a (for non-aerated CDP) represents the step change 0 - 0.1mg/L, thus it is plotted at 0.05mg/L and its y-axis value reads 0.37 (volume fraction). Hence, it can be said that 37% of the non-aerated region has a concentration between 0 and 0.1 mg/L. Figure 4.11(a) shows that in the non-aerated section the DO concentration ranges between 0 to 0.6 mg/L. However, the aerated section has a dissolved oxygen concentration range between 0 to 1.4 mg/L and does not exceed 1.4 mg/L. The CDPs clearly show more heterogeneity in the aerated section as compared to the non-aerated ones, which was already visually observed, but is now being quantified.–This quantification is needed in chapter 6 to derive the compartmental model from the integrated CFD-biokinetic model solution.

Figure 4.11b shows CDPs for dissolved oxygen in the aerated section for the two other flow scenarios (i.e. L-G & 2L-3G). The variation in dissolved oxygen distributions due to changes in operational conditions is evident. For the 2L-3G scenario, the CDP is widely spread and thus the use of a completely mixed assumption will not be a good estimate of the entire tank behaviour under such conditions. Indeed, several reactions depend on local concentrations and the average of the distribution will potentially mask reactions that do take place or underestimate process rates of reactions that do occur. Depending on the final objective of the modelling study this loss of detail could be acceptable or, on the contrary, could bring about incomplete and/or incorrect process conclusions or lead to significant calibration efforts to make up for these flaws.

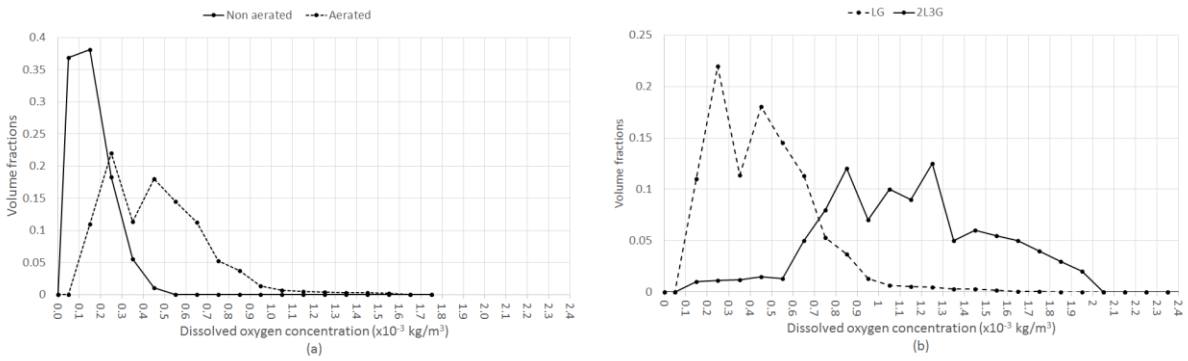

Figure 4.11 (a) Dissolved oxygen CDPs in different sections of the bioreactor for the L-G case and (b) comparison of dissolved oxygen CDPs in the aerated section for the L-G and 2L-3G scenarios

In order to investigate the actual impact of heterogeneous concentrations on the process rates, Figure 4.12 shows distributions of the autotrophic growth process rate. A step change (bin size) of 0.005 ($x10^{-4}$ kg/m^3.s) is used for these distributions. It can be seen that the distribution of autotrophic growth rate is more non-uniform for the aerated section as compared to the non-aerated section. For the aerated section, the growth rate CDP spreads between 0.018 to 0.07 ($x10^{-4}$ kg/m^3.s), whereas, in the non-aerated section it is between 0 to 0.02 ($x10^{-4}$ kg/m^3.s). Similar observations are made for the different scenarios in Figure 4.12b. The CDPs in the case of 2L-3G show that growth rate distribution is more non-uniform as compared to the L-G case. These findings are similar to the findings in Figure 4.11 with respect to non-uniformity among the different sections of the reactor as well as among the different operational conditions.

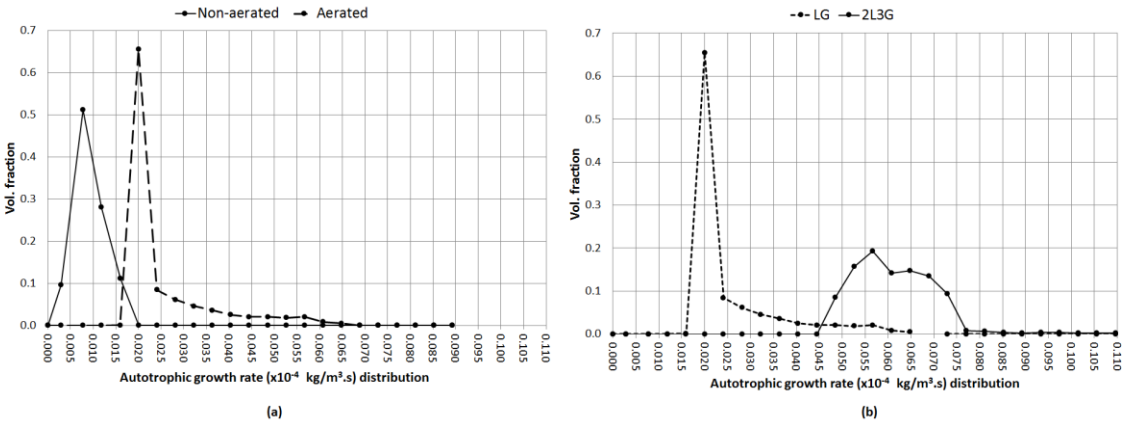

Figure 4.12 (a) Autotrophic growth rate distributions in different sections of the bioreactor for the L-G case and (b) comparison of autotrophic growth rate distributions in the aerated section for the L-G and 2L-3G scenarios

4.2.2.6. Comparison between the TIS and the CFD-biokinetic model

In order to compare the CFD results with those of the conventional TIS modelling, the CFD concentrations are averaged (similarly as in section 4.2.2.3) over different volumetric sections of the reactor as shown in Figure 4.1. The comparison between the TIS and CFD is performed for two cases i.e. L-G and 2L-3G because these two cases are closest to reality. Higher liquid flowrate likely gives higher loads and thus increased oxygen demand resulting in higher air flowrates. The dissolved oxygen and ammonium concentrations for both the modelling approaches under the two different operational conditions is shown in Figure 4.13. It must be noted that the TIS model assumes complete mixing in each of these sections. In contrast, the CFD average values are based on the local concentrations taking into account the mixing limitations and, hence, can be considered as the better representation of the average behaviour of the tanks. Notice that these average values are similar to the values plotted in the Figure 4.7 but with different number of sections. Moreover, the maximum and minimum bars are not shown here to not overwhelm the graph. For better understanding, the results for both the cases are discussed separately.

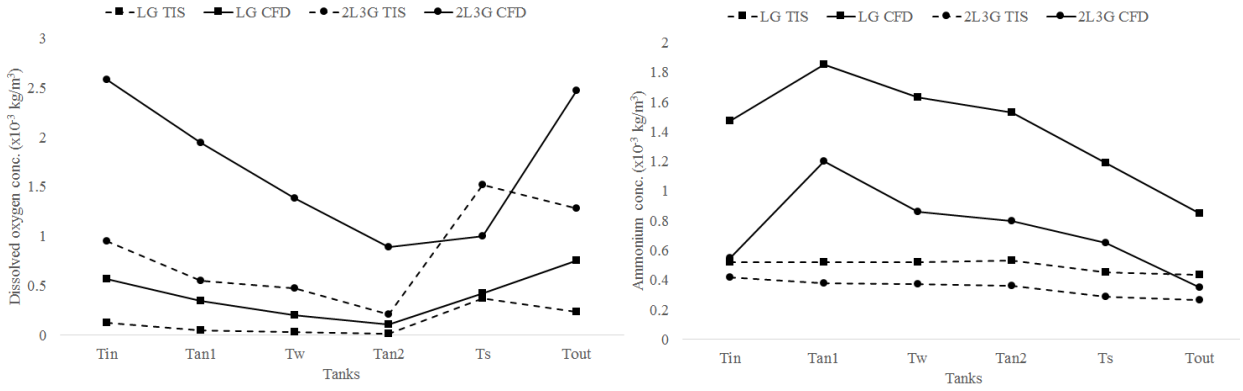

Figure 4.13 (a) Comparison between the TIS and CFD modelling for dissolved oxygen and (b) ammonium concentrations

In the L-G case, it can be seen that the TIS model predicted lower DO concentrations (except for the aerated tank T_S) as compared to the CFD model. This is due to the fact that the TIS model assumes complete mixing in each tank and thus overestimated the oxygen consumption resulting in lower DO concentrations. However, the CFD model took into account the mixing limitations resulting into higher DO concentrations. This can be explained by the fact that the dissolved oxygen concentrations are a result of two phenomena: 1) oxygen mass transfer from the gas phase and 2) oxygen uptake by the

substrate. Both phenomena are affected by mixing limitations. In the non-aerated regions there is no oxygen mass transfer occurring from the gas phase and hence mixing limitation is only hampering the oxygen uptake. This leads to higher average DO concentrations in the CFD model compared to the TIS model in the non-aerated regions. However, in the aerated regions, the mixing limitations impact both phenomena such that the dead zones cause less oxygen mass transfer and also cause less consumption of the substrates. Therefore, the difference between the CFD average DO concentrations and the DO values predicted by the TIS model reduces in the aerated region (T_S).

The trend in DO concentrations (from one tank to the next) is similar in both the models until the aerated tank (T_S). Further downstream in the outlet region (T_{out}), the DO concentrations decrease to 0.25mg/L for the TIS model but increase to 0.75 mg/L in the CFD model. This can be understood by considering the underlying flow patterns and mixing limitations inside the reactor shown in the Figure 3.10 and Figure 4.3. Figure 3.10 showed that the gas holdup is pushed in the direction of bulk flow and hence a high DO concentration is observed in the outlet region (Figure 4.3). This results in a higher average DO concentration in T_{out} in the CFD model (Figure 4.13). However, the TIS model is unable to take into account the impact of local hydrodynamics and thus predicts a low DO concentration. Similarly, the ammonium concentrations are lower for the TIS model due to the assumption of complete mixing and not taking mixing limitations into account. In short, the TIS model overrates the ammonium removal and may need to adapt the process rate through calibration to match experimental measurements.

In the 2L-3G case, the difference between the TIS and the CFD average values is even larger than in the L-G case. The TIS model ignores the impact of operational conditions on the detailed hydrodynamics (only dilution rate will be affected) but the CDP distributions (Figure 4.11b) for the 2L-3G case displayed a wider distribution of the DO concentrations compared to the L-G case and, hence, an even greater degree of heterogeneity. Therefore, it confirms the obvious that larger heterogeneity leads to larger deviation from the complete mixing assumption. Again the TIS model predicted lower DO concentrations compared to the CFD model except for the aerated region. In the aerated region (T_S), again it is a result of two phenomena (mass transfer from gas phase and uptake by the substrate) affected by the mixing limitations. However, the impact of the mass transfer limitation from gas to liquid phase in this case is larger resulting in lower DO concentrations compared to the TIS. Moreover, it can be noticed

that in the CFD model the DO concentration in the outlet and inlet regions is quite high as compared to the other regions due to the bulk flow impact on the gas dispersion.

These results show that the heterogeneities observed in the CFD-biokinetics model are not correctly captured by the TIS model leading to wrong conclusions. For example, in the L-G case the TIS model predicted 0.37 mg/L of DO in the aerated region, however, Figure 4.11 showed that the DO concentration in the aerated region ranges between 0 to 1.4 mg/L. Similarly, for the 2L3G case the TIS model predicted 1.5mg/L in the aerated region but Figure 4.11b showed that DO concentration ranges between 0 to 2.1 mg/L. The TIS model values are also not a good representative of the average tank behaviour as seen in Figure 4.13 and therefore, would lead to a calibration of the half saturation indices merely to fit the measurements.

In addition to the comparison between the concentrations, the autotrophic growth rates are calculated for both the models under different operational conditions (L-G & 2L-3G). The results are shown in the Table 4.3. It should be noted that the process rates for the CFD model are volume weighted average process rates calculated from the local concentrations. The process rates predicted by the TIS model are less than the CFD based process rates which is in correspondence with the oxygen concentrations. Figure 4.12 showed that the growth rate is not uniform and has a distribution similar to the concentration distributions. For example, in the aerated tank (TS) the TIS predicted the process rate to be 0.013 ($x10^{-4}$ $kg/m^3.s$), whereas Figure 4.12a showed that it varies between 0.018 and 0.07 ($x10^{-4}$ $kg/m^3.s$). The difference between the TIS and the volume averaged process rates can help in providing an insight about how much calibration will be needed for the TIS model. It can also provide a basis to devise a protocol for calibration procedures taking spatial variations and flow dynamics into consideration.

Table 4.3 Autotrophic growth rate (x10^{-4} kg/m^3.s) for the CFD model and the TIS model under different operational conditions

Cases	L-G		2L-3G	
Tanks	TIS	CFD	TIS	CFD
T_{in}	0.0076	0.0320	0.0193	0.0732
T_{an1}	0.0033	0.0277	0.0148	0.0907
T_W	0.0023	0.0189	0.0136	0.0688
T_{an2}	0.0008	0.0120	0.0084	0.0530
T_S	0.0130	0.0256	0.0163	0.0583
T_{out}	0.0100	0.0275	0.0148	0.0625

4.2.2.7. Sensor measurement/reading and calibration

The comparison between the TIS and CFD models displayed the imminent need for calibration for the TIS model to correct for the errors induced due to the assumption of complete mixing.

In the TIS modelling techniques, the $K_{O,A}$ (half saturation index of oxygen for aerobic growth of autotrophs) values are calibrated based on a measured dataset, collected at a specific (easily accessible) location in the reactor. The model should be able to take the sensor location into account for a robust calibration effort. The TIS model can take into account the location of sensor to a certain extent but is unable to distinguish between lateral locations of the sensors. However, Figure 4.5 showed that the measured dataset would be highly dependent on the sensor location (due to spatial variations across the cross section). Therefore, resulting calibrated $K_{O,A}$ values would potentially be different for different physical sensor locations in the bioreactor.

Moreover, the hydrodynamic results showed changes in flow patterns with the change in operational conditions (Figure 3.16) and their impact on the concentrations (Figure 4.8 & Figure 4.9). This can potentially impact the sensor measurements and hence the control and calibration. It can be investigated by assuming a fixed sensor location to be close to the inner wall (Figure 4.8) in the aerated section. For the L-G case, the measured DO concentration would be 0.22 mg/L (Figure 4.8), whereas, the TIS model predicts 0.4 mg/L for the aerated tank (T_S) (Figure 4.13). Therefore, for the L-G case, measured DO is lower than DO predicted by the TIS model. However, for the same sensor

location in the 2L-3G case, measured DO (1.82 mg/L) is higher than the DO (1.5 mg/L) predicted by the TIS model (Figure 4.13). Therefore, in order to calibrate the TIS model, for the L-G case, the $K_{O,A}$ value will have to be reduced whereas for 2L-3G case it needs to be increased to fit dynamically measured data (meaning that no single calibrated K-value can be found). Similarly, calibration of other half saturation indices will also depend on local mixing conditions.

In addition, Figure 4.11b provides the information about the sensor measurement/placement with respect to the CDPs under the different operational conditions. As the CDPs were drawn for a range of concentrations (step change) therefore it is important to indicate the step change where the measured value belongs. The sensor measurement for the L-G case is 0.22 mg/L, thus it corresponds to the 0.2-0.3 range. Hence, it can be said that the measured value represents at maximum 23% of the aerated region. Similarly, the sensor measurement for the 2L-3G case at maximum represents only 4% of the aerated region. Therefore, relatively the sensor measurements for the L-G case would be more reliable (in terms of representative of tank behaviour) as compared to the 2L-3G case. This information can certainly be useful while deciding the sensor location, accounting for this in control actions and for potential calibration efforts. The impact of the sensor location and the need of recalibration while extrapolating model results to different operational conditions such as from dry to wet weather conditions are often ignored. This clearly illustrates what this leads to and shows why dynamic calibration with a fixed mixing model will not work, i.e. never result in a single parameter set describing the system under both dry and wet weather conditions.

4.2.2.8. Impact of half saturation index on the concentrations

One major reason behind the calibration of k-values is the inability of TIS based ASM models to account for local hydrodynamics. Thus it is quite probable that these limitations are lumped into the k-values and hence the default k-values being used are potentially overestimated since they were derived in a TIS context. However, as is shown, the CFD takes local mixing limitations into account thus true k-values would be lower than the currently employed default values. Therefore, Figure 4.14 shows the impact of reducing the half-saturation index of dissolved oxygen ($K_{O,A}$) for autotrophic organisms by 15% on both the local dissolved oxygen concentration and autotrophic growth rate. This can be regarded as a reduction in “resistance” that a molecule senses when moving from the bulk to the cell internal (Arnaldos et al., 2015). The reduction

in $K_{O,A}$ value increases the growth rate (Figure 4.14b) and thus in turn increases the dissolved oxygen uptake resulting in lower dissolved oxygen concentrations. These results are useful to see how the reduced $K_{O,A}$ values locally impact the process rate and concentrations. In order to correctly capture these values, local concentrations of different species should be measured. This was, however, beyond the scope of this work.

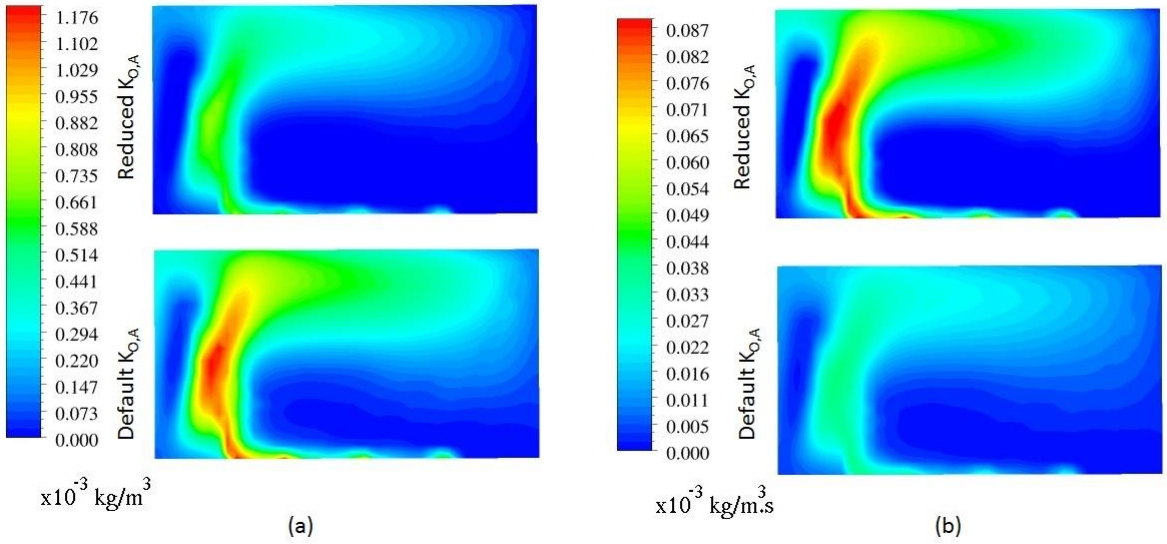

Figure 4.14 (a) Concentration of dissolved oxygen and (b) Autotrophic growth rate in the middle cross-section in aerated region (plot location indicated in the Figure 3.12 for L-G case

4.3. CFD-ASMGI integration

Nitrous oxide (N_2O) emissions are considered the most potent greenhouse gas emissions due to their high global warming potential which is 298 times greater than the carbon dioxide (IPCC, 2014). The N_2O emissions from wastewater treatment plants are also a growing concern and hence research has grown accordingly. However, the N_2O emission data collected from WWTPs show a huge variation in the N_2O emission factor (the fraction of influent nitrogen load emitted as N_2O), ranging between 0.01% and 1.8%, and in some cases even higher than 10% (Ahn et al., 2010a, 2010b; Foley et al., 2010; Kampschreur et al., 2009; Wang et al., 2011). A high degree of temporal variability in N_2O emission has also been observed within a WWTP (Ahn et al., 2010a;

Guo et al., 2013; Ye et al., 2014). The observed variability is in clear contrast with the fixed emission factors currently applied to estimating N_2O emissions from wastewater treatment (IPCC, 2014). A major problem with the use of fixed emission factors is that the link between emissions and process configurations and operating characteristics is not considered. The estimates do not account for the variable process conditions in different plants and thus do not encourage mitigation efforts (Ni et al., 2013; Ye et al., 2014).

Moreover, N_2O mathematical models (Guo and Vanrolleghem, 2014; Hiatt and Grady, 2008; Mampaey et al., 2013) show that the dissolved oxygen concentration (DO) plays a key role in quantifying N_2O production and, hence, emissions. Therefore, it is important to predict dissolved oxygen concentrations accurately to evaluate its impact on nitrous oxide production within a WWTP. However, as discussed earlier (chapter 2), current models (i.e. TIS based models) do not take spatial variations into account and thus resulting nitrous oxide predictions are based on the assumption of complete mixing. As illustrated in section 4.2.2, DO concentrations vary locally depending on the mixing conditions and, therefore, it is important to take spatial heterogeneities into account for an accurate prediction of nitrous oxide emissions. In this section, the CFD-biokinetic model presented in section 4.2 is extended by including equations needed to predict nitrous oxide concentrations.

4.3.1. Materials and methods

In order to model nitrous oxide production, the ASM1 needs to be extended with nitrous oxide models from the literature, i.e. including heterotrophic denitrification (Hiatt and Grady, 2008), AOB denitrification (Mampaey et al., 2013) and DO Haldane kinetics (Guo and Vanrolleghem, 2014). The combination of these models is referred to as the modified ASMG1 model. It comprises of 18 state variables and 15 processes. In this model, autotrophic biomass is subdivided into AOB (ammonium oxidizing bacteria) and NOB (nitrate oxidizing bacteria). Nitrates are subdivided into nitrate (NO_3^-), nitrite (NO_2^-), nitric oxide (NO), nitrous oxide (N_2O) and dinitrogen (N_2). The additional processes and variables lead to a tremendous increase in stoichiometric and kinetic parameters totalling 62. The detailed matrix for all the processes and default values for the kinetic parameters is provided by Guo and Vanrolleghem (2014).

Similar to the ASM1 integration (section 4.2), all state variables of the modified ASMG1 model are introduced as user defined scalars in the CFD hydrodynamic model.

This results in the solution of 18 additional equations. Default values for all kinetic and stoichiometric parameters are used. The same influent composition is used as for ASM1. However, nitrates are subdivided equally into NO_3, NO_2 and NO fractions (as these are not measured and not known). It is assumed that no nitrous oxide or dinitrogen is present in the influent. The autotrophic biomass is subdivided equally into AOB and NOB. Furthermore, the biokinetic modelling is performed on top of the converged hydrodynamic model. The biokinetic modelling in this case took 10-12 hours using 8 parallel processors. Four flow scenarios (L-G, 2L-G, L-3G & 2L-3G) similar to the CFD-ASM1 are simulated as well.

4.3.2. Results and discussion

The concentrations of nitrous oxide along with the DO concentrations at a horizontal cross section of the reactor at half depth (3.45m) are shown in Figure 4.15. It can be observed that the nitrous oxide concentrations vary along the length and width of the reactor. Higher nitrous oxide concentrations are observed where DO concentration is low and vice versa. The nitrous oxide concentrations in the middle of the reactor are higher compared to near the walls and a higher gradient exists where DO concentration is low. These details can be useful in determining the impact of local conditions on the production of nitrous oxide.

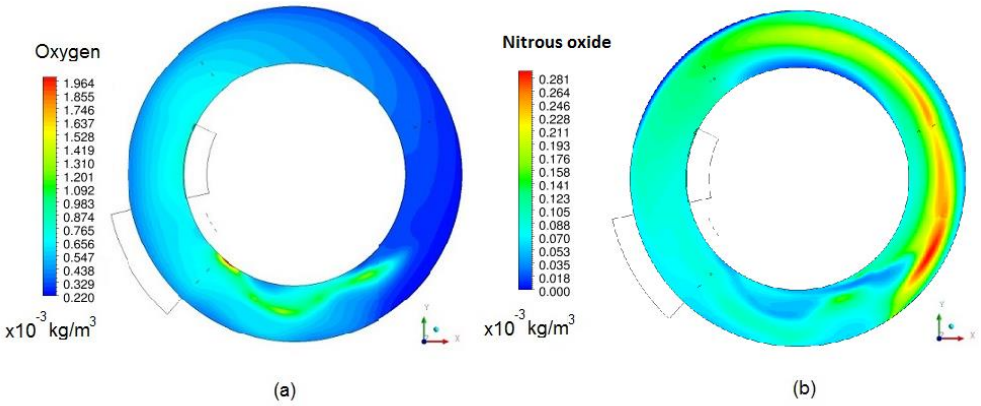

Figure 4.15 (a) The dissolved oxygen and (b) nitrous oxide concentrations at a horizontal cross section at half depth of the reactor

Nitrous oxide and DO concentrations at a vertical cross section in the reactor (at middle of the aerated region, Figure 3.14) are shown in Figure 4.16. The variations in nitrous oxide concentrations originating from variations in dissolved oxygen concentrations

can be observed. The flow patterns (dead zone and recirculating flow) impact the DO concentrations and thus the local nitrous oxide concentrations.

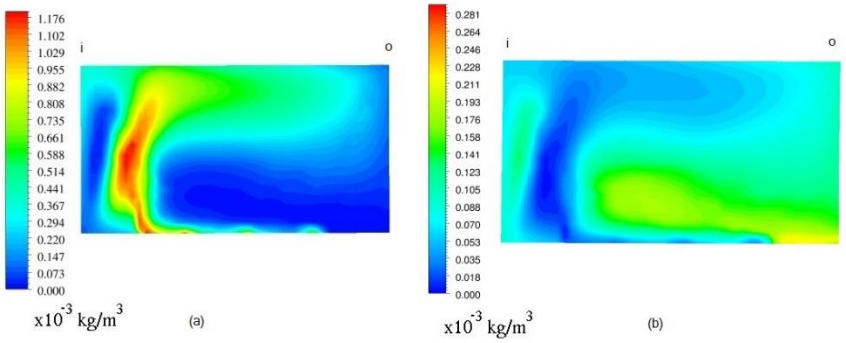

Figure 4.16 (a) The dissolved oxygen and (b) nitrous oxide concentrations at a vertical cross section in the middle of aerated region pf the reactor

Figure 4.15 and Figure 4.16 provide the local variation in the concentrations but in order to get an overall view of the reactor behaviour, concentrations are averaged over different sections in Figure 4.17 (similar to Figure 4.7). The minimum and maximum range bars are shown as well. There is a gradual increase in the N_2O concentrations from inlet (T1) to section T8 followed by a sudden decease in sections T9 and T10. This can be explained by the fact that the formation of the N_2O during heterotrophic denitrification results from reduction of nitric oxide under anoxic conditions using organic substrate as an electron donor. If the organic substrate is in abundance, N_2O under anoxic conditions is reduced into dinitrogen. However, there is a potential for accumulation of N_2O under limiting substrate conditions. Furthermore, in the aerated region there is a decrease in the N_2O concentration for the first part but then there is an increase towards the end part of the aerated region. These findings are similar to the findings by Guo and Vanrolleghem (2014) who performed N_2O off-gas measurements at the Eindhoven WWTP facility.

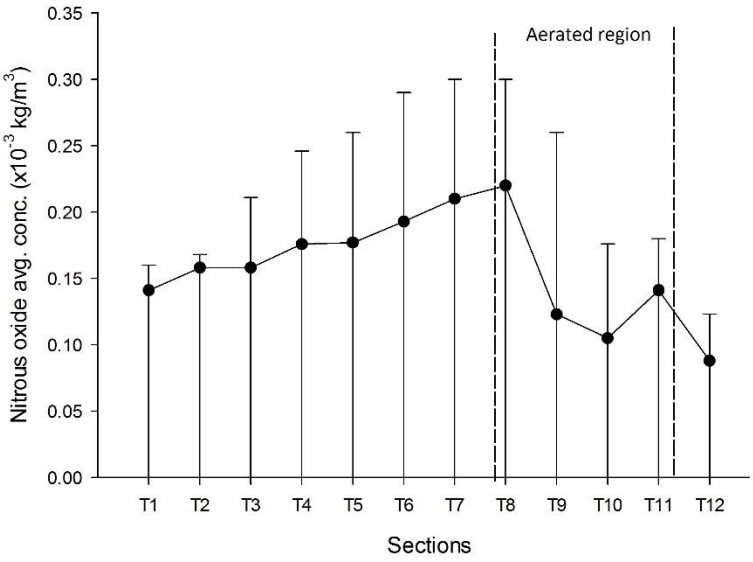

Figure 4.17 Average nitrous oxide concentration in different sections of the reactor for the L-G case

The results from the scenario analysis are provided in Figure 4.18. It shows N_2O concentrations at the vertical cross section in the middle of the aerated region of the reactor (plot location shown in Figure 3.14). It can be seen that with the change in operational conditions, flow patterns change and hence the nitrous oxide concentration as well. It can again be observed that nitrous oxide concentrations are higher where there is a low DO concentration (see Figure 4.8 for the DO).

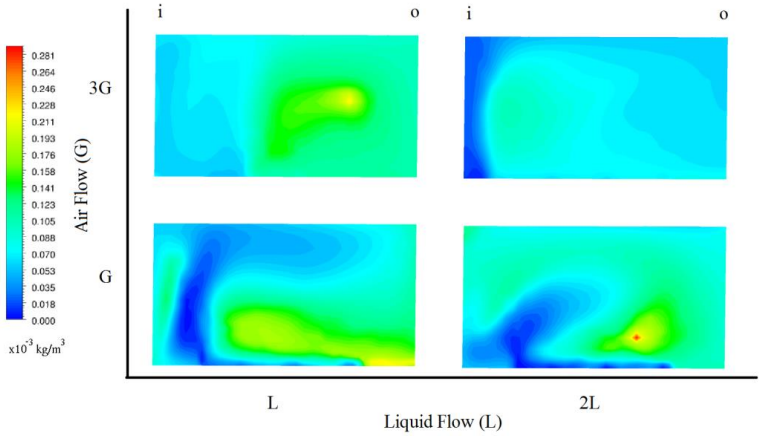

Figure 4.18 Nitrous oxide concentrations in the middle cross section (plot location indicated in Figure 3.12) of the aerated region at different air and liquid flowrates

4.4. General discussion

The impact of these findings on the way systems are currently modelled could be significant depending on the final objective of the modelling study. In general, this study has shown that detailed process design, evaluation and optimization will have to consider the effect of local mixing patterns and their effect on process performance. For instance, aerator design and placement for optimal process performance would benefit from a CFD-ASM model similar to the one developed in this study; conventional process engineering does not address the heterogeneities in the dissolved oxygen and contaminant concentrations caused by different aerator configurations and operational regimes. This potentially leads to suboptimal reactor design. It is therefore recommended to use such models in the design phase instead of using them for troubleshooting after construction.

Similarly, knowledge of local substrate conditions is required in order to make appropriate decisions in terms of sensor location for both process monitoring and control. Aerated zones are commonly perceived as homogeneously mixed; sensor location is thus normally decided upon depending on maintenance and operation convenience. Even though this should still be considered when deciding sensor location, it has been clearly shown that different locations along the width and depth of the reactor will bring about significantly different concentration measurements. Therefore, and depending on how conservative the monitoring and control strategy needs to be, the information shown will be necessary to carry out appropriate sensor placement decisions or account for the impact of location decision on controller performance by accounting for this in the control algorithm. A detailed account of sensor location impact on a controller performance is provided in Chapter 7.

Additionally, the results presented have far-reaching consequences in terms of process evaluation. For instance, phosphorus removal has been widely documented in systems with no anaerobic sections, such as aerobic membrane bioreactors (Rosenberger et al., 2002; Verrecht et al., 2010). The modelling results presented here provide evidence that this could be most probably due to the existence of anaerobic zones in the reactor, even in places supposedly aerated and well mixed. Another example where heterogeneous mixing could be of importance is in simultaneous nitrification-denitrification (SND) processes (and the nitrogen conversion processes taking place at low dissolved oxygen concentrations leading to N_2O production). Even though SND has been largely

attributed to diffusion limitation in flocs (Münch et al., 1996), from the results presented here, it is evident that non-uniform mixing will definitely also play a significant (and maybe even a leading) role.

In general, the previous discussion underlines the fact that an integrated CFD-ASM model approach provides extremely useful and detailed information about system behaviour which can be adopted in process understanding, improved design, optimisation and process evaluation. It is therefore recommended to use this information to revise certain conclusions taken with models that ignore mixing heterogeneity or start using models that better describe the reactor's mixing behaviour by means of e.g. compartmental models which are based on this increased understanding and will be derived for the present full-scale case in Chapter 6.

4.5. Conclusions

In the present study integrated hydrodynamic-biokinetic models (ASM1 and ASMG1) have been developed to describe the aerated compartment of a full-scale wastewater treatment plant. The model incorporates the detailed oxygen mass transfer using constant bubble size and local gas holdup. The model also takes into account local density variations as a function of local suspended solids concentrations. It was found that density has a significant impact (10-15% improvement in velocity predictions) on the hydrodynamics of the bioreactor. Furthermore:

- Regions of bad mixing resulting in non-uniform substrate (e.g. ammonium) and electron acceptor (e.g. dissolved oxygen) concentrations were shown to exist in areas commonly assumed to be aerated and well-mixed.
- The effects of changing influent and air flowrates on the substrate and electron acceptor distributions have been investigated. It was observed that a single tanks-in-series mixing model would not suffice for dynamic operational conditions and there would be a potential need for recalibration of e.g. half-saturation indices for TIS-based biokinetic models when moving from dry to wet weather conditions.
- The impact of sensor location on the corresponding measurements was evaluated and quantified; it was observed that the reliability of sensor measurement changed with the variation in the operational conditions.

- The CFD-ASMG1 modelling depicted the spatial variation in N_2O production due to variations in the local DO concentrations and also showed the impact of change in operational conditions leading to variations in N_2O production.

Therefore, the presented findings can have far-reaching consequences in the terms of optimal sensor location, control system design and process evaluation.

Chapter 5

Hydrodynamic-biokinetic model integration applied to an oxidation ditch WWTP

This chapter describes the CFD-biokinetic modelling of a full scale oxidation ditch located in La Bisbal d'Empordà (Spain).

5.1. Introduction

The oxidation ditch process is a widely used wastewater treatment technology. An oxidation ditch is a kind of artificial closed-loop channel, in which the wastewater is driven by the impellers of mechanical aerators. The impellers are intended to keep the wastewater mixed with activated sludge and introduce dissolved oxygen for the biological treatment. However, with the presence of the channel bend, the flow patterns in an oxidation ditch are complex and the distribution of the velocity is inhomogeneous (Yang et al., 2010). Thus, areas with a low velocity may exist and cause the activated sludge to settle in these regions, which will deteriorate the performance of the oxidation ditch process. The aerators are operating at the surface and there is a possibility of low dissolved oxygen regions (especially near the bottom of the tank) not only due to hydrodynamics but also due to operational limitations of the surface aerators. As a result, it is very important to understand the flow patterns and hydrodynamic characteristics and their impact on the system performance in terms of substrate concentrations in the operation and optimisation of oxidation ditches.

Current WWTP models, following the TIS approach, are unable to model these operational limitations and hence are unable to estimate their impact on the system performance (as discussed in chapter 2). In contrast, Computational fluid dynamics (CFD) is a tool which can be useful to investigate the complex flow in such bioreactors

(Glover et al., 2006). Previously, few CFD studies of oxidation ditches have been performed. Littleton et al. (2007) applied a three-dimensional fluid dynamic model for a rotor disc test tank and a full-scale oxidation ditch to investigate fluid flow features using momentum source calculated from the measured flow velocity in the oxidation ditch. Luo et al. (2005) used a 3D standard k - ε turbulence model and the moving mesh approach to simulate the motion of the brush aerators and their interaction with the fluid in a small-scale ditch. Fan et al. (2010) simulated the 3D solid–liquid two-phase flow field in a laboratory-scale oxidation ditch aerated with surface aerators using the multiple rotating reference frame approach (MRF) and the standard k-ε turbulence model. Yang et al. (2010) predicted the flow field in a full-scale carrousel oxidation ditch with the 3D standard k-ε turbulence model and a modified moving mesh approach. Jiang et al. (2010) proposed a momentum source term approach, only based on dimensions and the rotational velocity of aerators, to calculate the flow field in a full scale carrousel oxidation ditch. Even though these previous studies provide an account for the application of CFD modelling in oxidation ditches, still it will take some time for CFD to be used as a mainstream modelling tool.

All these previous studies have been stressing upon the need of detailed hydrodynamic modelling. However, biokinetic modelling along with the detailed CFD modelling has not been performed until now. Therefore, in the current study CFD-biokinetic modelling is performed on a full scale oxidation ditch WWTP to extend on the current state of the art in the open literature. As explained earlier in chapter 4, a two-step procedure is followed. First, the hydrodynamic modelling is performed and then on top of it a biokinetic model is integrated. The objective is to successfully model the local hydrodynamics and evaluate its impact on the biological process performance of the reactor under different operational conditions.

5.2. Material and methods

5.2.1. Configuration of the La Bisbal d'Empordà WWTP

The WWTP in La Bisbal d'Empordà (Spain) is used as a case study. The WWTP treats wastewater from the villages of La Bisbal d'Empordà, Corçà, Cruïlles, Monells, Sant Sadurní d'Heura, Forallac (Vulpellac) and Casavells. It has an average influent flow rate of 3,225 m^3/day. The WWTP consists of primary and secondary treatment steps

and a plant overview is given in Figure 5.1. The primary treatment consists of a coarse screen, a fine screen, a grit chamber-oil trap, a homogenisation tank with prolonged aeration and a sieve. The secondary treatment includes a biological reactor, an MBR (membrane bioreactor) and a secondary settler.

This plant is considered a hybrid or dual configuration plant, due to the use of a biological treatment with MBR technology and a secondary settler. In the secondary treatment, the biological reactor (carrousel type) pumps the water flow to the membrane tank. When the influent is more than 3225 m^3/day, the exceeding flow (bypassing the biological reactor) is treated with the secondary settler which can treat 3000 m^3/d.

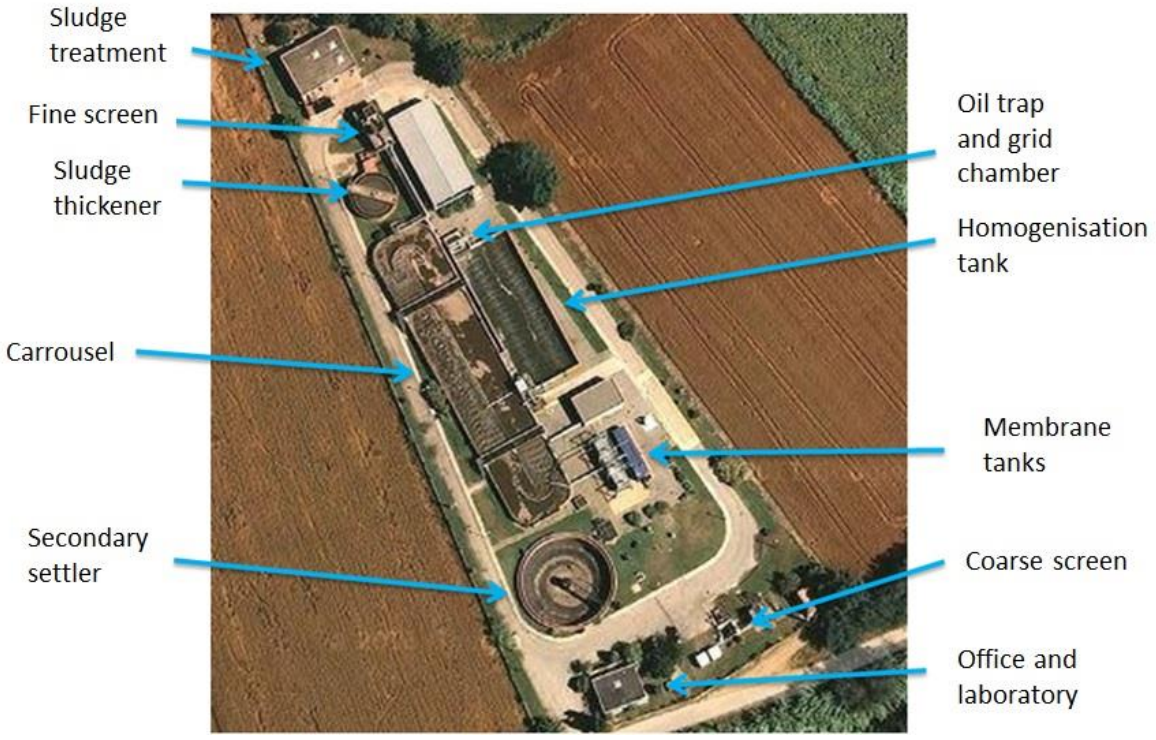

Figure 5.1 La Bisbal d'Empordà WWTP overview

In the present study, only the biological reactor of the WWTP is modelled. The reactor under study is a carrousel type oxidation ditch installed with surface aerators (rotors). The layout of the reactor is shown in Figure 5.2. It is 70m long, 14m wide and 4m deep. It has three inlet streams, i.e. one for the influent and two for the recycle streams from the MBR and secondary settler, respectively. It has an outgoing stream going to the MBR. There is a wall in the middle along the length of the reactor and two curved walls on either ends of the reactor to direct the flow in the carrousel. It must be noted that the

direction of the flow is clockwise as indicated in Figure 5.2 with the help of arrows. There are four submerged surface aerators (R1, R2, R3 & R4) installed in the reactor and their locations are shown in Figure 5.2. The aerators are brush type aerators which are each 6m long with a diameter of 1.2m. The surface aerators are the source of oxygen and also provide mechanical energy to maintain the sludge flow and avoid potential sludge settling. Therefore, the function of the surface aerators is very important for the performance of the bioreactor. However, operating all the aerators at all times results in high operational costs. Currently, only two aerators are used during the day (when electricity cost is high) and all four are only used at night (when electricity cost is low). This strategy reduces the operational costs, but the performance of the bioreactor is somehow compromised. Hence it is important to evaluate the performance of the reactor under both conditions.

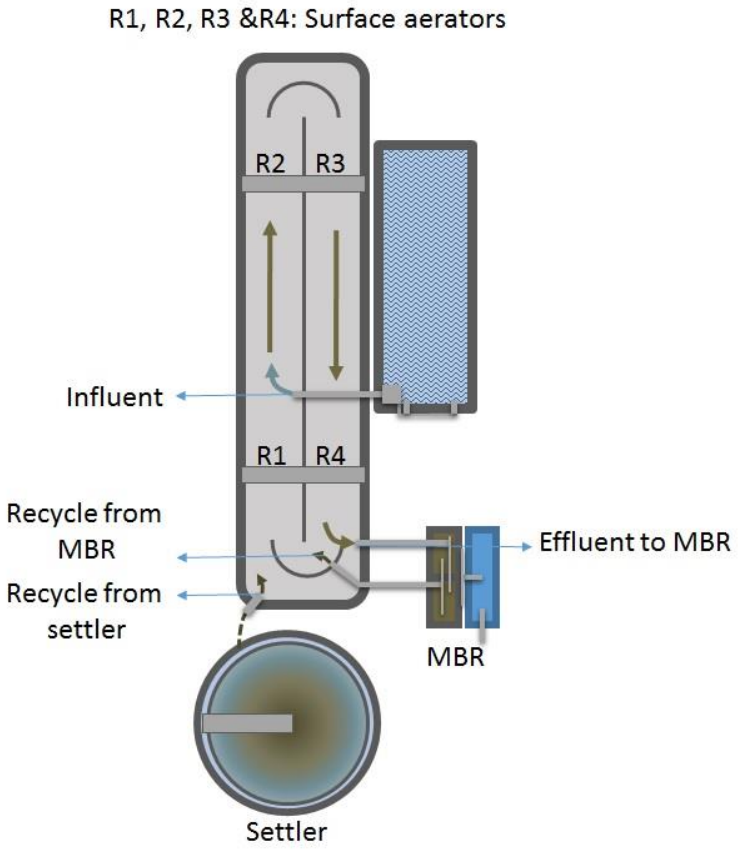

Figure 5.2 Configuration of the oxidation ditch bioreactor (La Bisbal, Spain)

5.2.2. Measurements

Flow measurements were performed for the validation of the hydrodynamic model of the reactor. It must be noted that all the measurements were performed during day time, thus when only two rotors were in operation. These measurements were performed using a simple flow measuring device (MC20, PCE inst., USA). Velocities were measured at a location 2 meters downstream of the rotor R2 (indicated in Figure 5.3). This location is chosen due to the ease of access. The measurements were performed at 7 points across the width and at 3 points along the depth (i.e. at the surface, 1m deep and 2m deep) of the reactor, totalling 21 measurement points. Each measurement was performed for 2-3 minutes and was repeated 3 times. The average standard deviation in the measurements was ± 0.01m/s. The results of these measurements are provided in section 5.3.1.

Dissolved oxygen measurements were also performed using a DO probe (497ADO, Emerson, USA) at two different locations i.e. 2m downstream from R2 (same as velocity measurements) and R4 (Figure 5.3). These measurements were performed primarily to calibrate the oxygen flux coming into the reactor due to surface aerators. These measurements were performed at three points across the width but only at 1m depth due to practical limitations. Again, the measurements were time averaged and repeated 3 times.

5.2.3. Simulation scenarios

Two scenarios i.e. with two and four operational rotors are simulated. It is assumed that the plant is operating at average influent rate and hence the recycle from the settler is turned off.

5.2.4. Computational fluid dynamic modelling

The stepwise approach provided in chapter 2 is followed to perform the CFD modelling of the reactor.

5.2.4.1. Geometry development

In the first step a 3-dimensional geometrical model of the reactor is developed taking into account all the necessary details. The developed 3D model is shown in Figure 5.3.

The size and location of the inlets, outlets and surface aerators are based on the exact dimensions of the reactor and can be seen in Figure 5.3. The outlet is divided into three because effluent is pumped to the MBR using three separate pumps. The surface aerators (rotors) are named individually R1, R2, R3 and R4 for reference. Moreover, CW1 and CW2 are the two curved walls at either end of the reactor and shall be used for reference during the discussion. Similarly, the wall in the middle will also be used in the discussion and hence will be referred as middle wall. Additionally, the red arrows show the direction of flow in the reactor.

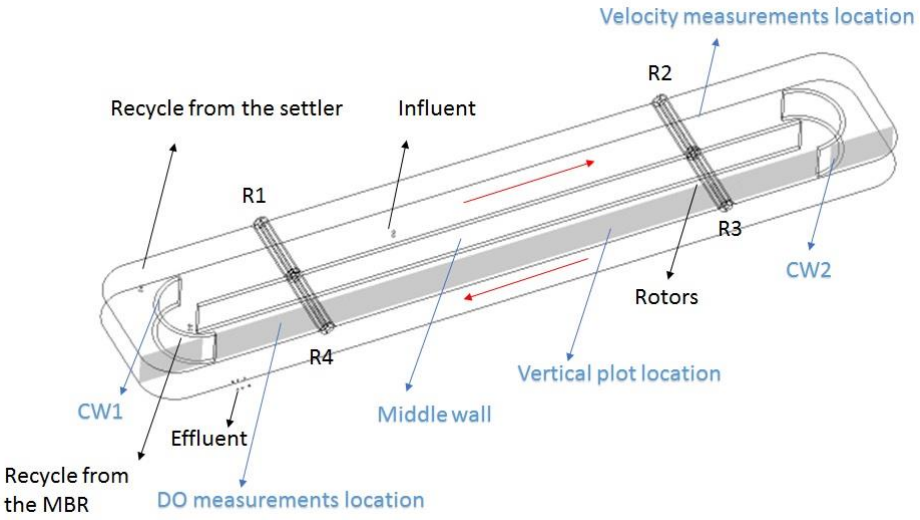

Figure 5.3 The 3-dimensional geometrical model of the oxidation ditch reactor (blue coloured text introduces terminology to be used in the results & discussion section)

The four surface aerators are simply modelled as long thin cylinders with a hollow core mimicking the shaft of the rotors. The modelling of rotors is illustrated in Figure 5.4. The inner diameter is the size of the shaft and the outer diameter is the size of the blades. The individual rotor blades are not modelled but it is assumed that the rotor acts merely as a source of extra momentum. Hence, the rotor is divided equally into four segments (across the cross-section) to implement a tangential momentum source in each segment of the rotor to mimic the real rotor behaviour.

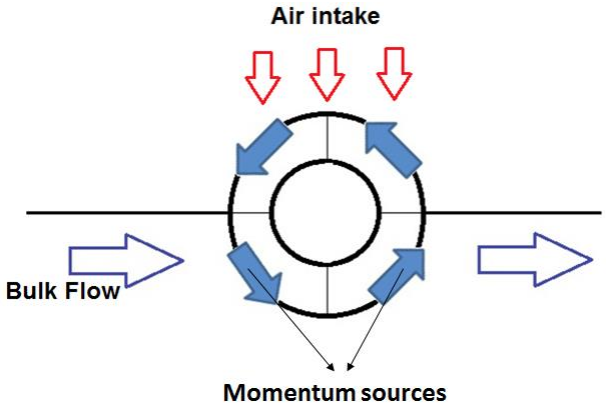

Figure 5.4 Illustration of the rotor modelling

5.2.4.2. Meshing

In the next step detailed meshing of the reactor is performed. Two separate meshes are generated for the two operating conditions i.e. 2-rotors and 4-rotors. In the 2-rotors case, the rotors R2 and R4 are operating. The 4-rotor mesh consists of 0.8 million cells, whereas, the 2-rotor mesh consists of 0.61 million cells. The mesh is kept fine in specific areas (such as near the rotors and inlet and outlet boundaries) where high gradients of pressure and velocity are expected. The resulting meshes for both the cases can be seen in Figure 5.5 and Figure 5.6. The only difference between both meshes is that in the 2-rotor mesh, two non-functioning rotors (R1 & R3) are not modelled and only their half immersed shaft is modelled (which acts as a wall).

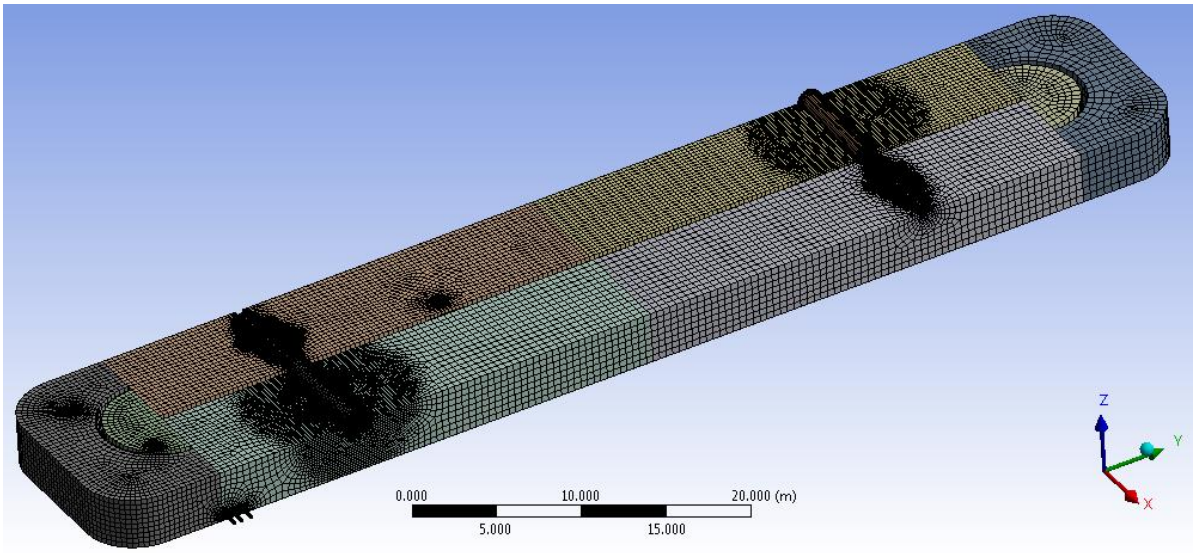

Figure 5.5 The 2-rotor mesh of the oxidation ditch

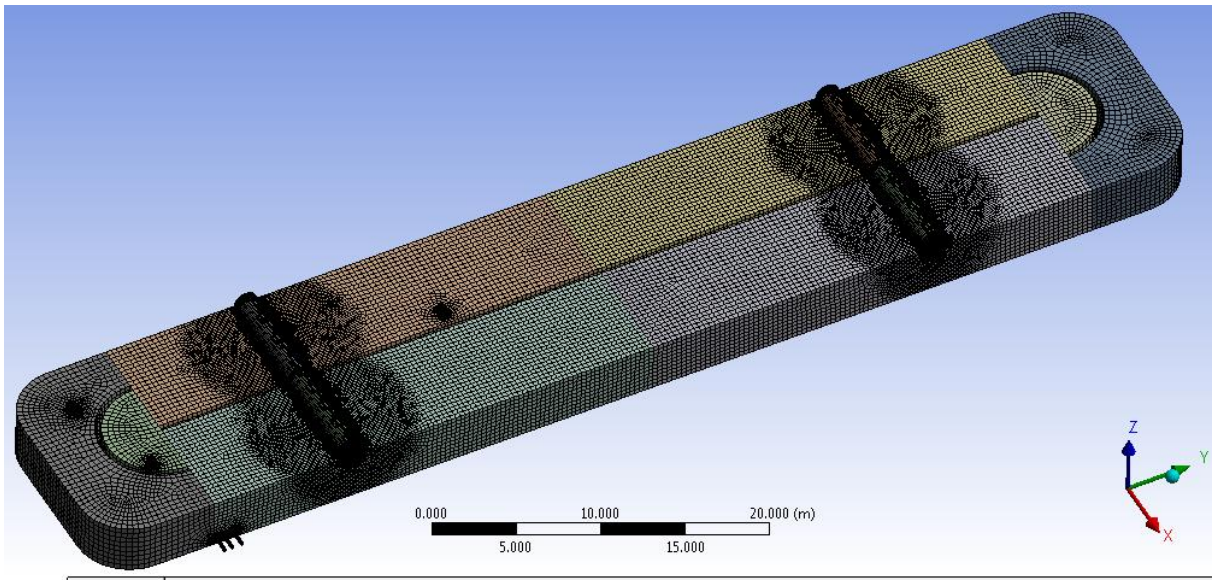

Figure 5.6 The 4-rotor mesh of the oxidation ditch

5.2.4.3. Boundary conditions

In the next step the boundary conditions are characterized and calculated for the system. As mentioned earlier, there are three inlets (i.e. influent, MBR recycle & settler recycle) and three outlets all going to the MBR. The top of the reactor is a free surface (i.e. not covered). The remainder of the surfaces are the physical bounds of the reactor.

The flow coming through influent and the MBR recycle stream is known therefore, it is set with the *'velocity inlet'* boundary condition. The settler recycle is turned off therefore it is set with the *'wall'* boundary condition type. The flow going out of the system through effluent streams is set with the *'outflow'* boundary condition type. The top surface of the reactor is set with the *'symmetry'* boundary condition to mimic a physical bound but with no wall friction. However, the tops of all the rotors are set with the *'wall'* boundary condition to be able to define the oxygen flux through it. This assumption is safe as top surface of the rotors does not impact the hydrodynamics of the system. The remaining boundaries are defined as *'wall'* boundary condition type.

The two inlet boundary conditions for the influent and the MBR recycle stream are calculated based on the average flow rate data. The average influent flow rate is chosen to be 3225 m^3/d and the MBR recycle flow rate to be 2995 m^3/d.

5.2.4.4. Flow modelling and other considerations

In this study only steady state simulations are performed bearing in mind that the biokinetic model will subsequently be integrated and, hence, in that case transient modelling would be highly computationally intensive. The flow inside the reactor is multiphase due to the presence of solids (biomass) in the liquid. However, in this study single phase (only liquid) modelling is performed to keep the computational demands as low as possible. The impact of solids concentrations on the flow is taken into account using a similar approach used in the chapter 4 (equation 4.5) by modelling density as a function of total suspended solids fraction. However, the detailed modelling of solids is not performed here.

Due to the presence of surface aerators, the flow inside the reactor is turbulent. Therefore, there is a need of a suitable turbulence model to model the flow as realistically as possible. In this case, the standard k-ε model is used which is a suitable model for high turbulent flows. It solves two extra transport equations (i.e. for turbulent kinetic energy and turbulent dissipation) in addition to continuity and momentum conservation equations (Versteeg and Malalasekera, 2007). The standard wall functions are used to model the near-wall regions and the second order upwind scheme is used for spatial discretization. The convergence criterion is set to be of the order of 10^{-4} for all the flow variables (i.e. continuity, momentum, turbulent kinetic energy and turbulent dissipation). The solution time for the hydrodynamic modelling of the 4-rotor case was approximately 4-5 hours using 4 parallel processers. However, the solution time reduced to 3-4 hours for the 2-rotor case (due to less number of cells in the mesh).

5.2.5. Biokinetic modelling

Given the objective to predict aerobic carbon and nitrogen removal, the hydrodynamic model is extended with a biokinetic model, i.e. the well-established Activated Sludge Model No. 1 (ASM1) (Henze et al., 2000, 1987). This integration is performed by adding 13 user defined scalars (UDS) representing each of the 13 components in the ASM1 model (similar to chapter 4). FLUENT solves 13 transport equations for these UDS. Each transport equation for a scalar ∅ can generally be written as

$$\frac{\partial \alpha_l \rho_l \emptyset_l^k}{\partial t} + \nabla.\left(\alpha_l \rho_l \vec{u}_l \emptyset_l^k - \alpha_l \Gamma_l^k \nabla \emptyset_l^k\right) = S_l^k \quad k = 1, \ldots, N \qquad \textbf{5.1}$$

The composition of the influent and the MBR recycle stream is taken from the plant data and is tabulated in Table 5.1 in ASM1 component form. However, the complete composition for the MBR recycle stream was unavailable. Only ammonium and nitrate concentrations were known and, therefore, the rest of the components are assumed based on the expert judgement, such that, the soluble and particulate substrates (S_S and X_S) are almost depleted and the biomass ($X_{B,H}$ and $X_{B,A}$) grow after passing through the MBR.

Table 5.1 The influent and MBR recycle stream composition

	ASM1 components	Influent (mg/L)	MBR recycle (mg/L)
1	S_I	30.8	30.8
2	S_S	75.01	1
3	X_I	684.9	1000
4	X_S	119.3	40
5	$X_{B,H}$	23.8	900
6	$X_{B,A}$	10.1	95
7	X_P	0	0
8	S_O	0	0
9	S_{NO}	2.7	3.6
10	S_{NH}	18.4	4.5
11	S_{ND}	0.4	0.4
12	X_{ND}	4	4

The oxygen intake due to surface aeration is modelled by defining a boundary flux of the oxygen scalar at the top surface of the rotors (as shown in the Figure 5.4). The flux of oxygen taken up by the rotors is difficult to measure therefore it is calibrated based on the downstream dissolved oxygen concentration measurements as mentioned in section 5.2.2. In order to implement the oxygen flux boundary condition, it is assumed that all the rotors are providing the same amount of oxygen and oxygen flux is uniformly distributed at the top surface of the rotors (i.e. oxygen intake is uniformly distributed). Therefore, instead of calibrating point to point (3 measurements) of the downstream oxygen with the measured DO, the average DO value is used. The results for this calibration are provided in Table 5.2. Initially, a "guess" of 1kg/s of oxygen flux was used to start comparing the simulated DO values with the measured DO values.

It resulted in very high DO concentrations (almost saturated) after which the flux was reduced gradually until the simulated DO values reached a magnitude in the order of the measured DO values (less than 1 mg/L). The results for different oxygen fluxes around the final calibrated value are presented in Table 5.2. It can be observed that the oxygen flux of 0.035 kg/s yields the best result with the minimum average difference (6.06%) between the measurements and the CFD dissolved oxygen values. Therefore, for all the simulations the oxygen flux of 0.035 kg/s is used as a boundary value for all the rotors.

Table 5.2 The oxygen flux calibration for the rotors

Oxygen Flux (kg/s)	Avg. DO measurement at R2 (mg/L)	Avg. DO CFD value at R2 (mg/L)	Avg. DO measurement at R4 (mg/L)	Avg. DO CFD value at R4 (mg/L)	Percent Difference
0.02	0.7	0.42	0.62	0.37	40.15
0.025	0.7	0.54	0.62	0.45	25
0.03	0.7	0.58	0.62	0.50	18.18
0.035	0.7	0.67	0.62	0.57	6.06
0.04	0.7	0.75	0.62	0.68	-8.33
0.045	0.7	0.86	0.62	0.77	-22.48

5.3. Results and discussion

5.3.1. Comparison between the velocity measurements and the CFD

In Figure 5.7 the comparison between measured velocities and the velocities predicted by the CFD modelling is presented. It can be seen that the velocities predicted by the CFD near the surface are in good agreement with the measured velocities. However, the velocities at 1m and 2m depths are predicted lower than the measured velocities. This difference could be due to the approximation method used for modelling the rotors and thus can be improved by more detailed modelling of the rotors. Moreover, impact of the solids concentration was taken into account by modelling density as a function of total suspended solids. However, detailed modelling of solids transport is needed to accurately model the potential sludge settling behaviour and hence it will improve the hydrodynamic predictions.

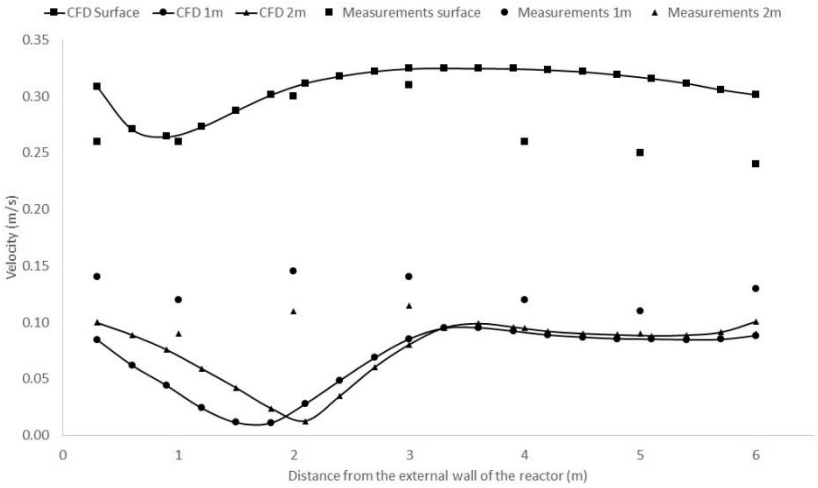

Figure 5.7 Comparison between the velocity measurements and the velocities predicted by the CFD (average standard deviation is ± 0.01m/s)

5.3.2. Hydrodynamic results

The hydrodynamic results for both the cases (i.e. 2-rotor and 4-rotor) are presented below separately.

5.3.2.1. The 2-rotor case

The velocity contour plots for the 2-rotor case in horizontal cross-sections at different depths (near the top, middle & bottom) in the reactor are shown in Figure 5.8. It must be noted that the flow is in clockwise direction in the carrousel. The impact of the rotors on the flow behaviour of the reactor is clearly visible in these plots. As expected, in Figure 5.8a higher velocities are observed in the vicinity of the rotors. However, regions of low velocity are also visible near the middle wall and in the corners of the reactor behind the curved walls (CW1 & CW2). This can be explained by looking at the velocity vector plots at these locations in Figure 5.9. The latter shows velocity vector plots in the horizontal cross-section near the top surface in the vicinity of the curved wall (CW1). It can be seen that two swirls are formed, one along the middle wall and one behind the curved wall in the corner. Both of these swirls are formed due to boundary layer detachment phenomena. These swirls are causing the low velocity regions observed in Figure 5.8.

Figure 5.8b & c show that the velocity profile changes along the depth of the reactor. It can be observed that the regions next to the rotors which have high velocity near the

top (Figure 5.8a), have low velocity near the bottom of the reactor (Figure 5.8c). This can be explained by looking at the velocity vector plots in the vertical sidewise cross section of the reactor in Figure 5.10. Here, it can be observed that a swirl is formed near the bottom which is causing the low velocities in Figure 5.8. It is the fluid moving at a higher velocity near the top surface that causes a region of low pressure and, hence, draws the fluid at bottom upwards leading to the formation of a swirl.

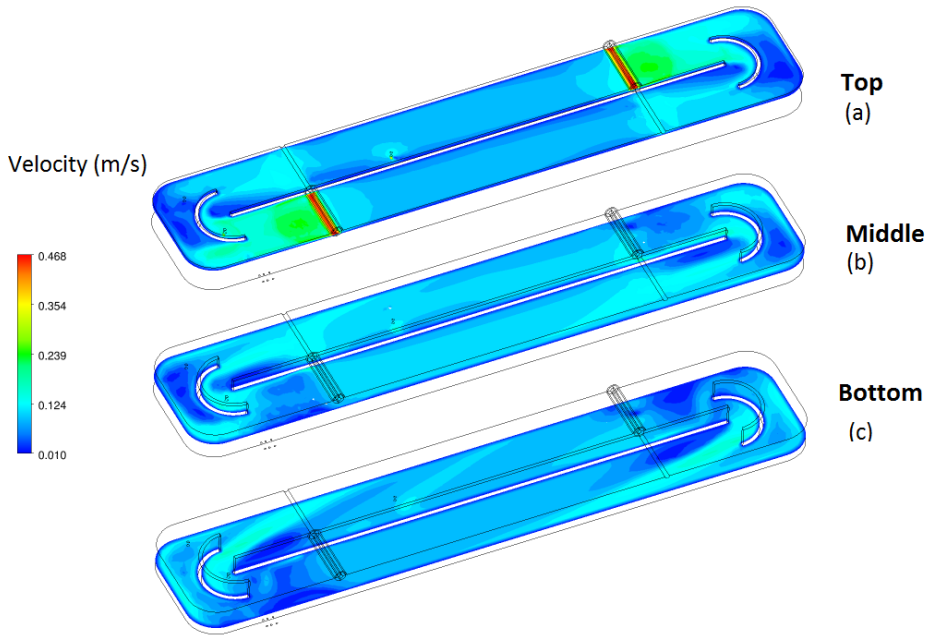

Figure 5.8 Velocity contour plot near (a) the top, (b) middle and (c) bottom of the reactor for the 2-rotor case

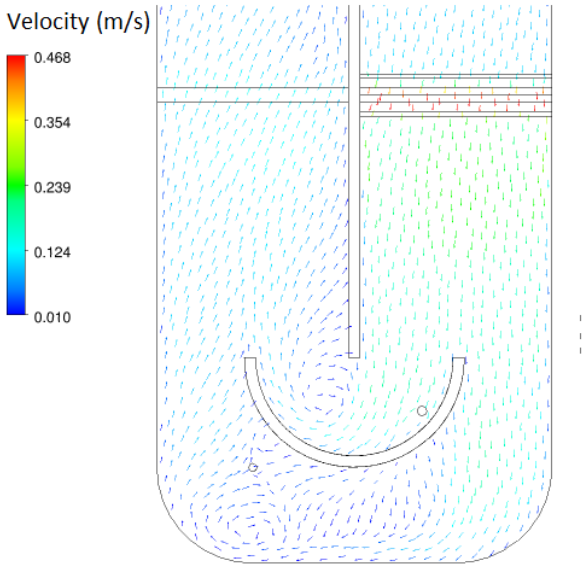

Figure 5.9 Velocity vector plots near the top surface of the reactor for the 2-rotor case

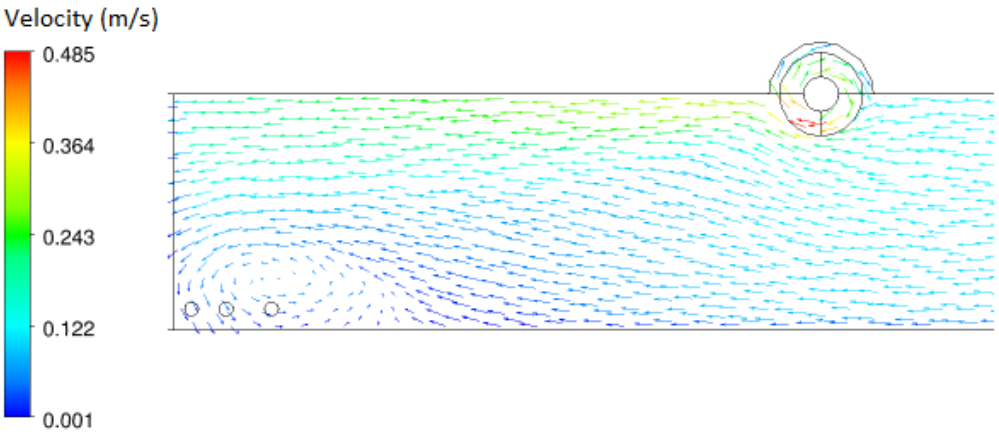

Figure 5.10 Velocity vector plot in the sidewise vertical cross-section of the reactor near the R4 rotor (plot location is shown in Figure 5.3)

5.3.2.2. The 4-rotor case

Similarly, the velocity plots for the 4-rotor case at different depths are shown in Figure 5.11. The impact of operating four rotors on the flow behaviour can be observed. The velocities in the reactor are higher in comparison to the 2-rotor case. However, the regions with low velocities can still be seen in Figure 5.11 due to the swirls being

formed near the middle wall and in the corners of the reactor. The velocity profile changing along the depth can also be observed.

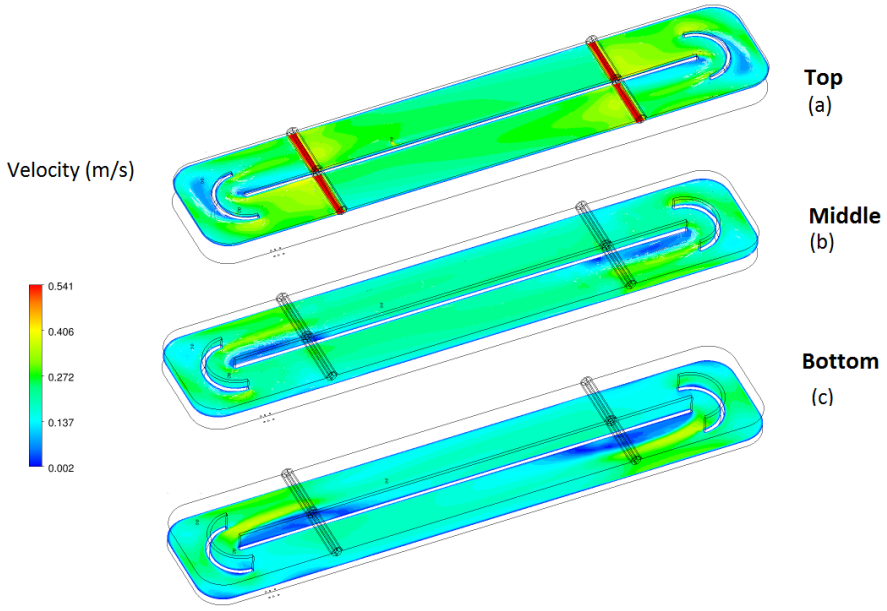

Figure 5.11 Velocity contour plot near (a) the top, (b) middle and (c) bottom of the reactor for the 4-rotor case

The impact of operating two or four rotors on the average velocities at different depths is summarized in Figure 5.12. In this figure, the velocities at different depths shown in Figure 5.8 & Figure 5.11 are averaged. It shows that the average velocities for the four rotor case are almost twice as high compared to the two rotor case. These are important operational differences that are usually not taken into account while modelling such systems using a TIS modelling approach.

Figure 5.12 Comparison of average velocities at different depths for 2-rotor and 4-rotor cases

The hydrodynamic CFD model showed the local flow variations and poor mixing regions in the reactor. It is observed that there are regions of low velocity in the corners and bends of the reactor. Due to the fact that the aerators are operating at the surface, low velocities are observed near the bottom of the reactor. The impact on the flow of operating four rotors is also observed as higher velocities exist compared to the two rotor strategy. However, the four rotor strategy does not entirely overcome the poor mixing zones, i.e. flow near the bends and in the corners. The liquid near the bottom still flows at a lower velocity compared to the top surface which 4-rotors strategy was intended to overcome. These flow variations are important to take into account while modelling such systems.

5.3.3. CFD-biokinetic modelling results

5.3.3.1. The 2-rotor case

Dissolved oxygen (DO) concentration plots at different depths of the reactor are presented in Figure 5.13. It can be observed that the DO levels vary across the reactor between 0.05 and 1.08 mg/L. Higher DO levels are observed in the regions next to the rotors in Figure 5.13a. However, the DO level decreases in the regions away from the rotors. Figure 5.13a shows that the DO level is higher near the top surface of the reactor. However, Figure 5.13b & c clearly demonstrate the decrease in DO level in the middle and near the bottom of the reactor as expected, but now quantified.

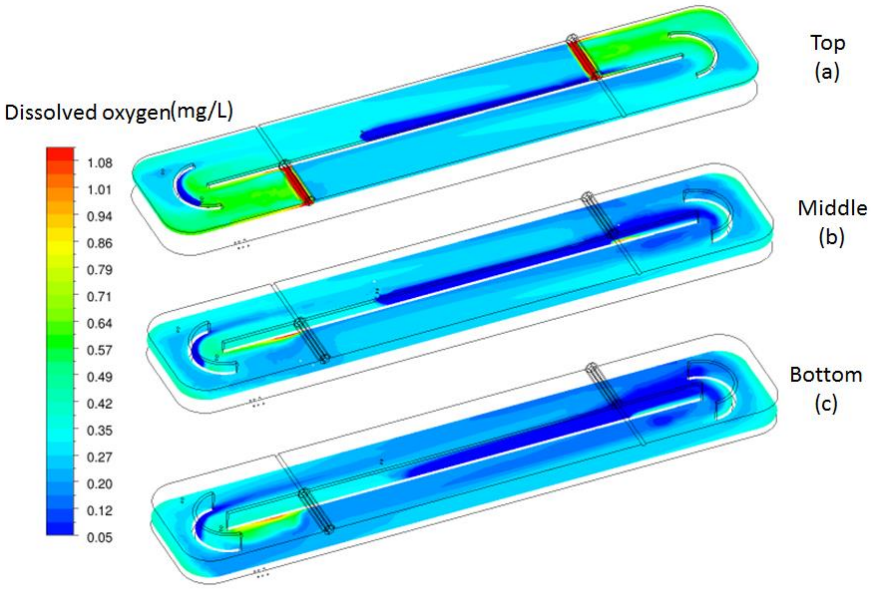

Figure 5.13 Dissolved oxygen concentration plots near (a) the top, (b) middle and (c) bottom of the reactor for the 2-rotor case

The ammonium concentrations at different depths are presented in Figure 5.14. The ammonium concentrations vary between 5.21 and 9.17 mg/L and it must be noted that blue colour does not really show good conversions as it is still high i.e. 5.21 mg/L. These variations are due to the hydrodynamics of the reactor and the local (un)availability of dissolved oxygen. In Figure 5.14a, it can be observed that the ammonium concentrations are higher (almost 9.1 mg/L) near the middle wall and lower in the rest of the reactor (almost 5.2 mg/L). This is because the influent flow is introduced from the top, near the middle wall (see Figure 5.3 for exact location of the influent) and then it flows in the direction of the flow. It can be observed that it is pushed towards the middle wall due to the bulk flow and does not flow behind the curved wall (CW2). However, after the bend it spreads due to the swirl behind the middle wall (see Figure 5.9 for the swirl formation). Similarly, in Figure 5.14b & c, the ammonium is higher near the middle wall before the bend and then it spreads after the bend. Moreover, it can be observed that ammonium after the bend spreads more uniformly near the bottom as compared to the top surface.

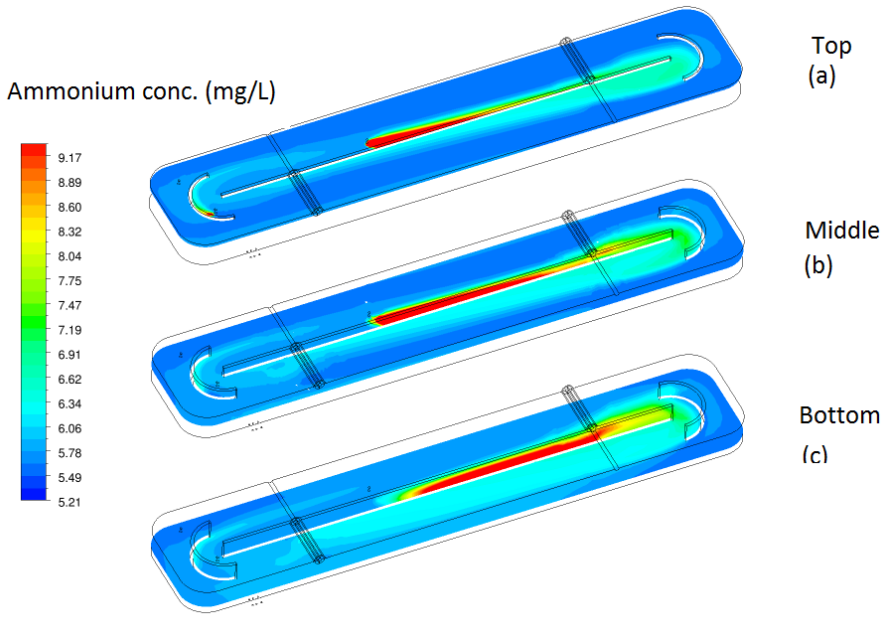

Figure 5.14 Ammonium concentration plots near the top (a), middle (b) and bottom (c) of the reactor for the 2-rotor case

Figure 5.15 shows the DO and ammonium concentrations at a vertical sidewise cross section of the reactor (plot location is shown in the Figure 5.3). The empty spaces in the plots are due to the presence of curved walls on either sides of the reactor. As observed in Figure 5.13 and here in Figure 5.15a as well, the DO concentration is low behind both the curved walls due to the formation of swirls. The impact of the rotor is also clearly visible as the DO concentration is higher near the top (almost 1.08 mg/L) and lower near the bottom (0.05 mg/L) in the vicinity of the rotor. Figure 5.15b shows the ammonium concentration being higher at the bottom which can be explained by the presence of low DO concentration at the bottom. The ammonium concentrations behind the curved wall (CW2) is lower compared to bulk because ammonium does not flow directly behind the curved wall (as seen in Figure 5.14). These results show that there is a non-uniformity in the concentrations of both dissolved oxygen and ammonium. These variations are higher in the vicinity of the rotors. The impact of the geometrical configuration (corners and bends) and operational limitations of the surface aerators in the reactor is also visible on the concentrations.

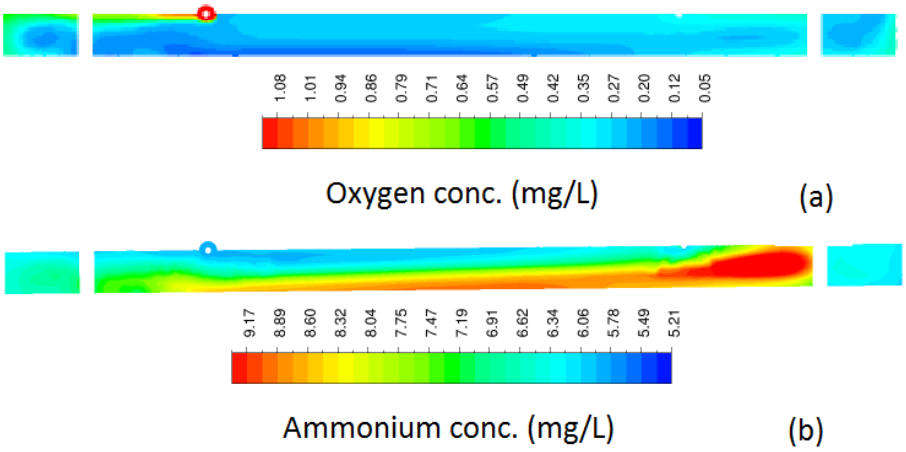

Figure 5.15 (a) The dissolved oxygen and (b) ammonium concentrations at a vertical sidewise cross section of the reactor for the 2-rotor case (plot location is shown in Figure 5.3)

5.3.3.2. The 4-rotor case

The DO and ammonium concentrations for the 4-rotor case in the horizontal cross section at different depths are shown in Figure 5.16 and Figure 5.17 respectively. The impact of operating all the rotors on the DO concentrations is visible, as the higher DO levels can be observed compared to the 2-rotor case in Figure 5.16. However, still there are areas with low DO concentrations due to the swirls near the bends. Similar to the 2-rotor case the DO concentrations are higher near the top surface and lower near the bottom. Figure 5.17 shows the ammonium concentrations indicating that the ammonium concentration patterns are similar to the patterns observed in the 2-rotor case. However, the ammonium concentrations are overall lower and vary between 2.16 and 5.9 mg/L which are still high (effluent ammonium concentration should be below 2-3 mg/L).

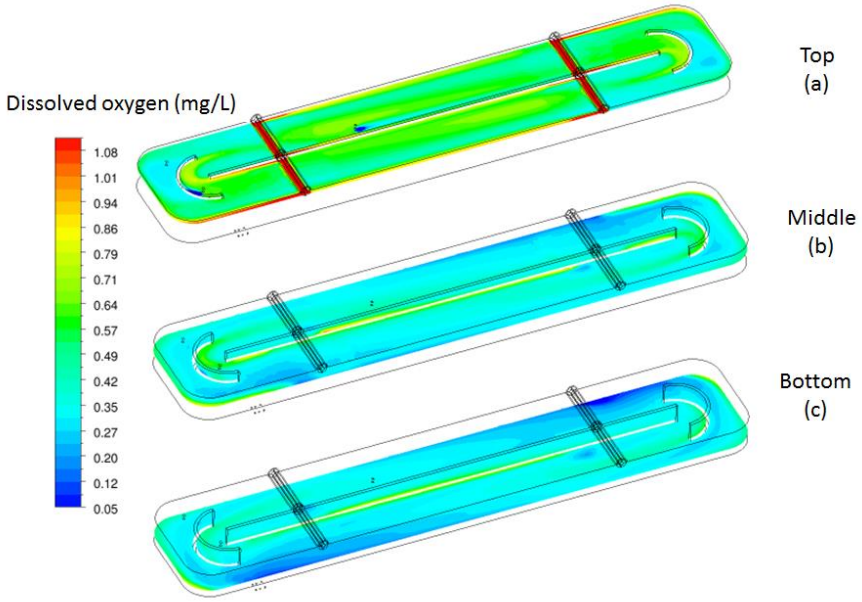

Figure 5.16 Dissolved oxygen concentration plots near (a) the top, (b) middle and (c) bottom of the reactor for the 4-rotor case

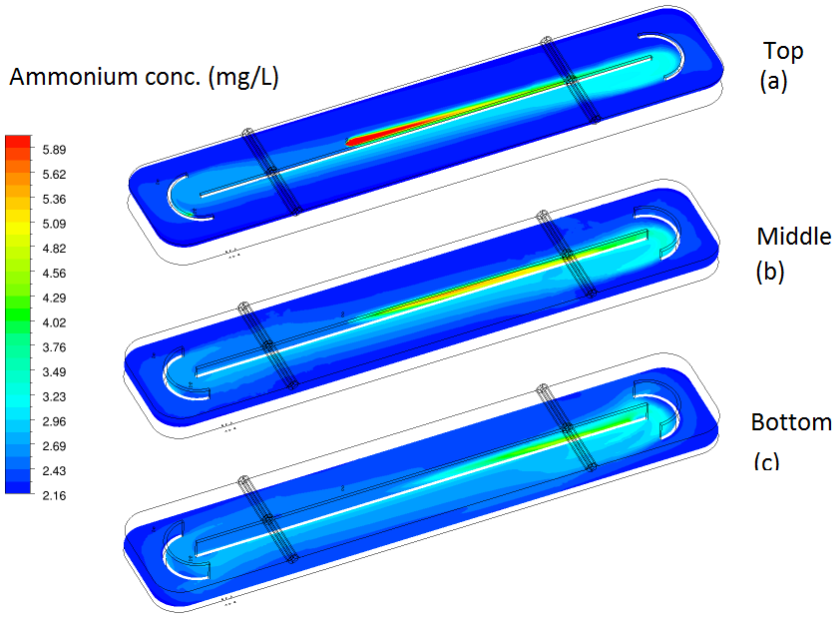

Figure 5.17 Ammonium concentration plots near (a) the top, (b) middle and (c) bottom of the reactor for the 4-rotor case

Similar to Figure 5.15, the dissolved oxygen and ammonium concentrations plots are presented in a vertical sidewise cross section of the reactor in Figure 5.18. As observed earlier in Figure 5.16, the DO is higher at the surface and lower near the bottom. Due

to the 4-rotor operation, higher DO can be observed in the region in between the rotors in the Figure 5.18a. As a consequence, the ammonium at the surface is lower and higher near the bottom in Figure 5.18b. This points out the impact of operational limitations of the surface aerators due to inadequate dissolved oxygen concentrations near the bottom and indicates that most of the bottom section is (near) anoxic.

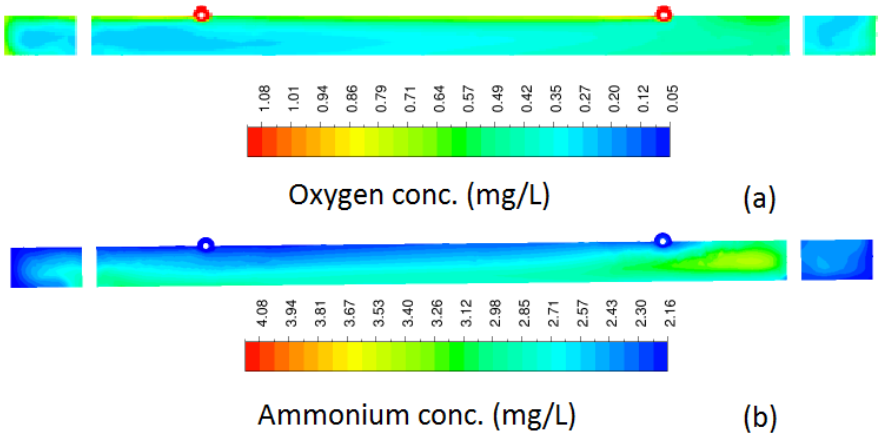

Figure 5.18 (a) The dissolved oxygen and (b) ammonium concentrations at a vertical sidewise cross section of the reactor for the 4-rotor case (plot location is shown in Figure 5.3)

The impact of the hydrodynamic results is also visible on the biokinetic results in terms of oxygen and ammonium concentrations. It is observed that there are regions of low oxygen concentrations near the bends and corners of the reactor. The low oxygen concentrations are observed near the bottom which impacts the ammonium concentrations. The bottom regions of the oxidation ditch are near anoxic even close to the rotors and this will be quantified in the chapter 6.

If the TIS modelling approach is implemented, it would not be able to consider these limitations. Hence, the TIS model will predict higher ammonium removal and thus modellers may need to calibrate the K-values to represent the reactors actual behaviour.

5.4. Conclusions

A detailed hydrodynamic model of an oxidation ditch is presented in this chapter. The poor mixing regions and operational limitation of surface aerators is observed. The ASM1 model is then integrated on top of the hydrodynamic model. It is observed that the poor mixing regions and operational limitations lead to non-uniform distribution of

substrates and, hence, negatively impact the system performance. Furthermore, the implications of using two and four rotor strategies are also presented. The 4-rotor strategy provides mechanical energy, which keeps the liquid moving at a higher speed. It also provides extra oxygen and thus results in overall better conversion of ammonium. However, bad mixing regions and operational limitation due to the surface aeration still persist in the 4-rotor strategy as well. It can be concluded that the CFD-ASM model provides useful information about local concentrations and enables the evaluation of different operational strategies in terms of biological performance of the reactor. It points out the need of more robust models than conventional TIS which are able to take into account the concentration variations stemming from the flow variations.

PART III

Model reduction using CFD-biokinetic model

Chapter 6

Compartmental modelling of full scale WWTPs

This chapter describes the development of a reduced model using the CFD-ASM1 model results for two case studies: the Eindhoven WWTP & La bisbal d'Empordà WWTP.

6.1. Introduction

Current wastewater treatment (WWT) modelling practices typically use a tanks-in-series approach (TIS), which only takes into account spatial heterogeneities of the system in a very limited way. The TIS approach only considers the flow and dispersion in one direction and thus ignores the flows in the other two dimensions. The true mixing behaviour is, however, more complex in nature (e.g. the presence of dead or recirculation zones) and will result in significant deviations of predicted process variables from the monitored ones. Since the TIS structure is typically kept fixed, this leads to the requirement of calibration of biokinetic model parameters (most often affinity indices) as these are the only degrees of freedom available to do so (Arnaldos et al., 2015). Difficulties arise when considering dynamic operational conditions and further recalibration is usually needed when moving from dry to wet weather conditions. Except for a few articles, the contribution of dynamic mixing conditions is usually ignored (Le Moullec et al., 2008; Potier et al., 2005). Previous studies emphasized the importance of bulk mixing in calibration procedures and showed the inability of TIS models to incorporate certain important mixing conditions (Guha et al., 2006) and even Levenspiel (1999) alluded to this shortcoming in the introduction of his milestone textbook. Next to reduced predictive power of the model, due to calibration for the wrong reasons (phenomena are lumped), using the models for developing process control might lead to non-optimal controller operation and associated costs

given that sensor readings provided to the controller are not representative. This is investigated in chapter 7 in detail.

The previous chapters have provided the evidence that computational fluid dynamics (CFD) is a powerful tool that can provide detailed process information at a local scale. Currently, it is being used mostly for troubleshooting. However, when integrated with biokinetic models, it provides very detailed insight into the impact of local reactor conditions on overall process performance. One of the major bottlenecks in using CFD as a main modelling tool, however, is its high computational requirement. Hence, it will not become mainstream in the first decades to come and there is a need for a methodology that combines the improved insight of CFD and the low computational cost of TIS. Le Moullec et al. (2011, 2010b) and Alvarado et al. (2012) have previously used CFD results to develop a so-called compartmental model (CM). Le Moullec and co-workers showed that the CM gives similar results to those of CFD models (for a lab scale reactor) but with lower calculation time with the advantage of remaining almost as simple to manipulate as the TIS approach.

In this chapter, the integrated CFD-ASM1 model presented in Chapter 4 is used as basis for the development of a compartmental model for the Eindhoven WWTP and similarly the model presented in Chapter 5 is used for the compartmental modelling of the La bisbal d'Empordà WWTP. In first instance, the proposed general procedure for developing the CM, as it is the same for both cases, is explained before the detailed description of each case. In addition, a new idea of cumulative species distributions is introduced to quantify the degree of inhomogeneity using CFD-ASM results. These distributions are subsequently used as a decision support tool for deriving compartmental models. The impact of dynamic operational conditions on the process performance in terms of dissolved oxygen concentrations is also discussed. A proposal for a dynamic compartmental model, which can take into account a range of operational conditions, is provided.

6.1.1. Cumulative species distribution

The CFD-ASM model provides the knowledge of local concentrations. In order to quantify the variations observed in this vast amount of concentration data (over 1 million data points in some cases), 'cumulative species distributions (CSD)' are introduced here. A CSD summarises the range of observed values as well as their frequency of occurrence for a certain species present in the bioreactor.

The CFD-biokinetic model provides local concentrations for each cell of the grid (mesh). Figure 6.1 shows how the CSD is calculated from the CFD model. In a certain section of the reactor with volume '*V1'*, for each cell '*i*', the local concentrations '*Ci'* and the corresponding size '*Vi*' of the cell is retrieved from the CFD-biokinetic model. Therefore, the total volume of cells having a concentration in the range '*Ci* to *Ci*+Δ*C'* '*Ci'* would be $\sum Vi$ and the corresponding volumetric fraction would be $^{\Sigma Vi}/_{V1}$. Finally, with the knowledge of minimum and maximum concentrations and by choosing a small step change (Δ*C*), the CSD can be plotted for a user-selected volume '*V1*'. Hence, for each volumetric region selected by the user, a CSD can be constructed and this for every species computed by the integrated CFD-ASM model. The vertical axis of a CSD represents the cumulative fraction of the respective volume each concentration in the horizontal axis represents. Without going into exact numbers, the steepness/slope of a CSD provides an immediate indication of the degree of variability of any concentration in different sections. The steeper the curve, the more uniform distribution of the concentration and vice versa.

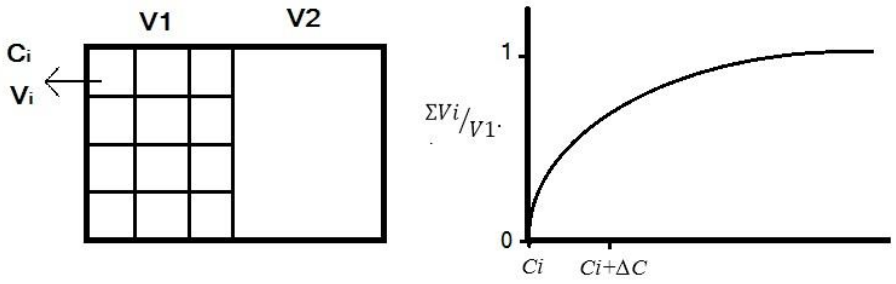

Figure 6.1 Illustration of cumulative species distribution

Practically, a CSD can be plotted for the whole reactor or any user selected section of the reactor. A single CSD for the whole reactor would provide an overview of the overall inhomogeneity of the reactor. Moreover, CSDs for different sections would enable quantifying and comparing variations occurring in different sections of the reactor. This is useful to determine which sections require more detailed modelling and which ones do not.

6.1.2. Compartmental modelling

A compartmental model describes the reactor as a conceptual network of spatially localized compartments connected through convective and exchange fluxes. The

convective flux mainly occurs in the direction of the bulk flow whereas exchange fluxes typically allow to conceptually mimic the occurrence of recirculation flows and dead zones in 3 dimensions as they occur in the actual reactor. In addition, the exchange fluxes are also used to include the turbulent characteristics of the flow and apparent hydrodynamics of the compartmental structure. For example, in Figure 6.2, a CM consists of a number of compartments C_i configured in more than one dimension and in which a recirculation flow Qr_i between compartments C_{i+1} & C_i occurs, along with the forward (convective) flow Q_i.

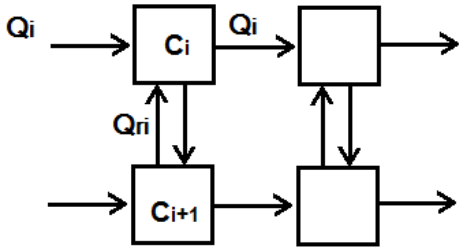

Figure 6.2 Illustration of compartmental model

The configuration of these compartments is typically based on the delimitation of homogeneous regions based on physical-chemical properties (in this case, derived from the CFD-ASM model). Shape, number and connectivity of these compartments can be determined based on various factors but will most likely be driven by the modelling objective.

The compartments of a reactor have traditionally been determined based on the flow distributions only. In the current study, however, it is found that the local mixing conditions impact the concentrations and thus the local process rates. Given the fact that the modeller is interested in these distributions, it makes more sense to base the compartmentalisation on species distributions rather than only hydrodynamics (although these are inherently embedded too as the concentration distributions are governed by the hydrodynamics). As the availability of DO determines the extent of both nitrification and, hence, indirectly the denitrification processes, DO is adopted as species of which the heterogeneity was used to derive the CM. Note that for other purposes, the user could select another species. Likely, this will be quite similar as many of the species in ASM are closely linked and will lead to similar-shaped CSDs. Moreover, the DO occurs in the fast reactions and hence by considering this, the time scales for slower reactions are automatically taken into account.

6.1.3. General compartmental modelling procedure

The development of a compartmental model is a laborious and iterative procedure. In this section, a general stepwise procedure is formulated (Figure 6.3). This procedure is followed in development of the compartmental models for both the case studies, however, improvisations are made where deemed necessary.

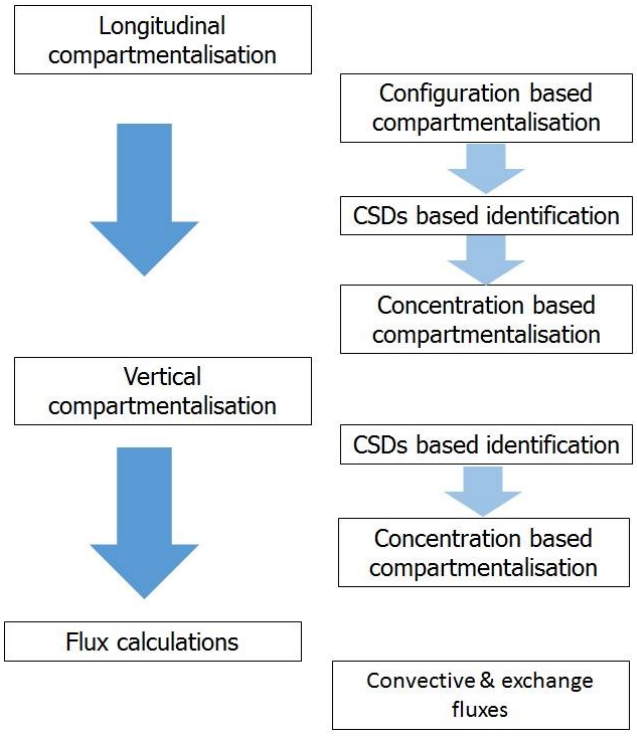

Figure 6.3 Compartmental modelling procedure

A compartmental model being the spatially localized network of several reactors can be developed based on the determination of the following parameters.

1. Number and size of compartments in the longitudinal and/or lateral direction **(longitudinal compartmentalisation)**
2. Number and size of compartments in the vertical cross-section of any of the longitudinal compartments **(vertical compartmentalisation)**
3. Convective and exchange flux between all compartments decided on in steps 1&2 (**flux calculations)**

These parameters are determined by means of the derived CSDs and the concentrations plots derived from the CFD-ASM model as described in more detail in the following sections (6.1.3.1-6.1.3.3).

6.1.3.1. Longitudinal compartmentalisation

First, the longitudinal compartmentalisation is performed which can be divided into the following steps.

Step I. Configuration based compartmentalisation

The configuration based compartmentalisation of the reactor is a postulation taking into account the operational significance of different regions and components of the reactor. The regions can be aerated/non-aerated or anoxic/aerobic/anaerobic depending on the system under study. The components of a reactor can be aerators, propellers, recycle pumps, inlets and outlets etc. At this stage it is unknown if a component plays a significant role in the non-uniformity of the reactor or not. Hence it is not a strict division of the reactor and must be amended if needed, based on the CSDs and/or concentration plots.

Step II. Cumulative species distributions

In the next step, the CSDs are plotted. Firstly, the CSD of the whole reactor is plotted to get an overview of the overall non-uniformity of the bioreactor. This provides a good measure of system heterogeneity and also serves as a reference to a worst case scenario (i.e. assuming one completely mixed tank). Next, the CSDs are plotted for the configuration based compartments of the reactor decided on in Step I. Additional CSDs might be plotted for different regions of the reactor to build up the knowledge of the system. The CSDs provide a comparison of the degree of variations between different zones in the reactor. Based on a threshold, the compartments with higher variations are then identified for further compartmentalisation. A threshold can be a measure of variation in concentrations or an absolute concentration. The determination of a threshold variation is driven by the objective of the study. Generally, the compartmental modelling aims at separating badly mixed regions from the rest of the regions and hence initially threshold can be an absolute concentration. Once regions are separated based on a concentration, the threshold can be a concentration range or a gradient of the CSD curve based on which further compartmentalisation can be done. The threshold values can also be different for different regions. However, it must be noted that CSDs are a

volumetric representation of the concentrations and do not include any spatial information on the occurrence of a specific concentration within a user selected volume. Therefore, compartmentalisation in itself cannot be performed solely based on the CSDs. Instead, concentration contour plots are needed to determine the exact location of occurrence of a certain concentration.

Step III. Concentration based compartmentalisation

In this step, the compartments are examined and further divisions are proposed based on the horizontal DO concentration profiles. The DO concentration profiles provide a good indication of variations and regions of bad mixing can be distinguished from the rest. However, at this stage it is important to examine the origin of these variations. The variations observed in a horizontal cross-section of a reactor can be either due to lateral or vertical hydrodynamics. The variations due to lateral hydrodynamics (such as due to bends and corners) are taken into account in the longitudinal compartmentalisation. In contrast, the variations due to vertical hydrodynamics (such as due to submerged aeration diffusers) are left for the vertical compartmentalisation. It must be noted that this procedure is based on the detailed knowledge of the system gained during the CFD hydrodynamic modelling of the system and hence certain decisions shall be taken based on the expert judgement of the practitioner.

6.1.3.2. Vertical compartmentalisation

In the next step vertical compartmentalisation is performed. The general procedure for vertical compartmentalisation is similar to the longitudinal compartmentalisation, with the exception of the first step (configuration based compartmentalisation).

Step I. Cumulative species distributions

First, CSDs are plotted for all longitudinal compartments decided in the previous step. The compartments with high variations (again based on a threshold) are identified and selected for further compartmentalisation. Again, additional CSDs can potentially be plotted to assess specific variations in different sections.

Step II. Concentration based compartmentalisation

The concentration plots along with hydrodynamic patterns in the vertical cross-section of the selected compartments are examined. Based on the observed concentration

patterns further compartmentalisation is proposed in the vertical cross-section. The size and shape of the proposed compartments is determined based on the homogeneous concentration profiles with a certain level of tolerance.

6.1.3.3. Flux calculations

The final step is to calculate the convective and exchange fluxes between the compartments. The convective flux is the volumetric flow rate of the liquid from one longitudinal compartment to the next longitudinal compartment. The exchange flux generally refers to a recirculating flow between any two compartments. It can be a flow rate between neighbouring sub-compartments within a longitudinal compartment or a counter current flow between two longitudinal compartments.

The compartments are multifaceted structures and, hence, fluxes need to be calculated separately through each facet. The flux through a facet (the interface between two adjacent compartments) is calculated as a product of the liquid velocity through a facet and area of the facet. The CFD hydrodynamic model provides the local velocities at each interface between two compartments. However, these velocities are provided in global coordinates of the system, thus local coordinates are created at the centre of each interface to calculate the velocity heading into and out of a certain compartment.

6.2. Case study of the Eindhoven WWTP

A complete integrated hydrodynamic and biokinetic model (CFD-ASM1), presented in chapter 4, is used to derive a compartmental model for the outer ring (Figure 6.4) of the full scale wastewater treatment plant (WWTP) of Eindhoven (The Netherlands). In order to achieve this principal objective, firstly the relevant CFD-ASM biokinetic results are briefly discussed and then the compartmental model is developed following the procedure described in section 6.1.3.

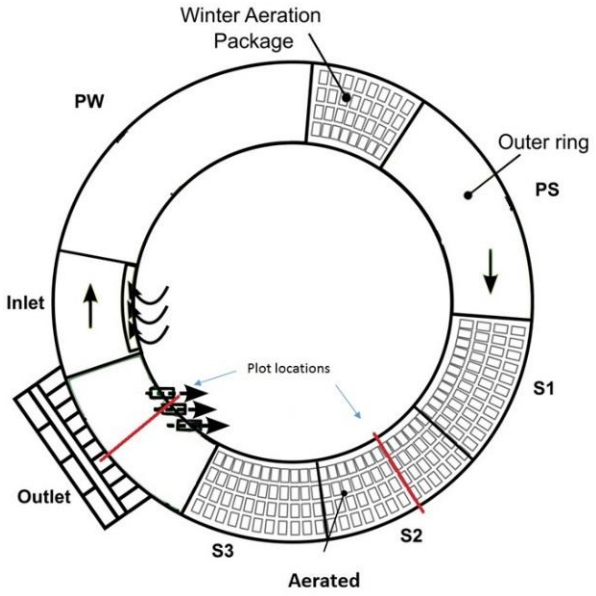

Figure 6.4 The configuration of the bioreactor of Eindhoven WWTP

6.2.1. CFD-biokinetic results

Several steady state simulations were performed at varying operational conditions ranging between dry and wet weather conditions. However, results of only three scenarios i.e. the L-G case being the base case, 2L-3G being the high flow rate case and a case in between 1.5L- 2G, are presented here.

Figure 6.5 shows the distribution of DO concentration at half the depth of the reactor in the horizontal cross-section for three scenarios i.e. L-G, 1.5L-2G and 2L-3G. These distributions are useful to determine the longitudinal discretization of the reactor. Given the fact that the aerators cover the entire bottom surface, it seems that the bubble plume that is created is "compressed" (Figure 6.5, left) leading to quite variable DO concentrations in a cross-section, especially at the start of the summer package. Increasing the gas flow rate seems to counteract this phenomenon (Figure 6.5, right).

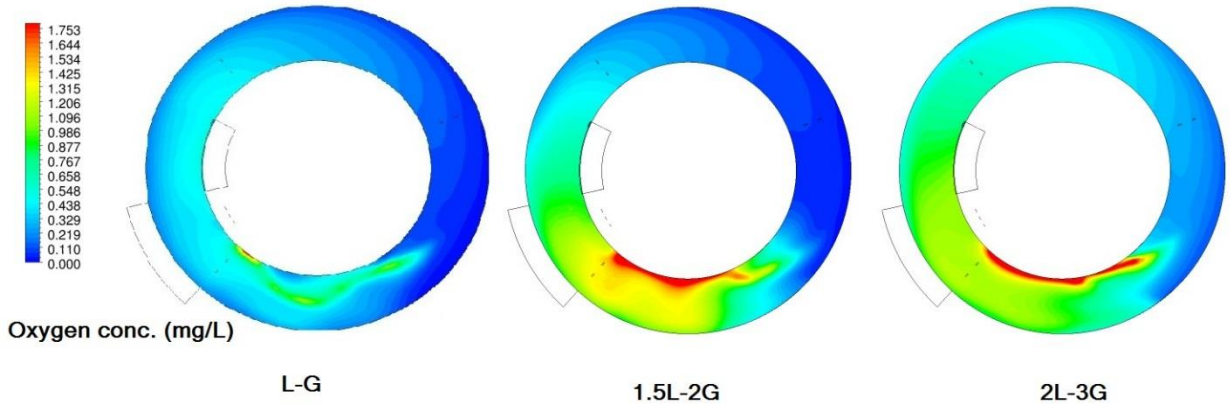

Figure 6.5 DO concentration at the horizontal cross-section of the Eindhoven WWTP bioreactor for different scenarios

Figure 6.6 presents the flow patterns and respective DO concentrations at a vertical cross-section in the middle of the aerated region (plot locations shown in Figure 6.4). Similarly, flow patterns and DO concentration distribution near the outlet and recycle region are shown in Figure 6.7. It can be observed that (1) dead and recirculation zones prevail and (2) there is a clear impact of (gas) flow conditions on the patterns developing.

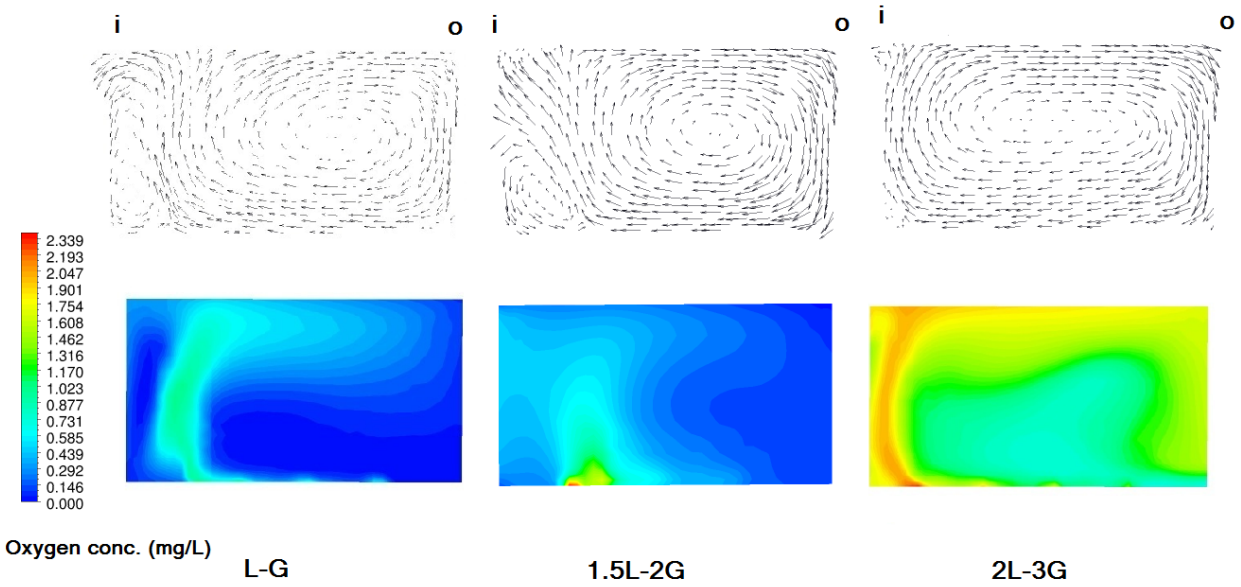

Figure 6.6 Flow pattern and DO concentration at a vertical cross-section in the middle of aerated region

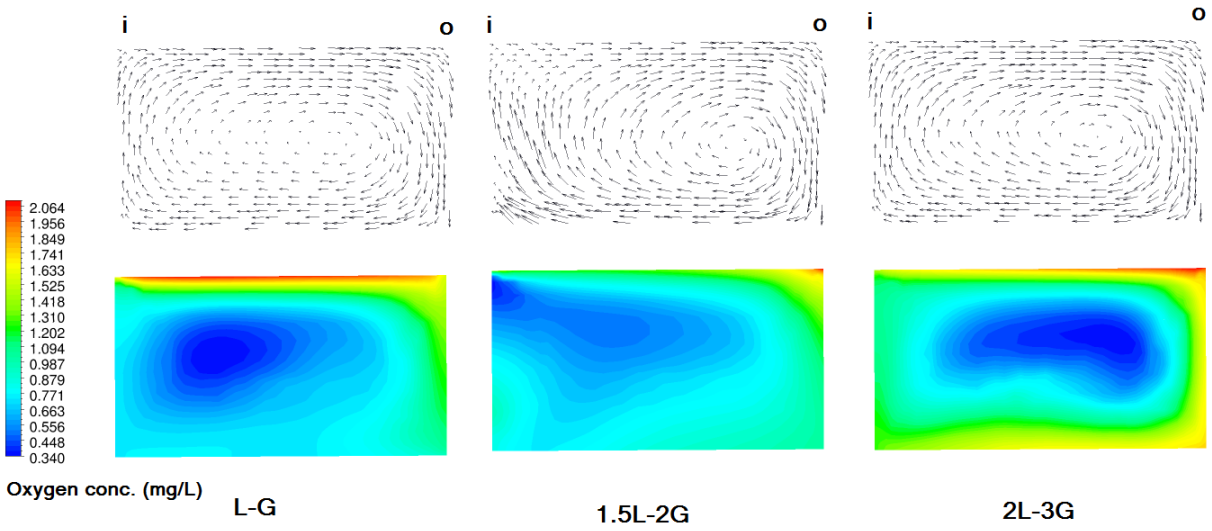

Figure 6.7 Flow pattern and DO concentration at a vertical cross-section in the middle of outlet region

6.2.2. Compartmental modelling of the Eindhoven WWTP

First, the stepwise procedure provided in section 6.1.2 is followed to derive the compartmental model for the L-G case. Next, the compartmental modelling for other cases (1.5L-2G & 2L-3G) is discussed and at the end, a dynamic compartmental modelling approach is proposed.

6.2.2.1. Longitudinal compartmentalisation for the L-G case

Step I. Configuration based compartmentalisation of the reactor

The reactor under study can be divided into two major regions i.e. an aerated and a non-aerated region. There are two separate aerated regions in the reactor i.e. winter package and summer package (Figure 6.4). However, for the current study, the winter package has not been used and therefore, the aerated region only refers to the summer package here. In addition to these regions, the reactor consists of different operational components which include an inlet, an outlet, three recycle pumps, and three pairs of propellers. Therefore, at first, the reactor was divided into 9 longitudinal compartments based on the reactor configuration (including separate compartments for each propeller). Later, during the concentration based compartmentalization it was found that the propellers do not cause significant variations and, therefore, three propeller

compartments were merged into neighbouring compartments to reduce the computational requirements. Now, primarily the reactor is divided into 6 zones named with reference to the reactor's configuration as Inlet (Inlet zone), PW (Pre Winter package zone), W (Winter package zone), PS (Pre summer package zone), S (Summer package zone) and Outlet (Outlet & recycle zone) (see Figure 6.4). The resulting initial guess for the compartmental network is shown in Figure 6.8.

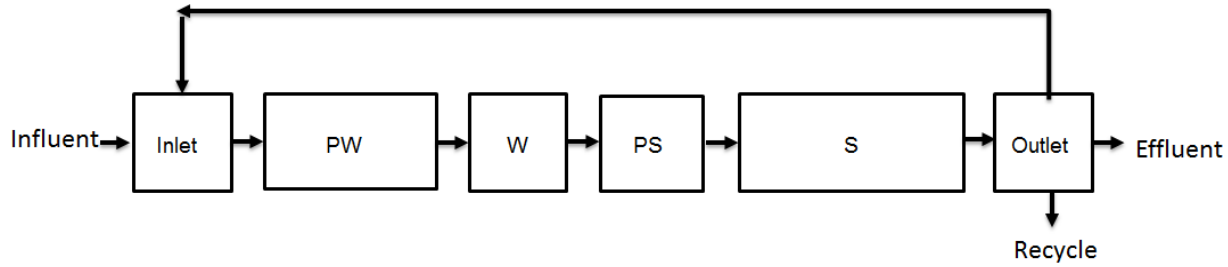

Figure 6.8 Configuration based longitudinal compartmentalisation

Step II. Cumulative species distributions

In the first instance a CSD is set up for the whole reactor for the base case, i.e. L-G case, (Figure 6.9) based on the dissolved oxygen concentration (with an ordinate resolution of 0.1 mg/L). The vertical axis represents the cumulative fraction of the respective volume each concentration represents. For example, this curve shows that almost 50% of the reactor volume has a dissolved oxygen concentration less than 0.5 mg/L and the rest of the reactor has a concentration between 0.5 and 2.4 mg/L. Overall the oxygen varies between 0 and 2.4 mg/L in the reactor. Therefore, modelling such a system based on the assumption of one completely mixed tank would definitely result in erroneous predictions.

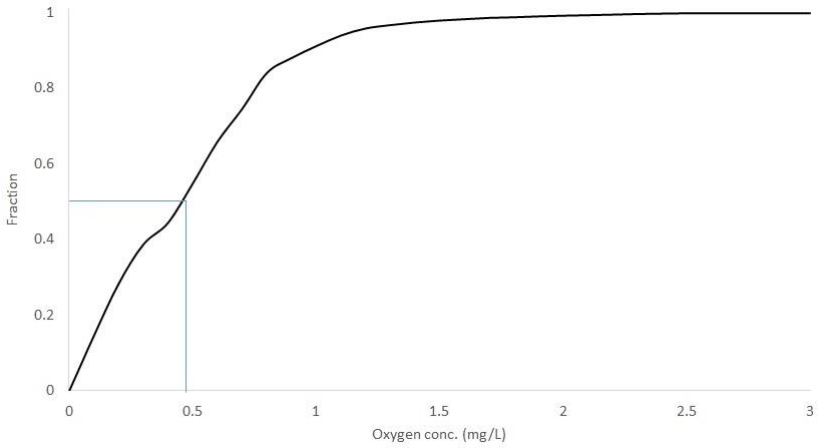

Figure 6.9 The CSD of dissolved oxygen for the whole reactor for the L-G case

In order to investigate further, CSDs for the aerated region and the remaining sections are plotted separately in Figure 6.10. Although it provides more information regarding the variations as compared to Figure 6.9, it can be observed that the variations in both the curves is still ranging between 0 and 2.4 mg/L. Hence, it is still hard to assume complete mixing in these separate regions and there is a need of further zooming into smaller sections of the reactor.

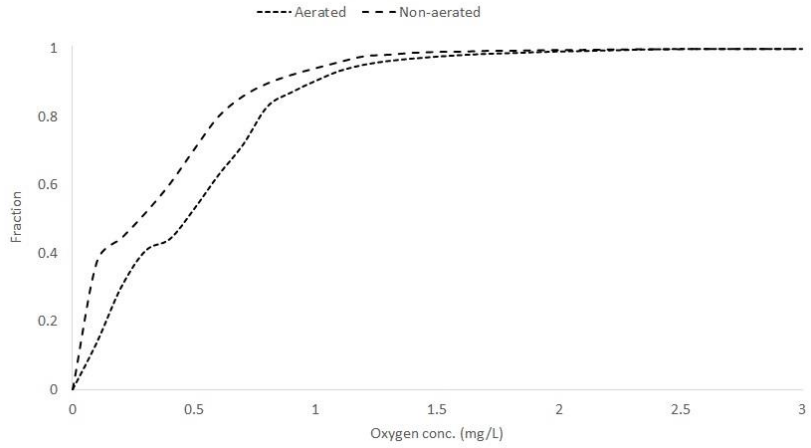

Figure 6.10 The cumulative species distribution of dissolved oxygen for the aerated and non-aerated sections of the reactor for the L-G case

Furthermore, the CSDs are plotted for the compartments decided in Step I as shown in the Figure 6.8. The resulting CSDs are provided in Figure 6.11. Now, these curves clearly show a difference in variations among different compartments. It can be observed that the PS and PW curves vary from 0 to 0.25 mg/L and 0.1 to 0.3 mg/L

respectively. In contrast, the outlet and inlet curves vary from 0.4 to 2.4 mg/L and 0.4 to 1.5 mg/L respectively. The aerated curve varies from 0 to 2.4 mg/L. The steepness/slope of the curves provide an immediate comparison of variability among these compartments. The curves for PW and PS are the steepest and hence, it can be said that the PW & PS regions have least variability. The aerated region has the least steep curve and thus highest variations in the DO concentrations. The inlet and outlet regions, as their slope indicates, have an intermediate variability i.e. more than PW and PS but less than the aerated region. It can also be confirmed from the CFD results (Figure 6.5) that the aerated region has the highest variation as compared to the rest of the reactor and the inlet and outlet regions have a higher variation compared to the other non-aerated regions.

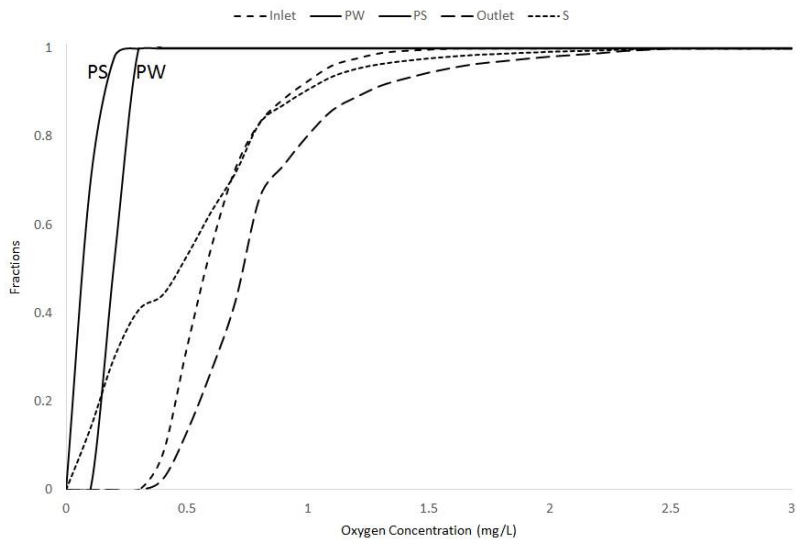

Figure 6.11 The cumulative species distribution of dissolved oxygen for the aerated, non-aerated, inlet and outlet sections of the reactor for the L-G case

It can be concluded that as the PW and PS compartments showed little variations (0 to 0.25 mg/L), these compartments need no further compartmentalisation. However, the inlet, outlet and S compartments still showed significant variations and thus need further compartmentalisation based on the DO concentration profiles in the next step.

Step III. Concentration based compartmentalisation of the reactor

Further compartmentalisation of the selected compartments (S, inlet & outlet) is based on the horizontal DO concentration contour plots. Figure 6.12 shows the DO

concentration for the L-G case in a horizontal cross-section of the reactor. It clearly illustrates DO concentration variations along the length of the reactor.

In the aerated region, the oxygen distribution varies along the reactor length such that in the beginning it is higher near the centre; in the middle it is higher near the inner wall and at the end it is again higher near the centre (Figure 6.5a). Therefore, considering these concentration patterns, the aerated region can be further split into three longitudinal sub-compartments namely S1, S2 & S3. It may seem that these regions can be compartmentalised differently as for example the S1 region can be split into two compartments. However, it should be recalled from the discussion in chapter 3 (section 3.3.4) that the gas plume does not rise perpendicularly towards the top, but instead the bulk flow pushes the gas plume in its direction. Therefore, at this stage, the S1 compartment is not further split longitudinally instead it will be accounted for in the vertical compartmentalisation. Even after dividing the aerated region into three (or even more), the variations across the width still persist. These variations are mainly due to vertical hydrodynamic behaviour caused by aeration. Hence, further longitudinal compartmentalisation cannot improve the non-uniformity.

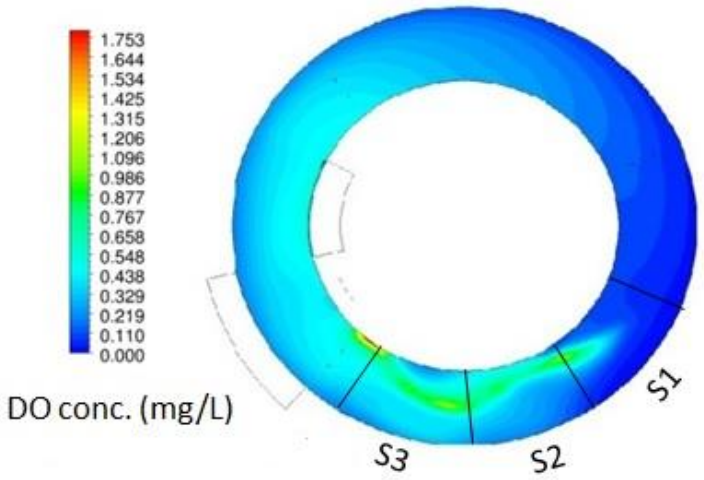

Figure 6.12 The DO concentration in the horizontal cross-section at 3.45m depth in the reactor for the L-G case

The DO concentrations pattern in the outlet and inlet regions (Figure 6.12), however, do not show significant variations along the length but show the DO variation across the width. These variations stem from the major recirculation zone (shown in Figure

6.7) and hence it is a vertical hydrodynamic behaviour which will be addressed in the vertical compartmentalisation. Therefore, at this stage, the outlet and inlet regions are not further compartmentalized.

The total number of compartments at the end of the longitudinal compartmentalisation now equals 8 and the overall intermediate compartmental network is shown in Figure 6.13.

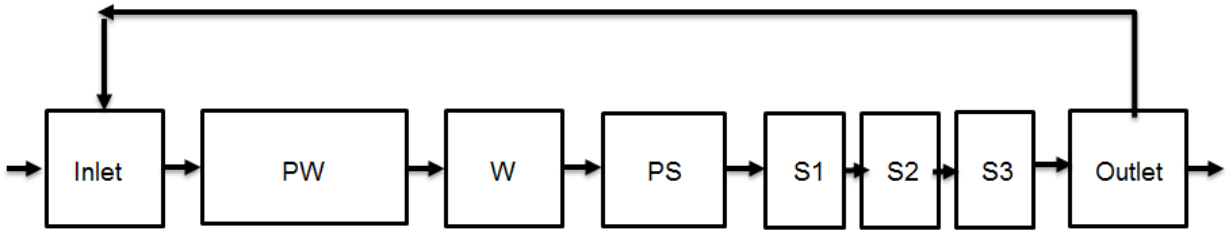

Figure 6.13 Overall longitudinal compartmentalisation

6.2.2.2. Vertical compartmentalisation for the L-G case

Step I. Cumulative species distributions

In this step, the CSDs are plotted for the longitudinal compartments (shown in Figure 6.13) to evaluate and quantify the variations. The resulting CSDs are provided in Figure 6.14.

There is no difference in previously plotted inlet and outlet CSDs (Figure 6.11) as further compartmentalisation was not done. However, it can be observed that now three curves (S1, S2 & S3) are plotted for three sub-compartment of the aerated region. It can be seen that the S1 curve has a concentration variation between 0 and almost 2 mg/L whereas, S2 & S3 vary between 0.2-2 mg/L and 0.25-2.2 mg/L. Even though the overall concentration ranges in these curves (S1, S2 & S3) are still high, the steepness of these individual curves has increased compared to the single CSD for the aerated region in Figure 6.11. The steeper parts of a curve indicate the presence of homogeneous regions inside a compartment. Therefore, it can be observed that most part of the S1 curve is quite steep as 82% of the S1 compartment has a DO concentration less than 0.2 mg/L and for the remaining 18% the DO concentration varies between 0.2-1.5 mg/L. Similarly, the S2 curve shows that 38% of the compartment has a DO concentration less than 0.2 mg/L. This can be explained by looking at Figure 6.6, showing the vertical

cross-section of the S2 compartment, which reveals a dead zone in the aerated region which has less variability within its core and, hence, causes an increase in steepness of the respective CSD. The increase in the DO concentration is mainly happening in the region between the two dead zones and, hence, overall the DO concentration variation in this region remains high. The S1 compartment, being located in the beginning of the aerated region, understandably has lower DO concentrations compared to the S2 & S3 compartments. Whereas, S3 being at the end of the aerated region has the higher DO concentrations compared to S1 & S2. The S2 compartment being in the middle has higher DO concentrations than S1 but lower than S3. This can be quantified given that the S1 curve shows that 90% of the region has a DO concentration below 0.5 mg/L, the S2 curve shows that 75% of the region has a DO concentration below 0.5 mg/L and S3 shows that only 35% of the region has a DO concentration below 0.5 mg/L.

From this discussion it can be concluded that further compartmentalisation is required for the S1, S2 & S3 compartments as the overall concentration variations are high. As discussed in section 6.2.2.1, the inlet and outlet also need further compartmentalisation due to high variations observed in their CSDs.

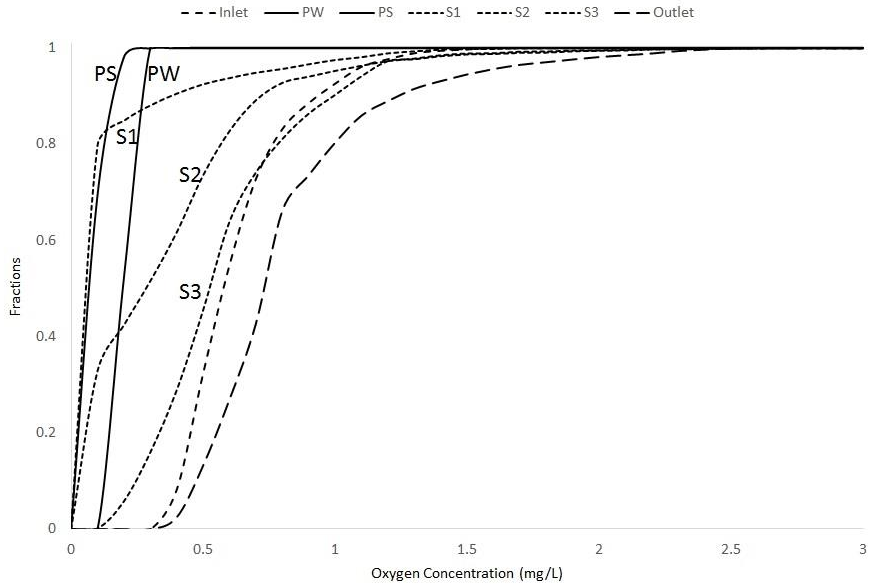

Figure 6.14 The cumulative species distribution of dissolved oxygen for the compartments shown in the Figure 6.13 for the L-G case

Step II. Concentration based compartmentalisation

Figure 6.15 shows the compartmentalisation process of the aerated region based on the hydrodynamics and the CFD-biokinetic results. The flow patterns in Figure 6.15a show that there are two recirculation zones i.e. one minor and one major recirculation zone which lead to DO variations in the cross-section. If the compartmentalisation is performed based only on the hydrodynamics, then this region can be divided into three respective compartments (C1, C2 & C3) as shown in Figure 6.15a. The minor recirculation is named C1, the major is named as C2 and the rest of the region is named as C3. These regions are not completely isolated and thus share exchange fluxes (Q13 and Q23) between them. Q13 is the exchange flux between the C1 and C3 compartments, similarly, Q23 is the exchange flux between C2 and C3 compartments. However, when the respective DO concentration plot is analysed in Figure 6.15b, it can be observed that the DO concentration is similar in both the recirculation zones i.e. C1 and C2. Therefore, these compartments can actually be considered as one compartment C1+C2 with their combined exchange flux being Q12+Q23. This approach reduces the overall number of compartments and, hence, the computational demands. It must be noted that the combined compartment C1+C2 is based on the DO concentration similarities and the configurational symmetry among C1 and C2 compartments (i.e. both share boundaries with the C3 compartment and hence exchange flux can simply be combined). This approach cannot be applied to those compartments where configurational symmetry is absent, even if they have the same DO concentrations.

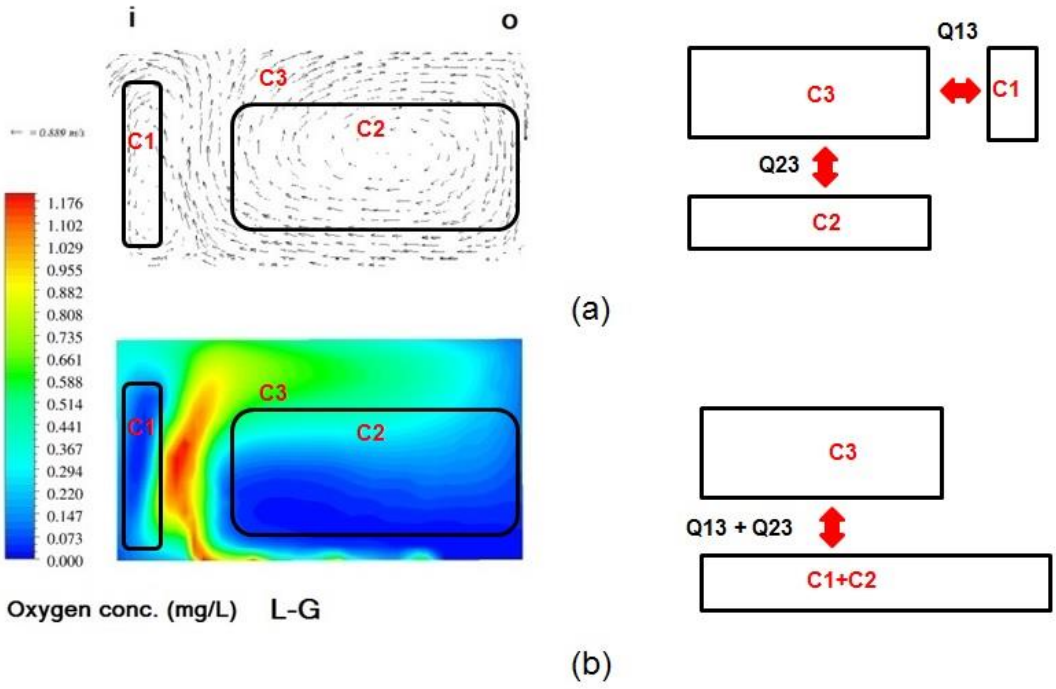

Figure 6.15 The compartmentalisation of the aerated region based on (a) the hydrodynamic and (b) the CFD-biokinetic results

The compartmentalisation process for the outlet region is shown in Figure 6.16. It can be seen that there is a major recirculation zone which is responsible for the DO variations in the cross-section. Therefore, the region having uniform DO concentrations can be considered as a separate compartment C1 and the rest of the region can be considered as the C2 compartment. In this region the compartmentalisation based on hydrodynamics and CFD-biokinetic both result into the same compartmental model, i.e. two compartments. Similarly, the inlet region is also divided into two compartments which is not shown here to avoid repetition.

Overall, applying the same process, the vertical compartmentalisation results in two compartments for the inlet, outlet and in each of the longitudinal compartments of the aerated regions (S1, S2 & S3). Therefore, the final compartmental network of the reactor consists of 13 compartments and is shown in Figure 6.17. The sub-compartments in each of the longitudinal compartments are denoted by ‘a’ and ‘b’. The black arrow between the compartments refers to the convective flux, whereas, a red double arrow refers to the exchange flux between two neighbouring compartments.

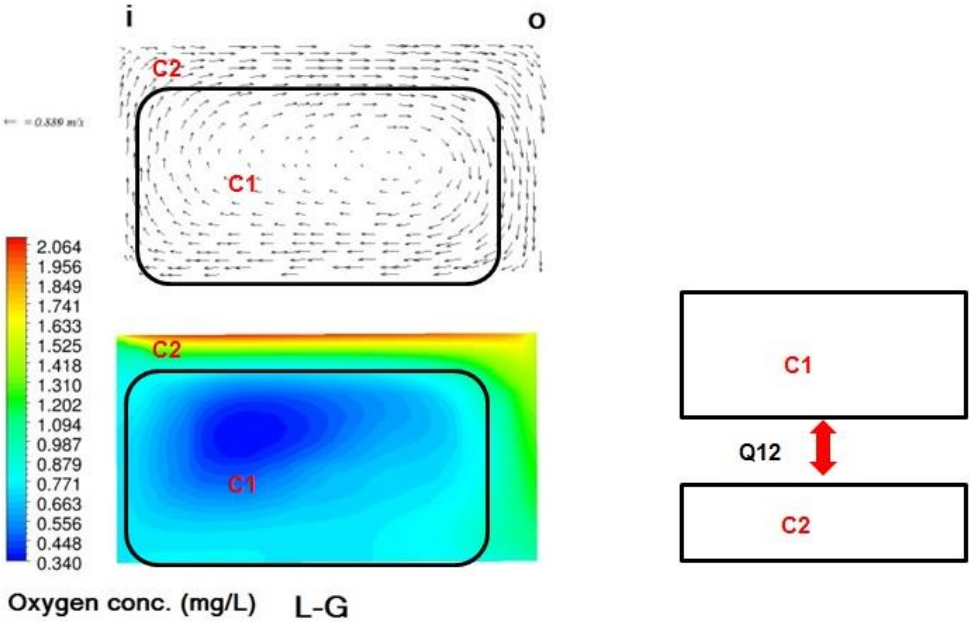

Figure 6.16 The compartmentalisation of the outlet region of the reactor

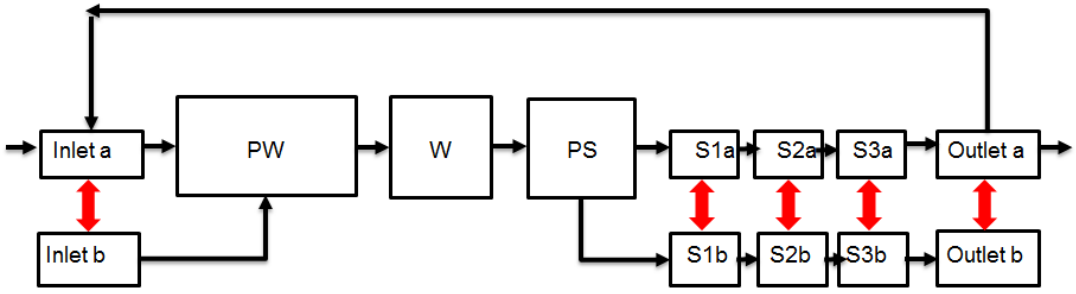

Figure 6.17 Overall compartmental network of the reactor for the L-G case

Figure 6.18 shows the resulting CSD plots for the compartments shown in the Figure 6.17. It can be observed that the variability has significantly reduced in these compartments. However, the S2b and S3b curves still show high variation range of 0.8 mg/L to 2.5mg/L and 1mg/L to 2.5mg/L respectively. These variations are due to the presence of high air availability near the diffusers and can be further reduced by more

compartmentalisation. However, these regions are negligible compared to the overall volumes and hence it is deemed unnecessary to further compartmentalise at this stage.

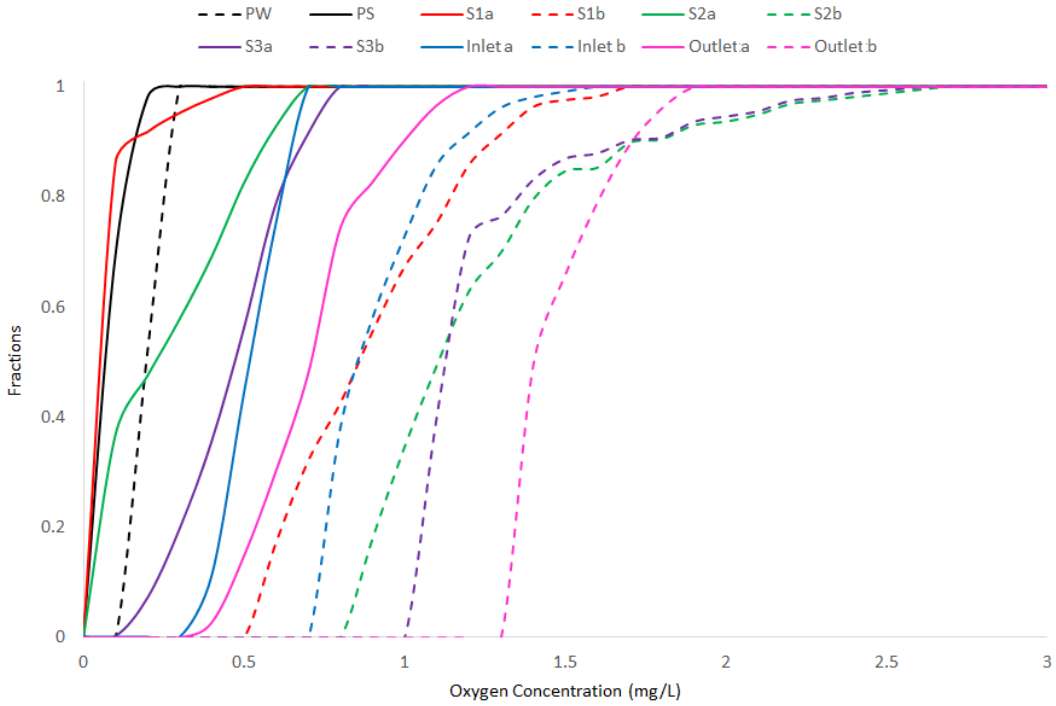

Figure 6.18 The cumulative species distribution of dissolved oxygen for the compartments shown in the Figure 6.17

6.2.2.3. Flux calculations

The final step is to calculate the convective and exchange flux (flow rates) between the compartments. For example, the flow rate from the PW to the W compartment indicated in Figure 6.17 is a convective flux and the flow rate between 'Outlet a' and the 'Outlet b' is the exchange flux. With the knowledge of exact locations of the interfaces between the compartments, one can compute the velocities at these interfaces from the CFD model. Figure 6.19 shows the shape of an actual compartment (S2a) in the aerated region and indicates the two types of fluxes.

As the velocities are in global coordinates, therefore, as shown in Figure 6.19, local coordinates are created at the centre of each interface to calculate the velocity heading into and out of a certain compartment.

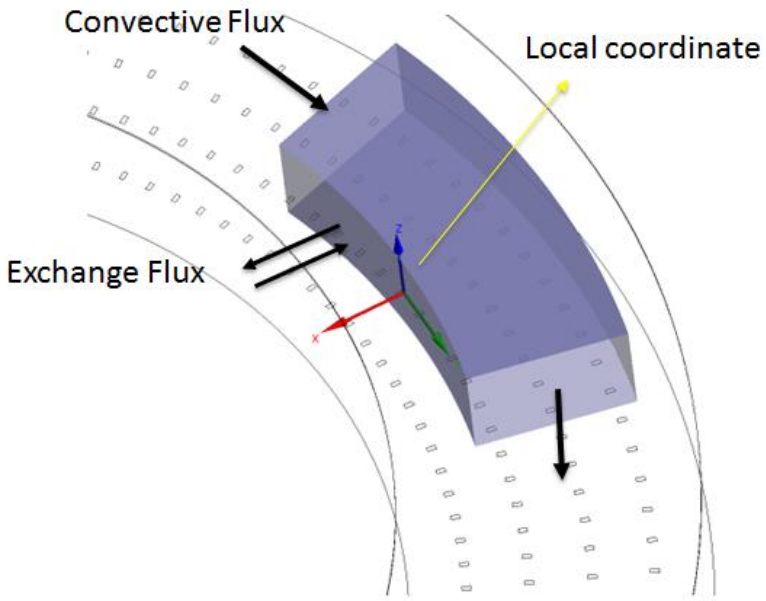

Figure 6.19 The S2a compartment in the aerated region indicating convective and exchange fluxes

6.2.2.4. Compartmental model for the other cases

Figure 6.5, Figure 6.6 & Figure 6.7 also show the flow patterns and oxygen distributions for the other two cases (1.5L-2G & 2L-3G). As seen in the L-G case, Figure 6.5 shows that the DO concentration is also non-uniform in the aerated region for these cases as well. Due to the change in aeration rates and thus the flow patterns, the only difference compared to the L-G case is the higher DO concentration near the wall. Similarly, Figure 6.6 & Figure 6.7 show the change in DO concentration across the vertical cross-section due to the changes in aeration rates.

In Figure 6.20, CSD curves are plotted for the 2L-3G case. Here as well, PS & PW are the steepest, however, the steepness of these curves decreased compared to the L-G case, thus pointing to an increased variability. Similarly, other curves for this case are less steep than the respective curves in the L-G case, thus indicating higher variability in 2L-3G case.

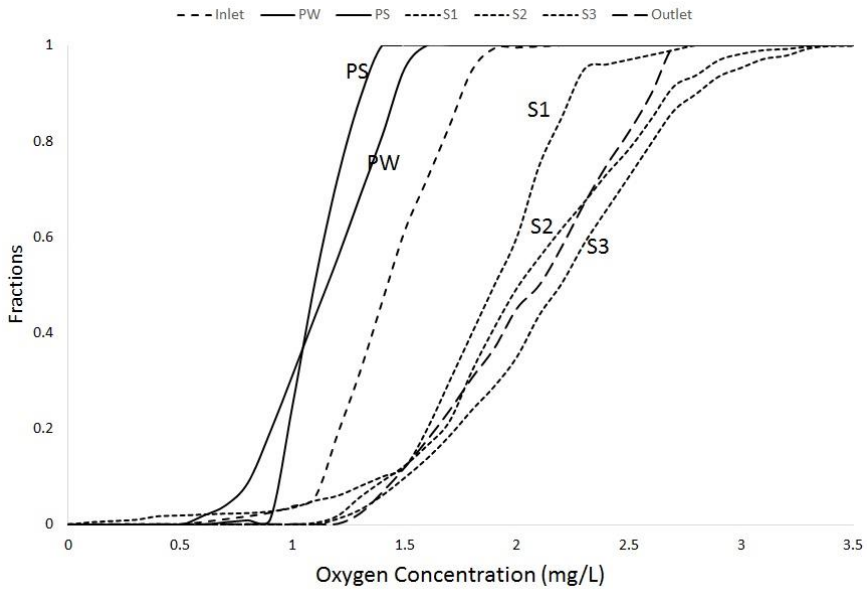

Figure 6.20 The cumulative species distribution of dissolved oxygen for the compartments shown in the Figure 6.13 for the 2L-3G case

The CSD curves show increase in the DO concentrations in the case of 2L-3G due to a change in conditions. Given the similarity in behaviour, the number of compartments is kept the same but the size of the compartments is adapted to account for the changed flow patterns. For example, the recirculation zone in the case of 1.5L-2G is smaller than in the other two cases (Figure 6.6), thus the resulting compartment is also smaller in size. Next to the changes in compartment sizes also the respective exchange fluxes to and from the compartment are different. However, a same compartmental network is employed as it simplifies the exercise of making the CM dynamic in nature.

6.2.2.5. Dynamic compartmental model

The above findings lead to the fact that a single CM with compartments having fixed volumes and fluxes is not sufficient under dynamic conditions and will lead to wrong predictions (although already more accurate compared to TIS). Therefore, compartments that have different volumes under different conditions (e.g. sub-compartments of the S1, S2, S3, Inlet & Outlet regions) need to be modelled as 'variable volume' tanks, where the volume is a function of the flow rate coming into the compartment (which equals the influent flow). In addition, the exchange fluxes need to be dynamic as function of the inflow rate. The development of the dynamic CM as well

as the comparison with the plain TIS model is currently on-going and outside the scope of this work.

Development of such a complex dynamic CM enables the model to operate under dynamic conditions within the flow rate ranges mentioned earlier (L-G & 2L-3G). It takes into account mixing limitations as well as resulting DO concentration distributions. Subsequently, the calibration efforts are reduced (by taking into account mixing limitations) and additionally the calibration should be more robust.

6.3. Case study of the La bisbal d'Empordà WWTP

The CFD-biokinetic model (CFD-ASM1) presented in chapter 5 for La bisbal WWTP is used to derive a compartmental model for the oxidation ditch. In order to achieve this principal objective, first the relevant CFD-ASM biokinetic results are briefly discussed and subsequently the compartmental model is derived.

The detailed configuration of the oxidation ditch is provided in chapter 5, however, a simple configuration is provided in Figure 6.21. It includes different divisions of the oxidation ditch, which are used for the CSDs and the compartmentalisation in the following sections.

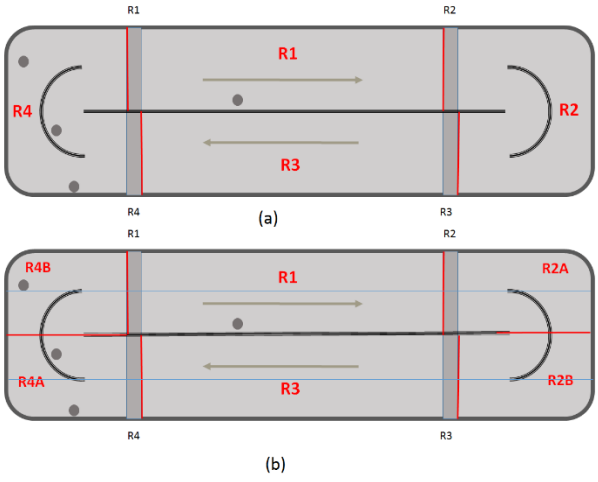

Figure 6.21 Simple configuration and different divisions of the oxidation ditch (red lines show the division and blue lines show the plot locations)

6.3.1. CFD-biokinetic results

The dissolved oxygen concentrations for the 2-rotor and 4-rotor cases are provided in Figure 6.22. In Figure 6.22a, it can be observed that the DO concentrations vary along the length and the depth of the reactor. The variations originate from the hydrodynamics of the reactor which are governed by the surface aerators and the configuration of the oxidation ditch. The surface aerators are installed at the top and, hence, cause low DO concentrations near the bottom of the reactor. The bends and corners in the oxidation ditch cause the formation of dead zones which consequently lead to variations in the DO concentrations in these regions. Similarly, variations are also visible in Figure 6.22b for the 4-rotor case. However, the regions next to R1 and R3 rotors now have higher DO concentrations because all rotors are in operation. In both cases, the influent stream flows close to the centre wall before the bend. However, after the bend the impact of the influent stream disappears, first due to the R2 rotor and second due to the dead zone behind the centre wall on the other side. However, the ammonium concentration distribution provided in Figure 5.14 and Figure 5.17 showed that even after the bend the influent stream flows close to the centre wall near the top surface and distributes evenly towards the bottom. These are important findings and are needed to be taken into account for the compartmentalisation of the reactor.

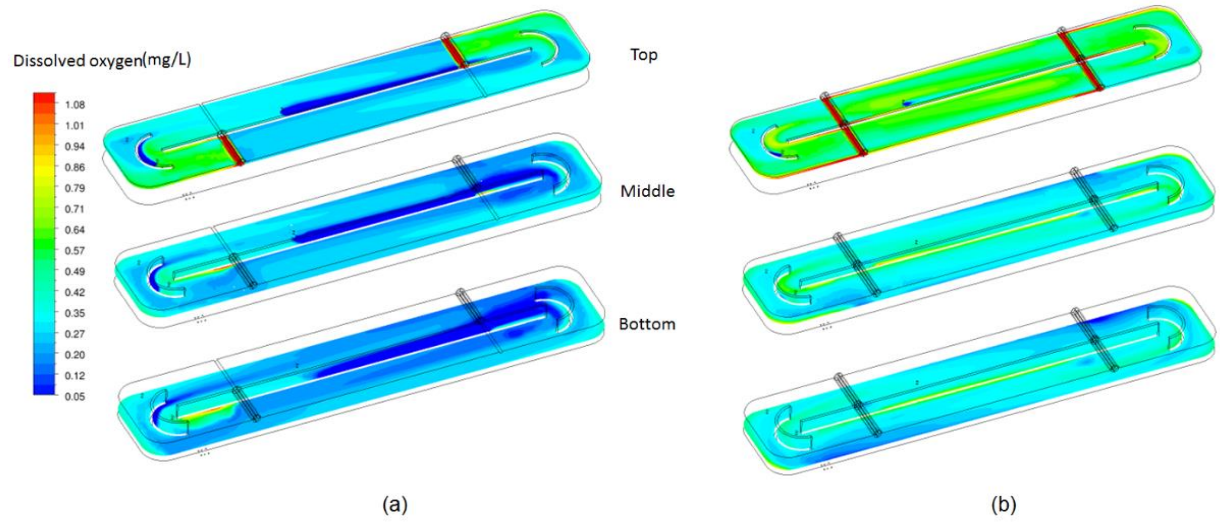

Figure 6.22 The DO concentrations in the horizontal cross-section of the oxidation ditch at different depths for (a) the 2-rotor and (b) 4-rotor cases

Figure 6.23 provides the DO concentrations at two vertical cross-sections at either side of the centre wall in the reactor (arrows show direction of the flow) for the 2-rotor case.

The plot locations are shown in Figure 6.21b. It can be observed that in the vicinity of the rotors the DO concentrations near the top are higher than the bottom. The bends at either end of the reactor are causing the dead zones being formed and in the process the top layer tends to mix with the bottom layer leading to less variation across the depth in the regions after the bend.

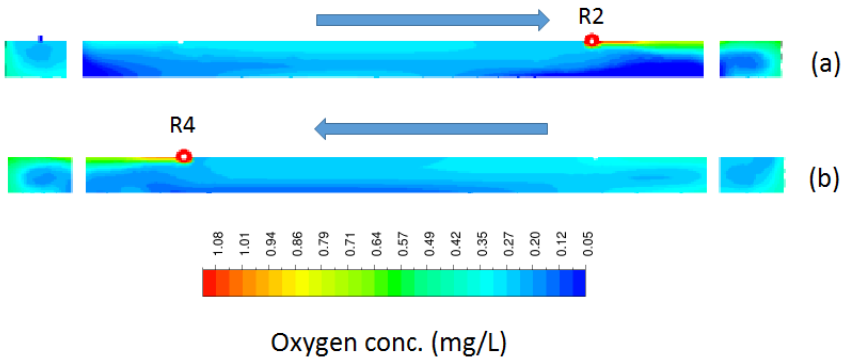

Figure 6.23 The DO concentration in the two vertical sidewise cross-sections of the reactor (plot location shown in Figure 6.21b) for the 2-rotor case

Similar to Figure 6.23, the DO concentrations for the 4-rotor case are provided in Figure 6.24. Similar patterns can be observed in the regions of the bends. However, due to the functioning of the extra rotors R1 and R3, the concentration variations along the depth in the subsequent regions is higher as compared to the 2-rotor case.

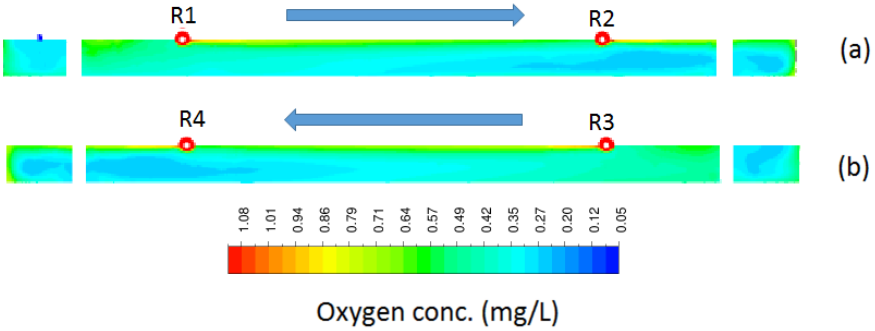

Figure 6.24 The DO concentration in the two vertical sidewise cross-sections of the reactor (plot location shown in Figure 6.21b) for the 4-rotor case

6.3.2. Compartmental modelling of La bisbal d'Empordà WWTP

First, the stepwise development of the compartmental model of the oxidation ditch for the 2-rotor case is presented. Next, a compartmental model is anticipated for the 4-rotor case and subsequently a dynamic compartmental model is proposed for both cases.

6.3.2.1. Longitudinal compartmentalisation for the 2-rotor case

Step I. Configuration based compartmentalisation

Based on the configuration, the oxidation ditch is firstly divided into four compartments such that each compartment consists of one rotor (as shown in Figure 6.21a) and is named conveniently with reference to the respective rotor as R1, R2, R3 & R4. It is done keeping in mind that a similar compartmental model is needed for the 4-rotor case. It must be noted that each inlet (influent, MBR recycle and settler recycle streams) and outlet are not separately compartmentalised here but will be taken into account in the next steps.

Step II. Cumulative species distributions

First, the dissolved oxygen CSD for the entire reactor volume is plotted in order derive some insight into the overall heterogeneity of the system. The resulting CSD is shown in Figure 6.25. It shows that 58% of the whole reactor volume has DO concentrations less than 0.2 mg/L and overall it does not exceed 1.2 mg/L. Therefore, considering such a system to be completely mixed is a flawed approach.

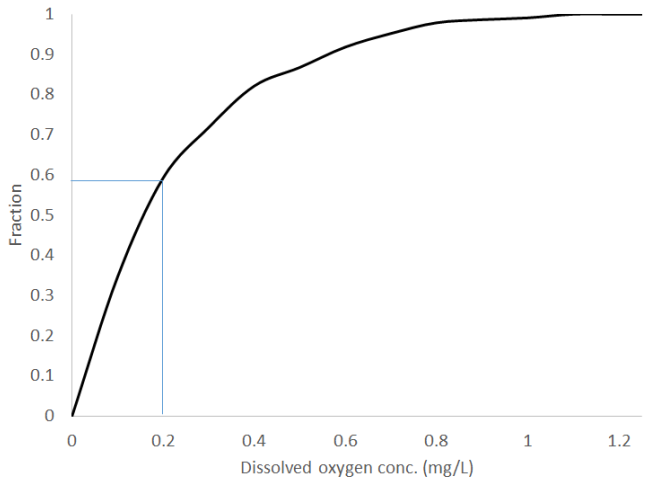

Figure 6.25 The dissolved oxygen CSD for the whole oxidation ditch bioreactor

Next, CSDs are plotted for the four compartments (R1, R2, R3 & R4) defined in the previous step (Figure 6.26). It can be observed that the CSDs for the R1 and R3 compartments show the steepest curves and, hence, exhibit the least variability. The overall variation however, ranges between 0-0.5 mg/L for these compartments. This variation is mainly due to the influent stream present in the R1 compartment (Figure 6.22). However, the CSDs for R2 and R4 regions show more variability in the DO concentrations due to the presence of surface aerators in these regions. The overall variation in the R2 and R4 ranges between 0-1.2 mg/L. Even though these regions are aerated, their respective CSDs show significant volumes of these regions having low DO concentrations. For example, 55% of the R2 region and 45% of the R4 region have DO concentrations less than 0.2 mg/L. These low DO concentrations are firstly due to the functional limitation of the rotors (rotors are at the surface) and secondly due to the presence of dead zones caused by the curved walls and the corners of the reactor in these regions.

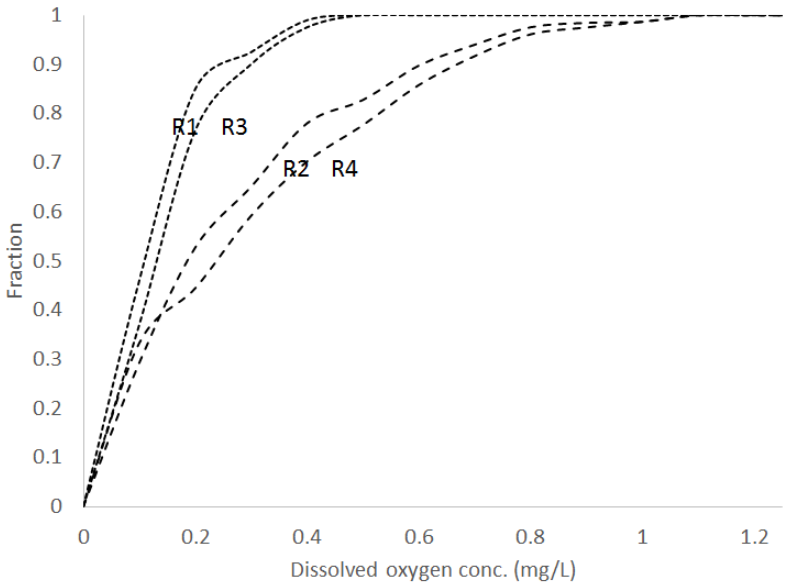

Figure 6.26 The dissolved oxygen CSDs for the R1, R2, R3 and R4 compartments

Henceforth, it can be concluded that the R2 and R4 compartments due to the high variations need further compartmentalisation. However, before going into the next step, additional CSDs are plotted to further investigate the R2 and R4 regions. Two CSDs are plotted for each of the R2 (R2A and R2B) and R4 (R4A and R4B) compartments such that the R2A and R4A constitute the regions before the bends and similarly R2B and R4B form the region after the bends (Figure 6.21b). The resulting CSDs are shown

in Figure 6.27. It can be observed that separating the regions before and after the bends has significantly changed the overall DO variations in these regions. The overall DO ranges from 0 to 0.9 mg/L for R2B and R4B regions, whereas, for the R2A and R4A the DO ranges from 0 to 1.3 mg/L. However, the origin of the variations in these regions can now be attributed differently. The DO variations in the R2A and R4A can be attributed to the presence of the rotors at the top resulting into higher DO concentration near the top and inadequate DO concentrations at the bottom. In contrast, the variations in R2B and R4B regions are mainly due to the presence of dead zones caused by the bends and the DO seeping through the inner side of the curved wall (as shown in Figure 6.22a). The CSDs for R2B & R4B regions are steeper as compared to the R2A & R4A regions because the DO concentrations are delimited (cannot be less than zero) in these regions due to their low values.

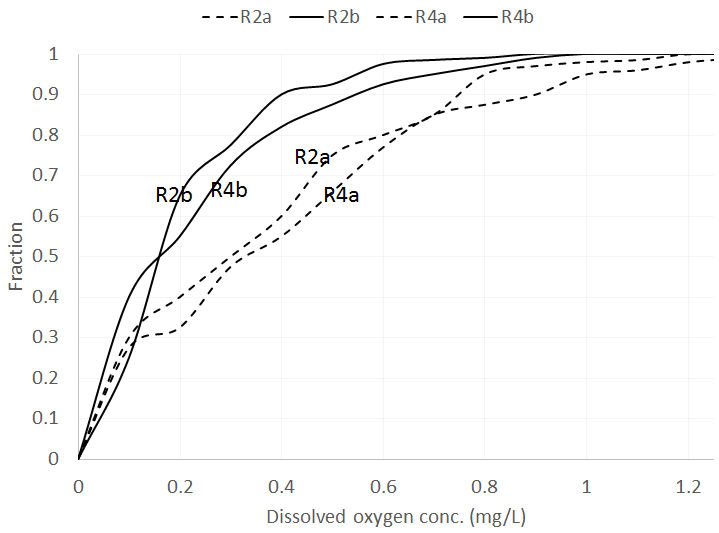

Figure 6.27 The dissolved oxygen CSDs for different sections of the oxidation ditch shown in the Figure 6.21b for the 2-rotor case

Step III. Concentration based compartmentalisation

In the next step, compartmentalisation further fine-tuned on DO concentrations and underlying hydrodynamics in the individual compartments R1, R2, R3 & R4.

The description for the compartmentalisation of the R4 region firstly based only on the hydrodynamics and then on the CFD-biokinetic model is provided in Figure 6.28a & b respectively. Considering only hydrodynamics leads to the formation of four compartments R4a*, R4b, R4c and R4d (it must be noted that small letters are being

used here for the compartments and are different than the capital letters used earlier for the CSDs). The R4a* represents the region next to the rotor, R4b represents the dead zone behind the curved wall, R4d represents the dead zone behind the middle wall and R4c represents the rest of the compartment. However, the DO concentrations in Figure 6.28b show that the MBR recycle stream does not mix with the R4a compartment, instead it is short circuited to the next compartment. Therefore, taking this into account, an additional compartment R4e is considered.

Considering the complexity of the system, it must be noted that a certain level of tolerance is used to form these compartments to avoid small facets and sharp angles between the compartments that can eventually lead to difficulties in the flux calculations. Moreover, the sub-compartments are connected with two types of flows i.e. convective and exchange flux. The convective flux is the bulk flow whereas, the exchange flux is the flow due to recirculating and counter current flows between the adjacent compartments.

The R2 and R4 regions showed similarity among them in terms of configuration, hydrodynamics and their CSDs. However, the R2 compartment does not have an MBR recycle stream and it does not need an additional compartment. Therefore, the R2 region is compartmentalized likewise and results into similar compartments namely R2a, R2b, R2c & R2d.

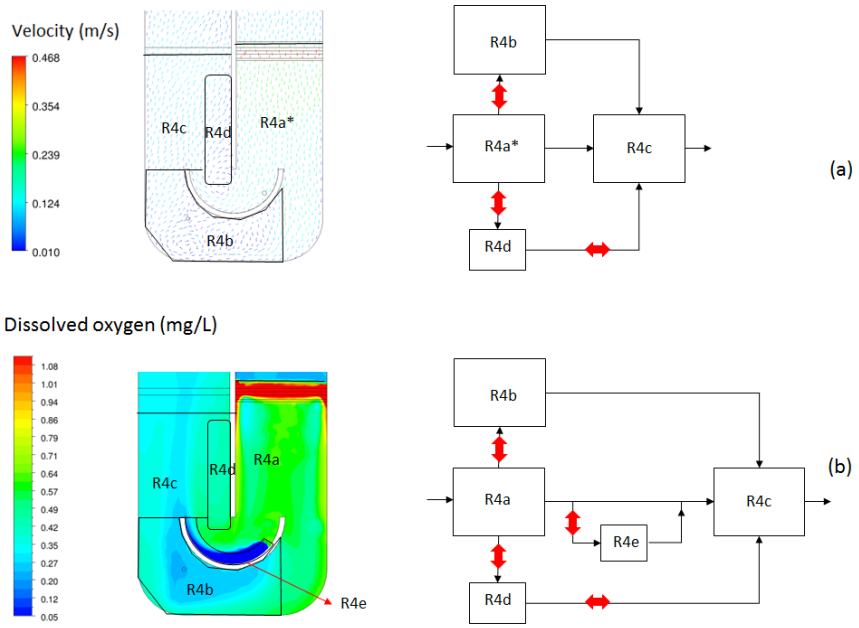

Figure 6.28 The compartmentalisation of the R4 region (a) using hydrodynamics and (b) CFD-biokinetic results (black and red arrows are the convective and exchange fluxes respectively) (R4a*=R4a+R4e)

Even though the CSDs for R1 and R3 do not show significant variations, but considering the underlying hydrodynamics, the influent stream in the R1 compartment flows close to the middle wall and does not mix with the bulk flow. The DO variations are low because the values are delimited here as well, however, the impact of this hydrodynamic behaviour can be concluded from the ammonium concentrations provided in the Figure 5.14 in Chapter 5. Therefore, seeing the R1 region as one completely mixed tank is hard to assume and hence it is further compartmentalised into three compartments R1a, R1b and R1c (Figure 6.29). The R1b & R1c incorporate the DO variations along the width due to the influent stream. Whereas, the R1a compartment is formed to take into account the variations along the length. Similarly, in the R3 region as well, the influent stream keeps on flowing close to the wall. Although, the variations in the DO concentrations are not substantial in this region as the DO values are delimited but the impact of influent flow is visible. Therefore, the R3 region is initially further divided into four compartments R3a, R3b, R3c & R3d such that the R3a & R3b and R3c & R3d divisions take into account variations along the width and the R3a & R3c and R3b & R3d divisions take into account the variations along the length in the R3 region. The R3 compartment is a little different from the R1 compartment as the influent stream flows through its entire length. However, in the R1

compartment the inlet is near the middle of the region and does not impact the upstream region and, hence, there is no need of compartmentalisation along the width in the region before the inlet.

As result of the longitudinal compartmentalisation, a total of 16 compartments are proposed. Figure 6.30 shows the overall longitudinal compartmental distribution in the reactor.

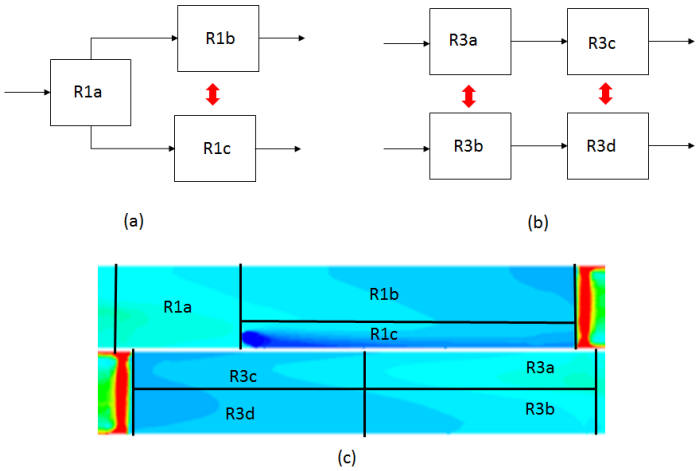

Figure 6.29 The compartmentalisation of (a) the R1 and (b) the R3 regions of the reactor using (c) the CFD-biokinetic results

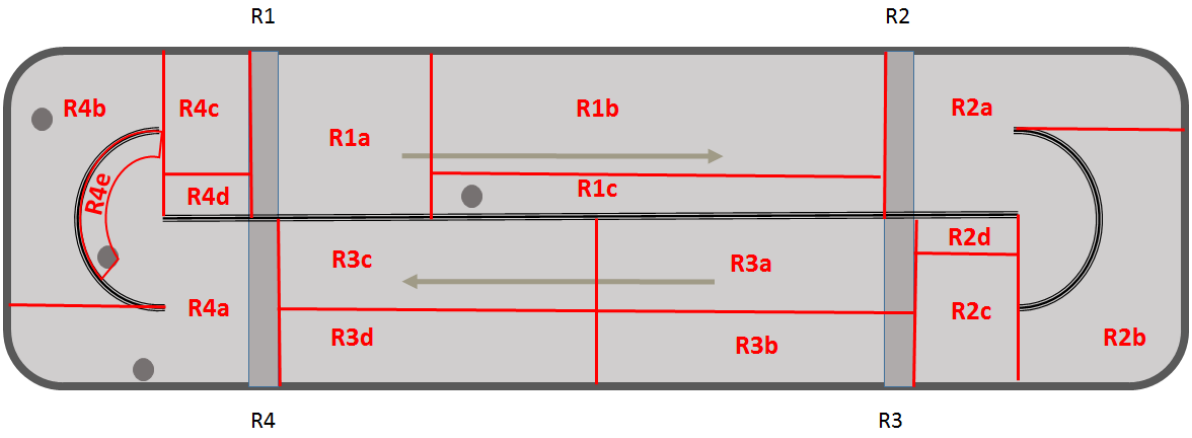

Figure 6.30 The longitudinal/lateral compartmentalisation of the reactor

6.3.2.2. Vertical compartmentalisation for the 2-rotor case

As observed in Figure 6.23, the DO variations along the depth are more pronounced in the R2 and R4 regions where the rotors are operating. Therefore, only these regions are compartmentalized along the depth into two compartments (top and bottom) as shown in Figure 6.31 for the R4 region. For the convenience, the top and bottom compartments are named R4a_T and R4a_B respectively. The compartments are connected by the respective convective and exchange flux. The exchange flux exists due to the formation of a dead zone at the bottom that leads to recirculation between both compartments.

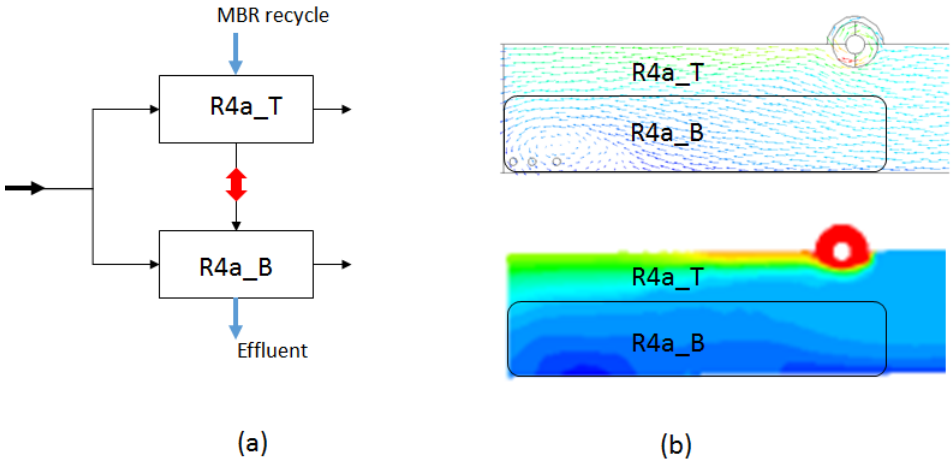

Figure 6.31 (a) Vertical compartmentalisation of the R4 region using (b) the CFD-biokinetic results

As a result of the two extra compartments along the depth, the total number of compartments is now 18. The overall compartmental network including all the sub-

compartments is provided in Figure 6.32. The complexity of the network is evident, as several sub-compartments have multiple incoming and outgoing fluxes.

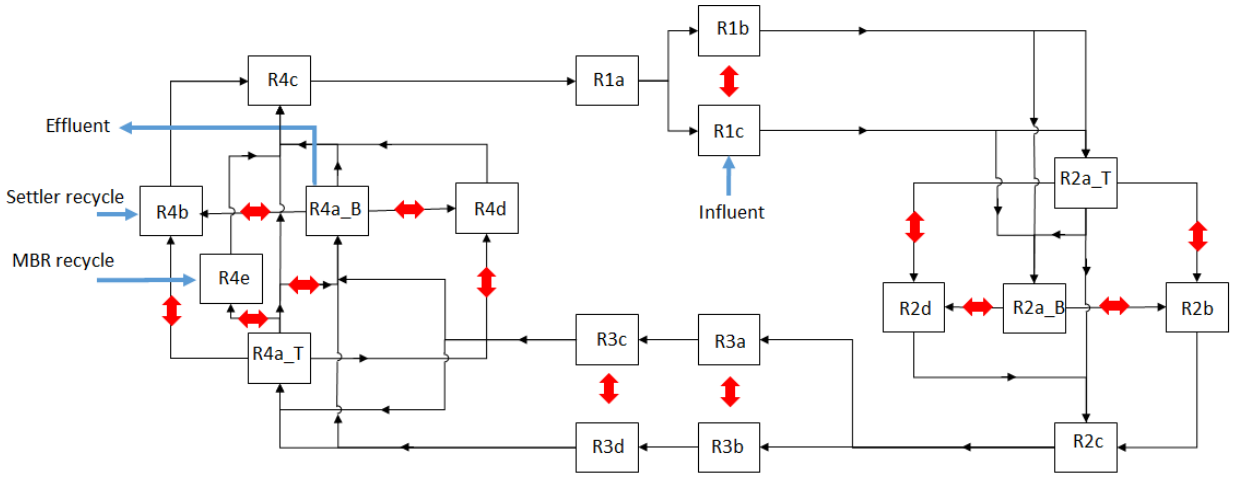

Figure 6.32 The overall compartmental network of the oxidation ditch for the 2-rotor case

6.3.2.3. Flux calculations

As discussed earlier in the section 6.2.2.3, the convective and exchange fluxes are calculated from the CFD hydrodynamic model as a product of velocity and the area of the compartmental facet. Here as well, the local coordinates are created at the centre of interfaces between two adjacent compartments to compute the local velocities going into and out of a compartment.

6.3.2.4. Compartmental model for the 4-rotor case

The CSDs for the 4-rotor case are presented in Figure 6.33. The overall variation in the 4-rotor case ranges from 0 to 1.7 mg/L in comparison to 0 to 1.3 mg/L for the 2-rotor case. The oxygen concentrations have increased generally in the reactor, for example, only 15% of the reactor had DO concentrations more than 0.6 mg/L in the 2-rotor case (Figure 6.25) whereas, in the 4-rotor case 30% of the reactors volume has a DO concentration of more than 0.6 mg/L. Similar to the 2-rotor case, the CSDs for the regions R1 & R3 are steeper than the R2 & R4 regions for the 4-rotor case. However, in comparison to the 2-rotor case the R1 and R3 CSDs show more variation. The increased variations are due to the extra rotors functioning in the 4-rotor case and, hence, increasing the concentration differences between the top and bottom of the reactors. The CSDs for the R2 & R4 regions have similar steepness for both the cases

with the only difference being the overall concentration range has increased for the 4-rotor case. The impact of dead zones and the inadequate oxygen concentrations at the bottom still persist in the 4-rotor case as observed in Figure 6.22b.

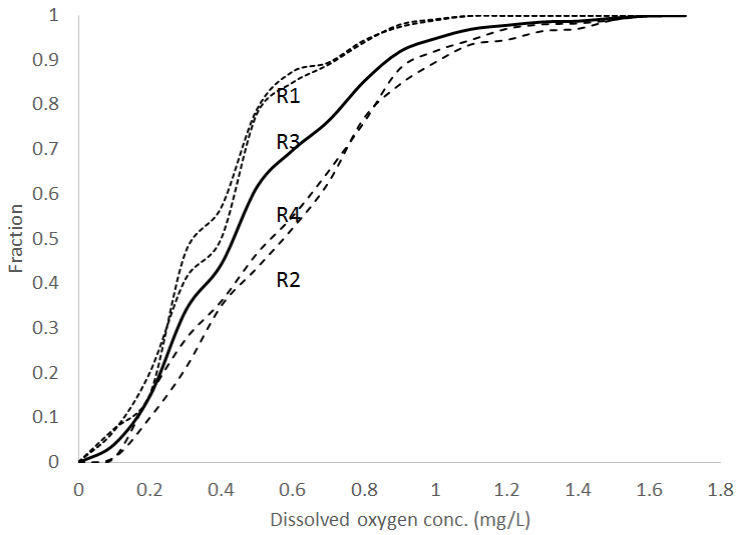

Figure 6.33 The oxygen CSD for different sections of the oxidation ditch shown in Figure 6.21b for the 4-rotor case

The DO variations (as observed in Figure 6.22, Figure 6.24 & Figure 6.33) in the R1 and R3 regions increase when all four rotors are operating. These variations exist mainly along the depth of the reactor. The variations in other parts of the reactor are similar to the 2-rotor case. Therefore, for the 4-rotor case, the R1 and R3 regions are further compartmentalized along the depth. This results in 7 additional compartments (four for the R3 region and three for the R1 region) along with additional convective and exchange fluxes. In total there are now 25 compartments for the 4-rotor case. In addition, the fluxes between the existing compartments are different as compared to the 2-rotor case due to extra momentum induced by the additional rotors.

6.3.2.5. Dynamic compartmental model

The above findings lead to the fact that under different operating conditions a single CM with a fixed number of compartments and fluxes is not sufficient. However, the number of compartments can be kept to 25 for both the cases because increasing the number of compartments from 18 to 25 for the 2-rotor case would not negatively impact the results. However, fluxes would be different and, hence, there is a need of a dynamic compartmental model which can account for the changes in the operational conditions.

This can be achieved by making the fluxes dynamic as a function of operating rotors. In order to make it more robust, the fluxes can be correlated to the speed of the rotors and, hence, the dynamic CM is able to take into account the variations in the speed of the rotors. However, extra CFD simulations with varying rotor speeds would be needed to achieve this. This is not covered in this study but it can be a future refinement to make the CM more robust and applicable to a broader range of operational conditions.

6.4. General conclusions

A comprehensive method and approach for deriving compartmental models from CFD-biokinetic results is presented and applied for two case studies. In addition, the concept of cumulative species distributions is defined and applied to quantify the DO variations in the reactors. The CSDs provided an easy way to compare DO variations occurring in different sections of the reactors. It proved to be an important method to evaluate the system heterogeneities in detail and can be used as decision support for deciding on the compartmentalisation of the system.

The compartmental model significantly reduces the computational demands as compared to the CFD-biokinetic model. For example, the CFD-biokinetic model for the Eindhoven case is based on 1.5 Million cells, whereas, the compartmental model consists of only 13 compartments capturing the majority of the important macroscale flow patterns. The development of such a simple and reduced model definitely needs laborious calculations of fluxes, nevertheless, compared to the TIS it is more robust and incorporates the detailed knowledge of the system. Such models will further reduce the need for calibration and reduce model uncertainty. They allow the possibility of modelling the specific processes that require low DO predictions (e.g. anammox, N/DN,…). Furthermore, they pave the way to devise robust control strategies and choose better sensor location and controller setpoints.

The compartmental modelling also enables the development of a dynamic CM which can ultimately take into account the impact of varying operational conditions on the system performance.

Chapter 7

Impact of sensor location on the performance of wastewater treatment plant control

This chapter is redrafted from "Rehman, U., Vesvikar, M., Maere, T., Guo, L., Vanrolleghem, P.A., Nopens, I., 2015. Effect of sensor location on controller performance in a wastewater treatment plant. Water Sci Technol 71, 700–708. doi:10.2166/wst.2014.525".

Abstract

Complete mixing is hard to achieve in large bioreactors in wastewater treatment plants. This often leads to a non-uniform distribution of components such as dissolved oxygen and, hence, the process rates depending on them. Furthermore, when these components are used as input for a controller, the location of the sensor can potentially affect the control action. In this contribution, the effect of sensor location and the choice of setpoint on the controller performance were examined for a non-homogeneously mixed pilot bioreactor described by a compartmental model. The impact on effluent quality and aeration cost were evaluated. It was shown that a dissolved oxygen controller with a fixed setpoint performs differently as function of the location of the sensor. When placed in a poorly mixed location, the controller increases the aeration intensity to its maximum capacity leading to higher aeration costs. When placed just above the aerated zone, the controller decreases the aeration rate resulting in lower dissolved oxygen concentrations in the remainder of the system, compromising effluent quality. In addition to the location of the sensor, the selection of an appropriate setpoint also impacts controller behaviour. This suggests that mixing behaviour of bioreactors should be better quantified for proper sensor location and controller design.

7.1. Introduction

The discharge of treated wastewater and the disposal of sludge from treatment plants treating domestic or industrial wastewater are subject to regulations imposed by the authorities. The main focus of wastewater treatment plants (WWTPs) is to reduce the BOD (biochemical oxygen demand), COD (chemical oxygen demand) and nutrients in the effluent discharged to natural waters, meeting the discharge regulations. WWTPs are designed to function as "microbiology farms", where bacteria and other microorganisms (activated sludge) are fed wastewater containing organic waste. Aeration plays a vital role in a wastewater treatment process and its purpose is twofold. First, oxygen must be dissolved in wastewater, in sufficient quantities, to support the biological activities associated with BOD reduction and nitrification. Second, the contents of the tank must be sufficiently mixed to keep the wastewater solids in suspension and uniformly mixed during the treatment. Wastewater treatment plants are typically operated at at least 1-2 mg/L dissolved oxygen (DO) to ensure enough aerobic process conditions. This is required for effective BOD removal, maximal rates of nitrification, and a reduction in the volume of sludge remaining after wastewater treatment.

Like any other process, wastewater treatment systems need to be operationally and cost-effectively optimized and aeration is one of the most energy intensive operations associated with the treatment process. Up to 60-65% of the total energy consumption is used for the activated sludge part of the treatment plant, i.e. for the stirring and aeration systems and pumping recycles (Duchène et al., 2001; Rieger et al., 2006). This shows the importance of proper design and operation of such systems and it thus indicates the need for an optimized control strategy.

The increasing demands on effluent quality at lower operational costs have promoted the development of new technologies and the implementation of control concepts to improve the overall performance of WWTPs (Fikar et al., 2005; Olsson, 2012; Olsson et al., 2015). Here, on-line sensors are used to gather process information and action is undertaken depending on the system’s state (feedback control). Full-scale applications have shown the feasibility of automatic control in aeration systems, chemical dosage and recycle flows (Devisscher et al., 2002; Ingildsen et al., 2002; Olsson et al., 2015; Onnerth et al., 1996). Dynamic simulation studies have also been used to compare the performance of different control strategies (Corominas et al., 2006; Flores-Alsina et al.,

2008; Machado et al., 2009; Spanjers et al., 1998; Stare et al., 2007; Zhao et al., 1995) or to evaluate them before full-scale implementation (Ayesa et al., 2006). Plant-wide operation has also been introduced to take into account the interactions between the processes (Gujer, 2006; Jeppsson et al., 2007; Lessard and Beck, 1993; Nopens et al., 2010). In this regard, the location of sensors has also been discussed (Waldraff et al., 1998), but these studies often has to do with the development of observers whose results are used as input to controllers.

Controllers for WWTPs are typically designed based on process models that approximate the mixing by a tanks-in-series (TIS) approach. In the TIS approach, the mixing behaviour of the whole reactor is modelled as a number of completely mixed continuous stirred tank reactors considering the flow in only one direction. This approach can only account for some back-mixing by maintaining the liquid longer in the system by adjusting the back-mixing rate (Le Moullec et al., 2010b). Hence, at most, sensor locations in the advective flow direction (1D) can be considered, whereas in reality these might not represent the overall reactor behaviour. Therefore, sensors should be placed in those regions that are a good approximation of the reactor behaviour. An optimal number of tanks (to some extent) can better predict the overall behaviour of the reactor. However, all the tanks are considered completely mixed. In this way they average out local variations occurring in the other two dimensions. In reality perfect mixing never occurs because only a portion of the reactor is directly aerated and oxygen is transferred to the rest of the reactor through advective transport (air bubble flow along with the liquid flow). The effectiveness of this advective transport mainly depends on reactor design and induced hydrodynamics of the system (Jin et al., 2006). Mass transfer between air and water occurs depending on the local concentration gradient and inter-phase resistance. Therefore, inefficiently mixed reactors possess less mixed regions or even completely dead zones resulting in a non-uniform environment. Thus, in conclusion, the TIS approach is unable to take into account the reactor inhomogeneity. This drawback of TIS modelling implies its limitation for evaluating the effect of sensor location on the controller performance.

Computational Fluid Dynamics (CFD) has emerged as a useful tool which allows more accurate evaluation of local phenomena such as mixing (Brannock et al., 2010; Cockx et al., 2001; Glover et al., 2006; Laborde-Boutet et al., 2009; Le Moullec et al., 2010a; Wang et al., 2010). Furthermore, biokinetics and CFD have been integrated to understand the system in more detail (Le Moullec et al., 2011, 2010b). However, CFD is computationally very intensive for a complex system such as a WWTP. Therefore,

an intermediate solution between TIS approaches and CFD modelling, called Compartmental Modeling (CM) has been used in previous studies (Alvarado et al., 2012; Gresch et al., 2009; Le Moullec et al., 2010b). A CM consists of a number of compartments C_i of volume V_i configured in more than one dimension and in which a recirculation flow Qr_i from compartment C_{i+1} to C_i occurs, along with the forward flow. It has been concluded that this approach reduces the computational requirements (with respect to the CFD) and improves the hydrodynamic predictions (with respect to the TIS) by taking recirculation flows into account and by modelling the flow in all three dimensions.

The main driver, today, for choosing the location of on-line sensors is easy accessibility for maintenance and installation. The fact whether the sensor is located in a place that severely deviates from the average behaviour in the monitored process is usually not considered. However, since this local value provides the input to the controller, it directly impacts its behaviour and success. This contribution illustrates the impact of sensor location in an aerated bioreactor of a WWTP on the process performance by using a compartmental model derived from CFD predictions.

7.2. Materials & methods

The compartmental model used in this study is borrowed from the study of (Le Moullec et al., 2010b) who developed it for a pilot plant reactor based on a CFD model. The reactor was a pilot gas/liquid channel reactor with a very long length compared to its height and width (Le Moullec et al., 2010a, 2010b) and thus leading to water flow along the length of the reactor (Figure 7.1). The total length of the reactor was 3.6m with a rectangular cross-section of 0.18m width and 0.2m height. One side of the walls was fitted at the bottom with stainless-steel tubes in which 1mm holes were present every centimetre for air sparging. The mixed liquor was recycled at the inlet keeping a recycle ratio of 4. A 0.88m^3 settler was used to clarify the mixed liquor and to produce sludge which was also recycled at the reactor inlet keeping a recycle ratio of 1. As the biological kinetics involved in the reactor are well represented by Monod equations with apparent reaction orders higher than zero, thus the pollution removal efficiency depends on the hydrodynamics (Levin et al., 1993).

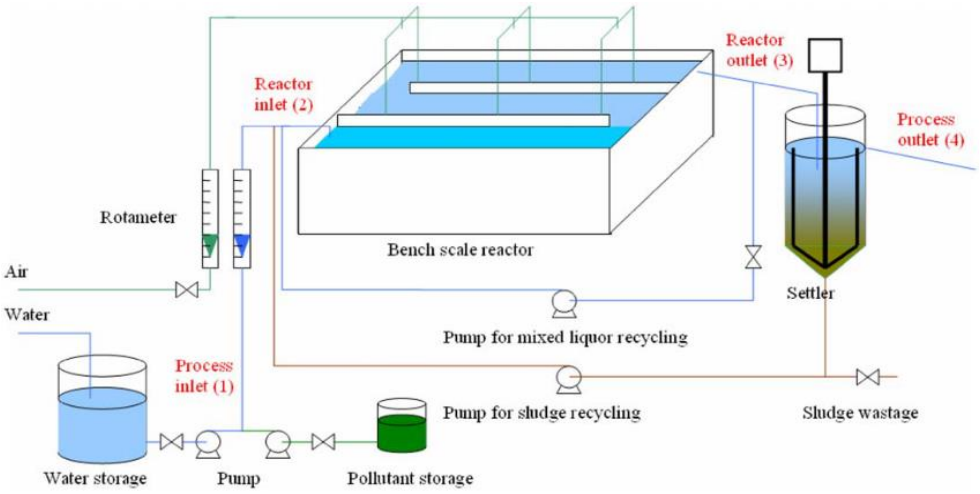

Figure 7.1 Channel reactor configuration (Le Moullec et al., 2010b)

7.2.1. Compartmental modelling

Compartmental modelling describes the reactor as a network of spatially localized compartments. Compartments are chosen on the basis of process knowledge and CFD results. The configuration of the compartments is based on the determination of homogeneous physical-chemical properties within a given tolerance. Shape, number and connectivity of these compartments are determined on the basis of the following parameters:

- The distribution of gas fraction i.e. extent of mixing
- The liquid velocity field to compute flow rates
- Liquid turbulence characteristics (k & ε), A previous study (Le Moullec et al., 2010a) has shown that the dispersion coefficient along the reactor is mainly dependent on these characteristics

As the studied system was a channel reactor, flow remains invariant along the length. Thus, the reactor could be split into just six slices of equal size along the length. It was obvious from the design of the reactor and also observed from the velocity and turbulence profiles of the CFD studies that air rises along the side of the wall and causes recirculation in the reactor. This recirculation creates dead zones in the middle and in the corners of the reactor. Hence, the reactor cross-section was divided into 4 different zones on the basis of flow dynamics. For clarity, each zone is labelled as GR (gas rich

zone), RL (recirculating liquid zone), CR (corner zone) and CN (centre zone) (Figure 7.2).

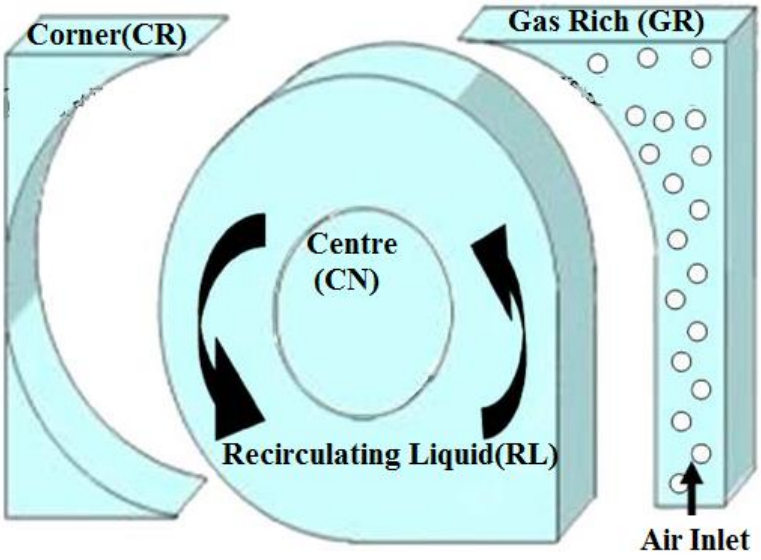

Figure 7.2: Cross-sectional compartments (Le Moullec et al., 2010b)

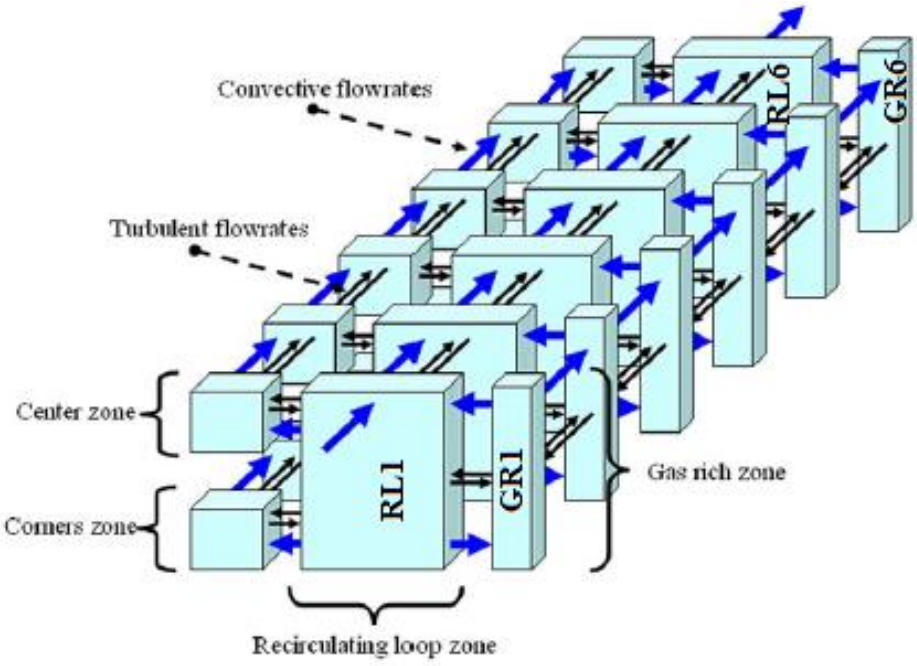

Figure 7.3 The compartmental layout of the reactor (Le Moullec et al., 2010b)

These labels are accompanied by the numbers 1 to 6 where 1 represents the first slice at the reactor entrance and 6 is the last zone near the outlet. This eventually resulted in a total of 24 compartments, i.e. 4 zones in each of the 6 slices (Figure 7.3). All

compartments are coupled through bidirectional fluxes. The model was implemented in the modelling and simulation platform WEST (http://www.mikebydhi.com) and used the BSM1 dry weather influent with dynamic diurnal effects (Jeppsson, 2014). In order to study the effect of sensor location, controller performance was evaluated in terms of both aeration cost and effluent quality.

7.2.1.1. Model configuration in WEST

The compartmental layout in the WEST simulation platform is shown in Appendix A 3. It consists of a network of 24 reactors, where each reactor represents one compartment in which reaction conditions are created. Each compartment has also inter-compartmental connections for respective convective and exchange fluxes. Convective fluxes in principle are the flow rates due to the main flow patterns (determined by velocity profiles through CFD) of fluid in the reactor. Exchange fluxes are calculated based on the turbulent characteristics of the flow along with the main flow. The reactors in this layout are distributed in a network of 4 rows which represent each of the 4 zones in a slice i.e. GR, RL, CR and CN. The top row represents GR reactors which account for 30% of the total reactor volume. These compartments are directly aerated as air is being pumped in these regions. All remaining compartments do not have direct aeration. Though, oxygen can be transferred to these reactors by convective or recirculation flows (i.e. through liquid transport terms). The 2^{nd} row from the top represents RL compartments which account for 50% of the total reactor volume. The inlet and outlet of the reactor are present in RL1 & RL6 compartments respectively. The 3^{rd} and 4^{th} rows respectively represent the corner and central dead zone compartments. Connections coming out of a reactor are accompanied with flow splitters to divide the flow between forward flow & recirculation fluxes. It can be seen that flow out of each GR (except GR6) reactor is partially sent back to the respective RL zones i.e. from GR1 to RL1 and partially forwarded to GR2. Similarly, in RL compartments, part of the flow is sent back as an exchange flow to the respective GR compartment i.e. from RL2 to GR2. CR & CN being dead zones do not exchange flow with other compartments through convective transport. For the GR6, CR6 and CN6 compartments all flows are directed towards the RL6 compartment and finally out of the reactor. Effluent from the reactor is carried to the secondary clarifier before discharge. Two recycle streams, one from reactor effluent and the other from the underflow of the secondary clarifier, are sent back to combine with the inflow to RL1.

The biological kinetics model chosen for this study is the ASM1 model (Henze et al., 2000, 1987) for the biological modelling of all reactors. This model is frequently adopted to simulate or predict performances of biological reactors. It is suitable to simulate carbon oxidation, nitrification and denitrification in the aerobic and anoxic zones of activated sludge reactors. It considers 12 different components and eight kinetic processes. The default values were used for all stoichiometric and kinetics parameters.

7.2.1.2. Simulations setup:

The PI controllers for maintaining the DO at a certain level were implemented in the WEST simulation platform. Two sets of simulations were performed: first the controller configurations were fixed and the sensor location was changed; second, the controller settings were varied, i.e. DO setpoint, at two different locations. All other parameters and influent composition remained the same for all simulations. Steady state conditions were achieved by running the simulation for 100 days. Subsequently, the controller was implemented for dynamic inflow conditions during 28 days.

7.3. Results & discussion

7.3.1. Simulations with varying sensor location:

For the first set of simulations, a PI controller was implemented and fed with the signal of a DO sensor placed in different compartments i.e. GR1, GR3, GR6, RL6 and CR6. These locations were selected based on the fact that usually DO is measured near the bioreactor outlet and at the water surface (easy access for maintenance). Controller settings (controller gain 200 & reset time 0.1hours) were kept fixed for each sensor location in order to only evaluate the impact of the location. The setpoint for DO concentration was chosen as 1.5 mg/l according to common industrial practices (Olsson, 2012). The effluent regulations in BSM1 impose constraints for effluent BOD, ammonium-nitrogen (NH_4-N) and total nitrogen, respectively at 10 mg/L, 4 mg/L and 18 mgN/L (Jeppsson, 2014). Effluent quality in terms of BOD, ammonia and DO in the effluent was sampled in the final compartment named RL6 as this is the actual outflow of the reactor.

The effect of sensor location on average effluent quality and aeration cost per day is shown in Figure 7.4. The aeration cost only includes the energy requirements for aeration. It is evident from the figure that when the sensor is placed in the GR compartments where aeration is actually taking place, BOD and ammonia concentrations in the effluent are quite high. Indeed, the aerated GR compartments have higher DO concentrations as compared to other compartments to which oxygen is transferred only by advection. The DO setpoint is easily reached and leads to local higher values of DO in the GR compartments. As a result, the controller reduces the aeration rate to bring the DO level back to 1.5 mg/L, which leads to much lower DO levels in the other, not directly aerated compartments. It can be seen in Figure 7.4 that the DO level in the effluent is as low as 0.03 mg/L in the cases where the sensor was located in GR1, GR3 & GR6. This of course explains the higher BOD and NH_4 levels in the effluent for these cases because lower reaction rates occur due to the low DO levels. Changing the location of sensor between GR1, 3 and 6 did not result in significantly different behaviour due to similar aeration conditions in these compartments. For this particular reactor, this behaviour indicates that there is no significant effect of inlet & outlet location as long as the sensor is placed in the aeration zone.

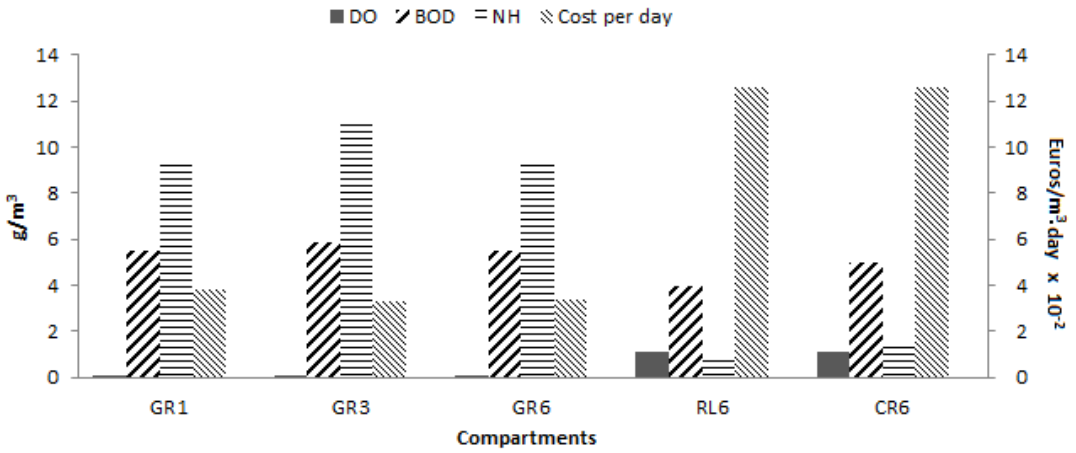

Figure 7.4: Average effluent quality & aeration cost per day with a fixed DO setpoint of 1.5mg/L

When the sensor was placed in the recirculating liquid and corner zones with relatively low DO values, the controller kept on increasing aeration (within the blower specs) to achieve the setpoint. In these poorly mixed zones the setpoint was hard to reach and the maximum capacity of aeration had to be imposed in order to reach the setpoint. The DO

concentration in the effluent was 1.1 mg/L resulting in good effluent quality in terms of ammonia removal but at very high aeration costs. The DO concentration in GR zones was found to be as high as 7 mg/L.

7.3.2. Simulations with varying setpoint:

The first analysis led to a 2nd set of simulations for obvious control optimization by changing the setpoint to higher values when the sensor is placed in GR zones or lowering it when placed in RL zones. A higher setpoint for GR zones will eventually result in increased aeration and better oxygen transfer to other zones, whereas a lower setpoint in the RL zone will cause a decrease in aeration and thus lower costs.

Three different setpoints were applied in both the GR6 and RL6 compartments. In the GR6 compartment, the setpoint was increased from 1.5 mg/L to 2 and 2.5 mg/L. In contrast, the DO setpoint in RL6 compartment was reduced from 1.5 mg/L to 1 and 0.5 mg/L. The results in terms of average effluent quality and cost of these six simulations are summarised in Figure 7.5 (RL6-1.5 corresponds to the sensor being placed in the RL6 compartment with a DO setpoint of 1.5 mg/L).

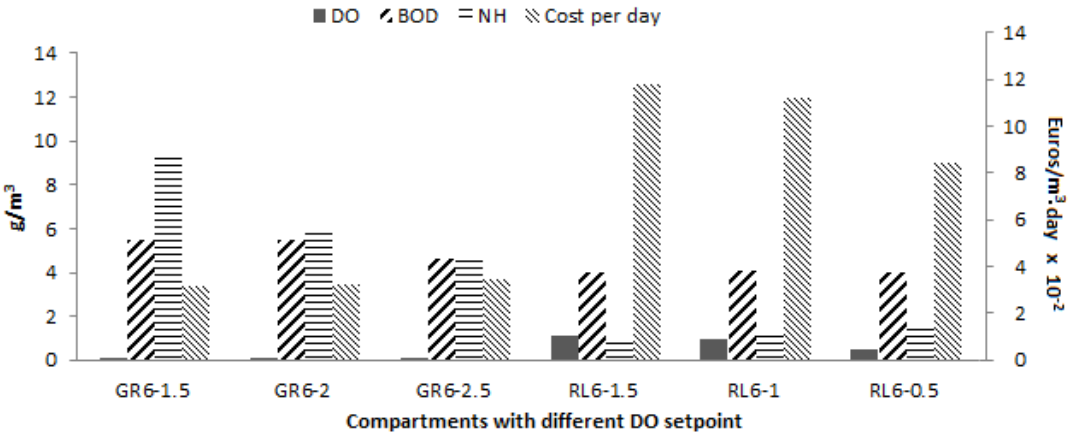

Figure 7.5: Effluent quality & aeration cost per day with varying DO setpoints

It can be observed that increasing the DO setpoint in the GR zones causes an increase in aeration and better oxygen transfer to the other compartments resulting in lower BOD and ammonia concentrations in the effluent, however at higher aeration cost. The gain from 1.5 to 2 mg/L is larger than from 2 to 2.5 mg/L (Figure 7.5). This observation leads to the conclusion that increasing the setpoint in aerated zones (e.g. GR compartments) will not linearly increase the effluent quality. Decreasing the DO

setpoint to 1mg/L in RL zones resulted in lower aeration costs while maintaining good effluent quality. It can be seen that further reducing the setpoint to 0.5 mg/L caused significant decrease in aeration costs but effluent quality significantly decreased as well. It is to be noted that the aeration cost in the case of RL6-0.5 is still two and a half times higher compared to GR6-2.5. The increase in cost relative to DO in the effluent can be seen in Figure 7.6.

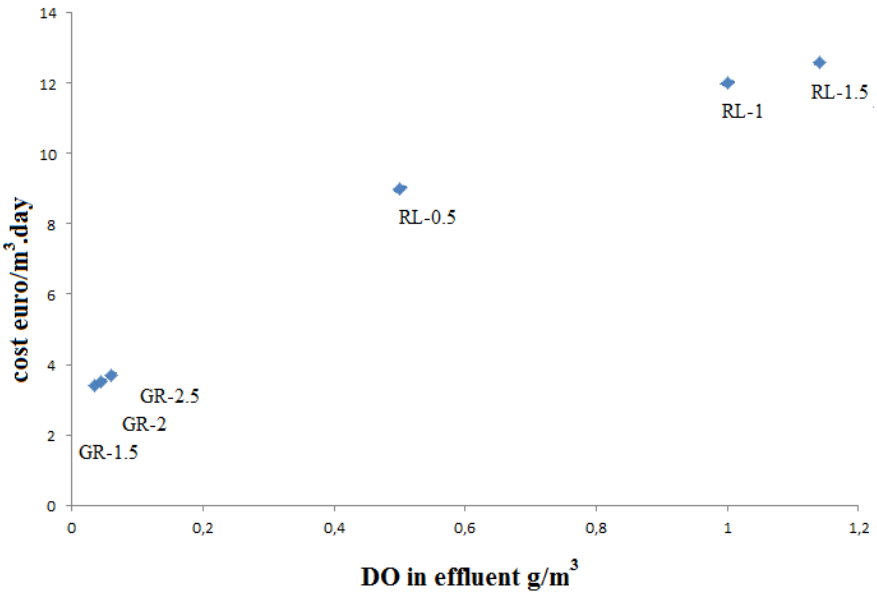

Figure 7.6: DO in effluent vs Cost for different setpoints in GR & RL zones

Figure 7.6 shows the level of DO in the effluent and the corresponding cost for aeration for all different setpoints in RL & GR compartments. The figure shows that only the cases RL-0.5 and RL-1 result in actual effluent DO levels equal to the controller's setpoint. In all other cases effluent DO failed to reach the actual setpoint in the effluent either due to bad mixing or physical limitations of the aerators (i.e. in RL-1.5).

7.3.3. Simulations with NH_4-DO control:

In addition to the above mentioned set of simulations, an NH_4-DO cascade control strategy was also applied to investigate its impact on the effluent quality. In this control strategy an NH4 controller selects the setpoint of a DO controller which directly controls the aeration rate (Zhang et al., 2008). A fixed setpoint of 2 mg/L was used for ammonia, while the DO controller gets its setpoint as an input from the ammonia controller. Both ammonia and DO probes were placed in the GR6 compartment. In order to achieve the desired setpoint of ammonia, a higher DO level is required which

leads to higher aeration in GR compartments. Thus, it resulted in lower BOD and higher DO concentrations in the effluent. A comparison in terms of DO, BOD and ammonia dynamics between DO control and NH_4-DO cascade control can be seen in Figure 7.7. It should be noted that in both cases, a steady state solution was achieved before applying the controllers. Therefore, starting points for both DO & NH_4-DO simulations were the same. It can be inferred that the cascade control partially corrects the bad sensor location resulting in improved effluent quality and DO concentration.

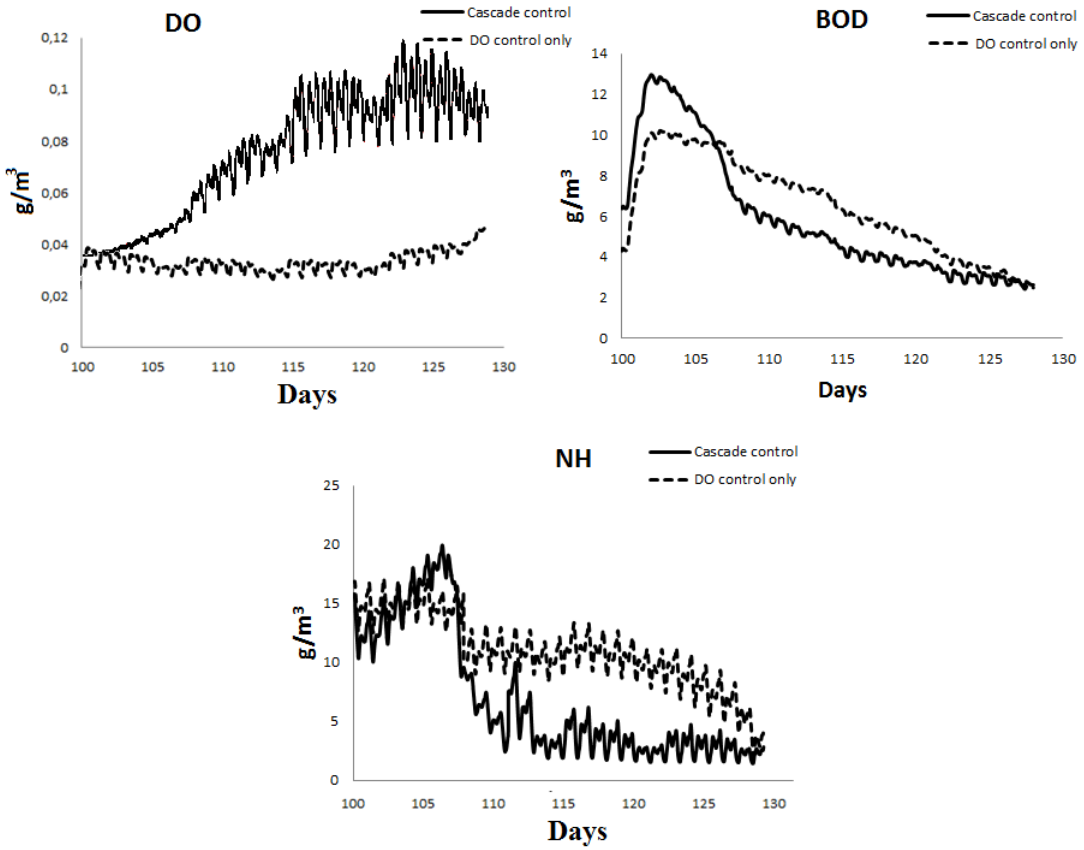

Figure 7.7: DO, BOD & NH dynamics for DO control and NH_4-DO cascade control

7.4. Conclusions and outlook

Due to the complex mixing behaviour of full-scale reactors, tanks-in-series models usually used to develop controllers, are not very realistic because they are severely oversimplifying real mixing behaviour. It is shown that knowledge of process hydrodynamics can be useful in deciding the appropriate location of sensors. A

compartmental model that refines the mixing behaviour of a pilot reactor illustrated clearly that in order to achieve cost-effective DO control the sensor location and setpoint are of importance. Hence, this should be embedded in a control design protocol. Another path forward is to redesign reactors and embedded aerators to better achieve completely mixed conditions. However, it must be ensured that such new design does not lead to reduced process efficiency or increased construction costs.

PART IV

Impact of bulk mixing on calibration

Chapter 8

Impact of bulk mixing conditions on the half saturation indices

This chapter is redrafted from "Arnaldos, M., Rehman, U., Naessens, W., Amerlinck, Y and Nopens, I., 2016. Understanding the Effects of Bulk Mixing on the Determination of the Affinity Index: Consequences on Process Operation and Design. (submitted to Water Research)". (It was joint first authorship and I did all the simulation work)

Abstract

The main objective of this study is to demonstrate the importance of mixing limitations as a source of inconsistencies between half-saturation indices in similar/identical systems when operated at different conditions. An exemplary system consisting of the second vessel of a hybrid respirometer has been studied. This system has been modelled both using a computational fluid dynamics (CFD)-biokinetic model (representing the physical system) and a tanks-in-series, completely stirred tank reactor (TIS-CSTR)-biokinetic model (representing the applied model). The results show that different mixing conditions cause deviations in the half-saturation indices calculated when matching the applied model to physical system performance. Additionally, sensor placement is shown to impact the calculation of half-saturation indices in the respirometric system. Thus, mixing conditions clearly affect operation and design of wastewater treatment systems with low substrate concentrations. Both operation and design can be improved with the development and application of integrated CFD-biokinetic or compartmental models.

8.1. Introduction

The Monod equation (Monod, 1942) has been used extensively for modelling the majority of biological treatment processes in the wastewater treatment field (Henze et al., 2000). Essentially, the Monod equation describes microbial growth through two kinetic parameters; the maximum specific growth rate and the so-called "affinity constant" (often termed the "half-saturation constant" and represented by K_S). Given that the "affinity constant" will affect the description of the treatment performance at low substrate conditions and the predominance of high-rate activated sludge processes (with high substrate concentrations), hitherto its importance on process evaluation and design has been relatively low. However, as effluent regulations are becoming more stringent and emerging wastewater treatment processes that operate with low substrate concentrations (e.g. simultaneous nitrification-denitrification, partial nitrification, anammox processes) are increasingly implemented at full-scale, there is a growing interest in determining the values of "affinity constants" for different substrates, biological reactions and organisms. Given the high variability in the values reported for "affinity constants" in different studies for similar processes (Arnaldos et al., 2015), research on this area has only partially improved the understanding of wastewater treatment systems. The reported variability has been pointed out to be due to the inherent limitations of the "affinity constant" concept. In order to reflect the real nature of this concept, the more appropriate terminology of "half-saturation index" has been adopted (Arnaldos et al., 2015). The novel terminology reflects the fact that the "affinity constant" is in fact not a constant, but rather an index influenced by numerous and heterogeneous phenomena. In fact, three distinct categories of phenomena influencing half-saturation indices have been identified: advectional, diffusional and biological. Arnaldos et al. (2015) concluded that the variety of factors influencing the half-saturation indices has caused the –seemingly- conflicting evidence when determining their values for different treatment systems. A factor that was pointed out to potentially hold more importance than it is accredited for when determining half-saturation indices in certain systems is bulk mixing conditions (pertaining to advectional phenomena). This factor and its impact on the half-saturation indices has not been systematically addressed, unlike other diffusional and biological factors, that have been granted significantly more attention by the wastewater process research community. However, it could be argued that, from a logical perspective, macroscopic factors should be analysed in the first place before descending to microscopic phenomena.

Furthermore, direct and indirect evidence that mixing conditions are important when determining half-saturation indices can be found in the published literature. For instance, Munch et al. (1996) studied a simultaneous nitrification-denitrification (SND) system and found that the half-saturation index for oxygen ($K_{O,A}$) in ammonia-oxidizing bacteria (AOB) of 4.5 mg O2/L represented the behaviour of the system appropriately. This high value has been suggested to result from limitations in oxygen diffusion through the activated sludge flocs (Daigger et al., 2007). In biofilm systems, however, maximum $K_{O,A}$ values for AOB of 2 mg O_2/L are commonly considered (Lackner and Smets, 2012); it is therefore logical to assume that values significantly higher than 2 mg O_2/L are not due to diffusional limitations only but include other effects as well. One of these effects could be hypothesized to be mixing conditions (advectional limitations) in the bulk liquid. This is consistent with SND being reported in many oxidation ditches, systems known to suffer from mixing limitations (Liu et al., 2010; Zhang and Qi, 2007). Likewise, in membrane bioreactors (MBR) half-saturation index determination can be affected by mixing limitations. For instance, biological phosphorus removal has been demonstrated in fully aerobic MBR systems (Rosenberger et al., 2002; Verrecht et al., 2010); this phenomenon is consistent with mixing limitations causing some fractions of the reactor to become anaerobic and as such to stimulate biological phosphorus removal. It is important to note that high liquid density and viscosity stemming from high solids concentrations in MBR systems can augment the effects of mixing limitations. Another recent study has shown that the observed process rates for organic matter removal changed in a moving bed biofilm bioreactor (MBBR) by an order of magnitude depending on the mixing energy imposed on the system (Nogueira et al., 2015). Furthermore, in the same study, the observed process rates for ammonium consumption were shown to also change significantly despite the fact that AOB were located deep in the biofilm (where they could be thought of not being affected by mixing conditions) (Nogueira et al., 2015). These observations could impact the calculated values of the half-saturation indices, especially when dealing with low substrate concentrations.

Beyond mixing deficiencies in full-scale and pilot systems, advection limitations have also been detected in more simple and downsized systems such as respirometers. Mixing limitations are not a common assumption in respirometric systems, but the consequences could be significant. For instance, Stenstrom and Song (1991) have reported different nitrification rates at different mixing speeds in respirometric assays. This observation was also made by Chu et al. (2003), who reported decreasing half-

saturation indices for dissolved oxygen at increasing mixing energies. This could be due to initial mixing limitations in the respirometer, enhanced oxygen dissolution in water, as well as to floc breakup due to excessive mixing. Additionally, Esquivel et al. (2014) reported very high half-saturation indices for different substrates as compared to values reported in the literature when using microrespirometers. This was linked by the authors to insufficient mixing in the respirometric vessels.

The main objective of the present study is to evaluate the importance of mixing limitations as a source of inconsistencies between half-saturation indices in similar or even identical systems when operated at different conditions. In order to accomplish this, an exemplary system consisting of the second vessel of a hybrid respirometer (Vanrolleghem and Spanjers, 1998) has been studied. This system has been modelled both using a computational fluid dynamics (CFD)-biokinetic model (same as chapter 4) and a biokinetic model using a very simple tank-in-series, completely stirred tank reactor (TIS-CSTR)-biokinetic model. Given the simplicity of the system, the hybrid CFD-biokinetic model is assumed to be the best feasible representation of the real physical system, while the TIS-CSTR-biokinetic model represents the applied model. Different mixing conditions are imposed on the CFD-biokinetic model and the associated process performance has been obtained; this has been considered to reflect the actual performance of a real respirometer. Then, this process performance has been compared to that obtained by the TIS-CSTR-biokinetic model; this would represent the results obtained when using an applied model. Subsequently, the half-saturation indices have been adjusted in the TIS-CSTR-biokinetic model in order to represent effluent quality for each mixing condition in the real system, mimicking one of the current process model calibration practices. The results for the calibrated half-saturation indices and their relative deviation from the real values have been presented and discussed. The importance of mixing conditions in half-saturation index determination has been further illustrated by calculating the resulting index as a function of sensor placement in the respirometer. Finally, the potential consequences of not taking into account mixing conditions in half-saturation indices in process operation and system design have been discussed.

8.2. Materials and methods

8.2.1. Description of the exemplary respirometric system

The system investigated for the effects of mixing conditions on half-saturation indices is the second vessel of a hypothetical hybrid respirometer. This system has been chosen to have a cylindrical shape, with a volume of 2 L (12 cm diameter and 20 cm height) (Figure 8.1a); these dimensions are representative of actual hybrid respirometers. An agitation device was not included in this hypothetical system because the mixing associated with the incoming flow is commonly assumed to be sufficient for complete mixing. This system has been chosen for its simplicity, which allows modeling it fairly easily using a CFD-biokinetic approach in a representative manner of actual process conditions. As stated in section 8.1 the governing assumption is that the CFD-biokinetic model represents the physical system, while the TIS-CSTR-biokinetic model represents the applied model.

The influent composition has been chosen to mimic a typical mixed liquor coming from the first vessel of a hybrid respirometer. As such, it contains readily biodegradable organic carbon and soluble nitrogen species (in concentrations typical of wastewater treatment plants) as substrates for heterotrophic and autotrophic biomass, respectively, as well as a high concentration of dissolved oxygen due to the fact that aeration is happening in the first vessel. The detailed influent composition has been shown in Table 8.1 and was collected from the wastewater treatment plant of Eindhoven (The Netherlands), except for the concentration of soluble ammonium, which was set to be present in abundance.

Table 8.1 Wastewater composition used in both the CFD-biokinetic and TIS-CSTR-biokinetic models.

Component	Concentration (mg/L)
Readily Biodegradable Carbon	41.00
Heterotrophic Biomass	500.00
Autotrophic Biomass	98.91
Dissolved Oxygen	9.00
Soluble Nitrites and Nitrates	15.21
Soluble Ammonium (Expressed as N)	40.00
Soluble Alkalinity	30.00

8.2.2. Description of the CFD-biokinetic model

First, the geometry of the respirometer was created in the design module of the commercial tool ANSYS (version R14.5, USA) taking into account all the details which can influence reactor hydrodynamics (such as accurate location, size and shape of inlet and outlet). Next, meshing using a commercial mesh generator tool (ICEM CFD, ANSYS, Pennsylvania, US) was performed. The mesh was kept very fine (67,000 cells, i.e. $3e^{-8}$ m^3 average cell size) in order to achieve a mesh-independent solution. Subsequently, steady state CFD simulations were performed in FLUENT (v14.5) (ANSYS, Pennsylvania, US) by solving the Navier-Stokes equations using a finite volume method for a single phase. Turbulence was modelled with a Reynolds Averaged Navier-Stokes (RANS) model and the realizable k-ε model (Ishii and Hibiki, 2011). In addition, the effect of gravity over the flow patterns was incorporated in the solution of the Navier-Stokes equations. It is important to take gravity into account for realistic hydrodynamic modelling of the system. The sludge density was calculated applying a correlation with the suspended solids concentration (De Clercq, 2003). At the inlet, velocity calculated from the volumetric flow rate was used as a boundary condition.

However, the outlet velocity was not known and thus a boundary condition of 'outflow' was used, so that the CFD model can calculate it itself using the continuity (mass balance) of the system. The details on the flow rates and the associated hydraulic retention times for the different mixing conditions scenarios in this study can be found in Table 8.2.

The approach used in chapter 4 (i.e. integrated CFD-biokinetic model) has been used in the present study. Specifically, the kinetic equations included in the CFD model are those describing carbon and nitrogen removal through aerobic and anoxic reactions in the ASM1 model (Henze et al., 2000). The kinetic parameter values (including the half-saturation indices) are the default values of the ASM1 model. Hence, in this study it is assumed that the half-saturation indices from the ASM1 model are the "real" values of the physical system, since the CFD-biokinetic model is more close to reality (note that this might not be true, but does not affect the qualitative outcome of the work).

Table 8.2 Simulated scenarios in terms of flow rates and hydraulic retention times

Simulation Scenario	Flow Rate (L/h)	HRT (min)
Base Case (X)	16	7.5
2X	32	3.75
0.75X	12	10
0.5X	8	15
0.25X	4	30

8.2.3. Description of the TIS-CSTR-biokinetic model

The TIS-CSTR-biokinetic model has been set up in WEST (MikebyDHI, Denmark). Virtual tracer tests were performed with this model and compared with a virtual CFD tracer test to determine the number of tanks required for the TIS-CSTR-biokinetic model. It was found that a single tank configuration would best represent the physical system; this would be a reasonable approach from a modelling perspective, given the scale and simplicity of the system. The biokinetic model chosen within the WEST platform has been ASM1, similar to the CFD-biokinetic model case. The influent flow rates and composition used in the TIS-CSTR-biokinetic model were chosen equal to

that used in the CFD-biokinetic model (Table 8.1 and Table 8.2, respectively), and the simulations were carried out under steady-state conditions.

8.2.4. Investigation of the effect of mixing conditions on half-saturation indices determination

A step-wise procedure has been followed to investigate the effects of mixing conditions on the determination of half-saturation indices. First, the mixing limitations in the real system have been studied by using the CFD model (without the integrated biokinetic model) for the base case mixing conditions. mixing patterns and the existence of dead zones have been described. Then, the effect of different mixing conditions on process performance in the real system has been studied by calculating the distribution of substrate concentrations and substrate consumption rates with the CFD-biokinetic model. Subsequently, the deviations in process performance between the modelled and physical systems at different mixing conditions have been investigated by fixing the kinetic parameters in the TIS-CSTR-biokinetic model to be equal to the ones used in the CFD-biokinetic simulations; the effluent quality at different flow rates has been compared. In a further step, the effects of mixing limitations on half-saturation index calibration have been studied; for each flow rate used in the CFD-biokinetic model, the half-saturation index for oxygen in autotrophic organisms ($K_{O,A}$) has been estimated in order to fit the physical system behaviour, thus mimicking one of the methods followed in modelling practices. It is important to note that the $K_{O,A}$ value of autotrophic organisms was the sole half-saturation index modified during calibration since oxygen was present in concentrations close to its half-saturation index in many of the scenarios; this was not the case for the rest of substrates/electron acceptors which were abundantly available (in the saturated zone of the Monod curve). The importance of mixing conditions in half-saturation index determination has been further illustrated by calculating the different indices obtained when locating a sensor in different parts of the respirometer.

8.3. Results and discussion

8.3.1. Mixing limitations in the physical System

First, mixing limitations in the physical system have been investigated by simulating it for the base case conditions using the CFD model without including the biokinetic equations. Figure 8.1 shows the velocity vector plots for the base case in both horizontal cross sections and a vertical cross section. As can be seen, the flow follows a very distinctive pattern, moving in a circular motion along the horizontal sections (Figure 8.1b). Furthermore, the flow proceeds from the inlet to the outlet and then part of it swirls back to the bottom of the tank where it swirls again to finally exit the system (Figure 8.1c). The consequence is the existence of two areas in the tank where flow slows down and thus the resulting mixing is deficient (centre of the previously described swirls); as can be observed, the major dead zone is located in the centre of the respirometer base (middle swirl). A minor dead zone can be found towards the top of the reactor (top swirl); both these dead zones have been pointed out in Figure 8.1b and c. These mixing limitations could result in a heterogeneous distribution of substrate concentration thus causing different effluent quality as compared to a fully-mixed system. It is noteworthy that this conclusion is intimately related to the reactor design (e.g. location of inlets and outlets). The latter is usually not accounted for in detail when studying mixing limitations by means of CFD studies. Hence, some sort of mixing limitations -that could be avoided with minor design adaptations- are likely to be present in most currently used reactors, which underlines the relevance of the present work.

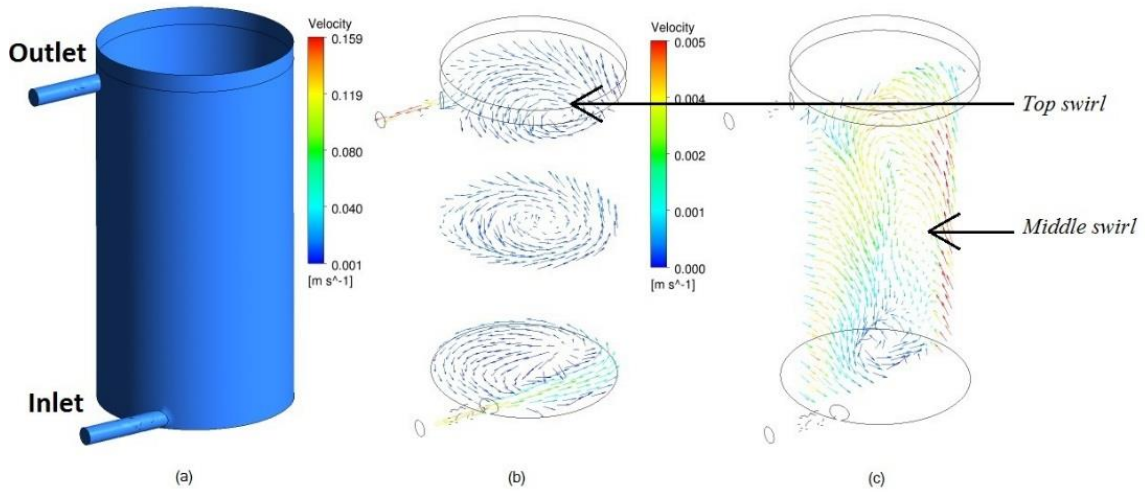

Figure 8.1 (a) Geometry of the respirometer and velocity vector plots in the base case in (b) horizontal cross sections and (c) a vertical cross section of the system (note the difference in scales used).

8.3.2. Effect of mixing conditions on process performance in the physical System

Figure 8.2 shows the steady state distribution of dissolved oxygen, ammonium and nitrate concentrations in the base case when using the CFD-biokinetic model. As can be seen, the distributions of oxygen and ammonium follow a similar pattern that is consistent with the velocity vector plots shown in Figure 8.1 (b and c). Substrate concentrations are lower in the area where the major dead zone is, indicating that the higher retention times promote high conversion efficiencies, but also advective mass transfer limitations. It is important to note that ammonium concentrations are well above the reported ammonium half-saturation index of 1.0 mg N/L for autotrophic organisms at 20ºC (Rittmann and McCarty, 2012) throughout the reactor. This means that there is no substrate limitation and thus, half-saturation indices are not playing a significant role in the description of the ammonium oxidation kinetics. The reported oxygen half-saturation index for autotrophic organisms at 20ºC is 0.4 mg O_2/L (Rittmann and McCarty, 2012). Given that the low range of oxygen concentrations is close to the half-saturation index (0.7 mg O_2/L, Figure 8.2), this index will probably play a significant role in the description of process kinetics (i.e. it will be sensitive). From a practical perspective, this means that it could be modified through a typical calibration process in order to fit model results with observed process performance.

Nitrate follows a trend that is also consistent with the flow patterns shown in Figure 8.1 (b and c). However, nitrate is different to ammonium and oxygen in the sense that it is both formed and consumed in the reactor, instead of solely being consumed (as is the case for the two former components). As can be deduced, the concentration of nitrates is maximal where ammonium and oxygen are minimal (major dead zone), which is consistent with an efficient aerobic transformation of ammonium to nitrate in this area (related to the higher HRT for the substrates in it); this process dominates the nitrate balance over the anoxic denitrification process. This can be verified by looking at in Appendix A 2a, where the simulation results excluding oxygen in the wastewater composition (thus only allowing denitrification) indeed show denitrifying activity. On the other hand, excluding the carbon source leads to a process where only aerobic nitrification is promoted (Appendix A 2b), and results show a similar but more pronounced nitrate distribution as in Figure 8.2 (nitrate concentrations are higher in the second dead zone near the top of the reactor).

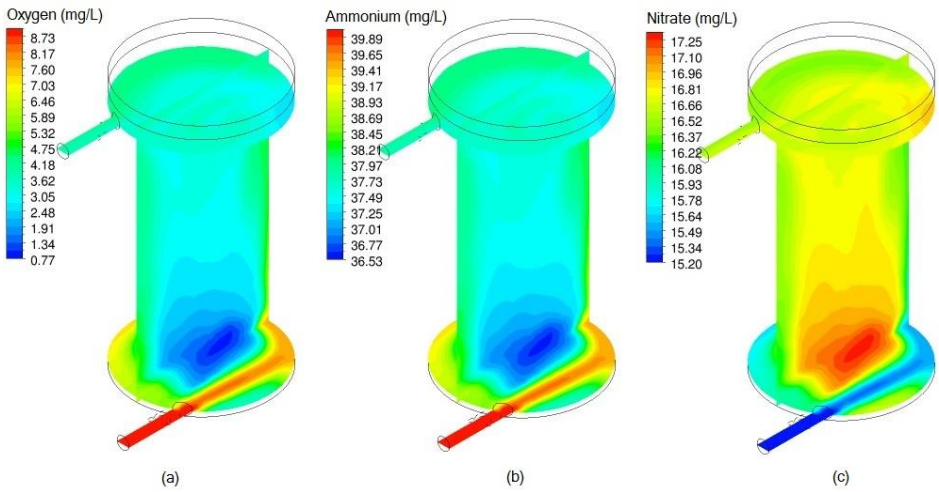

Figure 8.2 Spatial distribution of (a) dissolved oxygen, (b) ammonium and (c) nitrate in the base case

Figure 8.3 shows the distribution of organic carbon in the respirometer (a), together with the distribution of the substrate consumption rate in the system (b). As can be observed, the substrate consumption rates are lowest in the major dead zone due to the lower oxygen concentrations in this area (26% lower as compared to the maximum consumption rate achieved). This is consistent with the previous observations carried out for oxygen, ammonium and nitrate.

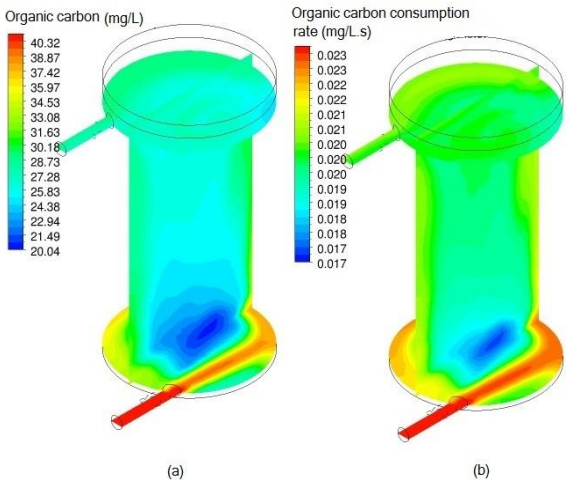

Figure 8.3 Spatial distribution of (a) organic carbon concentrations and (b) organic carbon consumption rates

Figure 8.4 shows the distribution of organic carbon consumption rates throughout the respirometer under different mixing conditions. Higher hydraulic retention times cause lower steady-state consumption rates due to the lower substrate concentrations that prevail under these conditions. For all mixing conditions, the substrate consumption rates are lower in the two reactor dead zones, similarly as was observed for the base case (Table 8.3, showing the decrease in organic carbon consumption rate as compared to the base case). It is important to note that at high flow rates (low HRTs), the differences in substrate consumption rates throughout the tank are significantly smaller than in the low flow rate cases (high HRTs) (Figure 8.5; Table 8.3). This is due to the fact that high HRT values have simultaneously better conversion efficiencies (due to the fact that there is more time available to degrade the substrates) and worse mixing conditions. From a practical perspective, this entails that the substrate concentration heterogeneity is higher in the high HRT cases, potentially causing significant departures between predicted and observed process performance.

Table 8.3 Decrease in organic carbon consumption rates at different mixing conditions.

Mixing Condition	Decrease in Organic Carbon Consumption Rate (%)
0.25X	34.25
0.5X	17.57
0.75X	8.45
X	0
2X	-7.73

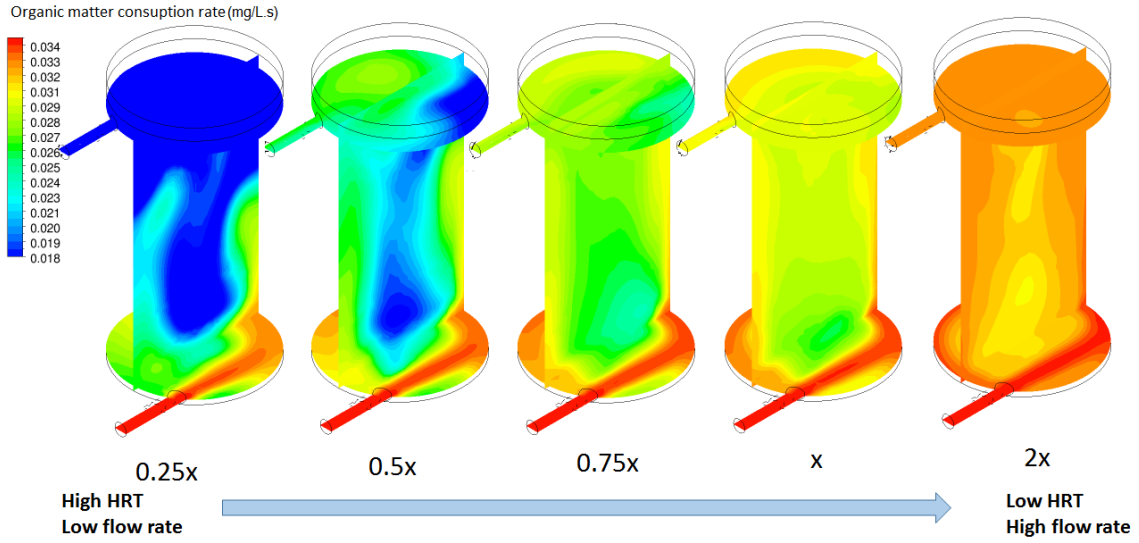

Figure 8.4 Spatial distribution of organic carbon consumption rates for different mixing scenarios in the system.

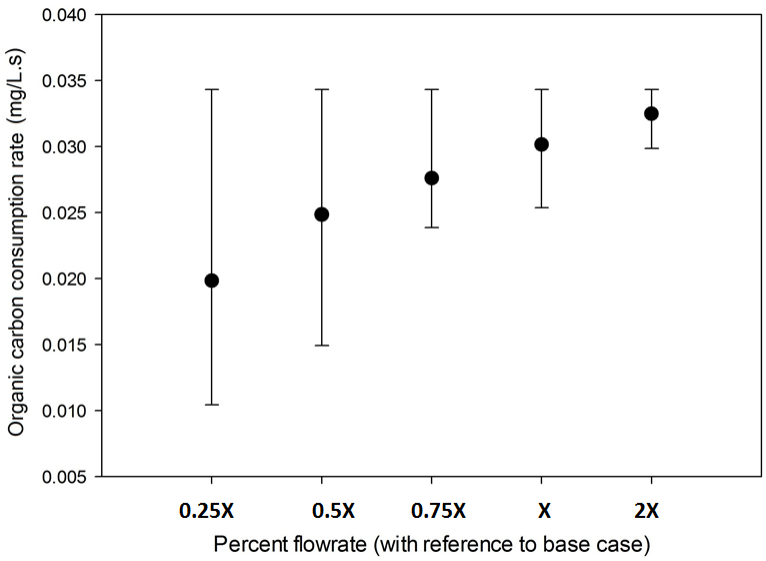

Figure 8.5 Range of maximum to minimum organic carbon consumption rates for the different mixing scenarios (the point shows the mean value).

Figure 8.6a shows the concentration of organic carbon for the different mixing scenarios considered. As can be seen, the organic carbon concentration is slightly lower in the dead zones for all cases; this was also observed for the base case. As can be seen, organic carbon concentrations in the majority of the reactor space vary between 20 and

30 mg/L throughout all mixing conditions. Given that the half-saturation index reported for aerobic and anoxic heterotrophs is 20 mg O_2/L (Rittman and McCarty, 2001), this entails that this half-saturation index will not affect the description of organic matter consumption rates between the different mixing scenarios. Thus, it will not be modified through a common calibration exercise (as a sensitivity analysis will report it to be insensitive). Figure 8.6b shows the distribution of oxygen concentrations in the different mixing scenarios. For all mixing conditions, the oxygen concentrations are lower in the two reactor dead zones, as was observed for the base case; this is coherent with the patterns observed in Figure 8.4. The existence of a wider range of concentrations at higher HRTs can also be observed for the oxygen concentrations in general. However, it is important to note that the heterogeneity in concentrations throughout the tank decreases at increasing HRTs given that most of the oxygen is consumed under these conditions. Ammonium follows a very similar trend as the one seen for oxygen concentrations (Figure 8.6), whereas nitrate does not (Figure 8.6d). As HRT values increase, there is a maximum nitrate concentration achieved around the two dead zones (found in the 0.75X case); however, nitrate concentration drops for the highest HRT case. This complexity is due to the fact that nitrate is again, besides being transported and converted by denitrification, being formed by nitrification. Moving from the highest HRT case towards lower HRTs increases nitrification rates, since ammonium concentrations as well as oxygen concentration are higher. This in turn leads to higher nitrate values in the (still nitrification dominated) nitrate balance. However, further decreasing HRT reduces the dead zones that are present allowing nitrate build-up. The consequence is that nitrate concentrations drop in both the tank and effluent as the formed nitrate is being washed out.

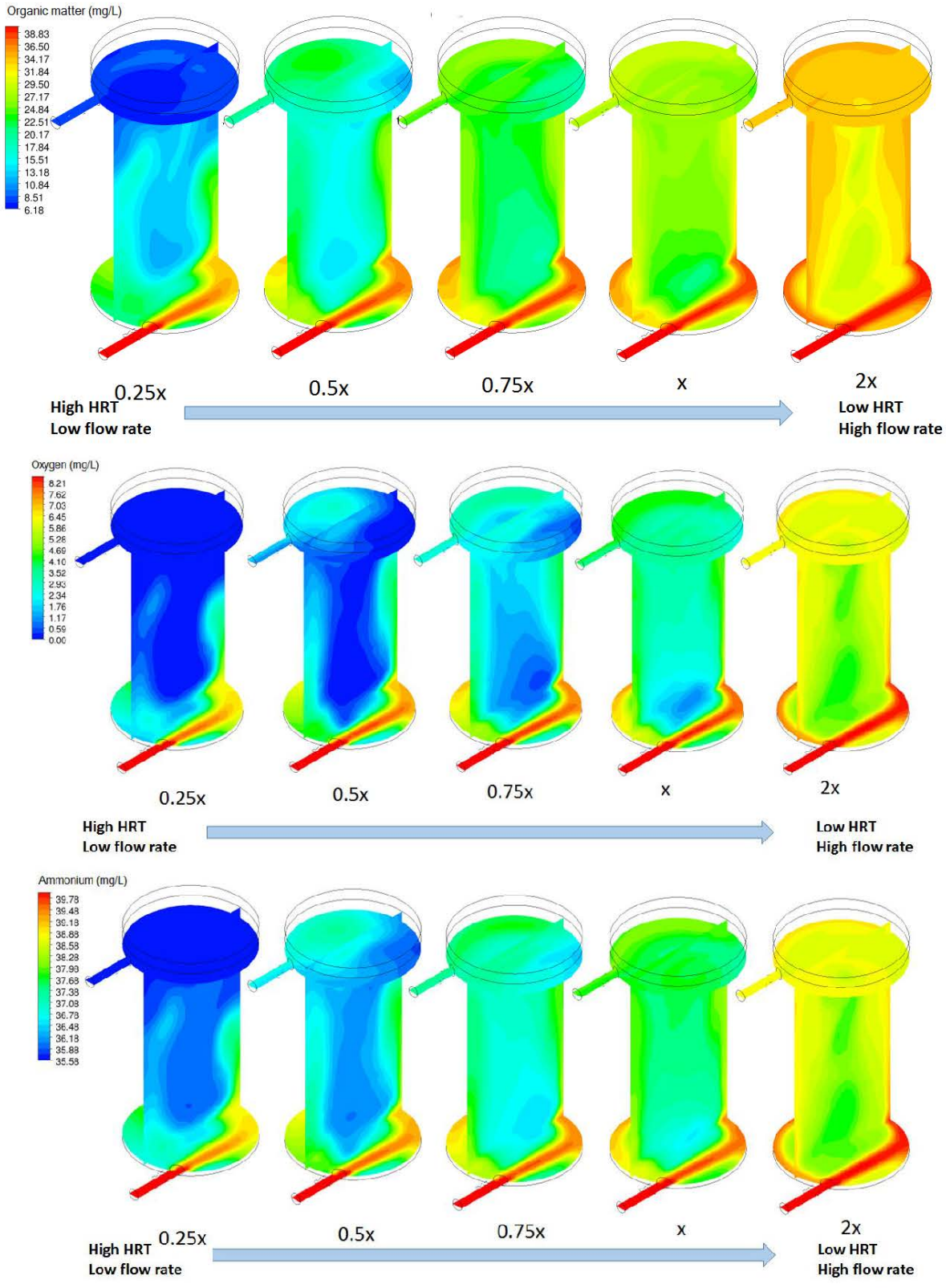
Organic matter (mg/L)
38.83
36.50
34.17
31.84
29.50
27.17
24.84
22.51
20.17
17.84
15.51
13.18
10.84
8.51
6.18
0.25x
0.5x
0.75x
x
2x
High HRT
Low flow rate
Low HRT
High flow rate
Oxygen (mg/L)
8.21
7.62
7.03
6.45
5.86
5.28
4.69
4.10
3.52
2.93
2.34
1.76
1.17
0.59
0.00
0.25x
0.5x
0.75x
x
2x
High HRT
Low flow rate
Low HRT
High flow rate
Ammonium (mg/L)
39.78
39.48
39.18
38.88
38.58
38.28
37.98
37.68
37.38
37.08
36.78
36.48
36.18
35.88
35.58
High HRT
0.25x
0.5x
0.75x
x
2x
Low flow rate
Low HRT
High flow rate

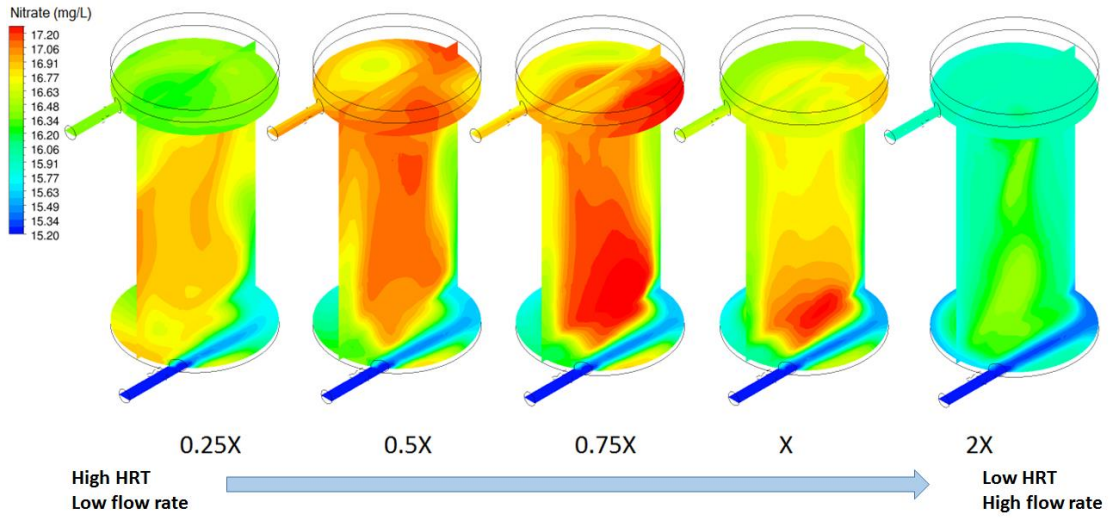

Figure 8.6 Distribution of (a) organic carbon, (b) oxygen, (c) ammonium and (d) nitrates concentrations for the different mixing scenarios.

8.3.3. Deviation in process performance between the physical and modelled systems at different mixing conditions

Figure 8.7 shows the difference between the effluent quality parameters (organic carbon, dissolved oxygen, ammonium and nitrate concentrations) for the CFD-biokinetic and TIS-CSTR-biokinetic models. As a general trend, the differences between models become more evident as HRT values become higher. This is consistent with the previous observation that there are wider concentration ranges with decreasing flow rates. This can be attributed to the combination of worse mixing conditions (i.e. worse advective transport) at lower flow rates together with higher times to degrade substrates through biological conversions at higher HRTs. As can be observed, the difference between predicted organic matter concentrations diminishes fast with decreasing HRT values (Figure 8.7a). This is in contrast to ammonium and nitrate, which only become equal at the lowest HRT level. This is due to the fact that oxygen only becomes limiting for heterotrophic aerobic reactions in the highest HRT case, affecting process rates in several areas of the tank and thus rendering effluent levels significantly dissimilar to the TIS-CSTR-biokinetic model results (Figure 8.7b). Aerobic autotrophic reactions, on the other hand, become oxygen limited at concentrations higher than the heterotrophic ones, given that nitrifying organisms are generally more intolerant to low oxygen concentrations as compared to heterotrophic organisms (i.e., they present higher half-saturation indices for oxygen). This causes a larger difference between predicted ammonium and nitrate concentrations between the

CFD-biokinetic model (physical system behaviour) and the TIS-CSTR-biokinetic model (Figure 8.7c). Recall that all concentrations are well above or approximately similar to their respective half-saturation indices, except for the oxygen values reached in the highest HRT case. It is also important to note that the TIS-CSTR-biokinetic model is not able to capture the change of ammonium oxidation and nitrate formation and reduction very accurately for the different mixing conditions (and particularly so for the nitrate case). As can be observed in Figure 8.7d, there exists a maximum nitrate concentration at intermediate HRT levels that is not at all captured by the TIS-CSTR-biokinetic model, due to the fact that it assumes perfect mixing.

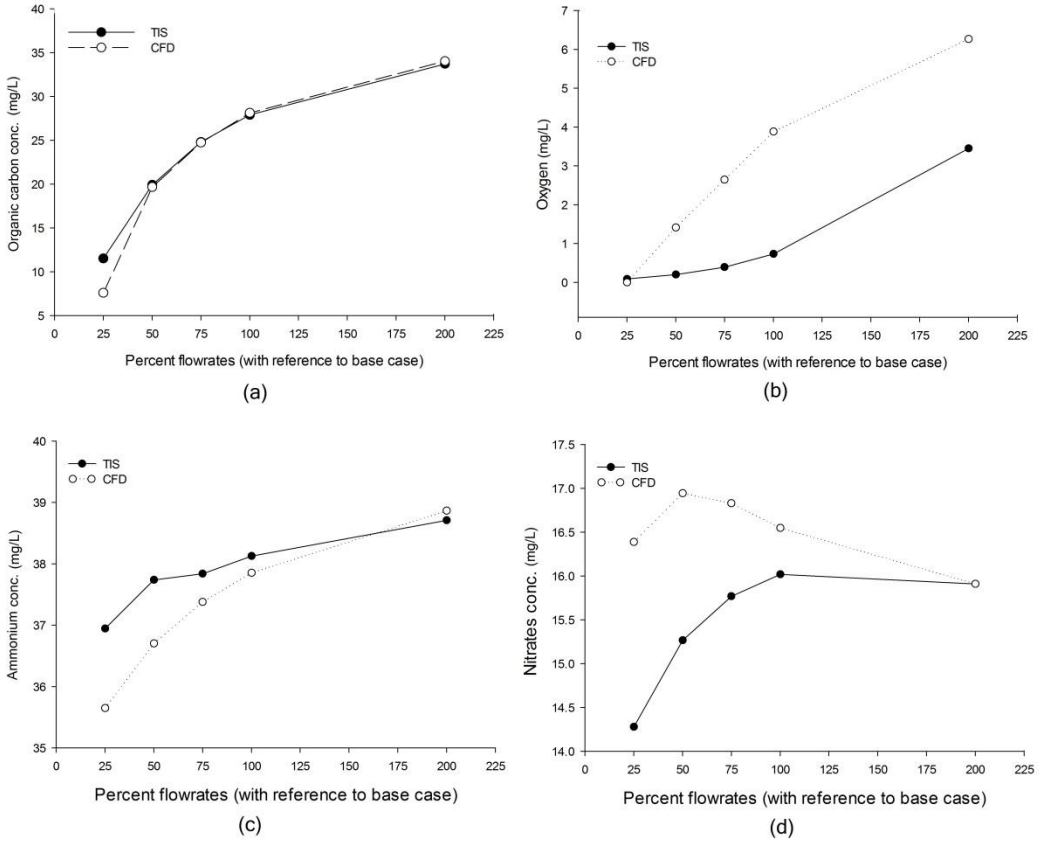

Figure 8.7 Difference between CFD-biokinetic and TIS-CSTR-biokinetic predicted concentrations for (a) organic matter, (b) oxygen, (c) ammonium and (d) and nitrates

8.3.4. Study of the effect of mixing conditions on half-saturation indices calibration

Based on expert knowledge (exposed in the previous sections), the $K_{O,A}$ index for autotrophic bacteria was the most sensitive of the calibration parameters given the fact

that oxygen was close to its value in several of the simulated scenarios and it varies significantly throughout the different mixing scenarios. Therefore, this system provides an opportunity to illustrate the effects of mixing conditions on the calculation of half-saturation indices when following commonly implemented methods for model calibration. Figure 8.8 shows the results for the calibrated $K_{O,A}$ for autotrophs for the TIS-CSTR-biokinetic model so the effluent predictions fit those of the CFD-biokinetic model; this is equivalent to closing the gap between both predictions in Figure 8.7. The calibrated $K_{O,A}$ values will be sensitive to the effluent concentrations when oxygen concentrations are of the order of $K_{O,A}$ values. As seen in Figure 8.7, the oxygen concentration for the 200% case is almost 3 mg/L, much higher than the default $K_{O,A}$ values (i.e. 0.4 mgO_2/L). Therefore, calibrated $K_{O,A}$ values are not sensitive to the effluent concentration in this case. As can be seen in Figure 8.8, the calibrated $K_{O,A}$ values are only shown for the 25-100% cases. In these cases, the half-saturation index would be calibrated to a value that is below the real one (results from 25 to 100%) and would change an order of magnitude with the change in mixing conditions. Commonly, respirometric systems are considered to present no mixing limitations and thus constitute an ideal system to measure the diffusional and biological contributions to half-saturation indices. Under the assumption of no mixing limitations, researchers neglect or postulate different explanations for the need for calibration of the $K_{O,A}$ index. An explanation that could be provided is that there has been a selection of organisms with improved substrate transport characteristics (Arnaldos et al., 2015) in the case of the half-saturation index values that fall well below the default (assumed real). Alternatively, another biology-related explanation that could be put forward is that either alternative enzymatic pathways have been activated in the organisms, or that the expression of transport enzymes has taken place (Arnaldos et al., 2015). Furthermore, a commonly provided diffusional-related explanation is the fact that high mixing energy has caused floc breakage in the full-scale system, bringing about lower half-saturation indices than expected. All of these explanations, that are based on basic biology and diffusional characteristics of the system, would theoretically match the obtained results and yet are not reflecting what is actually happening in the process. In this study, the respirometer presents mixing limitations that bring about an additional contribution (either by increasing or decreasing its value) to the half-saturation index when it is calculated as a result of the calibration of a TIS-CSTR-biokinetic model. As a result of incorrect $K_{O,A}$ calculation, suboptimal and even counter-productive process operational and design decisions could be taken. Additionally, opportunities for improved reactor design by modifying the advectional characteristics of the full-scale process will be lost.

In fact, in the present study, the respirometric analysis could indicate that advection limitations could be advantageous –in some occasions- for improved substrate removal by creating areas of relatively high retention times that still preserve adequate substrate and electron acceptor concentrations (i.e. complete mix might not be the best operational mode). It is important to note that this conclusion would have to be verified carrying out a similar study as the one presented here on a full-scale system.

In the case that the half-saturation index values fall above the real one, commonly provided explanations would refer to the diffusional conditions of the system, with the formation of flocs of large sizes and/or biofilm occurrence. This explanation also matches the results obtained from the respirometry, but would not reflect the actual behaviour of the full-scale process. As an example of the potential consequences of drawing this conclusion from the results obtained, a plausible operational decision would be to increase the mixing of the full-scale system in order to reduce the size of the flocs and improve process performance. This would increase energy consumption with no actual performance improvement (or at least, no guaranteed performance improvement with the information available).

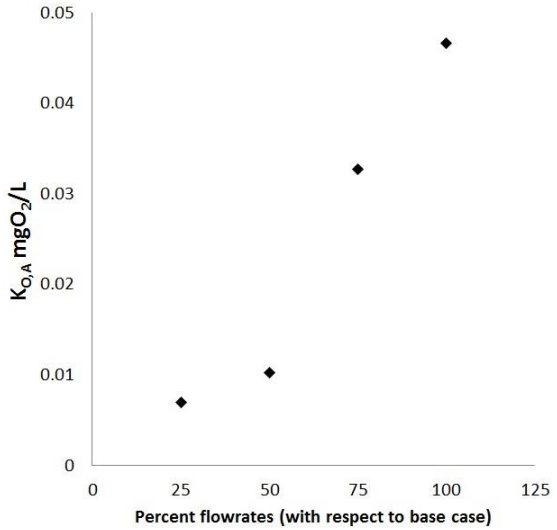

Figure 8.8 Calibrated values of $K_{O,A}$ for autotrophic organisms for 25-100% flow scenarios (default value for $K_{O,A}$ is 0.4 mgO_2/L)

8.3.5. Consequences of sensor placement on half-saturation indices calibration

In order to further illustrate the importance of mixing conditions, the effect of sensor placement in the respirometer on the calculated half-saturation indices has been quantified. A previous study using a combined CFD-biokinetic modelling framework has shown that bulk mixing can impact the performance of the control systems in full-scale plants, given that the sensors will provide inputs that are not representative of the entire treatment basin (Chapter 7 and Rehman et al., 2015). In this previous study, it was clearly demonstrated that a dissolved oxygen controller with a fixed set-point performs differently as a function of the location of the sensor. In the present study, it has been shown that these heterogeneities can also happen in downsized and simple bioreactors such as respirometers, commonly assumed to exhibit ideal completely mixed behaviour. This implies that sensor placement has the potential to also significantly affect the calibration of half-saturation indices through measurements that are not representative of a significant fraction of the reactor volume. This is very significant, given that an incorrect calculation of half-saturation indices can again lead to inappropriate design and/or operational decisions in processes where substrate concentrations are low or where effluent requirements are very stringent.

Figure 8.9 shows the distribution of calibrated $K_{O,A}$ values for autotrophic organisms for the base case if the ammonium sensor used was placed in specific locations (A: in the outlet of the reactor; B: middle of the reactor near the surface; C: near the wall and near the surface & D: near the wall at half depth of the reactor). As can be observed, these vary significantly, from 0.02 mg O_2/L in location B to 0.24 mg O_2/L in location D. This clearly confirms the hypothesis that sensor placement plays an important role in half-saturation index calibration and that mixing heterogeneities can affect the calculation of half-saturation indices not only in pilot and full-scale systems but also in simpler systems such as respirometers.

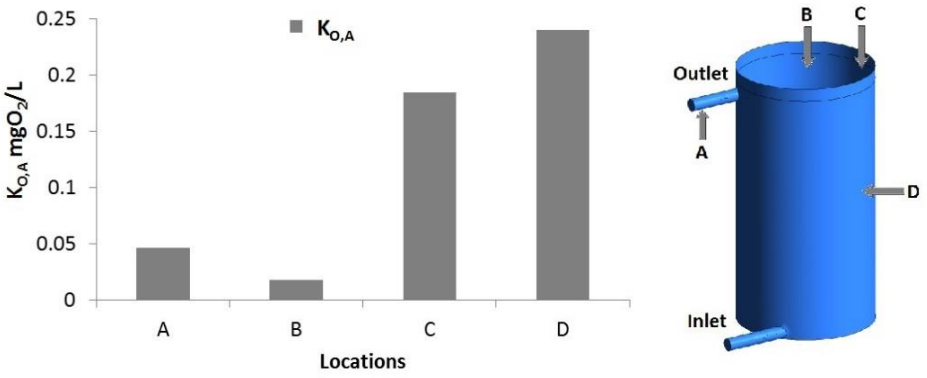

Figure 8.9 Calibrated $K_{O,A}$ values for autotrophic organisms based on the different sensor locations for the base case.

8.3.6. Implications at the process design and operational levels

This study provides important information that should be taken into account from an operational perspective. When trying to use half-saturation indices information for process evaluation or optimization, mixing conditions and sensor placement should be carefully considered. A possible approach to accomplish this would be to calculate half-saturation indices with well-characterized and standardized respirometers. This would allow the isolation of the biological and diffusional contributions from the advectional one in a calibration exercise. Afterwards, fine tuning of the calculated indices could be carried out with data taken from the full-scale system at different locations. In this case, the mixing characteristics of the full-scale plant should be well understood in order to select the appropriate sampling locations. This could be carried out through CFD studies that would lead to strong compartmental models and/or integrated CFD-biokinetic models that can be used to appropriately characterize the performance of the system.

From a design perspective, the added benefit of performing detailed CFD studies leading to robust CFD-biokinetic or compartmental models is that systems can be designed purposefully to create mixing limitations in certain sections. This could enable simultaneous oxic/anoxic/aerobic reactions to take place in different sections of the bioreactor. It could also be useful to create conditions to outcompete certain organisms (e.g. AOB vs. NOB in mainstream de-ammonification). Careful hydraulic process design that takes into account typical influent flow variations would ensure that this happens in a directed manner and in a way that operational and capital expenditures are minimized. As has been shown in the present study, varying influent flow rates can affect mixing patterns and subsequently impact process performance; this could be

accounted for in system design through advanced hydraulic analysis. However, bringing this in practice requires further studies to get a thorough understanding of the impact of reactor design on process performance. This study has laid out the basics for this.

8.4. Conclusions

The following conclusions can be drawn:

- The present study has demonstrated the importance of mixing conditions as a source of inconsistencies between calculated half-saturation indices values in an exemplary system consisting of the second vessel of a hybrid respirometer. These inconsistencies have been found to take place despite the simplicity and scale of the system. At larger scales, these effects can be expected to be even larger.
- The results have shown that the half-saturation index calculated from respirometric information might not reflect the actual half-saturation index of the full-scale plant. A possible solution to this issue is to calculate half-saturation indices from standardized and well-characterized respirometers. Afterwards, some fine tuning could be carried out on a case-to-case basis from full-scale plant data.
- Sensor placement has been shown to significantly impact the estimation of half-saturation indices in the respirometric system considered. This conclusion can be extended to full-scale systems, where half-saturation indices could be different depending on the measurement/sampling location chosen. This entails that mixing limitations could significantly affect decisions at the process monitoring and optimization levels.
- When designing a WWTP, the estimation/choice of a half-saturation index has to be considered carefully and in combination with CFD studies of the system that allow proper understanding of mixing conditions and the construction of robust CFD-biokinetic and/or compartmental models. This use of these models (beyond their current use as troubleshooting tools) could create opportunities at the design level by promoting certain biological reactions in different parts of the tank in a directed manner.

8.5. Acknowledgements

The research leading to these results has received funding from the People Programme (Marie Curie Actions) of the European Union’s Seventh Framework Programme FP7/2007-2013 under REA agreement 289193 (SANITAS Project). This publication reflects only the author's views and the European Union is not liable for any use that may be made of the information contained therein.

Chapter 9

Conclusions and perspectives

This chapter concludes the thesis and provides perspectives for future work.

Wastewater treatment plant (WWTP) modelling entails the modelling of the biological reactions (biokinetics) and underlying flow physics of the bioreactors (hydrodynamics). Currently, to model the hydrodynamics of a bioreactor, the tanks-in-series (TIS) modelling approach, which at best can model the flow variations in one direction, is widely used. These models assume a bioreactor as a series of completely mixed tanks and, hence, ignore any variation in the concentrations stemming from the design of a bioreactor or operational conditions. Therefore, these models eventually need rigorous calibration efforts to match measurements. This calibration is generally performed by manipulating kinetic parameters such as half saturation indices (K-values). The calibrated models are then used to assess or formulate different control strategies which includes the determination of an appropriate sensor location and a well-chosen setpoint for the controllers. In addition, the calibrated models are then extrapolated to predict the WWTP performance under different dynamic conditions (diurnal and dry/wet weather conditions) assuming that the flow patterns remain unchanged.

In this thesis, it was hypothesised and confirmed that the bioreactors are not at all completely mixed and, hence, current models wrongfully calibrate the kinetic parameters by correcting for the errors induced by the over-simplified modelling of mixing. The need for re-calibration arises at different operational conditions due to the limitation of the current models to incorporate changes in operational conditions.

This work contributes towards improving the currently employed models by performing detailed CFD hydrodynamic modelling of two full-scale bioreactors. The biokinetic models are then integrated with the CFD models to understand the impact of hydrodynamics on the process performance. Detailed scenario analysis with varying flow rates is performed to show the impact of changing operational conditions on the

process performance. The far reaching consequences on sensor location and calibration of half saturation indices are then demonstrated using this detailed modelling approach. A model reduction method is proposed which incorporates the knowledge gained from the integrated CFD-biokinetic models. The conclusions drawn from these studies are summarized and future work and perspectives are provided in the following sections.

9.1. Conclusions

9.1.1. Hydrodynamic modelling of WWTPs

Detailed 3D CFD hydrodynamic modelling was performed for two full-scale case studies, i.e. the Eindhoven WWTP (Chapter 3) and the La Bisbal d'Empordà WWTP (Chapter 5). Both cases were differently configured bioreactors and, hence, presented different challenges for the CFD modelling. However, similar conclusions can be drawn from both cases.

Chapter 3 confirmed the impact of reactor configuration and aeration on the mixing pattern in the reactor. The aeration system was modelled in detail by modelling each diffuser plate separately. The results showed areas of limited mixing and non-uniform gas dispersion along the length and across the cross-section of the bioreactor. These bad mixing zones were also found in the aerated regions, which are commonly assumed completely mixed. In order to grasp the effect of the changing and dynamic conditions occurring at the WWTP, multiple steady state simulations were performed, hereby varying gas and liquid flowrates. It was observed that the change in conditions leads to changes in flow patterns and, hence, the resulting gas dispersion. These are important findings, as the currently employed WWTP models (based on the TIS approach) are unable to capture these significant details and cannot translate the impact of dynamic conditions on the process performance.

Similarly, Chapter 5 demonstrated the impact of reactor configuration and the operating scheme of the surface aerators (rotors) on the flow patterns in an oxidation ditch. Two different operating conditions were modelled i.e. a 2-rotor strategy and a 4-rotor strategy. These rotors operate at the surface and, hence, only propel the liquid at the surface leading to low velocities at the bottom and therefore less mixing. It was shown that the bends and corners of the reactor induce the formation of swirls and poorly

mixed zones. It was found that using the 4-rotor strategy does not significantly improve the hydrodynamics. Again, these mixing patterns can only be discovered if detailed hydrodynamic modelling is performed as it is done in the current study. TIS based models over-simplify the mixing and, therefore introduce errors in the predictions.

An important finding was the impact of sludge density on the flow predictions. The sludge density was modelled as a function of total suspended solids and it was found that it improved the velocity predictions. Therefore, it is recommended to always use the sludge density instead of standard water density for modelling of wastewater flows.

9.1.2. Impact of hydrodynamics on the process performance of WWTPs

Biokinetic models were integrated with the CFD hydrodynamic model to assess the impact of hydrodynamics on the process performance for two case studies (Eindhoven and La Bisbal).

Two different biokinetic models were implemented. The first, ASM1, was integrated to predict the carbon and nitrogen removal. The second, ASMG1, was integrated to predict the nitrous oxide production in the bioreactors. The bioreactor at the Eindhoven WWTP is equipped with submerged diffusers for aeration. Therefore, the oxygen mass transfer from air to liquid phase was modelled in detail based on a constant bubble size, local gas holdup and relative velocities between the two phases (Chapter 4).

As a result of the CFD-biokinetic modelling, it was observed that the DO and ammonium concentrations vary not only along the length but also along the cross-section of the bioreactor (which is not taken into account at all by the TIS models). The impact of hydrodynamics was clearly observed on the DO and ammonium concentrations. The regions of limited mixing (dead zones) led to mass transfer limitations and, hence, depletion of dissolved oxygen. Moreover, reduced ammonium removal was observed due to the poor mixing conditions.

Concentration distribution plots (CDP) were used for the evaluation of the variability in concentrations. CDPs of the DO concentrations were generated for different sections of the reactor to analyse the overall variability. It was observed that variations are different in different sections of the reactor. Steady state simulations at varying liquid and gas flowrates demonstrated the change in concentration variations with the change

in operating conditions. It was observed that at increased gas flowrates the non-uniformity in the DO values increased despite the fact that the DO concentrations were higher. The impact of the DO variations was also observed on the nitrous oxide production. It proved that more nitrous oxide is produced where the DO concentrations are lower. Furthermore, the nitrous oxide production was also spatially non-uniform indicating that detailed modelling is needed to quantify and predict the emissions accurately.

A similar CFD-biokinetic integration (only ASM1) was performed for the oxidation ditch at La Bisbal d'Empordà WWTP. The impact of the operational limitation of the rotors on the process performance was revealed in terms of the DO and ammonium concentrations. The significant finding was the unavailability of the dissolved oxygen at the bottom of the reactor and thus creating a huge anoxic region in the oxidation ditch. Moreover, the 4-rotor strategy did not significantly improve the inadequate DO concentrations at the bottom.

9.1.3. Impact of mixing on the TIS model calibration

Impact of mixing on the TIS model calibration was partially discussed in chapter 4 and was further evaluated in detail in chapter 8 using a TIS-CSTR model.

In Chapter 4, the impact of mixing is demonstrated for the concentrations of oxygen and ammonium as well as the autotrophic growth rate. A clear impact on the process rate was observed as it decreased due to the unavailability of DO in the dead zones. It sheds light on the fact that the dead zones limit the process rates. However, for TIS models, common practice is to calibrate the process rates by changing the half saturation indices or maximum growth rates, therefore correcting for the errors which are actually induced by the mixing model's deviation from reality. Therefore, under different mixing conditions the TIS models will be calibrated differently. This was confirmed in chapter 8 through the detailed modelling of a lab-scale respirometer and evaluating the TIS modelling approach.

In Chapter 8, it was also shown that applying the TIS model resulted in the estimation of different $K_{O,A}$ (half saturation index of oxygen for autotrophic biomass) values for different mixing conditions and this even in a small, usually considered as completely mixed, respirometric reactor system. It shows that the TIS models tend to lump the advectional resistances (arising from mixing limitations) into the K-values which

should be modelled separately. It is mainly because the mixing conditions were not taken into account separately. This is one of the reasons for the wide ranges of K-values, e.g. $K_{O,A}$, reported in literature. These inconsistencies will be even more augmented in large bioreactors where mixing is more non-uniform as demonstrated in Chapter 4 & 5.

9.1.4. Impact of sensor location on calibration and controller performance

Sensor location is important for the calibration of a model as well as for the performance of a controller.

Chapters 4 and 8 described the impact of different sensor locations on the calibrated K-values. As the CFD-biokinetic model showed spatial heterogeneities in the reactor (chapters 4, 5 & 8), sensor readings become a function of the location. Normally, the TIS based models are calibrated on a measurement dataset measured at a certain location. The TIS models are too simple to take into account the exact location (especially lateral and along the depth locations) of a sensor and, hence, the model is calibrated assuming complete mixing in all three dimensions. However, if the location of the sensor in the real system is changed, the measured values will be different and, hence, the TIS model will result in different calibrated values. This is proved in chapter 8, where the $K_{O,A}$ values were calibrated based on different sensor locations inside the respirometer. It showed clearly the dependence of $K_{O,A}$ values on the sensor location. The dependence was more pronounced (sensitive) when the DO values were in the order of the magnitude of the $K_{O,A}$ default value. This indicates that at low substrate conditions the calibration procedure is highly dependent on sensor location and it must be considered while extrapolating the results.

In addition, the CDPs developed in chapter 4 provided a method for quantifying the sensor location's proximity to the average tank behaviour. Along with other benefits, this is an important feature of the CFD-biokinetic model which can be useful at a process level.

Chapter 7 showed the impact of a DO sensor location on the performance of the aeration control. The process models used for such a control are based on TIS models and, hence, consider variations only in one direction. Nonetheless, a more robust compartmental model (which incorporates the spatial heterogeneities) was used to evaluate the sensor placement in this study. It was observed that the DO controller performs differently at

different sensor locations. The results were presented in the form of effluent quality and aeration costs. It was observed that if a sensor was placed in a dead zone, the aeration costs will be too high. However, if it was placed just next to the aerators, the effluent quality will not be met. Normally, these issues are handled by changing the setpoint of the controller. Therefore, different DO setpoint values were examined at two different locations (i.e. in a dead zone and next to aerators). It improved the results to a certain extent and showed that the setpoint also should be a function of the sensor placement. Therefore, detailed hydrodynamic modelling is needed to better understand where to place a sensor and determine its optimal setpoint which leads to cost-effective control, i.e. minimising costs and maximising effluent quality.

9.1.5. Next Generation wastewater treatment models

The thesis stressed upon the need for more detailed and robust models for wastewater treatment plants. However, to date, even CFD hydrodynamic modelling is not fully endorsed by the practitioners due to the high computational demand, let alone CFD-biokinetic modelling. Henceforth, it will take some more time, probably decades, to fully utilize the benefits of CFD modelling. Therefore, a more suitable modelling approach, i.e. compartmental modelling was developed in this thesis (chapter 6). This modelling method combined the best of both worlds i.e. TIS and CFD. The general approach is summarized in Figure 9.1. It shows that detailed knowledge can be gathered from plain CFD models as well as CFD-biokinetic models. This detailed knowledge can be used to develop a network of spatially localized tanks-in-series in multiple dimensions, i.e. a so-called compartmental model.

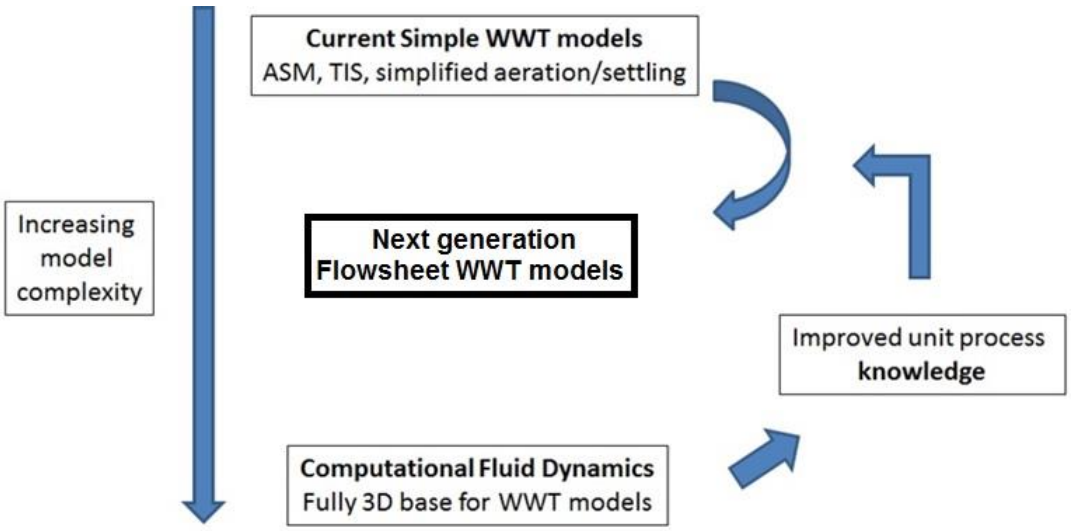

Figure 9.1 Illustration of Next Generation flowsheet WWT models (compartmental models)

The compartmental modelling of the two case studies was performed and presented in chapter 6. A general procedure for compartmental modelling was described in detail. In this thesis, a novel approach was used to develop the compartmental model (CM) which based the compartments on the DO concentrations and cumulative species distribution plots (CSDs) rather than only hydrodynamic characteristics. This approach proved to be modelling goal driven and in some cases (Eindhoven WWTP) can potentially reduce the number of compartments. The current approach does bring more realism in the modelling and, hence, more accurate predictions of the systems where oxygen plays a vital role (which is the case in most WWT bioreactors).

Moreover, the idea of cumulative species distribution (CSDs) is a novel way of quantifying species variations in the bioreactor. It brings a vast amount of information into a simple curve. The CSDs were used to compare the variations in different sections of the reactor as well as under different operational conditions. The CSDs provided a good measure of variations and are strongly recommended to be used as a decision support tool for compartmental modelling.

The CM was developed for different operational conditions, however, as the mixing patterns change, the compartmental model also changes. Therefore, a dynamic CM was suggested which can take into account all the possible mixing patterns and, hence, is more robust.

9.2. Perspectives

In this thesis, the benefits of detailed CFD modelling and development of compartmental models has been demonstrated. However, a lot of research work still needs to be done to validate their predictive power. A summary of perspectives and future work is provided below.

- The CFD-biokinetic models have not been fully validated due to lack of available data. In order to fully validate these models, detailed spatial data is required which is not straightforward to collect at a full scale WWTP and requires simultaneous measurements at multiple locations. Therefore, collection of data and validation of these models should be the utmost priority.

- The hydrodynamic model can be improved by more detailed modelling of aeration. Currently, it was done with a constant bubble size, however, in reality the bubbles are subject to breakage and coalescence. Therefore, the modelling of bubble size distributions and non-spherical bubbles are foreseen as a potential research that would definitely improve the oxygen mass transfer predictions and, hence, the biological reactions.

- The rheology of the sludge can be better predicted by modelling the solids transport. In the current study, it was shown that sludge density has a significant impact on the flow. Therefore, a lot of research potential lies there. The viscosity of wastewater is still a subject of research and improved viscosity models would also help modelling the sludge flows better.

- The propellers modelled in both case studies were approximated. A detailed modelling of propeller motion can result in better prediction of sludge velocity and hence overall hydrodynamics. Normally, the propeller motion in CFD can be either modelled with the help of the sliding mesh method or the multiple reference frame method. However, the sliding mesh method (at a higher computational cost) is more accurate and is recommended to be used.

- The ASMG1 modelling of nitrous oxide modelled the nitrous oxide production and did not include the modelling of stripping due to aeration. Therefore, it can

be very useful to actually model the stripping behaviour and hence be able to quantify the emissions accurately.

- The dynamic compartmental model is the solution to avoid recalibration efforts when moving from dry to wet weather conditions. The development of a dynamic CM can be rather complex, as there is a probability of ending up with two (or more) different CMs for different conditions. The difference between two CMs can be either the number of compartments or the respective fluxes (or both). However, more work needs to be done to develop a robust dynamic compartmental model. One way forward is to develop such a dynamic compartmental model which has the same number of compartments for different conditions with only differences in the fluxes. Therefore, the fluxes can be defined as a function of operating conditions (flow rates, operating rotors etc.). It can lead to an increase in the number of compartments, however, it will be more robust and applicable to a larger range of flow rates.

- The compartmental model provided in the thesis was based on the DO concentrations. It is assumed that it would not be too much different from a CM based on other species because most of the biological processes are driven by the availability and unavailability of the dissolved oxygen (e.g. nitrification and denitrification). However, this still needs to be evaluated and, therefore, it is a potential research area which can lead WWTP modelling in the right direction.

- The impact of sensor location on a controller performance was evaluated with a fixed compartmental model. However, as observed in this study, a fixed compartmental model might not be suitable under all the operational conditions. Therefore, it is suggested to broaden the research by evaluating impact of sensor location using a dynamic compartmental model.

- It is understood through this study that CFD can be really useful to evaluate and optimise the performance of existing bioreactors. However, optimisation is constrained to only altering process conditions (such as flowrates, recycle ratios and propeller speed etc.) in most cases. Whereas, it is plausible that the poor performance of a reactor is originating from the poor design (as it was observed in the chapter 5 for the oxidation ditch). Therefore, it would be more useful if detailed CFD modelling is included in the standard design protocol of the reactor

design to reduce the design related limitations as much as possible. A detailed CFD modelling at a design stage will also lead to overall better process design and control.

- Mixing is an important aspect of bioreactor operation and, hence, bioreactors are designed to achieve good mixing. However, it can be argued whether complete mixing is always to be pursued. This question becomes even more important when two different conditions are desired in a single bioreactor such as for nitrification and denitrification. In such instances, large gradients in the DO concentrations between different regions in a bioreactor might be suitable for the overall process. However, the problem arises when a certain region is expected to have a certain condition and it deviates due to mixing limitations (for example having denitrification conditions in the nitrification regions). Therefore, it becomes important to quantify those deviations and their impact on the process performance. The CFD-biokinetic modelling has shown its ability to quantify and understand the variations originating due to mixing. Therefore, when used at a design stage, the CFD-biokinetic model can help in designing bioreactors deliberately to exploit non-ideal mixing to maximise the process performance. It will certainly improve the process control and provide the opportunity to optimise the energy consumptions. Therefore, there is a lot of research potential and these ideas should be investigated thoroughly.

- The thesis has shown the potential of CFD-biokinetic modelling to evaluate the performance of a bioreactor. It might seem like that it will require a same amount of effort to perform this study for another case. However, the thesis can serve as a general guide to perform similar studies in less time as each modelling step has been explained in detail. Moreover, there is a need to build up on this knowledge by implementing similar approach on other cases to make it applicable to a wide range of WWTP technologies.

Bibliography

(IPCC) Intergovernmental Panel on Climate Change, 2014. Climate Change 2013 - The Physical Science Basis, 1st ed. Cambridge University Press, Cambridge, UK and New York, NY, USA. doi:10.1017/CBO9781107415324

Ahn, J., Daidou, T., Tsuneda, S., Hirata, A., 2001. Metabolic behavior of denitrifying phosphate-accumulating organisms under nitrate and nitrite electron acceptor conditions. J Biosci Bioeng 92, 442–446.

Ahn, J.H., Kim, S., Park, H., Katehis, D., Pagilla, K., Chandran, K., 2010a. Spatial and Temporal Variability in Atmospheric Nitrous Oxide Generation and Emission from Full-Scale Biological Nitrogen Removal and Non-BNR Processes. Water Environ Res 82, 2362–2372. doi:10.2175/106143010X12681059116897

Ahn, J.H., Kim, S., Park, H., Rahm, B., Pagilla, K., Chandran, K., 2010b. N2O emissions from activated sludge processes, 2008-2009: results of a national monitoring survey in the United States. Environ Sci Technol 44, 4505–4511. doi:10.1021/es903845y

Alvarado, A., Vedantam, S., Goethals, P., Nopens, I., 2012. A compartmental model to describe hydraulics in a full-scale waste stabilization pond. Water Res 46, 521–530. doi:10.1016/j.watres.2011.11.038

Alvarado, A., Vesvikar, M., Cisneros, J.F., Maere, T., Goethals, P., Nopens, I., 2013. CFD study to determine the optimal configuration of aerators in a full-scale waste stabilization pond. Water Res 47, 4528–4537. doi:10.1016/j.watres.2013.05.016

Amerlinck, Y., 2015. Model refinements in view of wastewater treatment plant optimization: improving the balance in sub-model detail (Doctoral dissertation).

Andersson, B., Andersson, R., Håkansson, L., Mortensen, M., Sudiyo, R., Van Wachem, B., 2011. Computational fluid dynamics for engineers. Cambridge University Press.

ANSYS Inc., 2011. ANSYS FLUENT Theory Guide. Southpointe 275 Technology Drive Canonsburg, PA 15317.

Ardern, E., Lockett, W.T., 1914. Experiments on the oxidation of sewage without the aid of filters. Journal of Chemical Technology & Biotechnology 33, 523–539. doi:10.1002/jctb.5000331005

Arnaldos, M., Amerlinck, Y., Rehman, U., Maere, T., Van Hoey, S., Naessens, W., Nopens, I., 2015. From the affinity constant to the half-saturation index: understanding conventional modeling concepts in novel wastewater treatment processes. Water Res 70, 458–470. doi:10.1016/j.watres.2014.11.046

Ayesa, E., De la Sota, A., Grau, P., Sagarna, J.M., Salterain, A., Suescun, J., 2006. Supervisory control strategies for the new WWTP of Galindo-Bilbao: the long run from the conceptual design to the full-scale experimental validation. Water Sci Technol 53, 193–201.

Ballot, B., 1845. Akustische Versuche auf der Niederländischen Eisenbahn, nebst gelegentlichen Bemerkungen zur Theorie des Hrn. Prof. Doppler. Annalen der Physik und Chemie 142, 321–351. doi:10.1002/andp.18451421102

Batchelor, G.K., 1967. An introduction to fluid dynamics. Cambridge University Press, Cambridge : Cambridge University Press.

Belia, E., Amerlinck, Y., Benedetti, L., Johnson, B., Sin, G., Vanrolleghem, P.A., Gernaey, K.V., Gillot, S., Neumann, M.B., Rieger, L., Shaw, A., Villez, K., 2009. Wastewater treatment modelling: dealing with uncertainties. Water Sci Technol 60, 1929–1941. doi:10.2166/wst.2009.225

Bock, E., Schmidt, I., Stüven, R., Zart, D., 1995. Nitrogen loss caused by denitrifying Nitrosomonas cells using ammonium or hydrogen as electron donors and nitrite as electron acceptor. Arch Microbiol 163, 16–20. doi:10.1007/BF00262198

Borghi, R., Anselmet, F., 2013. Turbulent multiphase flows with heat and mass transfer. ISTE Ltd/John Wiley and Sons Inc, Hoboken, NJ.

Brannock, M.W.D., Wang, Y., Leslie, G., 2010. Evaluation of full-scale membrane bioreactor mixing performance and the effect of membrane configuration. J Memb Sci 350, 101–108. doi:10.1016/j.memsci.2009.12.016

Çengel, Y.A., Cimbala, J.M., 2014. Fluid mechanics: Fundamentals and applications, Third edition. ed. McGraw Hill, New York.

Chachuat, B., Roche, N., Latifi, M.A., 2005. Optimal aeration control of industrial alternating activated sludge plants. Biochem Eng J 23, 277–289. doi:10.1016/j.bej.2005.01.012

Chandran, K., Stein, L.Y., Klotz, M.G., van Loosdrecht, M.C., 2011. Nitrous oxide production by lithotrophic ammonia-oxidizing bacteria and implications for

engineered nitrogen-removal systems. Biochem Soc Trans 39, 1832–1837. doi:10.1042/BST20110717

Cheng, C., Ribarova, I., 1999. Activated sludge system modelling and simulations for improving the effluent water quality. Water Sci Technol 39, 93–98. doi:10.1016/S0273-1223(99)00190-0

Chu, K.H., van Veldhuizen, H.M., van Loosdrecht, M.C., 2003. Respirometric measurement of kinetic parameters: effect of activated sludge floc size. Water Sci Technol 48, 61–68.

Cobb, E.D., 1993. Broad-band acoustic Doppler current profiler. Flow Measurement and Instrumentation 4, 35–37. doi:10.1016/0955-5986(93)90008-7

Cockx, A., Do-Quang, Z., Audic, J.M., Liné, A., Roustan, M., 2001. Global and local mass transfer coefficients in waste water treatment process by computational fluid dynamics. Chemical Engineering and Processing: Process Intensification 40, 187–194. doi:10.1016/S0255-2701(00)00138-0

Coen, F., Petersen, B., Vanrolleghem, P., Vanderhaegen, B., Henze, M., 1998. Model-based characterisation of hydraulic, kinetic and influent properties of an industrial WWTP. Water Sci Technol 37, 317–326. doi:10.1016/S0273-1223(98)00352-7

Commission Report, 2009. Report from the Commission to the European Parliament and the Council in accordance with Article 18.3 of the Water Framework Directive 2000/60/EC on programmes for monitoring of water status, COM(2009) 156 final þ accompanying commission staff working document (SEC(2009) 415). Brussels, Belgium: Commission of the European Communities.

Copp, J., 2000. The COST Simulation Benchmark–Description and Simulator Manual COST. European Cooperation in the field of Scientific and Technical Research), Brussels, Belgium.

Corominas, L., Sin, G., Puig, S., Traore, A., Balaguer, M., Colprim, J., Vanrolleghem, P.A., 2006. Model-based evaluation of an on-line control strategy for SBRs based on OUR and ORP measurements. Water Sci Technol 53, 161–169.

Daigger, G.T., Adams, C.D., Steller, H.K., 2007. Diffusion of oxygen through activated sludge flocs: experimental measurement, modeling, and implications for simultaneous nitrification and denitrification. Water Environ Res 79, 375–387.

De Clercq, B., 2003. Computational fluid dynamics of settling tanks: Development of experiments and rheological, settling and scraper submodels., PhD Thesis. ed. BIOMATH, Ghent University, Belgium.

Delafosse, A., Delvigne, F., Collignon, M., Crine, M., Thonart, P., Toye, D., 2010. Development of a compartmental model based on CFD simulations for description of mixing in bioreactors. Biotechnol. Agron. Soc. Environ. 14, 517–522.

Devisscher, M., Bogaert, H., Bixio, D., Van, D.E.V.J., Thoeye, C., 2002. Feasibility of automatic chemicals dosage control--a full-scale evaluation. Water Sci Technol 45, 445–452.

Duchène, P., Cotteux, E., Capela, S., 2001. Applying fine bubble aeration to small aeration tanks. Water Sci Technol 44, 203–210.

Eckenfelder, W.W.(W., Grau, P., 1998. Activated sludge process design and control, 2nd ed. ed. Technomic Pub., Lancaster, Pa.

Esquivel-Rios, I., Ramirez-Vargas, R., Hernandez-Martinez, G.R., Vital-Jacome, M., Ordaz, A., Thalasso, F., 2014. A microrespirometric method for the determination of stoichiometric and kinetic parameters of heterotrophic and autotrophic cultures. Biochem Eng J 83, 70–78. doi:10.1016/j.bej.2013.12.006

Fan, L., Xu, N., Wang, Z., Shi, H., 2010. PDA experiments and CFD simulation of a lab-scale oxidation ditch with surface aerators. Chemical Engineering Research and Design 88, 23–33.

Fayolle, Y., Cockx, A., Gillot, S., Roustan, M., Héduit, A., 2007. Oxygen transfer prediction in aeration tanks using CFD. Chem Eng Sci 62, 7163–7171. doi:10.1016/j.ces.2007.08.082

Fenu, A., Guglielmi, G., Jimenez, J., Spèrandio, M., Saroj, D., Lesjean, B., Brepols, C., Thoeye, C., Nopens, I., 2010. Activated sludge model (ASM) based modelling of membrane bioreactor (MBR) processes: a critical review with special regard to MBR specificities. Water Res 44, 4272–4294. doi:10.1016/j.watres.2010.06.007

Fikar, M., Chachuat, B., Latifi, M.A., 2005. Optimal operation of alternating activated sludge processes. Control Eng Pract 13, 853–861. doi:10.1016/j.conengprac.2004.10.003

Flores-Alsina, X., Corominas, L., Snip, L., Vanrolleghem, P.A., 2011. Including greenhouse gas emissions during benchmarking of wastewater treatment plant control strategies. Water Res 45, 4700–4710. doi:10.1016/j.watres.2011.04.040

Flores-Alsina, X., Rodríguez-Roda, I., Sin, G., Gernaey, K.V., 2008. Multi-criteria evaluation of wastewater treatment plant control strategies under uncertainty. Water Res 42, 4485–4497. doi:10.1016/j.watres.2008.05.029

Foley, J., de Haas, D., Yuan, Z., Lant, P., 2010. Nitrous oxide generation in full-scale biological nutrient removal wastewater treatment plants. Water Res 44, 831–844. doi:10.1016/j.watres.2009.10.033

García-Olivares, A., Becares, E., 1995. Calibration of a model for an A + B acivated sludge pilot plant treating industrial wastewater. Water Res 29, 2673–2680. doi:10.1016/0043-1354(95)00122-2

Gernaey, K.V., van Loosdrecht, M.C.M., Henze, M., Lind, M., Jørgensen, S.B., 2004. Activated sludge wastewater treatment plant modelling and simulation: state of the art. Environmental Modelling & Software 19, 763–783. doi:10.1016/j.envsoft.2003.03.005

Glover, G.C., Printemps, C., Essemiani, K., Meinhold, J., 2006. Modelling of wastewater treatment plants--how far shall we go with sophisticated modelling tools? Water Sci Technol 53, 79–89.

Gresch, M., Armbruster, M., Braun, D., Gujer, W., 2011a. Effects of aeration patterns on the flow field in wastewater aeration tanks. Water Res 45, 810–818. doi:10.1016/j.watres.2010.09.009

Gresch, M., Braun, D., Gujer, W., 2011b. Using reactive tracers to detect flow field anomalies in water treatment reactors. Water Res 45, 1984–1994. doi:10.1016/j.watres.2010.11.017

Gresch, M., Brügger, R., Meyer, A., Gujer, W., 2009. Compartmental models for continuous flow reactors derived from CFD simulations. Environ Sci Technol 43, 2381–2387.

Guha, D., Dudukovic, M.P., Ramachandran, P.A., Mehta, S., Alvare, J., 2006. CFD-based compartmental modeling of single phase stirred-tank reactors. AIChE Journal 52, 1836–1846. doi:10.1002/aic.10772

Gujer, W., 2006. Activated sludge modelling: past, present and future. Water Sci Technol 53, 111–119.

Gujer, W., Henze, M., Mino, T., Matsuo, T., Wentzel, M., Marais, G., 1995. The activated sludge model no. 2: Biological phosphorus removal. Water Sci Technol 31, 1–11. doi:10.1016/0273-1223(95)00175-M

Gujer, W., Henze, M., Mino, T., Vanloosdrecht, M., 1999. Activated Sludge Model No. 3. Water Sci Technol 39, 183–193. doi:10.1016/S0273-1223(98)00785-9

Guo, L., Lamaire-Chad, C., Bellandi, G., Daelman, M., Amerlinck, Y., Maere, T., Nous, J., Flameling, T., Weijers, S., Mark, V.L., Volcke, E., Nopens, I., Vanrolleghem, P.A., 2013. Comprehensive field measurement of nitrous oxide (N2O) gas emissions and influencing factors under dry and wet weather conditions.

Guo, L., Vanrolleghem, P.A., 2014. Calibration and validation of an activated sludge model for greenhouse gases no. 1 (ASMG1): prediction of temperature-dependent N_2O emission dynamics. Bioprocess Biosyst Eng 37, 151–163. doi:10.1007/s00449-013-0978-3

Guyonvarch, E., Ramin, E., Kulahci, M., Plósz, B.G., 2015. iCFD: Interpreted Computational Fluid Dynamics - Degeneration of CFD to one-dimensional advection-dispersion models using statistical experimental design - The secondary clarifier. Water Res 83, 396–411. doi:10.1016/j.watres.2015.06.012

Haldane, J.B.S., 1930. Enzymes Longmans, Green & Co. Ltd, London.

Harper, W.F., Takeuchi, Y., Riya, S., Hosomi, M., Terada, A., 2015. Novel abiotic reactions increase nitrous oxide production during partial nitrification: Modeling and experiments. Chemical Engineering Journal 281, 1017–1023. doi:10.1016/j.cej.2015.06.109

Hauduc, H., Rieger, L., Oehmen, A., van Loosdrecht, M.C., Comeau, Y., Héduit, A., Vanrolleghem, P.A., Gillot, S., 2013. Critical review of activated sludge modeling: state of process knowledge, modeling concepts, and limitations. Biotechnol Bioeng 110, 24–46. doi:10.1002/bit.24624

Henze, M., Grady, C.P.L.J., Marais, G., Matsuo, T., 1987. Activated Sludge Model No. 1. IAWQ Scientific and Technical Report No. 1, London, UK.

Henze, M., Gujer, W., Mino, T., 2000. Activated Sludge Models ASM1, ASM2, ASM2D and ASM3. IWA Publishing, London, UK.

Henze, M., Gujer, W., Mino, T., Matsuo, T., Wentzel, M., Marais, G., Vanloosdrecht, M., 1999. Activated Sludge Model No.2d, ASM2d. Water Sci Technol 39, 165–182. doi:10.1016/S0273-1223(98)00829-4

Hiatt, W.C., Grady, C.P., 2008. An updated process model for carbon oxidation, nitrification, and denitrification. Water Environ Res 80, 2145–2156.

Higbie, R., 1935. The rate of absorption of a pure gas into a still liquid during short periods of exposure. Transactions of the American Institute of Chemical Engineers 31, 365–389.

Hreiz, R., Latifi, M.A., Roche, N., 2015. Optimal design and operation of activated sludge processes: State-of-the-art. Chemical Engineering Journal 281, 900–920. doi:10.1016/j.cej.2015.06.125

Huang, W., Li, K., 2013. CFD Simulation of Flows in Stirred Tank Reactors Through Prediction of Momentum Source, in: Guillen, D. (Ed.), Nuclear Reactor Thermal Hydraulics and Other Applications. InTech. doi:10.5772/51754

Ingildsen, P., Jeppsson, U., Olsson, G., 2002. Dissolved oxygen controller based on on-line measurements of ammonium combining feed-forward and feedback. Water Sci Technol 45, 453–460.

IPCC, 2014. Climate change 2013: the physical science basis: Working Group I contribution to the Fifth assessment report of the Intergovernmental Panel on Climate Change.

Ishii, M., Hibiki, T., 2011. Thermo-Fluid Dynamics of Two-Phase Flow. Springer New York, New York, NY. doi:10.1007/978-1-4419-7985-8

Jeppsson, U., 2014. Benchmarking of Control Strategies for Wastewater Treatment Plants (Scientific and Technical Report), 1st ed. IWA Publishing.

Jeppsson, U., Pons, M.N., Nopens, I., Alex, J., Copp, J.B., Gernaey, K.V., Rosen, C., Steyer, J.P., Vanrolleghem, P.A., 2007. Benchmark simulation model no 2: general protocol and exploratory case studies. Water Sci Technol 56, 67–78. doi:10.2166/wst.2007.604

Jiang, C., Huang, W., Wang, G., Wang, Y., Xie, R., 2010. Numerical computation of flow fields in an oxidation ditch by computational fluid dynamics model. Huanjing Kexue yu Jishu 33, 135–140.

Jin, B., Yin, P., Lant, P., 2006. Hydrodynamics and mass transfer coefficient in three-phase air-lift reactors containing activated sludge. Chemical Engineering and Processing: Process Intensification 45, 608–617. doi:10.1016/j.cep.2005.08.007

Kampschreur, M.J., Picioreanu, C., Tan, N., Kleerebezem, R., Jetten, M.S.M., van Loosdrecht, M.C.M., 2007. Unraveling the Source of Nitric Oxide Emission During Nitrification. Water Environment Research 79, 2499–2509. doi:10.2175/106143007X220815

Kampschreur, M.J., Temmink, H., Kleerebezem, R., Jetten, M.S., van Loosdrecht, M.C., 2009. Nitrous oxide emission during wastewater treatment. Water Res 43, 4093–4103. doi:10.1016/j.watres.2009.03.001

Karpinska, A.M., Bridgeman, J., 2016. CFD-aided modelling of activated sludge systems - A critical review. Water Res 88, 861–879. doi:10.1016/j.watres.2015.11.008

Kinnear, D.J., Deines, K., 2001. ACOUSTIC DOPPLER CURRENT PROFILER CLARIFIER VELOCITY MEASUREMENT. Proceedings of the Water Environment Federation 2001, 500–515. doi:10.2175/193864701790861596

Kolarik, L.O., Priestley, A.J., 1995. Modern techniques in water and wastewater treatment. CSIRO, East Melbourne, Vic., Australia.

Kolev, N.I., 2005. Multiphase flow dynamics. Springer.

Laborde-Boutet, C., Larachi, F., Dromard, N., Delsart, O., Schweich, D., 2009. CFD simulation of bubble column flows: Investigations on turbulence models in RANS approach. Chem Eng Sci 64, 4399–4413. doi:10.1016/j.ces.2009.07.009

Lackner, S., Smets, B.F., 2012. Effect of the kinetics of ammonium and nitrite oxidation on nitritation success or failure for different biofilm reactor geometries. Biochem Eng J 69, 123–129. doi:10.1016/j.bej.2012.09.006

Laurent, J., Samstag, R.W., Ducoste, J.M., Griborio, A., Nopens, I., Batstone, D.J., Wicks, J.D., Saunders, S., Potier, O., 2014. A protocol for the use of computational fluid dynamics as a supportive tool for wastewater treatment plant modelling. Water Sci Technol 70, 1575–1584. doi:10.2166/wst.2014.425

Le Moullec, Y., Gentric, C., Potier, O., Leclerc, J.P., 2010a. CFD simulation of the hydrodynamics and reactions in an activated sludge channel reactor of wastewater treatment. Chem Eng Sci 65, 492–498. doi:10.1016/j.ces.2009.03.021

Le Moullec, Y., Gentric, C., Potier, O., Leclerc, J.P., 2010b. Comparison of systemic, compartmental and CFD modelling approaches: Application to the simulation of a biological reactor of wastewater treatment. Chem Eng Sci 65, 343–350. doi:10.1016/j.ces.2009.06.035

Le Moullec, Y., Potier, O., Gentric, C., Leclerc, J.P., 2008. A general correlation to predict axial dispersion coefficients in aerated channel reactors. Water Res 42, 1767–1777. doi:10.1016/j.watres.2007.10.041

Le Moullec, Y., Potier, O., Gentric, C., Leclerc, J.P., 2011. Activated sludge pilot plant: comparison between experimental and predicted concentration profiles using three different modelling approaches. Water Res 45, 3085–3097. doi:10.1016/j.watres.2011.03.019

Lessard, P., Beck, M.B., 1993. Dynamic modelling of the activated sludge process: a case study. Water Res 27, 963–978. doi:10.1016/0043-1354(93)90060-U

Levenspiel, O., 1962. Comparison of the tanks-in-series and the dispersion models for non ideal flow of fluid. Chem Eng Sci 17, 576–577. doi:10.1016/0009-2509(62)87010-9

Levenspiel, O., 1999. Chemical reaction engineering, 3rd ed. Wiley & Sons, New York.

Li, S., Ren, B., 2010. Meshfree Methods, in: Blockley, R., Shyy, W. (Eds.), Encyclopedia of Aerospace Engineering. John Wiley & Sons, Ltd, Chichester, UK. doi:10.1002/9780470686652.eae600

Levin, M., 1993. Biotreatment of industrial and hazardous waste. McGraw-Hill, Inc, United States.

Li, Z., Qi, R., Wang, B., Zou, Z., Wei, G., Yang, M., 2013. Cost-performance analysis of nutrient removal in a full-scale oxidation ditch process based on kinetic modeling. Journal of Environmental Sciences 25, 26–32. doi:10.1016/S1001-0742(12)60002-3

Littleton, H.X., Daigger, G.T., Strom, P.F., 2007. Application of computational fluid dynamics to closed-loop bioreactors: I. Characterization and simulation of fluid-flow pattern and oxygen transfer. Water Environ Res 79, 600–612.

Liu, X., García, M.H., 2011. Computational Fluid Dynamics Modeling for the Design of Large Primary Settling Tanks. Journal of Hydraulic Engineering 137, 343–355. doi:10.1061/(ASCE)HY.1943-7900.0000313

Liu, X., Wang, Y., Waite, T.D., Leslie, G., 2015. Numerical simulation of bubble induced shear in membrane bioreactors: effects of mixed liquor rheology and membrane configuration. Water Res 75, 131–145. doi:10.1016/j.watres.2015.02.009

Liu, Y., Shi, H., Xia, L., Shi, H., Shen, T., Wang, Z., Wang, G., Wang, Y., 2010. Study of operational conditions of simultaneous nitrification and denitrification in a Carrousel oxidation ditch for domestic wastewater treatment. Bioresour Technol 101, 901–906. doi:10.1016/j.biortech.2009.09.015

Lu, H., Chandran, K., 2010. Factors promoting emissions of nitrous oxide and nitric oxide from denitrifying sequencing batch reactors operated with methanol and ethanol as electron donors. Biotechnol Bioeng 106, 390–398. doi:10.1002/bit.22704

Luo, L., Li, W.M., Deng, Y.S., Wang, T., 2005. Numerical simulation of a combined oxidation ditch flow using 3D k-epsilon turbulence model. J Environ Sci (China) 17, 808–812.

Lyn, D.A., Stamou, A.I., Rodi, W., 1992. Density currents and shear-induced flocculation in sedimentation tanks. Journal of hydraulic Engineering 118, 849–867.

Machado, V.C., Gabriel, D., Lafuente, J., Baeza, J.A., 2009. Cost and effluent quality controllers design based on the relative gain array for a nutrient removal WWTP. Water Res 43, 5129–5141. doi:10.1016/j.watres.2009.08.011

Maere, T., Benedetti, L., Nopens, I., 2009. An update on mixing and pumping costs of BSM-MBR: a benchmark simulation model for membrane bioreactors to compare control strategies. Presented at the 1st IWA BeNeLux Regional Young Water Professionals Conference.

Mampaey, K.E., Beuckels, B., Kampschreur, M.J., Kleerebezem, R., van Loosdrecht, M.C., Volcke, E.I., 2013. Modelling nitrous and nitric oxide emissions by autotrophic ammonia-oxidizing bacteria. Environ Technol 34, 1555–1566. doi:10.1080/09593330.2012.758666

Manninen, M., Taivassalo, V., Kallio, S., 1996. On the mixture model for multiphase flow.

Maurer, M., Gujer, W., 1998. Dynamic modelling of enhanced biological phosphorus and nitrogen removal in activated sludge systems. Water Sci Technol 38, 203–210. doi:10.1016/S0273-1223(98)00405-3

MIKE Powered by DHI [WWW Document], 2016. URL https://www.mikepoweredbydhi.com/ (accessed 5.12.16).

Mohammadi, B., Pironneau, O., 1993. Analysis of the K-epsilon turbulence model. Institut National de Recherche d'Informatique et d'Automatique (INRIA), Paris, France.

Monod, J., 1942. Recherches sur la croissance des cultures bactériennes,. Hermann & cie, Paris.

Mullison, J., Wanis, P., Symonds, D., 2011. Field testing of a new ADCP. Presented at the IEEE/OES/CWTM tenth Working Conference on Current Measurement Technology, IEEE, pp. 87–92.

Münch, E.V., Lant, P., Keller, J., 1996. Simultaneous nitrification and denitrification in bench-scale sequencing batch reactors. Water Res 30, 277–284. doi:10.1016/0043-1354(95)00174-3

Nauman, E.B., 1987. Chemical reactor design. John Wiley and Sons Inc., New York, NY.

Ni, B., Yu, H., 2008. Simulation of heterotrophic storage and growth processes in activated sludge under aerobic conditions. Chemical Engineering Journal 140, 101–109. doi:10.1016/j.cej.2007.09.017

Ni, B.J., Yuan, Z., 2015. Recent advances in mathematical modeling of nitrous oxides emissions from wastewater treatment processes. Water Res 87, 336–346. doi:10.1016/j.watres.2015.09.049

Ni, B.J., Yuan, Z., Chandran, K., Vanrolleghem, P.A., Murthy, S., 2013. Evaluating four mathematical models for nitrous oxide production by autotrophic ammonia-oxidizing bacteria. Biotechnol Bioeng 110, 153–163. doi:10.1002/bit.24620

Nogueira, B.L., Pérez, J., van Loosdrecht, M.C., Secchi, A.R., Dezotti, M., Biscaia, E.C., 2015. Determination of the external mass transfer coefficient and influence

of mixing intensity in moving bed biofilm reactors for wastewater treatment. Water Res 80, 90–98. doi:10.1016/j.watres.2015.05.010

Nopens, I., 2013. IWA Working Group on Computational Fluid Dynamics (SG MIA) - IWA Water Wiki - Open Access Information for the Global Water Community [WWW Document]. URL http://www.iwawaterwiki.org (accessed 4.15.16).

Nopens, I., Batstone, D.J., Griborio, A., Samstag, R., Wicklein, E., Wicks, J., 2012. Computational Fluid Dynamics (CFD): What is Good CFD-Modeling Practice and What Can Be the Added Value of CFD Models to WWTP Modeling? Proceedings of the Water Environment Federation 2012, 7400–7405. doi:10.2175/193864712811704161

Nopens, I., Benedetti, L., Jeppsson, U., Pons, M.N., Alex, J., Copp, J.B., Gernaey, K.V., Rosen, C., Steyer, J.P., Vanrolleghem, P.A., 2010. Benchmark Simulation Model No 2: finalisation of plant layout and default control strategy. Water Sci Technol 62, 1967–1974. doi:10.2166/wst.2010.044

NX: Siemens PLM Software [WWW Document], 2016. URL https://www.plm.automation.siemens.com/en_us/products/nx/ (accessed 6.5.12).

Olsson, G., 2012. ICA and me--a subjective review. Water Res 46, 1585–1624. doi:10.1016/j.watres.2011.12.054

Olsson, G., Nielsen, M., Yuan, Z., Lynggaard-Jensen, A., Steyer, J.-P., 2015. Instrumentation, Control and Automation in Wastewater Systems. Water Intelligence Online 4, 9781780402680–9781780402680. doi:10.2166/9781780402680

Onnerth, T., Nielsen, M., Stamer, C., 1996. Advanced computer control based on real and software sensors. Water Sci Technol 33, 237–245. doi:10.1016/0273-1223(96)00176-X

Pan, Y., Ni, B.J., Yuan, Z., 2013. Modeling electron competition among nitrogen oxides reduction and N2O accumulation in denitrification. Environ Sci Technol 47, 11083–11091. doi:10.1021/es402348n

Petersen, E.E., 1965. Chemical reaction analysis. Prentice Hall.

Pittoors, E., Guo, Y., W. H. Van Hulle, S., 2014. Modeling dissolved oxygen concentration for optimizing aeration systems and reducing oxygen consumption in activated sludge processes: a review. Chemical engineering communications 201, 983–1002. doi:10.1080/00986445.2014.883974

Pons, M.N., Potier, O., Roche, N., Colin, F., Prost, C., 1993. Simulation of municipal wastewater treatment plants by activated sludge. Comput Chem Eng 17, S227–S232. doi:10.1016/0098-1354(93)80234-E

Potier, O., Leclerc, J.P., Pons, M.N., 2005. Influence of geometrical and operational parameters on the axial dispersion in an aerated channel reactor. Water Res 39, 4454–4462. doi:10.1016/j.watres.2005.08.024

Ratkovich, N., Horn, W., Helmus, F.P., Rosenberger, S., Naessens, W., Nopens, I., Bentzen, T.R., 2013. Activated sludge rheology: a critical review on data collection and modelling. Water Res 47, 463–482. doi:10.1016/j.watres.2012.11.021

Rieger, L., Alex, J., Gujer, W., Siegrist, H., 2006. Modelling of aeration systems at wastewater treatment plants. Water Sci Technol 53, 439–447.

Rittmann, B., McCarty, P.L., 2012. Environmental biotechnology: principles and applications. Tata McGraw-Hill Education.

Roeleveld, P.J., van Loosdrecht, M.C., 2002. Experience with guidelines for wastewater characterisation in The Netherlands. Water Sci Technol 45, 77–87.

Rosenberger, S., Krüger, U., Witzig, R., Manz, W., Szewzyk, U., Kraume, M., 2002. Performance of a bioreactor with submerged membranes for aerobic treatment of municipal waste water. Water Res 36, 413–420. doi:10.1016/S0043-1354(01)00223-8

Rostami, F., Shahrokhi, M., Md Said, M.A., Abdullah, R., Syafalni, 2011. Numerical modeling on inlet aperture effects on flow pattern in primary settling tanks. Appl Math Model 35, 3012–3020. doi:10.1016/j.apm.2010.12.007

Samstag, R.W., Wicklein, E.A., 2014. A Protocol for Optimization of Activated Sludge Mixing. Proceedings of the Water Environment Federation 2014, 3614–3640. doi:10.2175/193864714815939453

Samstag, R.W., Wicklein, E.A., Reardon, R.D., Leetch, R.J., Parks, R.M., Groff, C.D., 2012. Field and CFD Analysis of Jet Aeration and Mixing. Proceedings of the Water Environment Federation 2012, 4113–4139. doi:10.2175/193864712811708301

Samuelsson, P., Halvarsson, B., Carlsson, B., 2007. Cost-efficient operation of a denitrifying activated sludge process. Water Res 41, 2325–2332. doi:10.1016/j.watres.2006.10.031

Schiller, L., Naumann, Z., 1935. A drag coefficient correlation. Vdi Zeitung 77, 51.

Schreiber, F., Loeffler, B., Polerecky, L., Kuypers, M.M., de Beer, D., 2009. Mechanisms of transient nitric oxide and nitrous oxide production in a complex biofilm. ISME J 3, 1301–1313. doi:10.1038/ismej.2009.55

Schulthess, V.R., Wild, D., Gujer, W., 1994. Nitric and nitrous oxides from denitrifying activated sludge at low oxygen concentration. Water Sci Technol.

Shirazi, M.M.A., Kargari, A., Ismail, A.F., Matsuura, T., 2016. Computational Fluid Dynamic (CFD) opportunities applied to the membrane distillation process: State-of-the-art and perspectives. Desalination 377, 73–90. doi:10.1016/j.desal.2015.09.010

Spanjers, H., Vanrolleghem, P., Nguyen, K., Vanhooren, H., Patry, G., 1998. Towards a simulation-benchmark for evaluating respirometry-based control strategies. Water Sci Technol 37, 219–226. doi:10.1016/S0273-1223(98)00373-4

Stamou, A.I., Latsa, M., Assimacopoulos, D., 2000. Design of two-storey final settling tanks using mathematical models. Journal of Hydroinformatics.

Stare, A., Vrecko, D., Hvala, N., Strmcnik, S., 2007. Comparison of control strategies for nitrogen removal in an activated sludge process in terms of operating costs: a simulation study. Water Res 41, 2004–2014. doi:10.1016/j.watres.2007.01.029

Stenstrom, M.K., Song, S.S., 1991. Effects of oxygen transport limitation on nitrification in the activated sludge process. Research Journal of the Water Pollution Control Federation 208–219.

Tallec, G., Garnier, J., Billen, G., Gousailles, M., 2006. Nitrous oxide emissions from secondary activated sludge in nitrifying conditions of urban wastewater treatment plants: effect of oxygenation level. Water Res 40, 2972–2980. doi:10.1016/j.watres.2006.05.037

Tarpagkou, R., Pantokratoras, A., 2013. CFD methodology for sedimentation tanks: The effect of secondary phase on fluid phase using DPM coupled calculations. Appl Math Model 37, 3478–3494. doi:10.1016/j.apm.2012.08.011

Tchobanoglous, G., Burton, F.L., Stensel, H.D., 2003. Wastewater engineering: Treatment and Reuse, 4th ed. McGraw-Hill, New York, USA.

Torfs, E., 2015. Different settling regimes in secondary settling tanks: experimental process analysis, model development and calibration (Doctoral dissertation).

Valverde-Pérez, B., Fuentes-Martínez, J.M., Flores-Alsina, X., Gernaey, K.V., Huusom, J.K., Plósz, B.G., 2016. Control structure design for resource recovery using the enhanced biological phosphorus removal and recovery (EBP2R) activated sludge process. Chemical Engineering Journal 296, 447–457. doi:10.1016/j.cej.2016.03.021

Vanrolleghem, P., Spanjers, H., 1998. A hybrid respirometric method for more reliable assessment of activated sludge model parameter. Water Sci Technol 37, 237–246. doi:10.1016/S0273-1223(98)00338-2

Verrecht, B., Maere, T., Benedetti, L., Nopens, I., Judd, S., 2010. Model-based energy optimisation of a small-scale decentralised membrane bioreactor for urban reuse. Water Res 44, 4047–4056. doi:10.1016/j.watres.2010.05.015

Versteeg, H.K., Malalasekera, W., 2007. An introduction to computational fluid dynamics, 2nd ed. Pearson Education Ltd., Harlow, England.

Waldraff, W., Dochain, D., Bourrel, S., Magnus, A., 1998. On the use of observability measures for sensor location in tubular reactor. J Process Control 8, 497–505. doi:10.1016/S0959-1524(98)00017-1

Wang, J.S., Hamburg, S.P., Pryor, D.E., Chandran, K., Daigger, G.T., 2011. Emissions credits: opportunity to promote integrated nitrogen management in the wastewater sector. Environ Sci Technol 45, 6239–6246. doi:10.1021/es200419h

Wang, X., Ding, J., Guo, W.Q., Ren, N.Q., 2010. A hydrodynamics-reaction kinetics coupled model for evaluating bioreactors derived from CFD simulation. Bioresour Technol 101, 9749–9757. doi:10.1016/j.biortech.2010.07.115

Wang, Y., Waite, T.D., Leslie, G.L., 2013. Computational fluid dynamics (CFD) analysis of membrane reactors: modelling of membrane bioreactors for municipal wastewater treatment, in: Handbook of Membrane Reactors. Elsevier, pp. 532–568. doi:10.1533/9780857097330.3.532

Weiss, M., Plósz, B.G., Essemiani, K., Meinhold, J., 2007. Suction-lift sludge removal and non-Newtonian flow behaviour in circular secondary clarifiers: Numerical modelling and measurements. Chemical Engineering Journal 132, 241–255. doi:10.1016/j.cej.2007.01.004

Wicklein, E., Batstone, D.J., Ducoste, J., Laurent, J., Griborio, A., Wicks, J., Saunders, S., Samstag, R., Potier, O., Nopens, I., 2016. Good modelling practice in applying computational fluid dynamics for WWTP modelling. Water Sci Technol 73, 969–982. doi:10.2166/wst.2015.565

Wilcox, D.C., 1998. Turbulence modeling for CFD. DCW industries La Canada, CA.

Witt, P.J., Feng, Y., Eick, I., Schwarz, M.P., 2012. Modelling bubble flow with CFX and FLUENT for aluminium reduction cells. Presented at the Ninth International Conference on CFD in the Minerals and Process Industries CSIRO, Melbourne, Australia.

Wood, M., Greenfield, P., Howes, T., Johns, M., Keller, J., 1995. Computational fluid dynamic modelling of wastewater ponds to improve design. Water Sci Technol 31, 111–118. doi:10.1016/0273-1223(95)00498-C

Wood, M.G., Howes, T., Keller, J., Johns, M.R., 1998. Two dimensional computational fluid dynamic models for waste stabilisation ponds. Water Res 32, 958–963. doi:10.1016/S0043-1354(97)00316-3

Wunderlin, P., Lehmann, M.F., Siegrist, H., Tuzson, B., Joss, A., Emmenegger, L., Mohn, J., 2013. Isotope signatures of N_2O in a mixed microbial population system: constraints on N_2O producing pathways in wastewater treatment. Environ Sci Technol 47, 1339–1348. doi:10.1021/es303174x

Wunderlin, P., Mohn, J., Joss, A., Emmenegger, L., Siegrist, H., 2012. Mechanisms of N2O production in biological wastewater treatment under nitrifying and denitrifying conditions. Water Res 46, 1027–1037. doi:10.1016/j.watres.2011.11.080

Xie, W., Zhang, R., Li, W., Ni, B., Fang, F., Sheng, G., Yu, H., Song, J., Le, D., Bi, X., Liu, C., Yang, M., 2011. Simulation and optimization of a full-scale Carrousel oxidation ditch plant for municipal wastewater treatment. Biochem Eng J 56, 9–16. doi:10.1016/j.bej.2011.04.010

Xu, S., Hultman, B., 1996. Experiences in wastewater characterization and model calibration for the activated sludge process. Water Sci Technol 33, 89–98. doi:10.1016/0273-1223(96)00462-3

Yang, Y., Wu, Y., Yang, X., Zhang, K., Yang, J., 2010. Flow field prediction in full-scale Carrousel oxidation ditch by using computational fluid dynamics. Water Sci Technol 62, 256–265. doi:10.2166/wst.2010.240

Ye, L., Ni, B.J., Law, Y., Byers, C., Yuan, Z., 2014. A novel methodology to quantify nitrous oxide emissions from full-scale wastewater treatment systems with surface aerators. Water Res 48, 257–268. doi:10.1016/j.watres.2013.09.037

Yu, R., Kampschreur, M.J., van Loosdrecht, M.C., Chandran, K., 2010. Mechanisms and specific directionality of autotrophic nitrous oxide and nitric oxide generation during transient anoxia. Environ Sci Technol 44, 1313–1319. doi:10.1021/es902794a

Zhang, P., Qi, Z., 2007. Simultaneous nitrification and denitrification in activated sludge system under low oxygen concentration. Frontiers of Environmental Science & Engineering in China 1, 49–52. doi:10.1007/s11783-007-0009-1

Zhang, P., Yuan, M., Wang, H., 2008. Improvement of nitrogen removal and reduction of operating costs in an activated sludge process with feedforward–cascade control strategy. Biochem Eng J 41, 53–58. doi:10.1016/j.bej.2008.03.007

Zhao, H., Isaacs, S.H., Søeberg, H., Kümmel, M., 1995. An analysis of nitrogen removal and control strategies in an alternating activated sludge process. Water Res 29, 535–544. doi:10.1016/0043-1354(94)00174-6

Zhou, Z., Shen, X., Jiang, L., Wu, Z., Wang, Z., Ren, W., Hu, D., 2015. Modeling of multimode anaerobic/anoxic/aerobic wastewater treatment process at low temperature for process optimization. Chemical Engineering Journal 281, 644–650. doi:10.1016/j.cej.2015.07.017

Appendix A

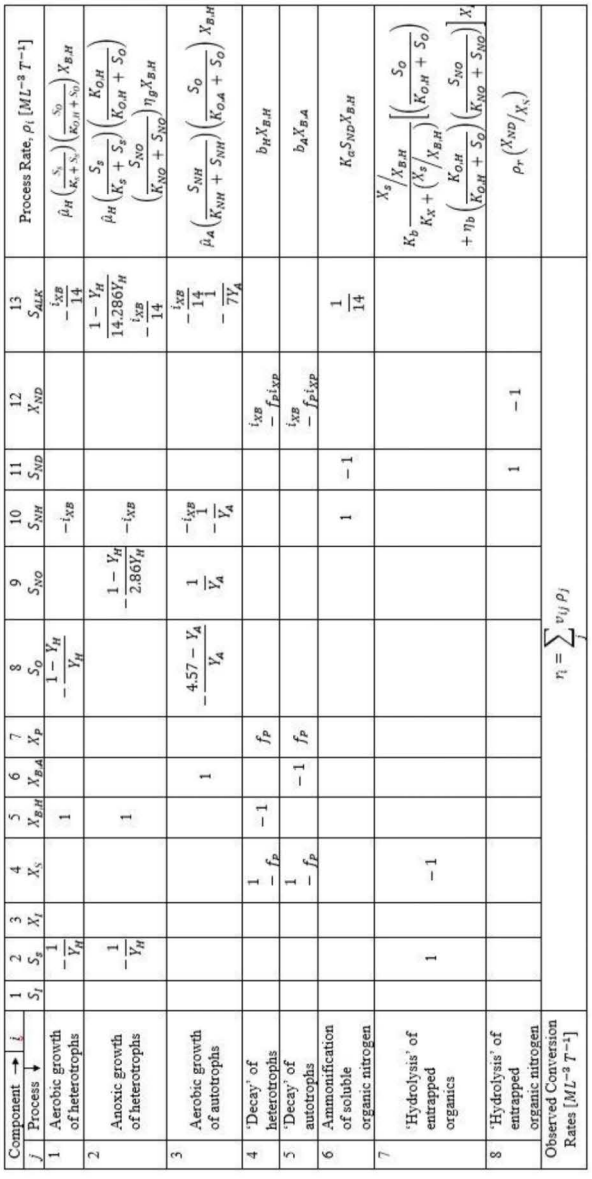

Component → / j	i	1 S_I	2 S_S	3 X_I	4 X_S	5 $X_{B,H}$	6 $X_{B,A}$	7 X_P	8 S_O	9 S_{NO}	10 S_{NH}	11 S_{ND}	12 X_{ND}	13 S_{ALK}	Process Rate, ρ_i $[ML^{-3}T^{-1}]$
1	Aerobic growth of heterotrophs		$-\frac{1}{Y_H}$			1			$-\frac{1-Y_H}{Y_H}$		$-i_{XB}$			$-\frac{i_{XB}}{14}$	$\hat{\mu}_H\left(\frac{S_S}{K_S+S_S}\right)\left(\frac{S_O}{K_{O,H}+S_O}\right)X_{B,H}$
2	Anoxic growth of heterotrophs		$-\frac{1}{Y_H}$			1				$-\frac{1-Y_H}{2.86Y_H}$	$-i_{XB}$			$\frac{1-Y_H}{14.286Y_H}$ $-\frac{i_{XB}}{14}$	$\hat{\mu}_H\left(\frac{S_S}{K_S+S_S}\right)\left(\frac{K_{O,H}}{K_{O,H}+S_O}\right)$ $\left(\frac{S_{NO}}{K_{NO}+S_{NO}}\right)\eta_g X_{B,H}$
3	Aerobic growth of autotrophs						1		$-\frac{4.57-Y_A}{Y_A}$	$\frac{1}{Y_A}$	$-i_{XB}-\frac{1}{Y_A}$			$-\frac{i_{XB}}{14}-\frac{1}{7Y_A}$	$\hat{\mu}_A\left(\frac{S_{NH}}{K_{NH}+S_{NH}}\right)\left(\frac{S_O}{K_{O,A}+S_O}\right)X_{B,H}$
4	'Decay' of heterotrophs			$1-f_P$	-1		f_P						$i_{XB}-f_P i_{XP}$		$b_H X_{B,H}$
5	'Decay' of autotrophs			$1-f_P$		-1	f_P						$i_{XB}-f_P i_{XP}$		$b_A X_{B,A}$
6	Ammonification of soluble organic nitrogen										1	-1		$\frac{1}{14}$	$K_a S_{ND} X_{B,H}$
7	'Hydrolysis' of entrapped organics	1			-1										$\frac{X_S/X_{B,H}}{K_b+\left(X_S/X_{B,H}\right)}\left[\left(\frac{S_O}{K_{O,H}+S_O}\right)\right.$ $\left.+\eta_b\left(\frac{K_{O,H}}{K_{O,H}+S_O}\right)\left(\frac{S_{NO}}{K_{NO}+S_{NO}}\right)\right]X_i$
8	'Hydrolysis' of entrapped organic nitrogen											1	-1		$\rho_r\left(X_{ND}/X_S\right)$
Observed Conversion Rates $[ML^{-3}T^{-1}]$		$r_i=\sum_j v_{ij}\rho_j$													

Appendix A 1 The gujer matrix for the Activated Sludge Model number 1 (Henze et. al 1987)

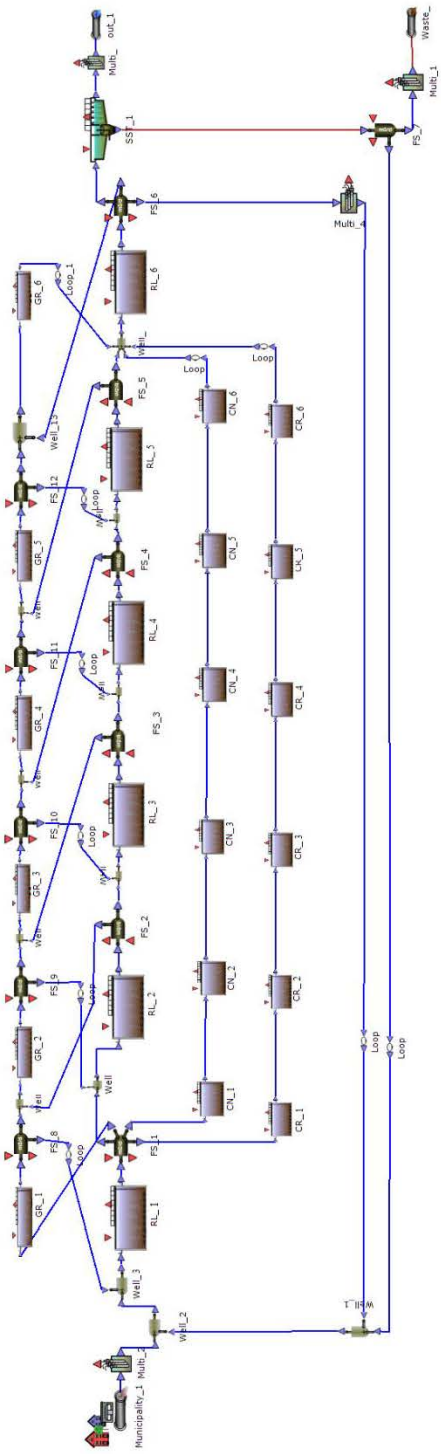

Appendix A 2 Layout in WEST for the compartmental model in chapter 8

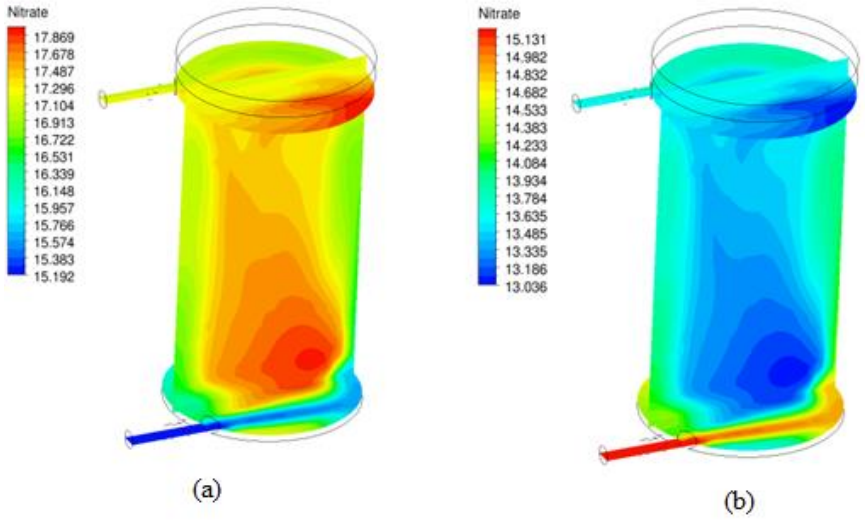

Appendix A 3 Distribution of the nitrate concentration in the absence of inflowing DO (a) and in absence of inflowing organic carbon (b).

Summary

Wastewater treatment plants (WWTP) are needed to treat municipal wastewater to reduce the impact of pollutants on the environment and the ambient nature. The discharge of treated wastewater and the disposal of sludge from treatment plants treating domestic or industrial wastewater are subject to regulations imposed by the authorities. Moreover, during the wastewater treatment process greenhouse gas emissions are produced. These emissions from WWTPs are a matter of growing concern.

The increased importance of wastewater treatment has led to development of mathematical models for optimization and design of wastewater treatment plants. WWTP modelling entails the modelling of the biological reactions (biokinetics) and underlying flow physics of the bioreactors (hydrodynamics). Currently, to model the hydrodynamics of a bioreactor, the tanks-in-series (TIS) modelling approach, which at best can model the flow variations in one direction, is widely used. These models assume a bioreactor as a series of completely mixed tanks and, hence, ignore any variation in the concentrations stemming from the design of a bioreactor or operational conditions. Therefore, these models eventually need rigorous calibration efforts to match measurements. This calibration is generally performed by manipulating kinetic parameters such as half saturation indices (K-values). The calibrated models are then used to assess or formulate different control strategies which includes the determination of an appropriate sensor location and a well-chosen setpoint for the controllers. In addition, the calibrated models are then extrapolated to predict the WWTP performance under different dynamic conditions (diurnal and dry/wet weather conditions) assuming that the flow patterns remain unchanged.

In this thesis, it is hypothesised and confirmed that the bioreactors are not at all completely mixed and, hence, current models wrongfully calibrate the kinetic parameters by correcting for the errors induced by the over-simplified modelling of mixing. Consequently, the need for re-calibration arises at different operational

conditions due to the limitation of the current models to incorporate changes in operational conditions.

The thesis comprises of four parts. The first part provides the detailed account of CFD (computational fluid dynamics) modelling of WWTPs. Second part is about integration of CFD hydrodynamic models with the biokinetic models to evaluate the impact of mixing on the process performance. Third part is about model reduction, where detailed knowledge gained from the CFD-biokinetic modelling is used to develop simple but spatially localized compartmental model. The fourth part provides the insight about impact of mixing on the TIS model calibrations.

In the first part, detailed CFD hydrodynamic modelling of a bioreactor of Eindhoven WWTP is performed. The impact of reactor configuration and process conditions on gas dispersion is observed. Potential regions of poor mixing are identified. The different flow patterns are discussed in detail. Similarly, hydrodynamic modelling of an oxidation ditch (OD) of La Bisbal d'Empordà WWTP is performed. The OD is equipped with four surface aerators (rotors). The impact of 2-rotor and 4-rotor strategy on the flow patterns is observed and discussed in detail.

In the second part, the CFD hydrodynamic model of Eindhoven WWTP is extended by integrating it with bio-kinetic models, firstly with ASM1 and secondly with ASMG1. The impact of local mixing conditions on the dissolved oxygen (DO) and ammonium concentrations is observed and described. Regions of poor mixing are observed and hence their impact on overall process heterogeneity is discussed. The impact of DO variations on the nitrous oxide concentrations is also observed and it is shown that low DO concentrations tend to increase the nitrous oxide production. Similarly, the OD is also extended with a bio-kinetic model i.e. the ASM1 model. It is observed that the surface aerators have an inherent operational limitation and the DO concentrations at the bottom are very low (nearly anoxic).

In the third part, the compartmental modelling (CM) was setup based on the DO concentrations using CFD-biokinetic model. A novel idea of cumulative species distribution (CSDs) to quantify the variations is introduced here as well. The CSDs serve as a decision support tool for the CM. A detailed stepwise procedure for the compartmentalisation is provided. Based on the procedure, the CMs are developed for both case studies. The CMs are also developed for different conditions and it is found that the CM network is different under varying conditions. Therefore, an idea of

dynamic compartmental model is suggested at the end. Furthermore, this part also illustrates the impact of sensor location on the controller performance using a compartmental model. It is found that the controller's performance highly depends on the sensor location and setpoint. An optimal sensor location can improve the effluent quality at reduced cost.

In the last part, the impact of mixing on a CSTR based model calibration is shown. It is shown that the TIS models predict different estimated values under different mixing conditions. Therefore, it is important to take into account the mixing conditions before performing calibrations. The impact of sensor locations on the TIS model calibrations is also shown. The TIS model calibrations vary significantly if the sensor location for data collection are changed.

It is concluded that this thesis has demonstrated the ability of CFD-biokinetic modelling to evaluate the process more accurately. Tthe derivation of a compartmental model has also provided the solution of high computational demands, commonly attributed to CFD modelling.

Samenvatting

Waterzuiveringsinstallaties (WZI) behandelen het huishoudelijk afvalwater om de impact van de vervuiling op het milieu en de ons omringende natuur te beperken. Het lozen van het behandelde afvalwater en het afvoeren van slib zijn onderworpen aan een strikte wetgeving. Daarnaast worden tijdens het waterzuiveringsproces broeikasgassen uitgestoten waarover een toenemende bezorgdheid bestaat.

Het toegenomen belang van waterzuivering heeft geleid tot de ontwikkeling van wiskundige modellen die gebruikt worden voor de optimalisatie en het ontwerp van waterzuiveringsinstallaties. De modellering van WZI's omvat de modellering van zowel de biologische reacties (bio-kinetiek) en de onderliggende stromingspatronen van de bioreactoren (hydrodynamica). Tegenwoordig wordt veelvuldig gebruik gemaakt van de tanks-in-serie (TIS) benadering. Modellen opgesteld volgens deze benadering stellen de bioreactor voor als een serie van aaneengeschakelde volledig gemengde tanks. Deze modellen kunnen echter enkel veranderingen in één richting beschrijven. Deze voorstelling negeert dan ook elke variatie in concentraties afkomstig van het ontwerp of het operationeel beheer van de bioreactor. Om de data te kunnen beschrijven moeten deze modellen daardoor soms gecorrigeerd worden tijdens een kalibratie. Deze kalibratie wordt vaak verwezenlijkt door de kinetische parameters, zoals de half-saturatie indices (K-waarden) te manipuleren. Deze gekalibreerde modellen worden dan gebruikt voor het evalueren of formuleren van verschillende controlestrategieën. Daarbij hoort onder andere het bepalen van een geschikte sensorlocatie en een goed gekozen regelwaarde. Bovendien worden deze gekalibreerde modellen geëxtrapoleerd om voorspellingen te maken van de prestatie van de WZI onder gewijzigde dynamische omstandigheden (zowel dagelijkse schommelingen als de impact van droog en regen weer) in de veronderstelling dat de stromingspatronen niet wijzigen.

De TIS-benadering gaat ervan uit dat de bioreactors volledig gemengd zijn. Door deze vereenvoudiging van de mengingspatronen worden mogelijks fouten geïntroduceerd in de kalibratie van de opgestelde modellen. De hypothese dat de bioreactors helemaal

niet volledig gemengd zijn wordt in deze thesis naar voor geschoven en bevestigd. Daarbij komt dan ook de nood om het model opnieuw te kalibreren voor verschillende operationele omstandigheden die door de beperkingen van het model niet beschreven kunnen worden.

Deze thesis bevat 4 delen. Het eerste deel geeft een gedetailleerd verslag over het gebruik van CFD (computational fluid dynamics) modellering voor de beschrijving (van de hydrodynamica) van WZI's. Het tweede deel behandelt de integratie van de CFD modellen en bio-kinetische modellen om de impact van menging op de prestaties van de installatie te evalueren. Het derde deel behandelt modelvereenvoudiging, waarbij gebruik gemaakt wordt van de kennis opgedaan bij de geïntegreerde modellering van CFD en bio-kinetiek om een eenvoudiger ruimtelijk 'compartimenteel model (CM)' op te stellen. Het vierde deel ten slotte verschaft inzicht over de invloed van menging op de kalibratie van TIS gebaseerde modellen.

In het eerste deel werd een gedetailleerd CFD model voor de hydrodynamisch modellering van een bioreactor op de WZI van Eindhoven ontwikkeld. De invloed van de reactorconfiguratie en de procesomstandigheden op dispersie werd vastgesteld. Daarbij werden mogelijke regio's met slechte menging geïdentificeerd. Verschillende stromingspatronen werden in detail besproken. Een gelijkaardige studie werd ook uitgevoerd op een oxidatiesloot (OS) van de WZI La Bisbal d'Empordà. De OS is uitgerust met vier oppervlaktebeluchters (rotors). De invloed van een regeling gebruikmakend van ofwel twee of vier beluchters op de stromingspatronen werd bestudeerd en besproken.

In het tweede deel wordt het CFD hydrodynamisch model van de WZI Eindhoven uitgebreid door het te integreren met bio-kinetisch modellen, ten eerste het ASM1 model en ten tweede met het ASMG1 model. De impact van de lokale condities voor menging op opgeloste zuurstof (OZ) en ammonium werd berekend en beschreven. Regio's met slechte menging werden vastgesteld en hun impact op de algemene procesheterogeniteit werd besproken. Verder werd de invloed van variaties in OZ op het voorkomen van lachgas bestudeerd. Lage OZ concentraties lijken namelijk een verhoging in de aanmaak van lachgas te stimuleren. Ook voor de WZI La Bisbal d'Empordà, werd het CFD model van de OS uitgebreid met een bio-kinetisch model, namelijk ASM1. Het kon worden vastgesteld dat de oppervlaktebeluchters een inherente operationele beperking hebben die leidt tot heel lage OZ concentraties (bijna anoxische omstandigheden) bij de bodem.

In het derde deel, werd het ‘compartimenteel model’ opgesteld op basis van de OZ concentraties berekend met het geïntegreerde CFD-bio-kinetiek model. Een nieuw concept werd ontwikkeld om het CM op te stellen door cumulatieve species distributies (CSD), die de concentratievariaties in de reactor kwantificeren, als beslissingsondersteunend instrument te gebruiken. Een gedetailleerde, stapsgewijze procedure voor het compartimenteren werd opgesteld en toegepast voor de twee WZI’s. Deze procedure werd herhaaldelijk toegepast onder verschillende operationele omstandigheden en het werd zodoende aangetoond dat het CM daarbij wijzigt. Op basis van dit resultaat werd een voorstel gedaan om een dynamisch compartimenteel model te ontwikkelen. Verder werd in dit deel, met behulp van het CM, ook de impact van de sensorlocatie en regelwaarde op de prestatie van een regelaar geïllustreerd. Een optimale sensorlocatie is belangrijk omdat het leidt tot een verbeterde effluentkwaliteit aan een verlaagde kost.

In het vierde en laatste deel, werd de invloed van menging op de kalibratie van een TIS gebaseerd model aangetoond. Daarbij werd het duidelijk dat een TIS gebaseerd model leidt tot andere geschatte parameter waarden voor verschillende mengingscondities. Het is daarom belangrijk om de menging in rekening te brengen voor het uitvoeren van een kalibratie. Ook hier werd de invloed van de sensorlocatie aangetoond, deze wijzigt namelijk de kalibratie in hoge mate.

Als conclusie kan men stellen dat deze thesis heeft aangetoond dat geïntegreerde CFD-bio-kinetische modellering een nauwkeurigere evaluatie van het proces toelaat. Verder heeft de ontwikkeling van een compartimenteel model tot een oplossing geleid voor de hoge computationele belasting typisch voor een CFD model.

Curriculum vitae

Personal information

Name	Usman ur Rehman
Address	Zwijnaardsesteenweg 664C 9000 Gent, Belgium
Cell Phone	+32 488 66 44 98
Email	usman_cr@yahoo.com
Date of birth	January 17, 1986
Place of birth	Jhelum, Pakistan
Nationality	Pakistan

Education:

2012-	**PhD in Applied Biological Sciences,** Ghent University (UGent), Belgium PhD title: Next generation bioreactor models for wastewater treatment systems by means of detailed combined modelling of mixing and biokinetics
2009-2011	**MSc. Innovative and sustainable Chemical Engineering,** Chalmers University of Technology (CTU), Sweden.
09.2010-02.2011	**MSc Chemical Engineering (Exchange Program)** Technical University Delft (TU Delft), Netherlands.
2004-2008	**B.Sc. Chemical Engineering,** University of Engineering and Technology Lahore (UET), Pakistan.

Positions:

06.2012-06.2015	Marie-Curie Early Stage Researcher, Part of ITN 7th Framework Programme 2011. Programme Acronym: SANITAS
09.2009-	Member of Board of European Students of Technology (BEST) Gothenburg
01.2009-08.2009	Management Assistant at Sapphire Textiles Ltd. Lahore Pakistan

Extra trainings:

1. Complementary skills and water policy, University of Exeter, United Kingdom
2. Modelling and control of urban wastewater system, Lund university, Sweden and Technical university of Denmark
3. Practical fieldwork for WWTPs, Ghent university, Belgium
4. Decision-making and multi-criteria for urban water systems, Girona university, Spain

International conference – Symposia:

Participant & workshops:

1. 10th IWA Leading Edge Conference on Water and Wastewater Technologies (LET) (2013), Bordeaux, France (Workshop presentation)
2. 4th IWA/WEF wastewater treatment (WWT) modelling seminar (WWTmod) (2014), Spa, Belgium
3. 2nd IWA Specialized International Conference "Ecotechnologies for Wastewater Treatment" EcoSTP (2014), Verona, Italy (Workshop presentation)
4. 1st IWA Resource recovery conference (RR 2015), Ghent, Belgium

Oral presentations:

1. Rehman, U., Vesvikar, M., Maere, T., Guo, L., Vanrolleghem. P.A. & Nopens, I. (2013) Effect of sensor location on controller performance in a wastewater treatment plant. In proceedings: 11th IWA conference on instrumentation control and automation (ICA), Narbonne, France
2. Rehman, U., Maere T., Vesvikar, M., Amerlinck, Y. & Nopens, I. (2014) "Hydrodynamic – biokinetic model integration applied to a full scale WWTP." In proceedings: World Water Congress (WWC), Lisbon, Portugal.
3. Rehman, U., Amerlinck Y., Arnaldos M. & Nopens I. (2014) "CFD and biokinetic model integration applied to a full scale WWTP." In proceedings: The Water Quality Event (WEFTEC), New Orleans, USA.
4. Rehman, U., Amerlinck, Y., Arnaldos, M., Porro, J., De Mulder C. & Nopens I. (2015) "Elucidating the effects of mixing on nitrous oxide emissions using computational fluid dynamics in a full scale WWTP". In proceedings: 9th IWA Symposium on Systems Analysis and Integrated Assessment (WATERMATEX), Gold Coast, Australia
5. Rehman, U., De Mulder, C., Amerlinck, Y., Arnaldos, M., Weijers, S. R., Potier, O. & Nopens, I. (2016) "Towards better models for describing mixing using compartmental modelling: a full-scale case demonstration". In proceedings: 5th IWA/WEF Wastewater Treatment Modelling Seminar (WWTmod), Annency, France.

Peer reviewed publications – A1:

1. Rehman, U., Vesvikar, M., Maere, T., Guo, L., Vanrolleghem. P.A. & Nopens, I. (2015) Effect of sensor location on controller performance in a wastewater treatment plant, Water Science & Technology, 71(5), 700-708
2. Arnaldos, M., Amerlinck, Y., Rehman, U., Maere, T., Van Hoey, S., Naessens, W., & Nopens, I. (2015) From the affinity constant to the half-saturation index: Understanding conventional modeling concepts in novel wastewater treatment processes. Water Research, 70, 458-470.
3. Arnaldos, M., Rehman, U., Amerlinck, Y., Naessens, W., & Nopens, I. (2016) Understanding the Effects of Bulk Mixing on the Determination of the Affinity Index: Consequences on Process Operation and Design. (Submitted) Water Research.